WL-TR-96-4021

CERAMIC BEARING TECHNOLOGY PROGRAM

VOLUME 2   APPENDICES

R. KOMANDURI

OKLAHOMA STATE UNIVERSITY

STILLWATER OK

JULY 1995

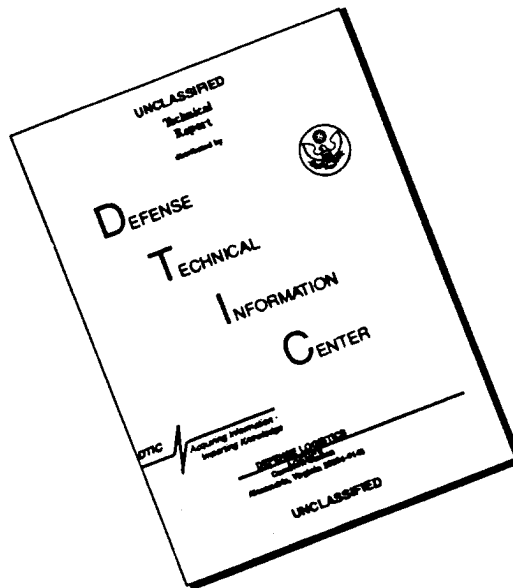FINAL REPORT FOR 08/01/92 - 07/01/95

APPROVED FOR PUBLIC RELEASE; DISTRIBUTION IS UNLIMITED.

19961018 137

DTIC QUALITY INSPECTED 3

MATERIALS DIRECTORATE

WRIGHT LABORATORY

AIR FORCE MATERIEL COMMAND

WRIGHT PATTERSON AFB OH 45433-7734

DISCLAIMER NOTICE

THIS DOCUMENT IS BEST QUALITY AVAILABLE. THE COPY FURNISHED TO DTIC CONTAINED A SIGNIFICANT NUMBER OF PAGES WHICH DO NOT REPRODUCE LEGIBLY.
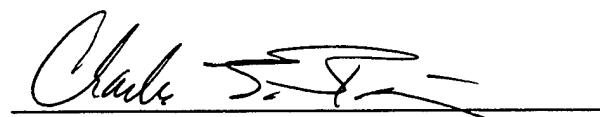
NOTICE

When government drawings, specifications, or other data are used for any purpose other than in connection with a definitely related government procurement operation, the United States Government thereby incurs no responsibility nor any obligation whatsoever; and the fact that the government may have formulated, furnished, or in any way supplied the said drawings, specifications, or other data, is not to be regarded by implication or otherwise as in any manner licensing the holder or any other person or corporation, or conveying any rights or permission to manufacture, use, or sell any patented invention that may in any way be related thereto.

This report is releasable to the National Technical Information Service (NTIS). At NTIS, it will be available to the general public, including foreign nations.

This technical report has been reviewed and is approved for publication.

KARL R. MECKLENBURG, Project Engineer
Nonstructural Materials Branch
Nonmetallic Materials Division

KENT J. EISENTRAUT, Chief
Nonstructural Materials Branch
Nonmetallic Materials Division

CHARLES E. BROWNING, Chief
Nonmetallic Materials Division
Materials Directorate

If your address has changed, if you wish to be removed from our mailing list, or if the addressee is no longer employed by your organization, please notify WL/MLBT, Bldg 654, 2941 P Street, Suite 1, Wright-Patterson AFB OH 45433-7750 to help maintain a current mailing list.

Copies of this report should not be returned unless return is required by security considerations, contractual obligations, or notice on a specific document.

REPORT DOCUMENTATION PAGE

Form Approved
OMB No. 0704-0188

Public reporting burden for this collection of information is estimated to average 1 hour per response, including the time for reviewing instructions, searching existing data sources, gathering and maintaining the data needed, and completing and reviewing the collection of information. Send comments regarding this burden estimate or any other aspect of this collection of information, including suggestions for reducing this burden, to Washington Headquarters Services, Directorate for Information Operations and Reports, 1215 Jefferson Davis Highway, Suite 1204, Arlington, VA 22202-4302, and to the Office of Management and Budget, Paperwork Reduction Project (0704-0188), Washington, DC 20503.

1. AGENCY USE ONLY (Leave blank)	2. REPORT DATE JUL 1995	3. REPORT TYPE AND DATES COVERED Final Report 08/01/92--07/01/95

4. TITLE AND SUBTITLE CERAMIC BEARING TECHNOLOGY PROGRAM

VOL 2 Appendices A-L

6. AUTHOR(S) KOMANDURI

5. FUNDING NUMBERS
C F33615-92-C-5933
PE 62712
PR 8355
TA 00
WU 10

7. PERFORMING ORGANIZATION NAME(S) AND ADDRESS(ES)

OKLAHOMA STATE UNIVERSITY
STILLWATER OK

8. PERFORMING ORGANIZATION REPORT NUMBER

9. SPONSORING/MONITORING AGENCY NAME(S) AND ADDRESS(ES)

MATERIALS DIRECTORATE
WRIGHT LABORATORY
AIR FORCE MATERIEL COMMAND
WRIGHT PATTERSON AFB OH 45433-7734

10. SPONSORING/MONITORING AGENCY REPORT NUMBER

WL-TR-96-4021

11. SUPPLEMENTARY NOTES

12a. DISTRIBUTION/AVAILABILITY STATEMENT

APPROVED FOR PUBLIC RELEASE; DISTRIBUTION IS UNLIMITED.

12b. DISTRIBUTION CODE

13. ABSTRACT *(Maximum 200 words)*

This project deals with the development of advanced manufacturing technologies for finishing silicon nitride balls and rollers for bearing applications. Magnetic field assisted polishing was used for finishing the balls and magnetic abrasive finishing for finishing rollers. By applying low levels of controlled force (1 N/ball or less) the damage on the finished surface is expected to be minimal. Also chemo-mechanical polishing was used to minimize the brittle fracture. Using these techniques the polishing time was reduced from some 10- 20 weeks to about 20 hours. The finish obtained was about 5-10 nm and the sphericity in the range of 0.5 -1 μm. In this report various technical papers dealing with various aspects of the finishing of silicon nitride balls and rollers prepared on this contract are included as appendices. They include the technology of polishing, optimum polishing conditons, the thermal model of the spot temperature generated in polishing, and finally the material removal mechanisms in polishing.

14. SUBJECT TERMS Silicon nitride, balls and rollers, finishing, bearings, chemo-mechanical polishing, magnetic field assisted polishing, the thermal models, and polishing mechanisms.

15. NUMBER OF PAGES 212

16. PRICE CODE

17. SECURITY CLASSIFICATION OF REPORT UNCLASSIFIED	18. SECURITY CLASSIFICATION OF THIS PAGE UNCLASSIFIED	19. SECURITY CLASSIFICATION OF ABSTRACT UNCLASSIFIED	20. LIMITATION OF ABSTRACT SAR

NSN 7540-01-280-5500

Standard Form 298 (Rev. 2-89)
Prescribed by ANSI Std. Z39-18
298-102

Table of Contents

APPENDIX A

ON THE FINISHING OF SILICON NITRIDE BALLS

M. Raghunandan and R. Komanduri

FINISHING OF SILICON NITRIDE BALLS

M. Raghunandan and R. Komanduri
Mechanical and Aerospace Engineering
Oklahoma State University
Stillwater, OK 74078, USA

SUMMARY

A batch of 12, HIPed silicon nitride balls (NBD 200 from CERBEC) of 13.4 mm nominal diameter was finished by magnetic float polishing process. These balls contained nearly a 200 μm thick x 5 mm wide band of material around the periphery at the parting plane for HIPing. The finishing process consisted of three stages - rough polishing using 30 μm boron carbide at 4000 rpm spindle speed to remove the rim on the silicon nitride balls, intermediate finishing 30 μm boron carbide at 2000 rpm spindle speed to reduce diameter and sphericity, and final finishing using 10 μm silicon carbide, followed by 1 μm silicon carbide and 1-5 μm chromium oxide. The balls were finished to a final diameter of 12.7 mm with an average sphericity of 1.3 μm (0.5 - 2.0 μm) and an average surface finish, R_a, of 24.6 nm (16.6 - 39.8 nm). The total time for finishing was about 21 hours. This, however, included an intermediate stage of finishing with chromium oxide in order to address the problems we experienced earlier in attempting to obtain good finish. As this stage is not required under normal circumstances, some 4 1/2 hours of polishing time can be saved resulting in total polishing time of about 16 1/2 hours.

EXPERIMENTAL SETUP AND TEST PROCEDURE

Figure 1(a) is a schematic diagram and Figure 1 (b) is a photograph of the magnetic float polishing apparatus showing permanent magnets located at the base of the apparatus. Table I lists typical test conditions used with the magnetic float polishing apparatus. The magnets were located with alternate N and S poles underneath the float chamber. A guide ring was mounted on top of the float vessel to contain the magnetic fluid. Magnetic fluid containing fine abrasive particles was filled in the chamber. The ceramic ball blanks were held in a 3-point contact between the float at the bottom, chamber wall on the side, and a top

plate connected to the shaft at the top. The shaft was connected to the spindle of the Bridgeport CNC milling machine or the Professional Instruments Inc. (PI) spindle which is capable of operating in the speed range of 60 - 6,000 rpm and upto 10,000 rpm respectively. The balls and the float were pushed upwards against the shaft by the magnetic buoyancy force. When a magnetic field was applied, the ceramic balls, abrasive grains, and the float made of non-magnetic material all float and were pushed upwards by the magnetic fluid. The balls were pressed against the drive shaft and were finished by the rotation of the drive shaft.

The magnetic fluid is a colloidal dispersion of extremely fine (100 to 150 A) sub-domain ferro-magnetic particles, usually magnetite (Fe_3O_4), in various carrier fluids, such as water or kerosene. The ferrofluids are made stable against particle agglomeration by the addition of surfactants. The chemical, mechanical, and physical properties of a ferrofluid correspond very closely to those of a carrier fluid. For example, all commercial ferrofluids utilizing organic carrier liquids are essentially electrically nonconductive and they have good lubrication properties. Magnetically, a ferrofluid is perfectly soft. The fluid has no net magnetization because the magnetic moments of individual particles are randomly distributed. When a magnetic field is applied to a ferrofluid, the magnetic moments of the particles orient along the field lines almost immediately to changes in the applied magnetic field (H). When the applied field is removed, the moments randomize quickly. Ferrofluids belong to a class of materials defined as super-magnetic. The magnetization (M-H) curve for the magnetic fluid used in the present study is given in Figure 2. The fluid possesses susceptibility up to 10^4 times greater than natural liquids and exhibits saturation magnetization (the maximum possible magnetization) up to 10^5 A/m.

Ferrofluids are strongly affected by an applied magnetic field. In a uniform magnetic field, the particles in a ferrofluid experience only torque and align with the field. When a magnetic fluid is placed in a magnetic field gradient, it is attracted towards the regions of higher magnetic field. If a non-magnetic substance (e.g., abrasives in this case) is mixed in the magnetic fluid, the substance is discharged towards the regions of lower field. When the field gradient is set in the gravitational direction, the non-magnetic material is made to float on the fluid surface by the action of the magnetic levitational force. In a field

with a gradient, however, the particles experience a force such that the fluid itself responds as a homogeneous magnetic liquid which moves to the region of highest field. Due to this, any non-magnetic material (float, balls, and abrasives in this case), when placed in ferrofluid, experiences a force which tends to expel the non-magnetic body from the fluid. This force, called the buoyancy or levitational force, is proportional to the gradient of the external field, the strength of the external field, and the magnetization of the fluid. Thus, the balls are pushed, by the float, against the top plate with a buoyant force F_b. The magnetic buoyant force F_b can be changed by changing the gap between the float and the magnet, and, by changing the magnetic field. This force is now utilized for polishing purposes.

TEST PROCEDURE

Table II lists the different polishing stages used to finish a batch of 12, 1/2 in HIPed silicon nitride balls. The process parameters such as spindle speed, abrasive type, abrasive size and spindle type, for different stages of polishing are also listed in the Table III. Except for the two tests (I and Q), a load of 1N/ball was used. The loads used in tests I and Q are indicated in Table III. The choice of these process parameters were based on the results of previous polishing stage and the aim of the next polishing stage. The batch size was chosen as the largest number of balls that could be used in the present experimental setup. After each polishing stage the balls were characterized as follows:

1. The ball diameter measurements were taken at ten points on each ball for all the balls for Tests A, B, C, and Q. For other tests, diameter measurements were on 3 or 4 balls and for each ball 3 or 4 measurements were taken.

2. The weight change was measured for the balls and the material removal rate in mg/min was computed as the weight change per ball per minute.

3. The ball roundness was measured using TalyRond at three different points on each ball for three different balls. For Test H, the TalyRond measurements were not taken.

4. In some cases (Tests G, H, I, N, P, and Q), the surface finish was measured using the Talysurf. Measurements were taken at three different points on each ball for three balls for Tests G, N and Q. For Tests I, H, and P, three measurements on one ball were taken.

5. At the end of Test Q, the balls were characterized using a Zygo laser interference microscope and an ABT 3200 Scanning Electron Microscope (SEM). The measurements were taken at two different points on the ball for two balls.

TEST RESULTS

A large rim of material was found at the perimeter of the as-received balls. This rim measured about 200 μm thick x 5 mm in height. The as-received balls had a mean diameter of about 13.4 mm. In Figure 3 (a), a TalyRond trace of the ball through this rim of material is shown. The sphericity of the ball as measured by TalyRond was 203.4 μm (244.9 - 183.1 μm). After about 11 hours of polishing (Test I) the sphericity was improved to 1.6 μm (2.3 - 0.9 μm). The diameter of the ball was about 13 mm at this stage. Another 10 hours of polishing was needed to reduce the diameter to 12.7 mm. At this stage (Test Q), a sphericity of 1.3 μm (2.0 - 0.5 μm) and a surface finish (R_a) of 24.6 nm (16.6 - 39.8 nm) were obtained. Figure 3 (b) and 3 (c) give the TalyRond traces of the polished ball (stages I and Q) in the same scale as Figure 3 (a) for comparison. Figures 4 (f) and (j) show the same traces (for Tests I and Q, respectively) at higher magnification to show the undulations on the ball on a micro-level.

The strategy used for finishing the balls was as follows. Initially the polishing was aimed at removing the rim and reducing the diameter. This required high removal rate so that the ball shape could be improved quickly. Hence, the polishing was performed with a 500 grit (about 30 μm mean diameter) boron carbide abrasive at 4000 rpm (Tests B and C). Tests B and C summarize three tests of 45 minutes each for a total of 180 minutes. These tests were conducted on the Bridgeport CNC milling machine in order to protect the precision PI air bearing spindle from impact loads caused by the large sphericity of the balls. In Table III, the maximum, minimum and average sphericity of the balls and the material removal rates (mg/min) for different stages of polishing are

given. The test numbering in this table corresponds to the numbering used in Table II, where the conditions used for polishing are given. Figures 4 (a) and (b) are TalyRond traces showing the progressive improvement of sphericity of the ball with polishing duration (for Tests B and C, respectively). After the first duration of polishing [Figure 4 (a)], i.e. after 135 minutes, the rim of material on the silicon nitride balls was completely removed. Thus, 135 minutes are sufficient to remove the rim completely. Test C was aimed primarily at removing material so that the required diameter can be reached.

Further polishing tests were aimed at improving the sphericity and reducing the diameter. For this purpose, polishing with boron carbide at a speed of 2000 rpm on a PI spindle was carried out (Tests D, E, and F). This decision was based on the previous experience that a speed of 2,000 rpm and use of PI spindle would produce good sphericity. Figures 4 (c), (d), and (e) show the TalyRond plots for Tests D, E, and F, respectively. At the end of Test F, a sphericity of 2 μm (1.8 - 2.8 μm) was obtained. At this stage, the diameter was about 13 mm.

In the finishing of silicon nitride balls in some of the previous batches, problems were encountered in obtaining good surface finish (Ra less than 50 nm). It was observed that good surface finish was obtained with chromium oxide in some tests but not in others. It was felt that this was due to changes in the polishing load. Though nominally 1 N/ball was used in the polishing experiments, a variation of about 10 - 20% was expected in some of the tests due to electronic drift in the amplifier. After detecting the drift, the amplifier was replaced with one that was stable. To analyze this, tests with chromium oxide abrasive were planned. Before polishing with chromium oxide, an intermediate polishing with smaller grit size (10 μm) boron carbide was carried out (Test G). Only a slight improvement in sphericity was seen. The surface finish parameters R_a and R_t (minimum, average and maximum values of measurement) are listed in Table IV. Polishing with chromium oxide was then carried out (Test H) at a load of 1 N/ball. As was expected, no improvement in surface finish was obtained. The load was then increased to 1.5 N/ball (Test I), with all the remaining parameters similar to Test H. An R_a of 35 nm (29.1 - 38.4 nm) was obtained, which is about half the previous value. Figures 5 (a), 5 (b), and 5 (c) give the Talysurf surface roughness traces for Tests G, H, and I, respectively. The TalyRond plot for Test I

is shown in Figure 4 (f) [see also Figure 3 (b)]. On comparing Figures 5 (a) and (b), it is clear that there was no change in surface finish between Tests G and H. The removal of peaks, which is characteristic of chromium oxide polishing, can be seen in Test I [Figure 5 (c)]. Thus, it is clear that loads higher than 1 N/ball are needed for producing good surface finish using chromium oxide abrasive. A slight reduction in sphericity was also obtained.

Polishing tests J, K, and L were aimed at rapidly reducing the diameter while maintaining the sphericity. In Test J boron carbide abrasive (30 μm) was used. In Test K , the abrasive was changed to softer silicon carbide (38 μm), so that the surface damage could be reduced to some extent. However, this resulted in a large reduction of removal rate. Hence, in Test L, boron carbide abrasive (30 μm) was again used. The sphericity was maintained in the range of 1 - 3 μm for all these tests. The ball diameter at the end of this test was in the range of 12.785 - 12.791 mm.

The emphasis in the final stage of polishing was to obtain the desired surface finish and sphericity while maintaining the required diameter. Tests M - Q correspond to this stage of polishing. In Test M, silicon carbide (12 μm) size was used for polishing. This resulted in good improvement in sphericity to an average value of 1 μm (1.8 - 0.5 μm). Figure 4 (g) shows a TalyRond plot of the ball. However, the removal rate was low. In order to reduce the total polishing time, silicon carbide of the next larger grit size (15 μm) was used in polishing in Tests N and O. In Test N, an average sphericity of 0.9 μm (0.7 - 1.2 μm) was obtained. Figure 4 (h) shows a TalyRond plot of the roundness of the ball and Figure 5 (d) shows the Talysurf surface roughness plot of the ball at the end of this test. In Test O, evaporation of the water base and consequent drying of the magnetic fluid was observed. This lead to improper movement of the ball in the polishing chamber and hence poor sphericity. The sphericity at the end of polishing Test O was 3.1 μm (1.8 - 4.2 μm). Since the diameter at the end of this test was 12.703 - 12.705 mm, no attempt was made to correct this increase in sphericity by further polishing with silicon carbide of 15 μm grit size. Instead, silicon carbide of 1 μm grit size was used for polishing with the aim of improving surface finish (Test P). It was found that Test P resulted in both improvement of surface finish and sphericity. Figures 4 (i) and 5 (e) show the TalyRond and Talysurf plots respectively for Test P. Next a final polishing test using chromium

oxide (1 - 5 μm) with a load of 1.2 N/ball was performed (Test Q). A sphericity of 1.3 μm (0.5 - 2.0 μm) was obtained. The TalyRond roundness plot is shown in Figure 4 (j) [see also Figure 4 (c)]. The surface finish R_a was 24.6 nm (16.6 - 39.8 nm). Figure 5 (f) shows the Talysurf surface roughness of the polished ball. The polishing by removal of peaks as seen in Test I is also found in this case. Figure 6 shows the 2-D surface roughness plot obtained from ZYGO laser interference microscope. ZYGO plot shows a mostly smooth surface with few shallow pits. These pits are believed to be left over from the previous polishing stages.

DISCUSSION

The total polishing process can be divided into three stages:

1. Removal of the rim of material - This took about two hours (135 min.) of polishing. In this stage the emphasis was placed on obtaining high removal rate so that the rim could be quickly removed. At this stage, surface finish is important only to the extent that it is useful in controlling the amount of damage to the surface.

2. Reduction in diameter and improvement of sphericity - The emphasis here was on quick improvement in sphericity with a moderate removal rate. The improvement in sphericity was quicker than the reduction in diameter. Thus, a sphericity of about 1 μm was obtained in about five hours of polishing, while the diameter at this stage was nearly 300 μm oversize. Reduction of diameter needed about 2 hours of polishing.

3. Final finishing - This stage has two sub goals - control of final diameter and sphericity, and, production of final surface finish. Low removal rates are prefered here so that better control can be exercised on the final diameter. Also, a graded surface finish is needed between the rough polishing of earlier stages and final chromium oxide polishing. Abrasives of smaller grit size were used for this purpose which would also give rise to low removal rates. Further, the sphericity needs to be held at a low value. This stage of polishing took about 8 hours.

In the present test, a total of about 21 hours was needed to complete polishing of 1/2 in. silicon nitride balls to final size, finish, and sphericity. As pointed out earlier, some experiments on polishing with chromium oxide were carried out at the intermediate stage. As this was not required, the total polishing time could be about 16 1/2 hours. Also, in the present test, we were able to achieve the polishing stages 1 and 2 successfully. The maximum diametrical removal rate was about 1.2 μm/min. Thus, from the initial diameter of 13.4 mm, the final diameter of 12.7 mm can be obtained in about 10 hours. However, to obtain low values of sphericity and surface finish, small abrasives/low speed need to be used. This implies that a large amount of time was spent in removing the final 100 μm of diameter. Also, the variability of removal rates was sufficiently large, especially at higher removal rates. This we believe was due to repeated use of the ferrofluid instead of a fresh batch. We have done this as our stock of ferrofluid was rapidly depleting. This implies that there may be considerable variation in finishing times. Also, some amount of intermediate inspection is needed. However, we feel that by incorporating appropriate monitoring and control systems (for example for load and speed), better control over the process can be achieved.

As pointed out earlier, the as-received (HIPed) silicon nitride balls from CERBEC (NBD 200) were about 13.4 mm in diameter and contained nearly a 200 μm (diameter difference) x 5 mm band of material around the periphery. To finish these balls to a diameter of 1/2 in took nearly 21 hours. However, some 4 1/2 hours was not required in the normal procedure. Also, the diameter of the as-received balls need not be 13.4 mm and the rim of material can also be reduced significantly during HIPing . This should bring the polishing time down quite significantly. It also shows the capability of the magnetic float polishing technique to handle balls of such initial size and shape.

Figure 7 shows the variation of average sphericity with time. The maximum and minimum sphericity values measured are also shown in the figure as error bars. In this plot the three stages of polishing discussed earlier are indicated. It should be noted that the Y-axis (sphericity) is plotted in log scale. Hence, the error bars would appear disproportionately large at smaller values of sphericity when compared to larger values. In this plot the intermediate tests conducted to study the effect of load on chromium oxide polishing were

eliminated and the time correspondingly adjusted. The thick lines are the best-fit exponential functions. In the curve fitting, the data after 405 minutes of polishing (Test F) was considered separately as the slope of the line was different. Thus the two exponential functions approximate a more complicated function. Also the data for Tests O, P, and Q (the last three tests) were not considered for curve fitting. This was due to the fact that the fluid dried up during Test O, causing a degradation in sphericity. As this dry up was a peculiarity of this particular test and should not occur in general practice, it was eliminated from the analysis. Also, since the degradation in sphericity at one test will be carried over to subsequent tests, these data points were also eliminated from analysis. The extrapolation of the best fit curve is shown in broken lines. It can be seen that this line is almost parallel to the line through the last three points. This clearly indicates that the test results would have followed the line indicated by the broken line had the fluid not dryed up. This gives us further confidence that our analysis is valid.

The change in slope of the best fit occurs at about 2 μm average sphericity. This slope is about 3 times smaller than that of the previous curve. Thus to reduce sphericity by half (say from 1 to 0.5 μm) would take three times more time than it would take to the same reduction at larger values of sphericity (say 50 to 25 μm). The equations for the best fit are given in the following:

$$\text{Sphericity} = 156.16\ e^{-0.011t} \qquad \text{Sphericity} > 2\ \mu m$$

$$\text{Sphericity} = 8.72\ e^{-0.003t} \qquad \text{Sphericity} < 2\ \mu m$$

Based on these equations, an estimated time of 1400 minutes from the beginning is needed to obtain a sphericity of better than 0.1 μm average.

Earlier, we have identified factors such as speed, wear of shaft, and wear of float to influence the sphericity of the ball. We now know that fluid dry-up as an additional factor influencing the sphericity in magnetic float polishing. This knowledge along with the bet fit relationships obtained here would be useful for producing high precision balls using MFP.

As mentioned earlier, the diameter of the finished balls were measured 10 times on each ball for all the balls. The measurements were performed using a micrometer with a resolution of 1 μm. From this the frequency of occurrence of each diameter value was determined. This frequency was divided by the total number of measurements to obtain the normalized frequency for each diameter. Figure 8 shows the normalized frequency for the different ball diameters. The average of diameters for the whole batch was 12.695 mm. It can be seen from the plot that most of the diameters (about 95%) are within ± 1 μm from the average diameter. This variation is same as the capability of the measuring instrument. Also, the difference in maximum and minimum diameter measurements was 4 μm. Of this, the average variation in the different diameter measurements of a single ball (i.e. average sphericity as measured by micrometer) was 2 μm. The variation among the average diameters of the balls in the batch was 2 μm.

CONCLUSIONS

1. A batch of 12, HIPed silicon nitride balls of 13.4 mm nominal diameter was finished to size, sphericity, and finish using magnetic float polishing technique. The finished balls were characterized using Talysurf, TalyRond, Zygo laser interference microscope, and a scanning electron microscope. The finished balls had a final diameter of 12.7 mm with an average sphericity of 1.3 μm (0.5 - 2.0 μm) and an average surface finish, R_a, of 24.6 nm (16.6 - 39.8 nm).

2. The finishing time to accomplish the task was about 21 hours from the as-received condition. However, under normal circumstances, this can be reduced to 16 1/2 hours or less as some 4 hours was taken to conduct other tests to assess surface finish achievable with chromium oxide abrasive. Also, both the initial diameter and shape can be considerably close to the finial requirements. This would significantly reduce the polishing time.

3. Unlike the conventional polishing technique, the batch size used is rather small. This was by choice as we were asked to develop technology for polishing small batches since conventional methods requires large number of balls and long polishing times. In a R & D environment or where small batches

11

are desired, the technique developed would be ideal. It is conceivable that the batch size can be increased to say 50 to 100 balls per batch.

TABLE I   TEST CONDITIONS

Work material	HIPed Silicon nitride(NBD 200), 1/2 in balls
Abrasive type	B_4C, SiC, Cr_2O_3
Abrasive size	1 - 40 μm
Abrasive concentration	10 % by volume
Ferrofluid	Water based ferrofluid (W-40) (400G saturation magnetization Viscosity 25 cp)
Magnets	Rare Earth Magnets (Nd-Fe-B) Width : 1/2 in Thickness : 2 x width Residual magnetization : 10500 G
Load	1.0, 1.2, 1.5 N/ball
Speed	2000, 4000 rpm
Machine Tool and Spindle Used	Bridgeport CNC Milling Machine PI Air Bearing Spindle

TABLE II   TEST DETAILS

Test	Time, min	Abrasive Type	Abrasive Size, μm	Speed, rpm	Load, N/ball	Spindle	Remarks
A	0	-	-	-			Stage 1
B	135	B_4C	30	4000	1.0	CNC	
C	270	B_4C	30	4000	1.0	CNC	
D	315	B_4C	30	2000	1.0	PI	Stage 2
E	360	B_4C	30	2000	1.0	PI	
F	405	B_4C	30	2000	1.0	PI	
G	495	B_4C	10	2000	1.0	PI	Study of
H	585	Cr_2O_3	1-5	2000	1.0	PI	finishing
I	675	Cr_2O_3	1-5	2000	1.5	PI	with Cr_2O_3
J	720	B_4C	30	2000	1.0	PI	Stage 2
K	765	SiC	38	2000	1.0	PI	
L	810	B_4C	30	2000	1.0	PI	
M	870	SiC	12	2000	1.0	PI	Stage 3
N	960	SiC	15	2000	1.0	PI	
O	1060	SiC	15	2000	1.0	PI	
P	1180	SiC	1	2000	1.0	PI	
Q	1270	Cr_2O_3	1-5	2000	1.2	PI	

TABLE III
SPHERICITY AND MATERIAL REMOVAL RATE
FOR DIFFERENT STAGES OF POLISHING

Test	Sphericity, μm			MRR
	Max.	Min.	Ave.	mg/min
A	244.9	183.1	203.4	-
B	29.8	17.4	22.9	1.03
C	14.8	7.7	11.1	1.22
D	5.6	2.5	4.4	1.33
E	5.5	3.4	4.3	1.13
F	2.8	1.8	2.0	0.87
G	2.7	1.0	1.7	0.02
H				0.01
I	2.3	0.9	1.6	-
J	2.7	1.6	2.3	-
K	2.3	1.2	1.5	0.64
L	2.9	1.2	2.0	1.23
M	1.8	0.5	1.0	0.16
N	1.2	0.7	0.9	0.30
O	4.2	1.8	3.1	0.30
P	2.3	1.5	1.8	0.06
Q	2.0	0.5	1.3	

TABLE IV SURFACE FINISH AT DIFFERENT STAGES OF POLISHING

Test	Surface finish R_a, nm			Surface finish R_t, µm		
	Min.	Ave.	Max.	Min.	Ave.	Max.
G	58.9	64.0	72.6	1.55	1.85	2.15
H	63.7	66.6	70.9	0.74	0.89	1.04
I	29.1	35.0	38.4	0.45	0.67	1.01
N	118.0	133.2	156.7	1.29	1.85	1.50
P	42.6	46.2	50.8	0.41	0.45	0.46
Q	16.6	24.6	39.8	0.28	0.38	0.54
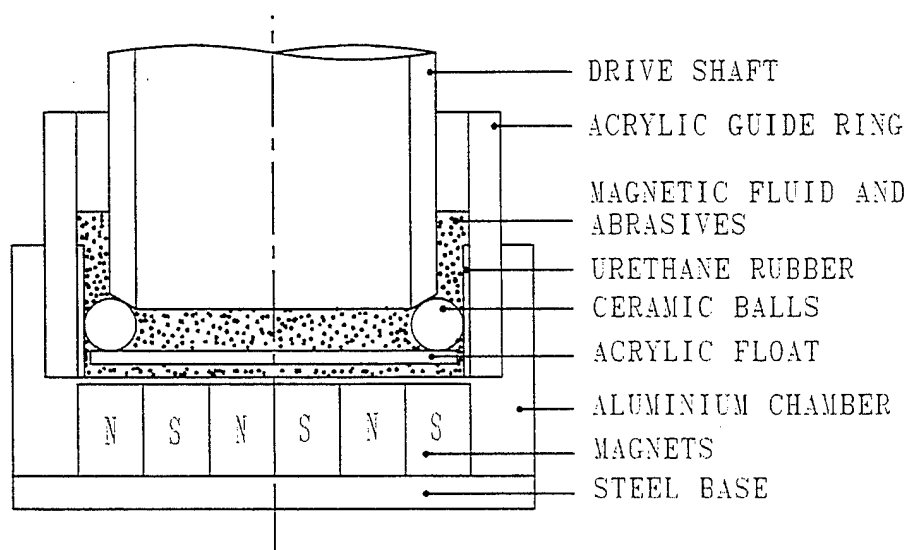
DRIVE SHAFT

ACRYLIC GUIDE RING

MAGNETIC FLUID AND ABRASIVES

URETHANE RUBBER

CERAMIC BALLS

ACRYLIC FLOAT

ALUMINIUM CHAMBER

MAGNETS

STEEL BASE

N S N S N S

Figure 1 (a)   Schematic of the magnetic float polishing apparatus showing the permanent magnets at the base.
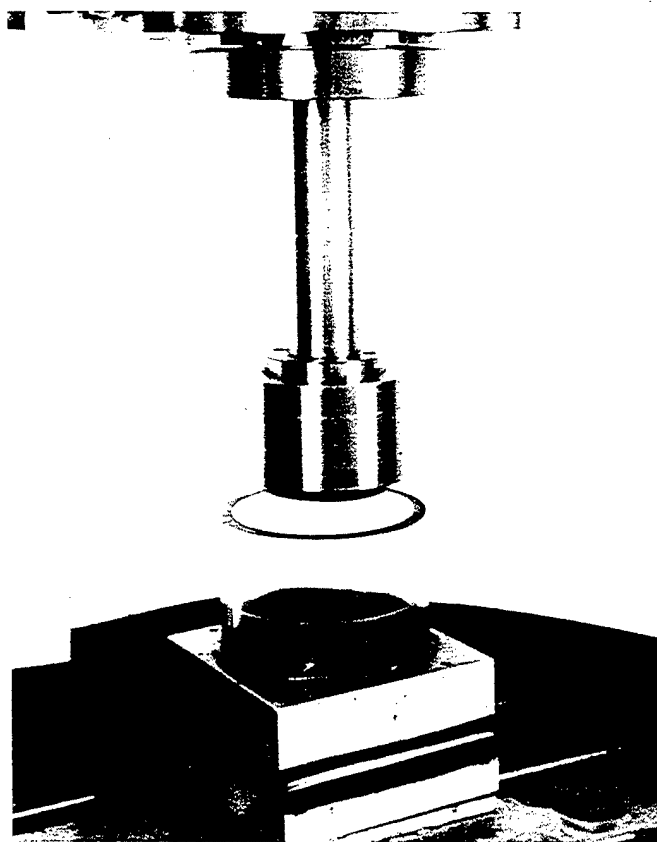
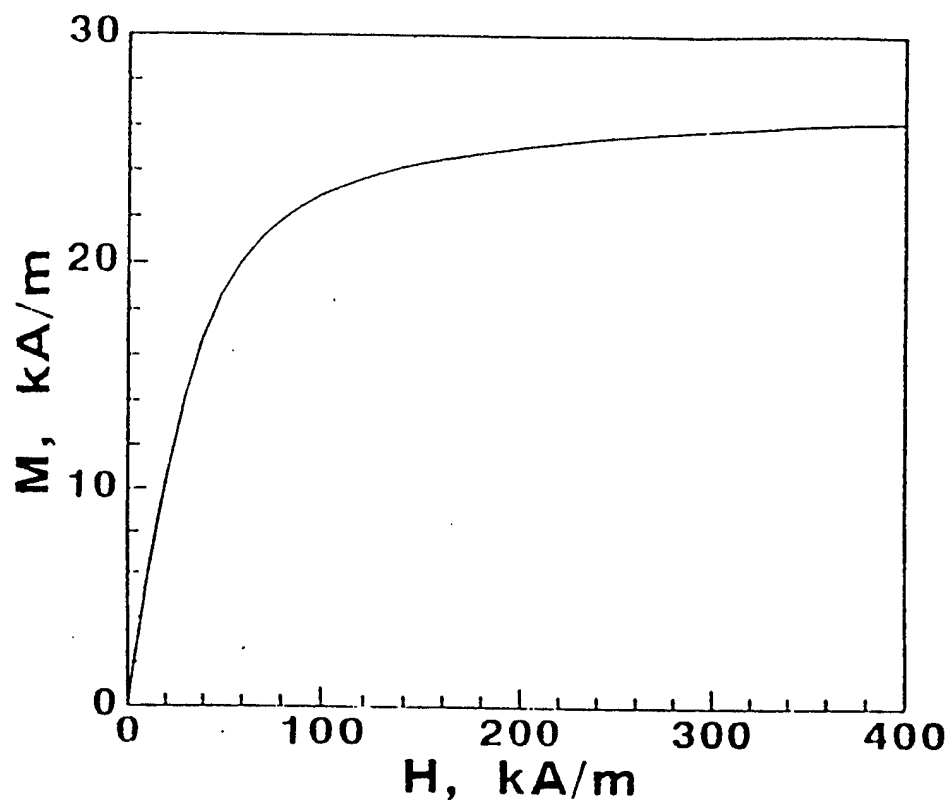Figure 1 (b)   Photograph of the magnetic float polishing apparatus

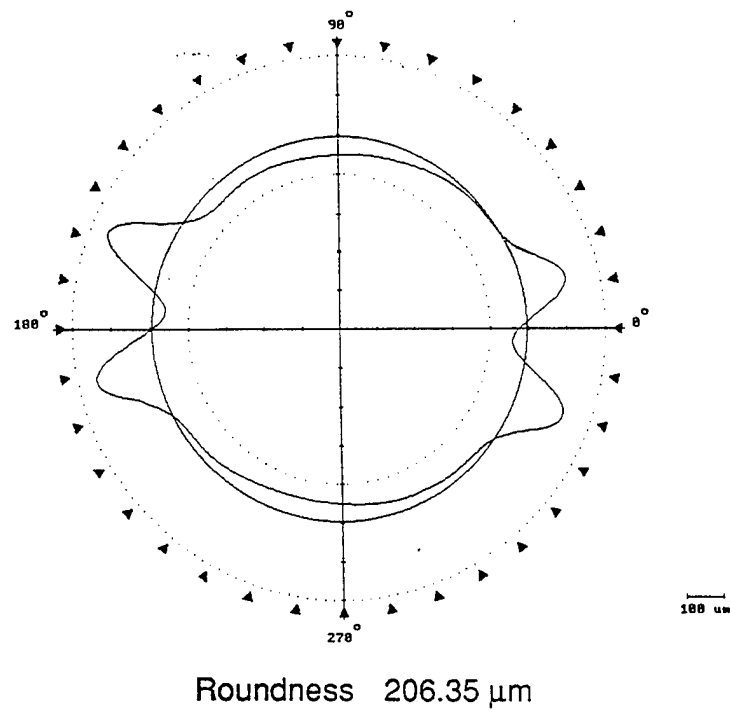Figure 2   Magnetization (M-H) curve for the ferrofluid

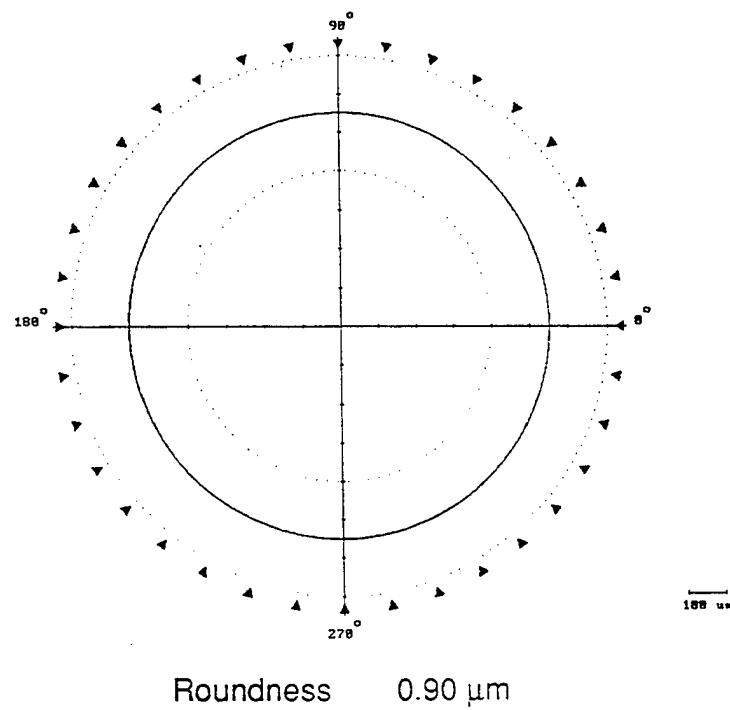Roundness   206.35 µm

Figure 3 (a)   TalyRond roundness trace of an as-received ball

Roundness   0.90 µm

Figure 3 (b)   TalyRond roundness trace of a polished ball after Test I
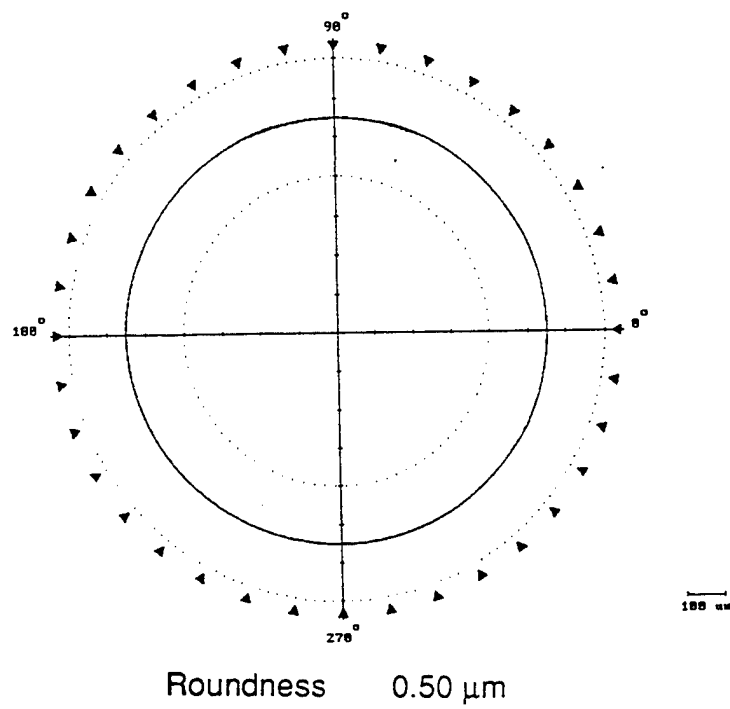Speed : 2000 rpm, Load : 1.5 N/ball, Abrasive : 1-5 µm Cr_2O_3

Roundness 0.50 μm

Figure 3 (c) TalyRond roundness trace of a polished ball after Test Q
Speed : 2000 rpm, Load : 1.2 N/ball, Abrasive : 1-5 μm Cr_2O_3

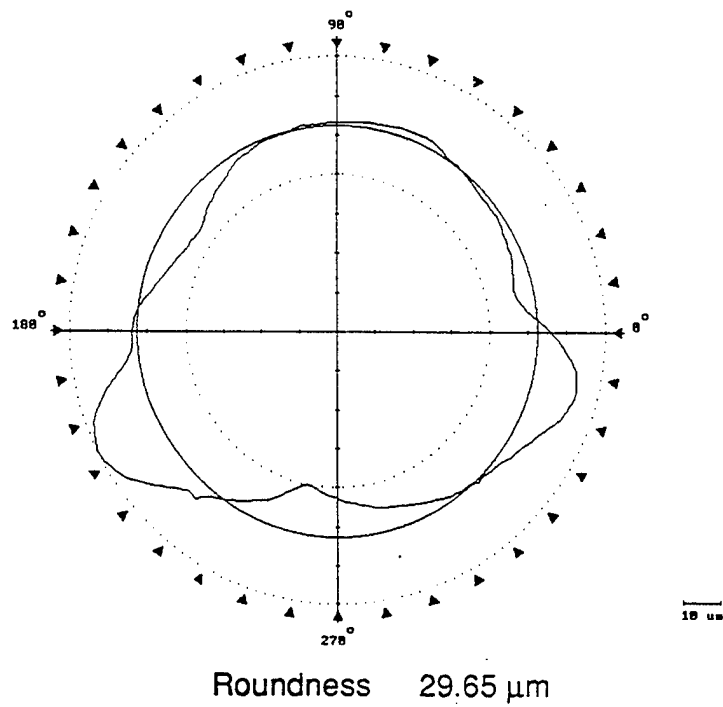Roundness   29.65 µm

Figure 4 (a)   TalyRond roundness trace of a polished ball
Test B, Speed 4000; Load: 1 N/ball; Abrasive: 17 µm B₄C

Roundness   9.90 µm
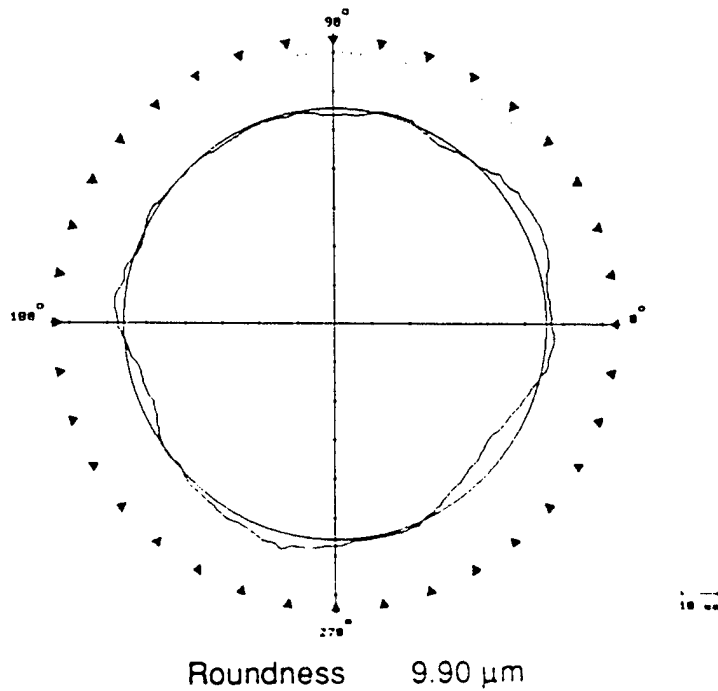
Figure 4 (b)   TalyRond roundness trace of a polished ball
Test C, Speed 4000; Load: 1 N/ball; Abrasive: 17 µm B₄C
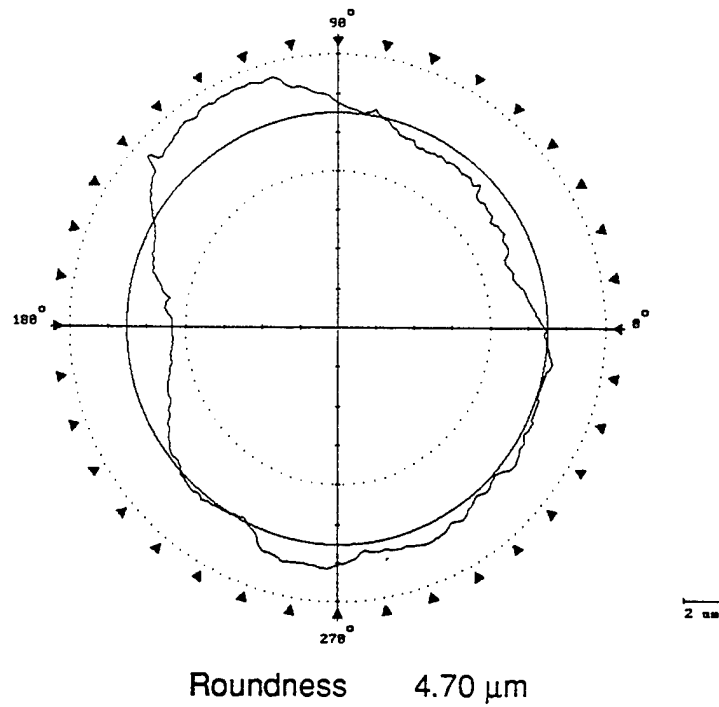
21

Roundness   4.70 μm

Figure 4 (c)   TalyRond roundness trace of a polished ball
                Test D, Speed 2000, Load: 1 N/ball ; Abrasive: 17 μm B4C

Roundness   3.65 μm
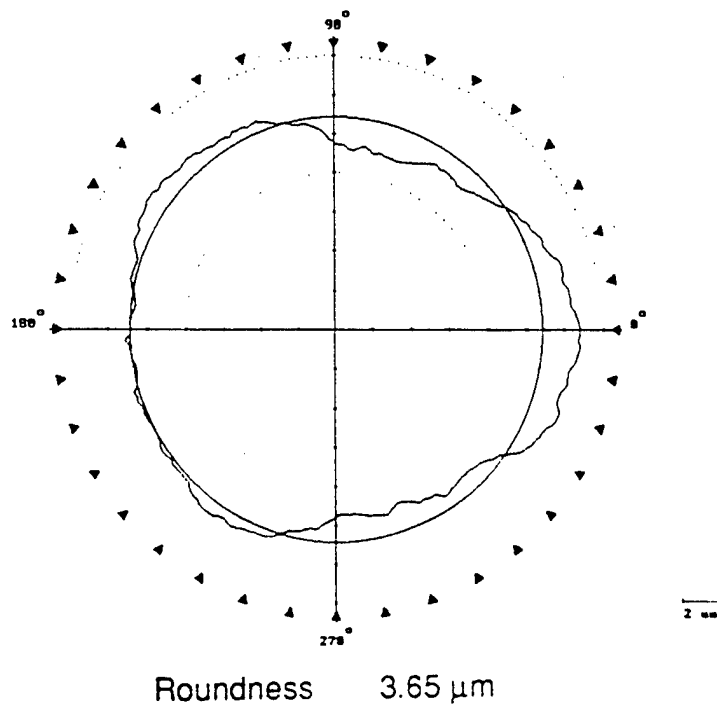
Figure 4 (d)   TalyRond roundness trace of a polished ball
                Test E, Speed: 2000; Load: 1 N/ball; Abrasive: 17 μm B4C

Roundness   2.15 μm

Figure 4 (e)   TalyRond roundness trace of a polished ball
Test F, Speed : 2000; Load: 1 N/ball; Abrasive: 17 μm B$_4$C

Roundness   0.90 μm

Figure 4 (f)   TalyRond roundness trace of a polished ball
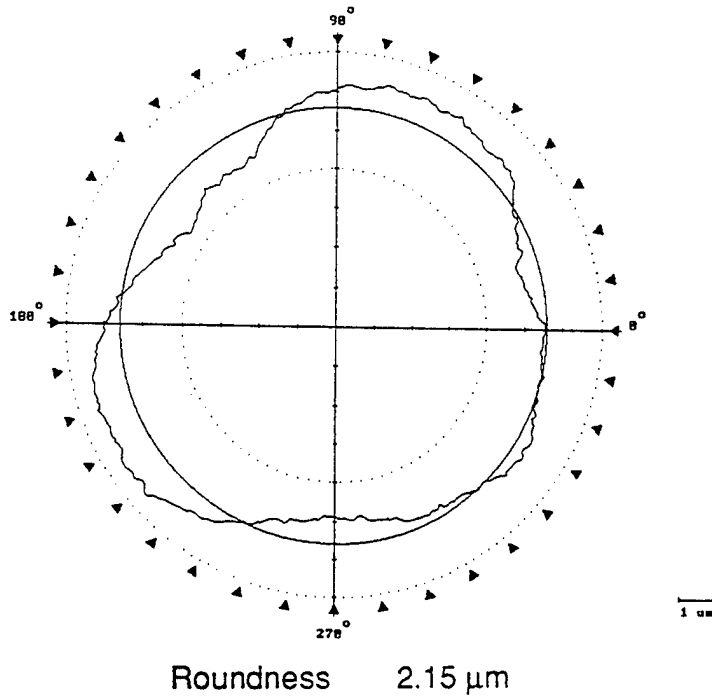Test I, Speed : 2000; Load: 1.5 N/ball; Abrasive: 1-5 μm Cr$_2$O$_3$

23

Roundness   0.60 μm

Figure 4 (g)   TalyRond roundness trace of a polished ball

Test M, Speed : 2000; Load: 1 N/ball; Abrasive: 3 μm SiC

Roundness   0.75 μm
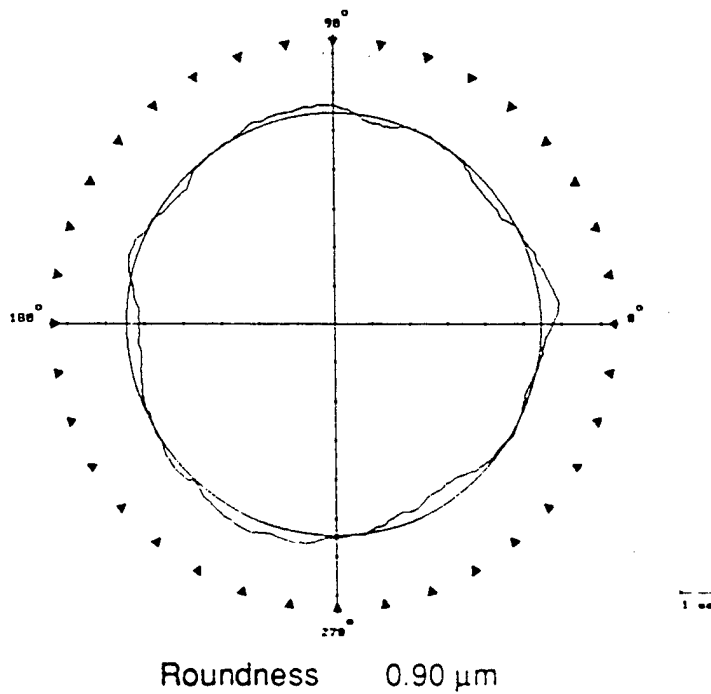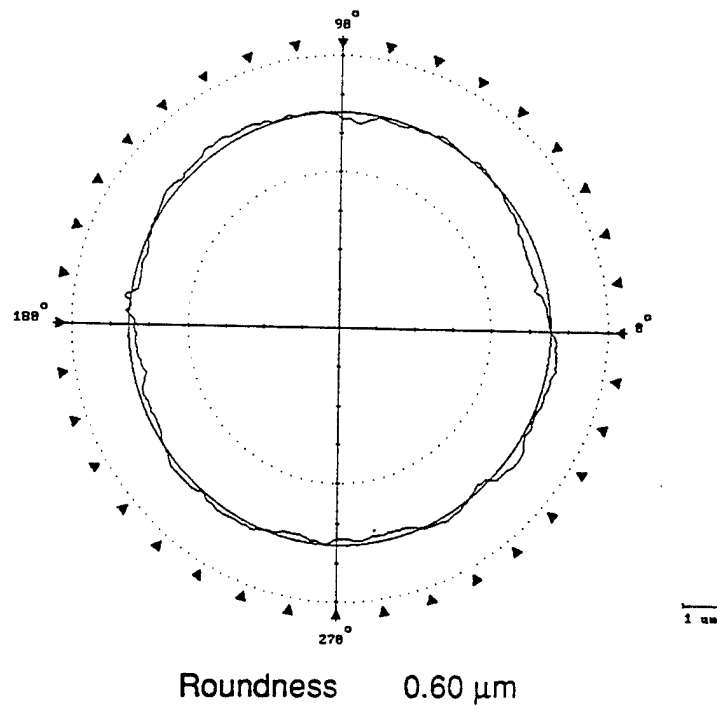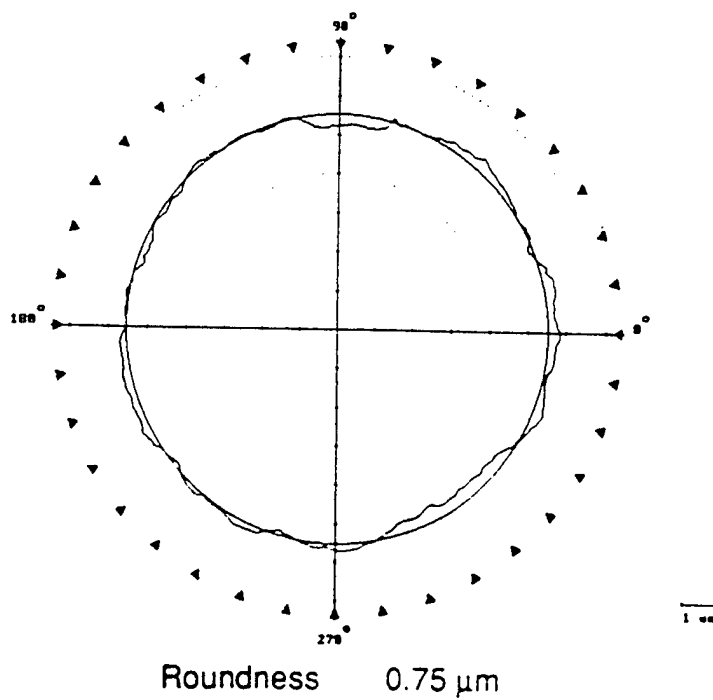
Figure 4 (h)   TalyRond roundness trace of a polished ball

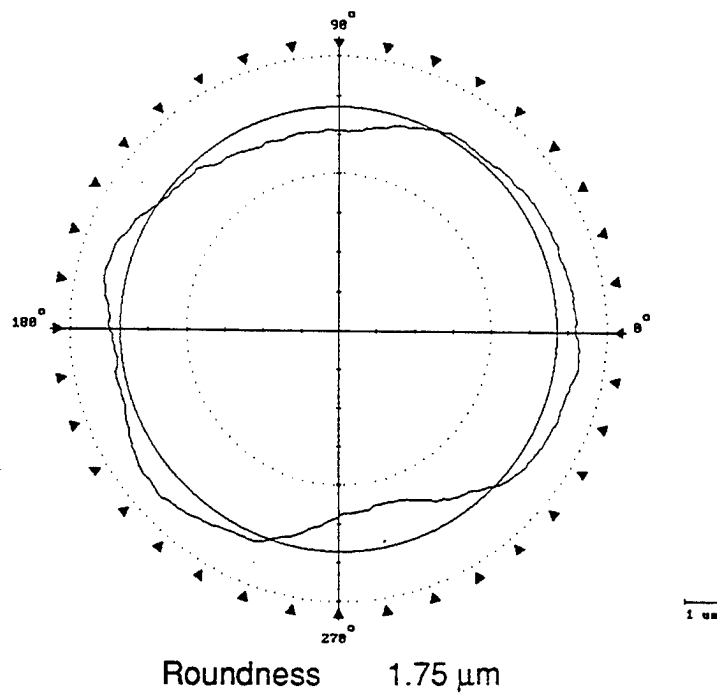Test N, Speed : 2000; Load: 1 N/ball; Abrasive: 5 μm SiC

Roundness   1.75 μm

Figure 4 (i)   TalyRond roundness trace of a polished ball after Test P
Speed : 2000 rpm, Load : 1 N/ball, Abrasive : 1 μm SiC

Roundness   0.50 μm
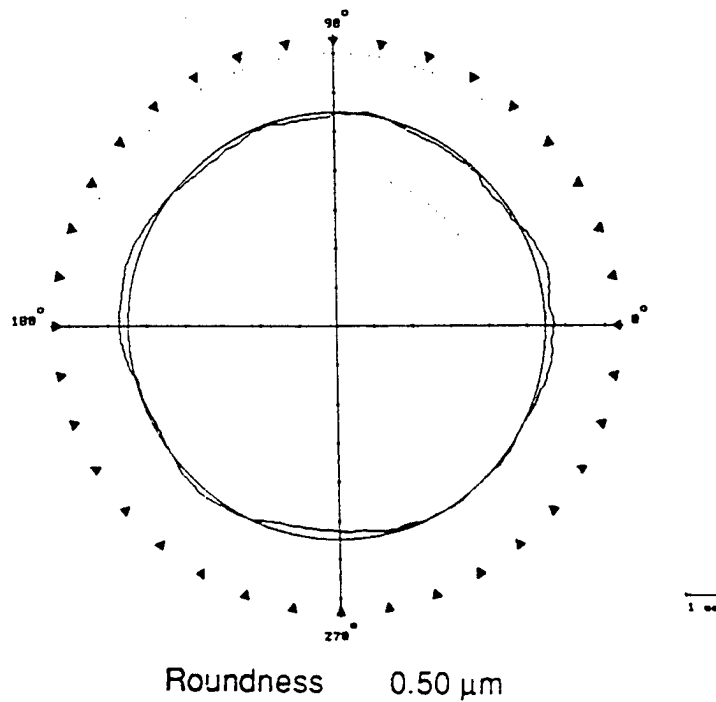
Figure 4 (j)   TalyRond roundness trace of a polished ball after Test Q
Speed : 2000 rpm, Load : 1.2 N/ball, Abrasive : 1-5 μm Cr_2O_3

R_a 62.8 nm R_t 0.65 μm
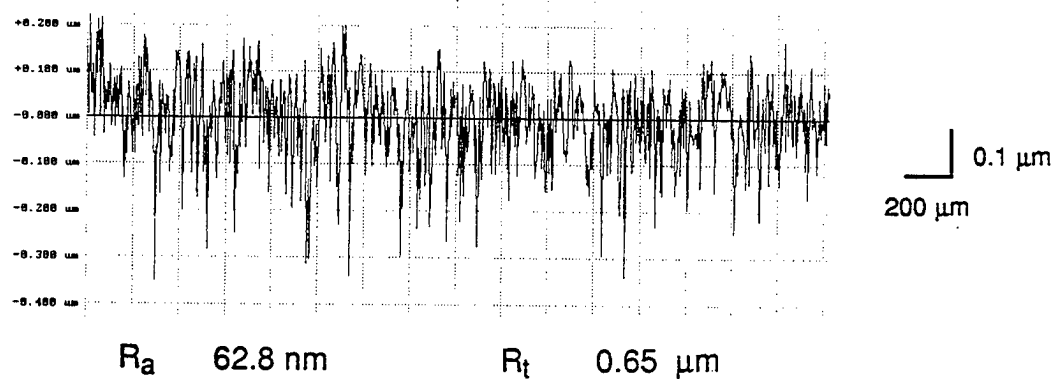
Figure 5 (a)   Talysurf surface roughness trace of a polished ball
             Test G, Speed: 2000; Load: 1 N/ball; Abrasive: 1-2 μm B_4C

R_a 70.9 nm R_t 0.65 μm
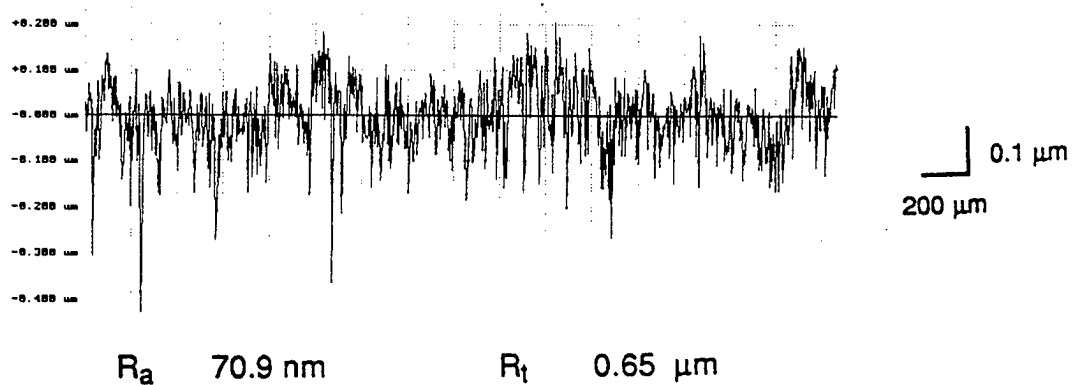
Figure 5 (b)   Talysurf surface roughness trace of a polished ball after Test H
             Speed : 2000 rpm, Load : 1 N/ball, Abrasive : 1-5 μm Cr_2O_3

R_a 34.2 nm R_t 0.47 μm
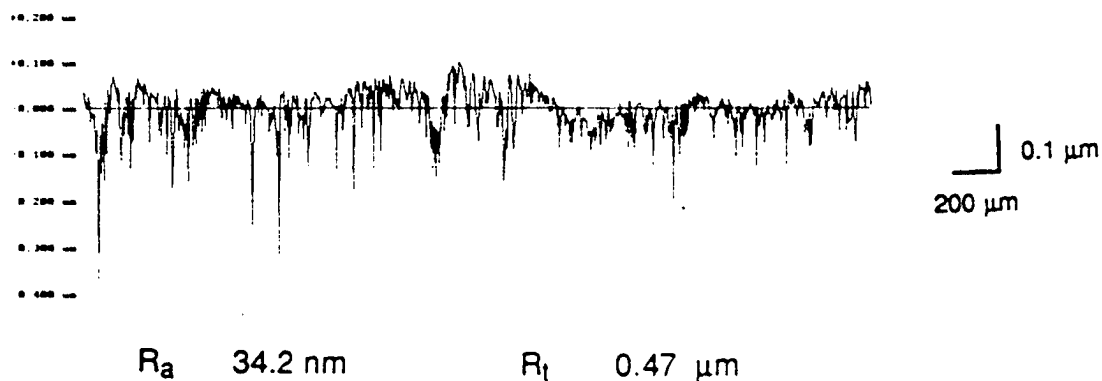
Figure 5 (c)   Talysurf surface roughness trace of a polished ball after Test I
             Speed : 2000 rpm, Load : 1.5 N/ball, Abrasive : 1-5 μm Cr_2O_3

R_a 124.9 nm R_t 1.29   μm
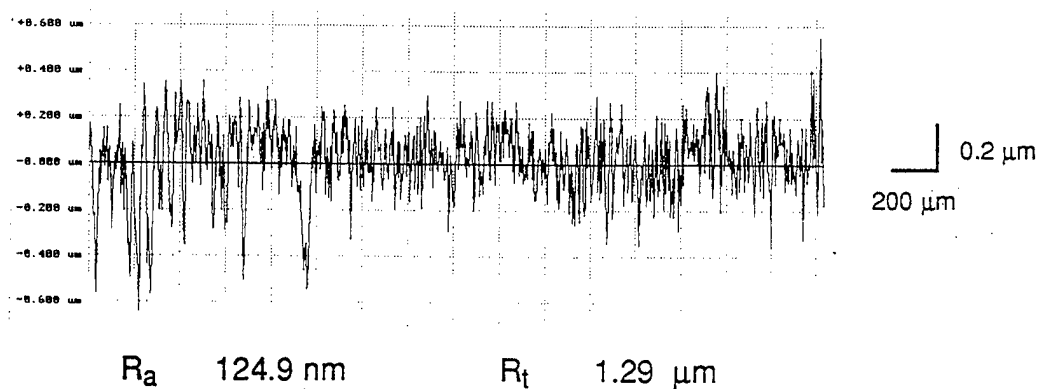
Figure 5 (d)   Talysurf surface roughness trace of a polished ball in Test N
Speed 2000; Load: 1 N/ball; Abrasive: 5 μm SiC

R_a 45.1 nm R_t 0.41   μm
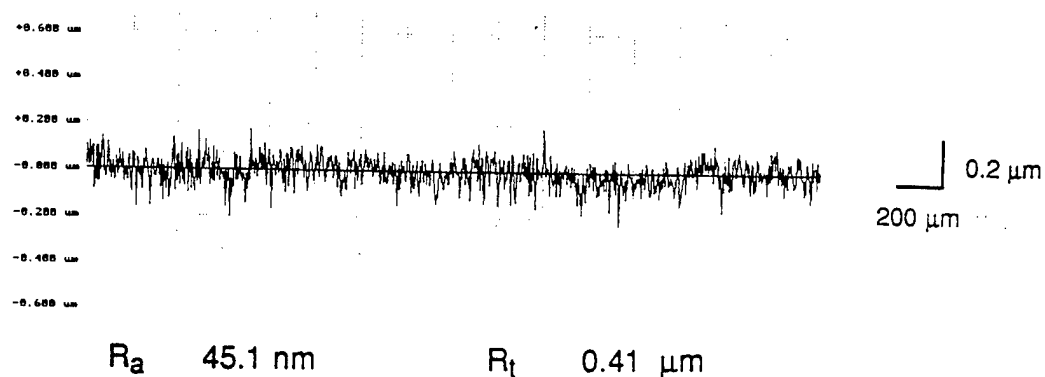
Figure 5 (e)   Talysurf surface roughness trace of a polished ball after Test P
Speed : 2000 rpm, Load : 1 N/ball, Abrasive : 1 μm SiC

R_a 18.3 nm R_t 0.49   μm
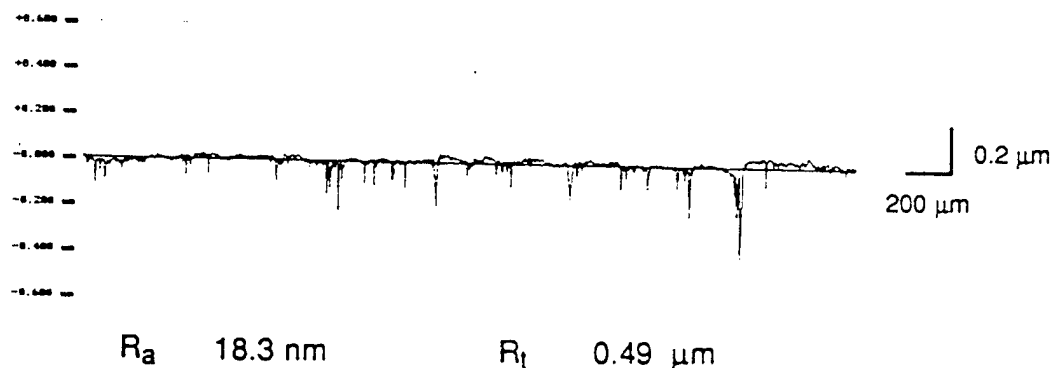
Figure 5 (f)   Talysurf surface roughness trace of a polished ball after Test Q
Speed : 2000 rpm, Load : 1.2 N/ball, Abrasive : 1-5 μm Cr_2O_3

Figure 6   ZYGO plot of a polished ball used in Test Q
            speed 2000, 1.2 N/ball, 1-5 μm chromium oxide
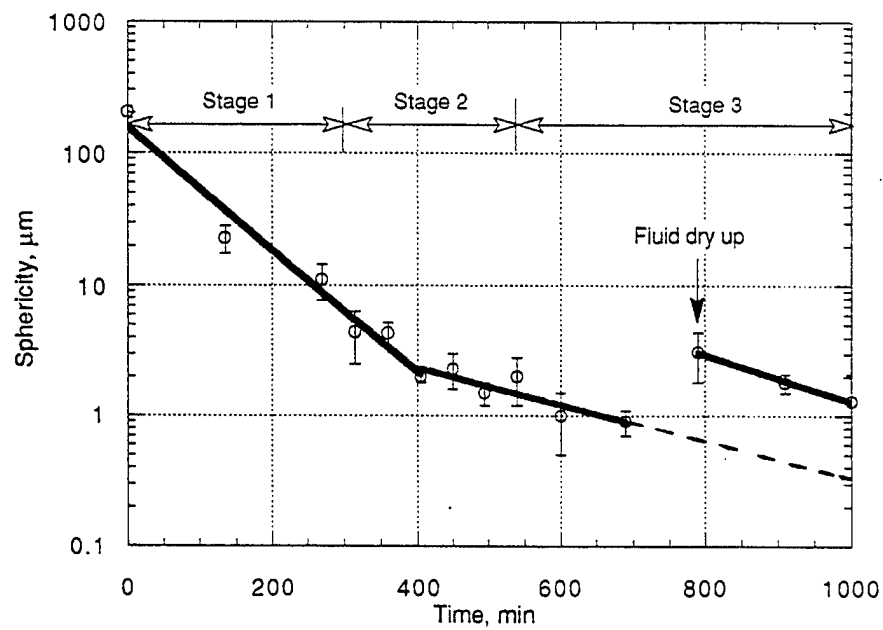
Figure 7   Variation of spharicity with time

Figure 8   Diameter distribution of the finished balls

APPENDIX B

MAGNETIC FLOAT POLISHING OF CERAMICS

M. Raghunandan, N. Umehara, A. Noori-Khajavi, and
R. Komanduri

MAGNETIC FLOAT POLISHING OF CERAMICS

M. Raghunandan, N. Umehara, A Noori-Khajavi, and R. Komanduri

Mechanical and Aerospace Engineering

Oklahoma State University

Stillwater, OK 74078, USA

ABSTRACT

Magnetic float polishing is a new technique developed for efficient finishing of advanced ceramics. The equipment for this application thus far has been developed on the basis of empirical designs and trial and error experimental approach which can be costly and time consuming. In the work reported here both analytical (FEM simulation) and experimental approaches were taken to determine such design parameters as the variation of magnetic float stiffness with buoyant force and variation of buoyant force with the gap between the magnet and the float. The agreement between the experimental and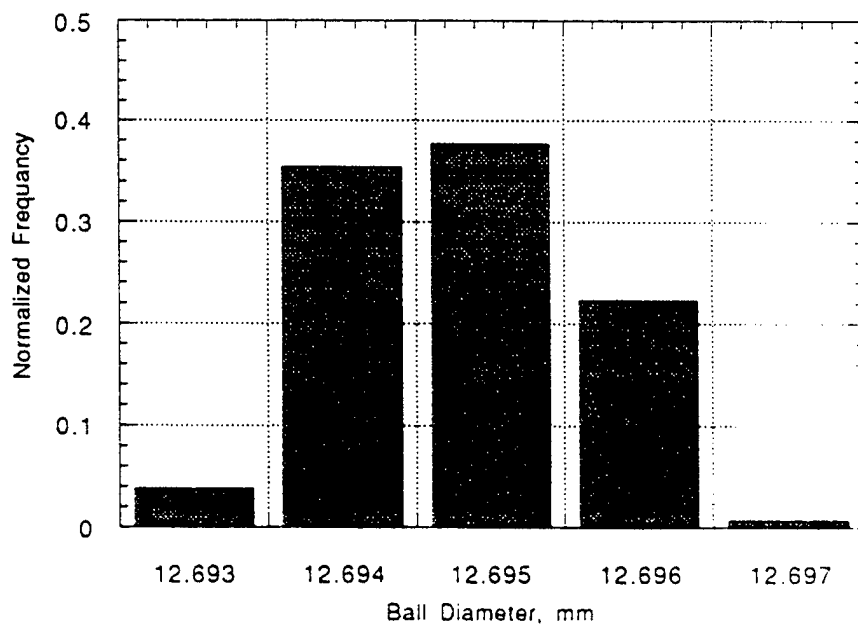 analytical results is found to be excellent. Consequently, it is possible to simulate different designs without actually building different equipment for the performance evaluation. Also, the effect of ball circulation speed in magnetic float polishing is discussed qualitatively for assessing the conditions for high removal rates and/or best finish. Such an approach can facilitate the development of operating conditions maps for magnetic float polishing.

INTRODUCTION

Finish, accuracy, and surface integrity of the parts produced by conventional machining (i.e. tool harder than the work piece) depend on the machine tool system, namely, the machine tool, cutting tool, workpiece, cutting conditions, and cutting fluid. For accomplishing higher removal rates or higher surface finish, the machine tools need to be rigid, free from quasi-static errors (deflections) as well as dynamic errors (chatter or vibration), and, workpiece and tooling errors. Often it is difficult to build economically machine tools that are extremely rigid, vibration free, and error free. With the introduction of many difficult-to-machine materials, such as hardened steels, and nickel-, cobalt- and titanium-based superalloys oscillations in the cutting process (cyclic variation of forces) have become inherent to the cutting process (cyclic chip formation) and can not be modified significantly by the machine tool system. Also, with the advent of advanced materials, such as ceramics and composites, very few cutting tool materials (including diamond and cubic boron nitride) with geometrically defined edges are capable of material removal. Ceramics and glasses are brittle and failure of parts made from these materials are

31

initiated by cracks formed during machining as well as by other defects in these materials. To minimize the damage due to machining, it is necessary to process them under 'gentle' conditions, i.e. very low forces. While improved machine tools will certainly facilitate in reducing deflections and chatter, need arises for controlling the force. Also, the finishing operation has to be economically attractive. This has led to the introduction of non-traditional machining where the cutting process is aided by a secondary energy source. For example, in ultrasonic grinding, the material removal operation is facilitated by the vibratory action. Similarly, in laser assisted machining, a laser compliments the cutting action.

Magnetic field assisted polishing is one such non-conventional machining technology in which the cutting force is controlled by the magnetic field. As a machine tool technology for finish polishing, it essentially accomplishes the task without the need for designing expensive, rigid, ultra-precision, vibration free, and error free machine tools. This new technology can be incorporated into existing conventional machine tools, thereby minimizing the cost of new equipment. The process can thus be very effective and economical. However, the design parameters are not established. In this paper some of the design parameters of importance to magnetic float polishing are evaluated analytically and verified experimentally.

MAGNETIC FIELD ASSISTED POLISHING OF ADVANCED CERAMICS

It is somewhat difficult by conventional grinding and polishing techniques to finish cost effectively advanced ceramics and glasses, such as silicon nitride, silicon carbide, and aluminum oxide, and at the same time to meet the requirements of high finish, high accuracy, and presence of minimal surface defects, such as cracks. This has necessitated the development of an alternate manufacturing technology, namely, magnetic field assisted polishing. There are two types of magnetic field assisted polishing techniques -- one for finishing rollers, known as magnetic abrasive finishing and the other for finishing balls, known as magnetic float polishing, the subject of this paper. It may be noted that the later process is also termed as magnetic fluid grinding [8] although in this paper we prefer to use the term magnetic float polishing. The salient features of the magnetic float polishing technique are the following :1) very high finish and accuracy can be obtained; 2) Very little or no surface damage, such as microcracks, is imparted to the ceramic parts during the finishing operation due to extremely low level of forces, 3) Finishing operation can be significantly faster than by conventional techniques. This is due to higher spindle speeds possible by this technique, 4) Small batches can be processed. Small batches of ceramic balls can be polishing by this process, unlike in conventional polishing where a large number is required for alignment and accuracy requirements. The number of balls used depends on the size of the balls and 5) Fewer polishing steps are needed. The balls can be processed from the rough to finished state in one operation by varying the strength of the magnetic field intensity. It

is, therefore, not necessary to change the polishing machines for roughing and finishing or clean the balls during the polishing cycle.

Although the magnetic field assisted polishing concept was originated in the U.S., it was in the former U.S.S.R. (Baron and his associates [1-5]) and Bulgaria (Mekedonski and his associates [6]) that much of the developments took place after World War II. These researchers have shown that the technique can be applied for a wide range of products. In the 80's, the Japanese researchers (chiefly, Professor Kato and his associates at Tohoku University [7-10], and Dr. Shinmura and his associates at Utsunomia University [11-14]) followed this work and began research for finish polishing applications. Several ceramic companies in Japan, including, Toshiba are actively working in this area. Studies are also underway in the U.K. (Childs et al [15,17,18]) and in the U.S. at Oklahoma State University under ARPA and NSF support.

In the following, magnetic field assisted polishing technique for finishing ceramic balls will be briefly reviewed.

MAGNETIC FLOAT POLISHING OF CERAMIC BALLS

Magnetic float polishing of ceramic balls was developed recently in Japan by Kato et. al [7-10] to rapidly finish (in a few hours) ceramic balls in small batches of ten to a hundred. The polishing operation in this process occurs due to the magnetic levitational force. The process works on the basis of the magneto-hydrodynamic behavior of a magnetic fluid that can float non-magnetic abrasives suspended in it. The process is considered highly effective for finish polishing because a levitational force is applied to the abrasives in a controlled manner. The forces applied by the abrasives to the part in this process are extremely small (about 1 N or less per ball). The time required to finish the balls to the same accuracy (or better) by this technique is at least an order of magnitude faster than by conventional polishing techniques. Consequently, this technique can be extremely cost effective and viable for the manufacture of ceramic balls.

Figure 1(a) is a schematic diagram and Figure 1 (b) is a photograph of the magnetic float polishing apparatus showing permanent magnets located at the base of the apparatus. The magnets are located with alternate N and S poles underneath the float chamber. A guide ring is mounted on top of the float vessel to contain the magnetic fluid. Magnetic fluid containing fine abrasive particles is filled in the chamber. The ceramic ball blanks are held in a 3-point contact between the float at the bottom, guide ring on the side, and a top plate connected to the shaft at the top. The shaft is connected to the spindle of the Bridgeport CNC milling machine which is capable of operating in the speed range of 60 - 6,000 rpm. When a magnetic field is applied, the ceramic balls, abrasive grains, and the float of non-magnetic material all float and are pushed

upwards by the magnetic fluid. The balls are pressed against the drive shaft and are finished by the rotation of the drive shaft.

The magnetic fluid is a colloidal dispersion of extremely fine (100 to 150 A) sub-domain ferro-magnetic particles, usually magnetite (Fe_3O_4), in various carrier fluids, such as water or kerosene. The ferrofluids are made stable against particle agglomeration by the addition of surfactants. When a magnetic fluid is placed in a magnetic field gradient, it is attracted towards the higher magnetic field side. If a non-magnetic substance (e.g., abrasives in this case) is mixed in the magnetic fluid, they are discharged towards the lower side. When the field gradient is set in the gravitational direction, the non magnetic material is made to float on the fluid surface by the action of the magnetic levitational force. The fluid has no net magnetization because the magnetic moments of individual particles are randomly distributed. Magnetically, a ferrofluid is perfectly soft. When a magnetic field is applied to a ferrofluid, the magnetic moments of the particles orient along the field lines almost immediately to changes in the applied magnetic field (H). When the applied field is removed, the moments randomize quickly. Ferrofluids belong to a class of materials defined as super-magnetic. The magnetization (M-H) curve for the magnetic fluid used in the present study is given in Figure 2. The fluid possesses susceptibility up to 10^4 times greater than natural liquids and exhibit saturation magnetization (the maximum possible magnetization) up to 10^5 A/m.

The chemical, mechanical, and physical properties of a ferrofluid correspond very closely to those of a carrier fluid. For example, all commercial ferrofluids utilizing organic carrier liquids are essentially electrically nonconductive and they have good lubrication properties. Ferrofluids are strongly affected by an applied magnetic field. In a uniform magnetic field, the particles in a ferrofluid experience only torque and align with the field. In a field with gradient, however, the particles experience a force such that the fluid itself responds as a homogeneous magnetic liquid which moves to the region of highest field. Due to this, any non-magnetic material, when placed in ferrofluid experiences a force which tends to expel the non-magnetic body from the fluid. This force, called the buoyancy or levitational force is proportional to the gradient of external field, strength of external field, and the magnetization of the fluid. Thus, the balls are pushed, by the float, against the top plate with a buoyant force F_b. The magnetic buoyant force F_b can be changed by changing the gap between the float and the magnet, and, by changing the magnetic field. This force is now utilized for polishing purposes.

In order to obtain an optimum magnetic circuit for this method, the effect of support stiffness of the float on removal rate, sphericity, and surface roughness were investigated by Umehara et al [16]. They found that higher supporting stiffness of the float results in an increase in the removal rate and the rate of sphericity improvement. However, it also leads to a larger value

of minimum sphericity and surface roughness. From this, it appears that larger supporting stiffness of the float is desirable for rough grinding of ceramic balls. However, it is not clear if smaller supporting stiffness of the float facilitates finish polishing. For successful use of this technique, it is necessary to investigate the optimal conditions for higher removal rate and for superior finish. However, it is clear that the design of the magnetic circuit is critical for obtaining better polishing characteristics.

Childs et al [17] recently investigated the mechanical aspects related to the material removal in magnetic fluid grinding of ceramic balls. They measured the ball circulation speed to investigate the ball motion during polishing. They calculated the removal rate by assuming it to be proportional to the load pressing the balls on to the drive shaft and to the skidding velocity at the drive shaft, in a manner expected of an abrasive wear process. They estimated a wear coefficient of 0.05-0.09 from the experiments, which they attributed is typical of a 2-body abrasion process. They only emphasized the influence of sliding speed between the balls and the drive shaft on the removal rate. For efficient polishing of high precision balls, both the sliding speed and the rolling speed between the ball and the drive shaft would be important.

Childs et al [18] also analyzed the kinematic motion of the balls in a magnetic fluid during magnetic float polishing. They developed a relationship between the drive shaft speed and the ball circulation speed and found it to agree reasonably well with the experimental results. But since the effect of such a motion of the ball on the polishing characteristics are still unknown, the optimum relative motion between the ball and the drive shaft as a consequence is also still unknown. It is clear from this that more polishing studies are needed for the determination of optimum operating conditions in magnetic float polishing.

THEORETICAL ANALYSIS

Ferromagnetic materials when placed in a magnetic field acquire magnetic polarization. The number of magnetic dipoles per unit volume of the material is known as the intensity of magnetization (or simply magnetization), and is represented by vector $\mathbf{M}$. In the presence of a magnetizable material, magnetic field density, $\mathbf{B}$ can be shown as:

$$\mathbf{B} = \mu_o(\mathbf{M} + \mathbf{H}) \tag{1}$$

where $\mathbf{H}$ is magnetic field intensity. In the absence of any electric current in the media we have according to Ampere's law

$$\nabla \times \mathbf{H} = 0 \tag{2}$$

Therefore, from the divergence theorem there is a scalar potential function ϕ such that

$$\mathbf{H} = \nabla \phi \tag{3}$$

The relation between $\mathbf{M}$ and $\mathbf{H}$ can be represented by

$$M = \chi H \tag{4}$$

Where χ is the magnetic susceptibility. For ferromagnetic materials, magnetization is strongly a function of H. Substituting Eq. (4) into (1), we get

$$B = \mu_o(1+ \chi)H \tag{5}$$

According to Maxwell's equations

$$\nabla \cdot B = 0 \tag{6}$$

Substituting (3) and (6) into (5), we get

$$\nabla \cdot [(1+ \chi)\nabla \phi] = 0 \tag{7}$$

This is a nonlinear equation because χ is a strong function of H and as no analytical solution is currently available, it can be solved only numerically. The magnitude of B, H, and M can be found from Eq. (1), (3), and (4) respectively.

If an object is immersed into the magnetic fluid, the magnetic buoyancy force, F_b (ignoring the conventional buoyancy forces) can be calculated using the equation given by Rosensweig [19].

$$F_b = \int_s \left(\frac{1}{2} \mu_0 M \,^2_n + \mu_0 \int_0^H M \, dH \right) \vec{n} \, ds \tag{8}$$

Where M, H, and M_n are the magnitudes of magnetization M, field intensity H, and magnetization normal to the surface of the floating object M_n, respectively. n is the unit vectors normal to the surface of the object.

As pointed out earlier, there is no analytical solution to Eq. (7), it can only be solved numerically either through finite element or finite difference methods. In either methods the entire domain of the problem will be divided into small elements by meshing the domain. The outputs of the program will be magnetic field H, magnetic flux density B, magnetic vector potential A, and magnetic potential, ϕ. Forces can be calculated from Eq. (8).

DESCRIPTION OF THE APPARATUS

Figure 3 is a schematic diagram of the experimental apparatus for measuring the magnetic buoyant force. The buoyant force of a non-magnetic body immersed in magnetic fluid under the magnetic field can be measured by the reaction force of the magnets. A vessel containing the magnetic fluid is placed on the magnets. The magnetic base and the vessel are supported on a load cell. An acrylic resin disk (2 mm thick and 40 mm in diameter) with a stem held at a fixed height is submerged in the magnetic fluid. It causes a reaction on the load cell which varies with the distance of the disk from the magnet. The reaction force of the disk along with the stem and that

with only the stem are measured. The difference between the forces gives the buoyant force F_b of a float disk.

A water-based magnetic fluid (W-45) was used whose saturation magnetization and viscosity are 0.04 T (at 637 KA/m of magnetic field intensity) and 7.0 x 10^{-3} Pa.s respectively. Magnetic field is applied by the assembly of Sm-Co permanent magnets (residual magnetization 0.96 T and coercivity 684.6 kA/m). In order to obtain a large magnetic buoyant force, the magnets are assembled such that the polarities of adjacent magnets are opposite. Three levels of magnetic field are applied by the assembly of magnets with three different widths (a_m), namely, 4 mm, 6 mm and 8 mm respectively. The length of the magnet is 30 mm for all magnets. Height of the magnet is twice the width. Magnetic field intensity in the Z-direction was measured using a Hall effect sensor.

SIMULATION RESULTS

Childs and Yoon [15] reported on the design of a magnetic fluid grinding cell (both theoretical and analytical work) to develop design parameters. They used finite difference (FD) analysis to analyze the magnetic force generation, to predict the depth at which the abrasives float, and to estimate the force the float exerts on each ball, all with a view to develop a methodology for the selection of the width of the magnet for a ball of a given diameter. Initially, we used the FD technique proposed by Childs and Yoon [15] to analyze the process. Unfortunately, due to limitations of this technique (compared to FEM) and the assumptions made in the analysis, the experimental values were found to differ significantly from the analytical values. Figure 4 is a plot of the variation of the buoyant force of the float with the distance from the magnet by FD and FEM analyses respectively for magnets of 6 mm width. It can be seen that the FD analysis overestimates the buoyant force at all distances from the magnet. As will be shown later in this section, the FEM analysis agrees well with the experimental values thus lending support to the analytical technique. Some of the reasons for the discrepancy between the values obtained by the FD and FEM analyses are the following.

1. In their analysis Childs and Yoon assumed the magnets to be infinitely long in the N-S direction. This gives rise to the assumption that flux density on the surface of the magnet is uniform, and equal to the residual magnetization (remenence) of the magnets. Childs and Yoon also neglected the internal resistance of the magnet. Figure 5 is a FEM plot showing the distribution of the magnetic flux density, B (contour map) on the surface of the magnet as well as within the magnet. The maximum values of flux density for each contour are shown in the figure. It can be seen that the magnetic flux density on the surface of the magnet is not constant but varies with the position on the magnet, namely, maximum of 0.5 T at the interface between any

two magnets and minimum of 0.3 T around the middle of the magnet. Also, the magnetic flux density on the surface of the magnet is much lower than the remenence (about 0.5 T compared to the remenence of 0.96 T). Further, it can also be seen from Figure 5 that the internal resistance of the magnet is quite significant and can not be neglected.

2. FEM analysis solves the differential equations of the system for each element, creating a piecewise continuous function of the output.FD analysis, in contrast, approximates the solution at the nodes.

3. For materials with nonlinear properties, as is the case in the present investigation, the solutions by both FD and FEM analyses are through repeated iteration. Analysis of such a nonlinear process by FD technique requires a special program to be written, which limits the complexity of the problem that could be analyzed. In contrast, standard software packages are available (such as ANSYS) to solve complex realistic problems on a routine basis using the FEM technique.

4. In the FEM analysis we used the surface integral of the pressure due to the presence of a magnetic field to compute the magnetic buoyancy forces (Rosensweig [19]) which is more accurate than computing the magnetic force per unit volume as adopted by Childs and Yoon.

Consequently, we attribute the lack of agreement between the values obtained using the FD technique and those from the FEM technique or the experimental results partially to the inaccuracies inherent to the FD technique and the simplifying assumptions made in the analysis. It was, therefore, decided to conduct FEM simulation studies using the ANSYS program to calculate the buoyant force and float stiffness in the magnetic float polishing.

FEM simulation studies were made using the ANSYS program to calculate the buoyant force and float stiffness in the magnetic float polishing for the apparatus shown in Figure 3. The geometrical information of the magnetic float polishing apparatus, such as the diameter of the chamber, float, magnet pole width, magnet thickness, as well as the magnetic properties of the magnet, such as residual magnetization and coercive force for magnet, M-H curve for magnetic fluid were provided as inputs to the system. A 40 mm chamber containing a 2 mm thick float was modeled. The magnets were modeled as having 0.96 T residual magnetization and coercivity of 684.6 kA/m. Three different widths of magnet - 4, 6 and 8 mm were considered. The length on magnets in each case was 2 times the width. Also, the number of magnets was different for each case (15 for 4 mm width, 12 for 6 mm width and 8 for 8 mm width). The magnet assembly was taken to have alternate N-S poles. About 25 cc of magnetic fluid was considered, equivalent to 20 mm height over the magnets. A steel plate (thickness equal to 1/2 the width of magnets) was considered placed below the magnets. The magnetic fluid properties were input as B-H table

based of the curve given in Figure 2. Similarly, the B-H table of the steel was input. All non-magnetic materials - float, guide ring and surrounding air are assumed to have permeability of that of vacuum. Using this, a 2-D FEM analysis was performed. From the ANSYS solution, the magnetic field intensity at the nodes for different distances from the magnet were obtained. The buoyant force, F_b was computed using Eq (8). The integral in Eq (8) was computed numerically using the field intensities obtained as above.

For simplicity, it was assumed that

$$M_n = \chi H_n \qquad H_n < H_{saturation}$$
$$= M_s \qquad H_n >= H_{saturation}$$
$$M = \chi H \qquad H < H_{saturation}$$
$$= M_s \qquad H >= H_{saturation}$$
$$\chi = M_s / H_{saturation}$$

where H_n is the field intensity normal to the surface, H is the magnitude of field intensity, $H_{saturation}$ is the field intensity beyond which the magnetic fluid is saturated, M_s is the saturation magnetization.

From the above computation, magnetic field intensity, H_z and the buoyant force, F_b for different distances, h from the magnet were obtained. Using these values, a functional relationship between F_b and h was obtained. The support stiffness of the float was computed by differentiating F_b with respect to h. These computations were performed for three different widths of the magnet, a_m, namely, 4 mm, 6 mm, and 8 mm and the results are summarized in Figures 6-8.

Figure 6 shows the variation of the magnetic field intensity, H_z with the distance from the magnet, h. It can be seen that the maximum field intensity occurs very close to the magnet. and drops at an exponential rate, with increasing distance from the magnet, resulting in negligible values beyond a distance of about 5 mm. Figure 7 shows the variation of the magnetic buoyant force, F_b with the distance from the magnet, h. It can be seen that the magnetic buoyant force of the float decreases with increasing gap between the magnet and the float for all widths of the magnet. It can also be seen that the magnet assembly with 4 mm wide magnets provides a more rapid increase in force with decreasing gap followed by 6 mm and 8 mm wide magnets respectively. This indicates that the gradients of these curves depend strongly on the width of the magnets. This effect is seen more clearly in Figure 8, which shows the variation of support stiffness of the float (i.e. the gradient of the F_b - h curve) with F_b. The support stiffness of the float is seen to increase linearly with the buoyant force of the float. It is clear from this figure that smaller widths of the magnet can provide larger support stiffness of the float. It can also be seen from

these results that different support stiffness values of the float can be obtained at the same buoyant force by changing the width of the magnets.

EXPERIMENTAL RESULTS

Figure 9 shows the magnetic field intensity, H_z above the center of a magnet as a function of the distance from the magnet, h. On comparing this with Figure 6, it can be seen that the experimental values appear to be consistently higher than the analytical values. Two possibilities exist for the discrepancy : i. The simulation gives values *at a point* while the Hall effect sensor measures values *over a finite area*, ii. Cross sensitivity can be a problem with Hall effect sensor and one may not be measuring exactly the z-component. If the assumptions made in the calculation of the magnetic field intensity are appropriate then the analytical values would be more reliable than the experimental values.

Figure 10 shows the magnetic buoyant force, F_b as a function of the distance from the magnet, h and Figure 11 shows the relationship between support stiffness of the float and buoyant force, F_b for different widths of the magnet, a_m. The supporting stiffness of the float was calculated from the gradient of the curves in Figure 10. On comparing the analytical results obtained using ANSYS (Figure 7) with the experimental results (Figure 10), a good agreement in the values of buoyant force can be seen when the distance of the float from the magnet is larger than 0.5 mm. At distances larger than 0.5 mm, the larger width of the magnet gives higher force. However, at distances smaller than 0.5 mm, the effect is reversed and smaller widths of the magnet gives larger force. In this region, the experimental values are much larger than the theoretically computed values. Very large magnetic field intensities (much larger than required to cause saturation of the magnetic fluid) are present close to the surface of the magnet. This causes the magnetic fluid to break down and agglomerate. Higher forces result when the float is pressed down on the agglomerates. However, the theoretical analysis assumes that the magnetic fluid is homogeneous at all values of field intensity, and hence, leads to lower values of forces. It can be seen from Figure 10 that the agglomeration appears to be more pronounced in the case of smaller widths of magnet. A similar effect can be observed by comparing Figures 8 and 11. The theoretical computation and experimental estimation of the supporting stiffness of the float are in good agreement for values of buoyant force less than about 12 N. This is about the same region where the agglomeration of magnetic fluid begins.

Agglomeration and breakdown of magnetic fluid is an undesirable effect, which leads to lower life of the fluid. Our experience is that the breakdown occurs after prolonged exposure to high intensity magnetic field. Also, the breakdown (when it occurs) is localized to regions of high intensity. Fe_3O_4 particles agglomerate after breakdown and occupy the regions of high field. and

prevents more fluid from being exposed to high field. The possibility of breakdown was identified in the present study. However, no attempt was made to model this phenomenon because any such analysis would be complex and would need to consider factors such as mechanism of breakdown and constitution of the magnetic fluid. As any breakdown is undesirable we have incorporated a 1 mm aluminium sheet on top of the magnets which would shield the fluid from exposure to high field intensities. Further it is desirable to determine the onset and amount of agglomeration and produce designs which will eliminate or reduce this effect without compromising on the force or stiffness. Work is currently in progress to address this issue.

From the above discussion it is clear that the theoretical analysis is capable of reproducing results of sufficient accuracy to the experimental, except under very severe magnetic field conditions which can cause breakdown of the fluid. Thus, the theoretical analysis can be a valuable design tool to analyze various design alternatives to optimize force and stiffness. The close agreement between the theoretical and experimental results allows one to optimize the design parameters analytically before building the equipment and testing. This will result in considerable savings in time, cost , and efforts needed in building the equipment and testing.

DESIGN CONSIDERATIONS

In the magnetic float polishing technique, an important consideration in the design of the apparatus is the design of magnetic field itself, namely, the magnetic field intensity and magnetic field gradient. This will govern both the buoyant force and the support stiffness of the float which in turn will control the static and dynamic grinding loads per ball. We believe these parameters are directly related to the removal rate and the finish obtainable.

Consider the arrangement shown in Figure 3 where the magnets are located with alternate N and S poles. With this type of magnetic circuit, magnetic intensity and magnetic gradient can be pre-selected by choosing different magnetic materials (i.e. different residual magnetic flux density) and of different sizes. The width of the magnetic pole a_m can change the magnetic buoyant force of the float especially for a given support stiffness of the float as shown in Figure 11 [16]. Preliminary experimental results indicate that the removal rate, sphericity, and surface roughness are influenced by the buoyant force and the supporting stiffness of the float. However, these experimental results are inadequate to develop the overall design methodology. The effect of the supporting stiffness of the float on the finish obtainable should be established by surface roughness analysis of the finished balls.

Thus, some of the principles for optimum design of the equipment for the magnetic field assisted polishing are established. Based on the optimal design of the equipment, optimum

41

operating conditions need to be established for polishing different materials (magnetic and non-magnetic) and different geometries (internal and external).

DISCUSSION

In the magnetic float polishing, the polishing characteristics, such as removal rate, sphericity, and surface roughness appear to depend on the relative sliding speed and rolling speed at the three contact points, namely, between the balls and the top plate, bottom float, and the side of the float vessel respectively. However, the relative contributions of each of these areas to the removal rate and finish are not known. Figure 12 shows various velocity and geometric components of the float polishing apparatus after Childs et al [17]. Below a certain drive shaft speed Ω_s, ball circulation speed Ω_b would be proportional to Ω_s. Above that critical value of Ω_s, skidding between drive shaft and balls would occur gradually. The ball circulation speed can be measured using the apparatus shown schematically in Figure 13. The polishing chamber is similar to one shown in Figure 1(a). A hole is drilled in to the side of the guide ring and a pin passed though it, such that it will contact the urethane rubber on the outside at the same height as the balls. As the balls move around the guide ring, the pin is moved back and forth. The pin is linked to a leaf spring, whose vibrations are measured by the use of a suitable transducer such as strain gages or a LVDT. The vibrational frequency of the leaf spring is proportional to the ball circulation speed. Ball circulation speed can also be calculated by making suitable assumptions for the friction coefficient at different interfaces and fluid drag on the ball. The relationship between ball circulation speed, Ω_b and drive shaft speed, Ω_s is shown in Figure 14. These results were measured experimentally while polishing a batch of fourteen 12.7 mm balls. The sliding speed, V_s between drive shaft and balls can be defined as the relative speed of the balls and the drive shaft. Direct measurement of sliding and rolling speeds is rather difficult. Instead, sliding speed V_s can be calculated using the following equation [17] based on the ball circulation speed, Ω_b.

$$\frac{V_s}{R_s\Omega_s} = 1 - \frac{R_f}{R_s}\frac{\Omega_b}{\Omega_s}(1 + \cos\theta + \sin\theta) + \frac{R_f}{R_s}\frac{\Omega_f}{\Omega_s}\cos\theta \qquad (9)$$

where R_s and R_f are the radius of contact point between the ball and the drive shaft, and between the ball and the float, respectively; Ω_s is the drive shaft speed; Ω_b is the ball circulation speed; Ω_f is the float rotational speed, and θ is the chamfered angle of the drive shaft.

Assuming a suitable value for the ratio Ω_f / Ω_s, the sliding speed, V_s can be calculated by substituting the values of Ω_s, R_s, R_f, θ, and Ω_b. In Figure 15, the relationship between sliding speed, V_s and drive shaft speed, Ω_s is shown for the ball circulation data plotted in Figure 14.

Using the above method for the estimation of sliding speed, the effect of sliding speed on polishing characteristics can be established experimentally.

In order to determine the effect of rolling speed on polishing characteristics, estimation of the rolling speed between the balls and the drive shaft is needed. Rolling velocity can be measured by the same method as that of sliding speed mentioned earlier. The rolling speed can be calculated using the following equation [17]:

$$V_R = R_s \Omega_s - \frac{R_f \Omega_b + V_s}{2} \tag{10}$$

The rolling speed V_R can similarly be calculated by substituting the values of Ω_s, R_s, R_f, θ, Ω_b, and V_s. Using the above method for the estimation of rolling speed, the effect of rolling speed on polishing characteristics can be determined experimentally.

From these results, optimum operating conditions, such as sliding and rolling conditions can be established for obtaining high removal rate, small sphericity and high surface finish. Such a relationship between operating conditions and polishing characteristics will enable one to develop optimum operating conditions maps for magnetic field assisted polishing as shown schematically in Figure 16. At low shaft speeds the frictional forces are sufficient to ensure the rolling motion of the balls. Under such conditions the material removal occurs by micro-slip. This ensures uniform removal of material from all points on the ball surface leading to good sphericity. However, the balls rolling over the abrasive could lead to micro-fracture and hence higher surface roughness. With increase in shaft speed the slippage between the ball and the shaft increases. This ensures higher removal rate. The surface roughness would be smaller as the removal occurs by abrasion rather than micro-fracture. However, too large a slippage implies insufficient rotation of the ball and the material will be removed at isolated spots leading to an increase in sphericity. However, there exists a optimum point where the transition from rolling to rolling-sliding (micro-sliding to macro-sliding) occurs. At this point the material removal rate can be maintained at high level without compromising on finish and sphericity. Such optimum operating conditions can be obtained by making use of the Eqs.(9) and (10). Also, the dimension of some parts of the apparatus, such as R_s and R_f, and contact geometry θ can be determined from the design process.

CONCLUDING REMARKS

Currently, the design of equipment for magnetic float polishing is arrived empirically by experimental trial and error which is a costly and time consuming approach. Need arises for the development of a design methodology based on first principles. Also, if analytical techniques can

be developed that can facilitate the design and optimization of the equipment without actually constructing different versions of the apparatus, it would result in significant savings in time and cost. Also for continued application of advanced ceramics for structural application, it is necessary to develop a cost effective and efficient finishing technology that finishes the surface with minimal defects. The analytical work reported here enables the machine tool builders to develop new designs for various applications. Many manufacturers are looking for alternate finishing technology to improve quality and reduce costs. The magnetic float polishing addresses this issue and some of the principles developed are expected to provide the knowledge-base for the design, construction, and optimization of the magnetic field assisted polishing technology.

ACKNOWLEDGMENTS

BIBLIOGRAPHY

1.   Baron, J. M, "Technology of Abrasive Machining in a Magnetic Field," Masino-strojenije, Leningrad (1975) (in Russian).

2.   Konovalov, E. G. and F. J. Sakulevich, "Principles of Electro-Ferromagnetic Machining," Naukaitechnika (1974) (in Russian).

3.   Sakulevich, F. J. and L. M. Kozuro, "Magneto-Abrasive Machining," Naukaitechnika, Minsk (1978) (in Russian).

4.   Sakulevich, F. J. and L. M. Kozuro, "Magneto-Abrasive Machining of Fine Parts," Vyssaja Skola, Minsk (1977) (in Russian).

5.   Konovalov, E. G. and G. S. Sulev, "Finishing Machining of part by Ferromagnetic Powder in Magnetic Field," Naukaitechnika (1967) (in Russian)

6.   Makedonski,. B. G. and A. D. Kotshemidov, "Schleifen im Magnetfeld," Fertigungs-technik und Betrieb, 24, H.4 (1974) 230 - 235

7.   Kato,K, " Tribology of Ceramics. ", Wear, 136 (1990)117-133.

8.   Umehara, N. and K. Kato, " Principles of Magnetic Fluid Grinding of Ceramic Balls," Int. J. of Applied Electromagnetics in Materials, 1, (1990) 37-43.

9.   Umehara, N and K. Kato, " A Study on Magnetic Fluid Grinding (1st Report), The Effect of the Floating Pad on Removal Rate of Si_3N_4 Balls," J. of Japan Society of Mechanical Engineers, 54, 503, (1988)1599-1604. (in Japanese)

10. Umehara, N. and K. Kato, "Hydro-Magnetic Grinding Properties of Magnetic Fluid Containing Grains at High Speeds," J. of Magnetism and Magnetic Materials, 65 (1987) 397-400

11. Takazawa, K., Shinmura, and E. Hatano, "Development of Magnetic Abrasive Finishing and Its Equipment," MR 83-678. Proc. of the SME'S 12th Deburring and Surface Conditioning Conference, Orlando , Nov 8-10, 1983

12. Takazawa, K., Shinmura, and E. Hatano, "Advanced Development of Magnetic Abrasive Finishing and Its Equipment,"Proc. of the SME'S Deburring and Surface Conditioning Conference '85, Orlando , (Sept 23-26, 1985) 30-46

13. Shinmura, T., Takazawa, K., and E. Hatano, "Study of Magnetic Abrasive Finishing," Annals of CIRP, 39/1 (1990) 325-328

14. Shinmura, T., Yamaguchi, H. and T. Aizawa, "A New Internal Finishing Process for Non-Ferromagnetic Tubing by the Application of a Magnetic Field - The Development of a Unit Type Finishing Apparatus Using Permanent Magnets," (1993)

15. Childs, T.H.C.and H. J. Yoon, "Magnetic Fluid Grinding Cell Design," Annals of CIRP, 41/1 (1993) 343-346

16. Umehara, N., Kato,K. and M. Takekoshi, " The Effect of Supporting Stiffness of a Float on Finishing Characteristics," to be published in the Proc.of the Annual Meeting of the Magnetic Fluid Research Society (1993) (in Japanese)

17. Childs,T.H.C., Mahmood,S and H.J. Yoon, "The Material Removal Mechanism in Magnetic Fluid Grinding of Ceramic Ball Bearings," Proc.of I. Mech. E. , 208, No. B1 (1994) 47--59

18. Childs, T.H.C., Jones, D.A., Mahmood, S., Kato, K., Zhang,B.,and N. Umehara,"Magnetic Fluid Grinding Mechanics," Wear, 175 (1994) 189-198

19. Rosensweig, R. E,"Ferrohydrodynamics," Cambridge University Press, Cambridge, U.K. (1985)

Figure 1 (a) Schematic and a photograph of the Magnetic Float Polishing Apparatus
    & (b)   Showing Permanent Magnets Located at the Base of the Apparatus.

Figure 2   Magnetization (M-H) Curve for the Magnetic Fluid

Figure 3   Schematic Diagram of the Experimental Apparatus used for Measuring the Magnetic Buoyant Force

Figure 4   Variation of the Magnetic Buoyant Force on the Float With the Distance From the Magnet, h (ANSYS Simulation, FEM) And Finite Difference (FD) Method

Figure 5   Contour Map of the Magnetic Field Density on the Surface and Inside the Magnets by ANSYS Simulation

Figure 6   Variation of the Magnetic Field Intensity, H_z with the Distance from the Magnet, h (ANSYS Simulation) a_m = width of magnet

Figure 7   Variation of the Buoyant Force on the Float, F_b with the Gap between the Magnet and the Float, h (ANSYS Simulation)
    a_m = width of magnet

Figure 8   Variation of Stiffness of the Float with Buoyant Force on the Float, F_b (ANSYS Simulation) a_m = width of magnet

Figure 9   Variation of the Magnetic Field Intensity, H_z with the Distance from the Magnet, h (Experimental Results) a_m = width of magnet

Figure 10   Variation of the Buoyant Force on the Float, F_b with the Gap between the Magnet and the Float, h (Experimental Results)
    a_m = width of magnet

Figure 11   Variation of Stiffness of the Float with Buoyant Force on the Float, F_b (Experimental Results) a_m = width of magnet

Figure 12   Schematic showing the Velocity and Geometric Components of the Float Polishing Apparatus [17]

Figure 13   Apparatus for Measuring the Ball Circulation Speed

Figure 14   Variation of Ball Circulation Speed, Ω_b with Drive Shaft Speed, Ω_s

Figure 15   Variation Between Sliding Speed, V_s with Drive Shaft Speed, Ω_s

Figure 16   Schematic of a Typical Optimum Operating Conditions Map

DRIVE SHAFT
ACRYLIC GUIDE RING
MAGNETIC FLUID AND ABRASIVES
URETHANE RUBBER
CERAMIC BALLS
ACRYLIC FLOAT
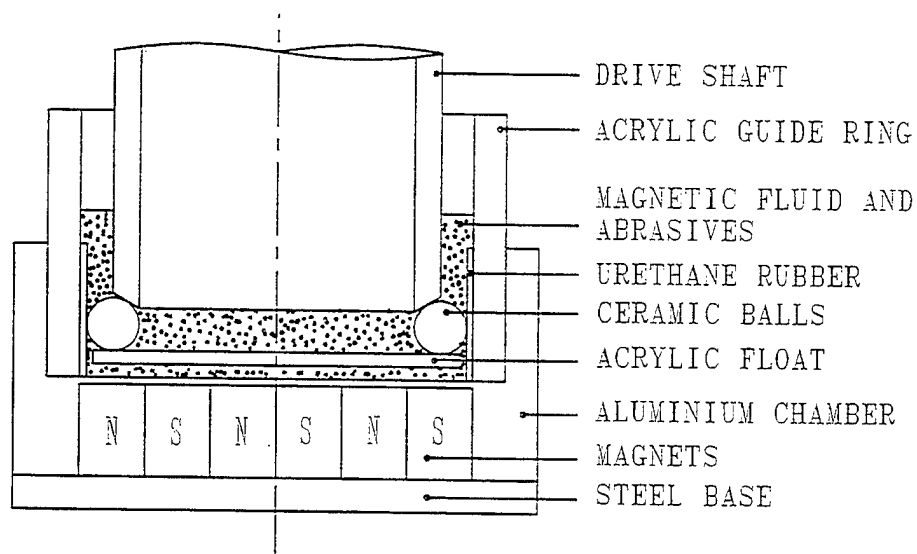ALUMINIUM CHAMBER
MAGNETS
STEEL BASE

N S N S N S

Figure 1 (a)   Schematic of the magnetic float polishing apparatus showing the permanent magnets at the base.
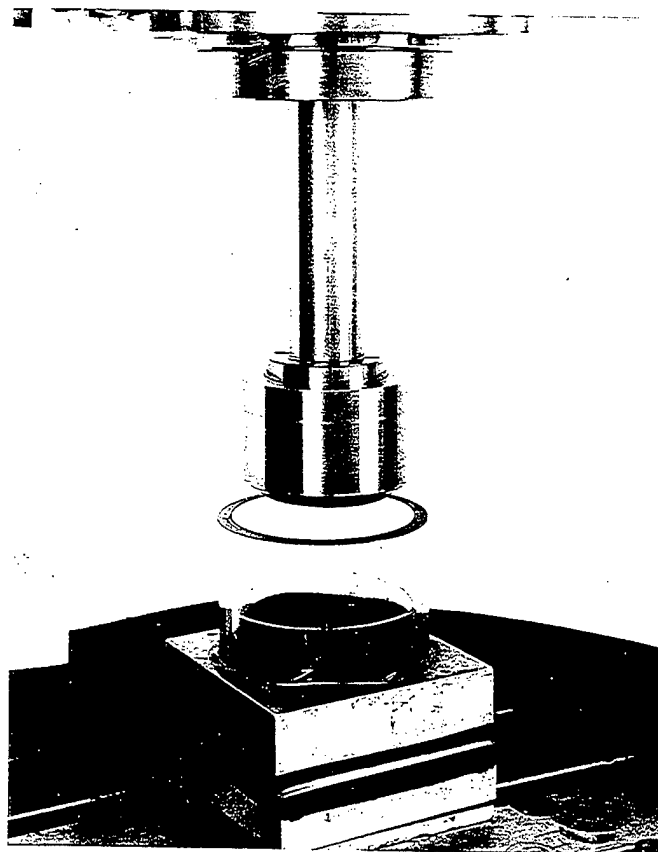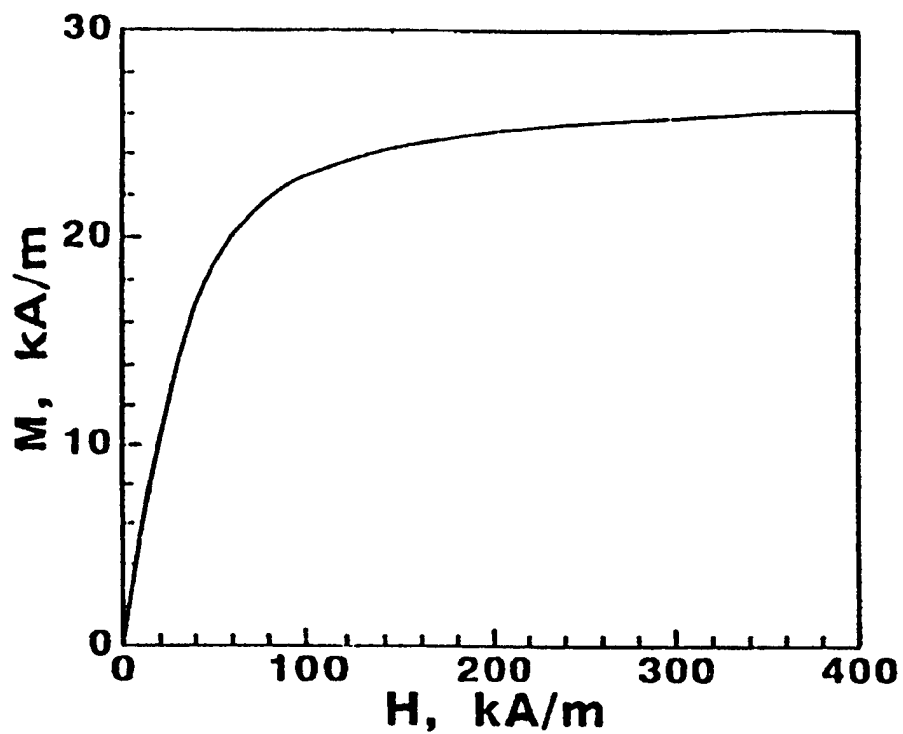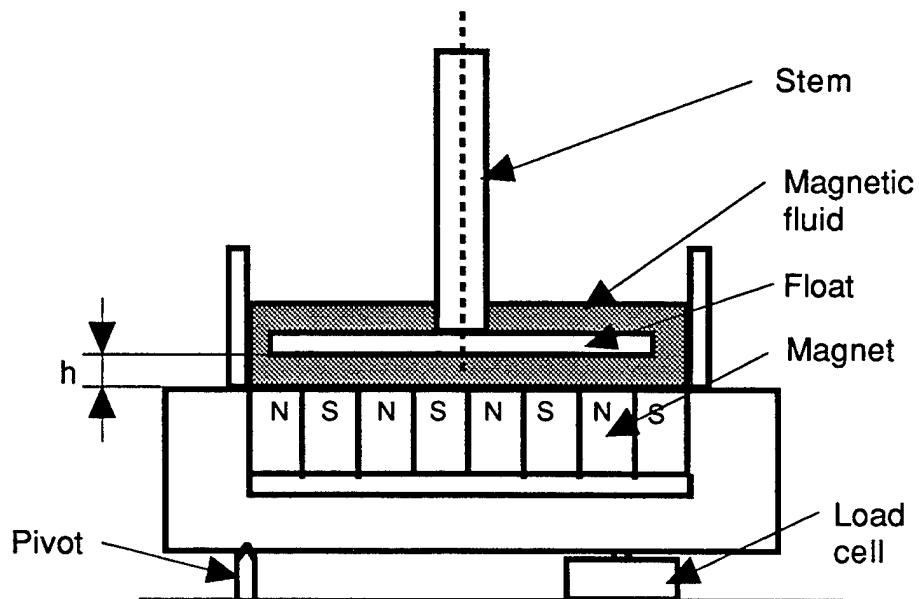

Figure 1 (b)   Photograph of the magnetic float polishing apparatus

Figure 2   Magnetization (M-H) Curve for the Magnetic Fluid

Figure 3   Schematic Diagram of the Experimental Apparatus used for
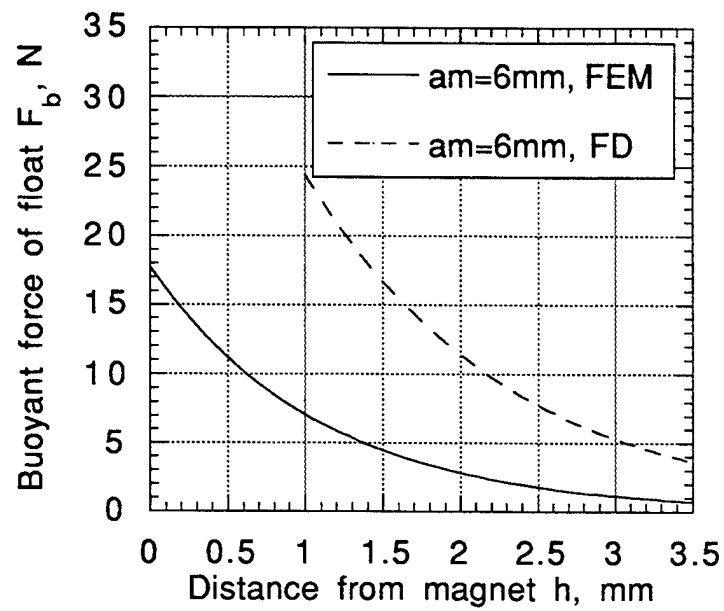Measuring the Magnetic Buoyant Force

Figure 4   Variation of the Magnetic Buoyant Force on the Float With the
Distance From the Magnet, h (ANSYS Simulation, FEM) And Finite
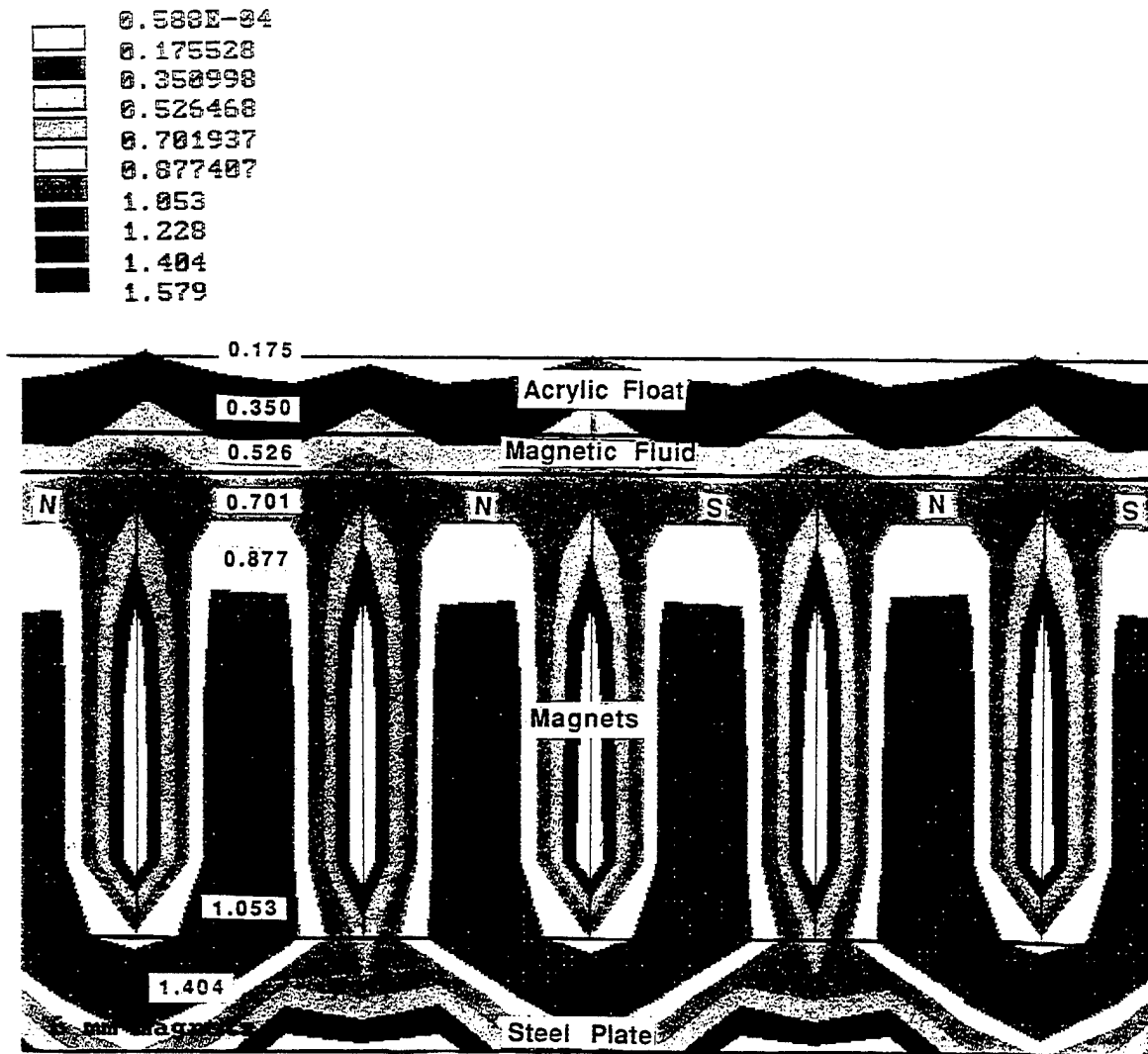Difference (FD) Method

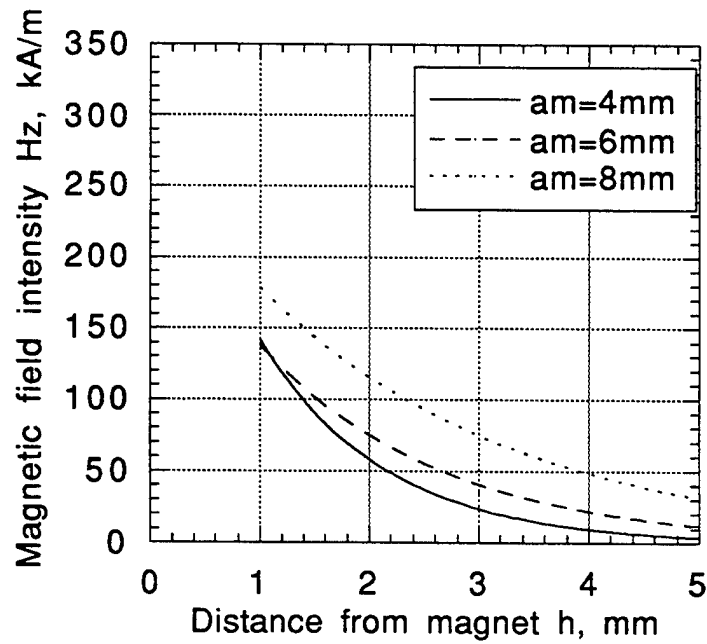Figure 5   Contour Map of the Magnetic Field Density on the Surface and Inside the Magnets by ANSYS Simulation

Figure 6   Variation of the Magnetic Field Intensity, H_z with the Distance from the Magnet, h (ANSYS Simulation) a_m = width of magnet
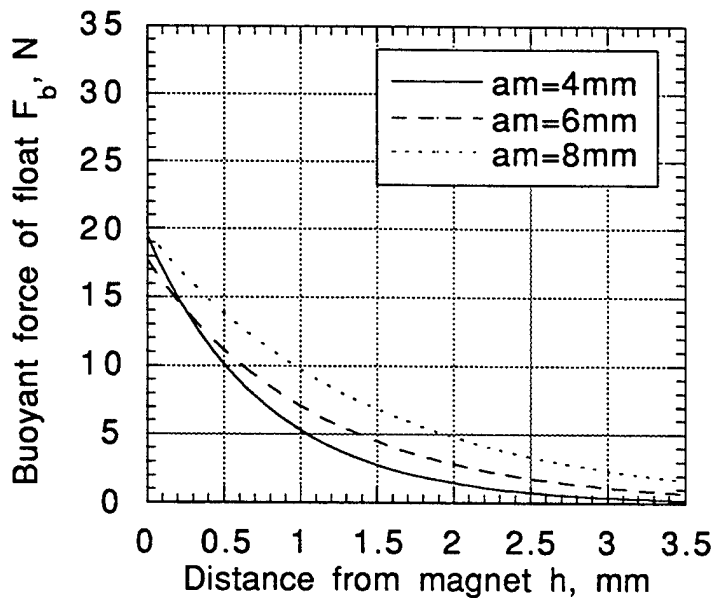

Figure 7   Variation of the Buoyant Force on the Float, F_b with the Gap between the Magnet and the Float, h (ANSYS Simulation) a_m = width of magnet
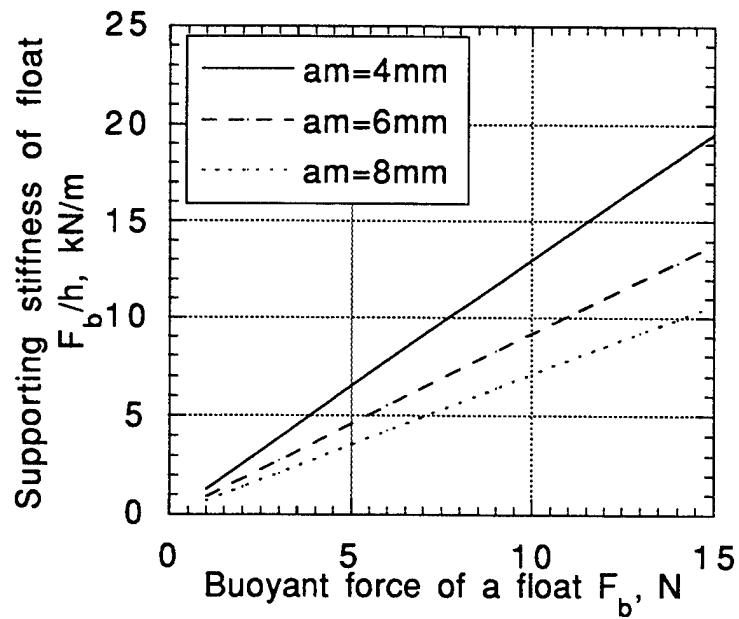
Figure 8   Variation of Stiffness of the Float with Buoyant Force on the Float, F_b
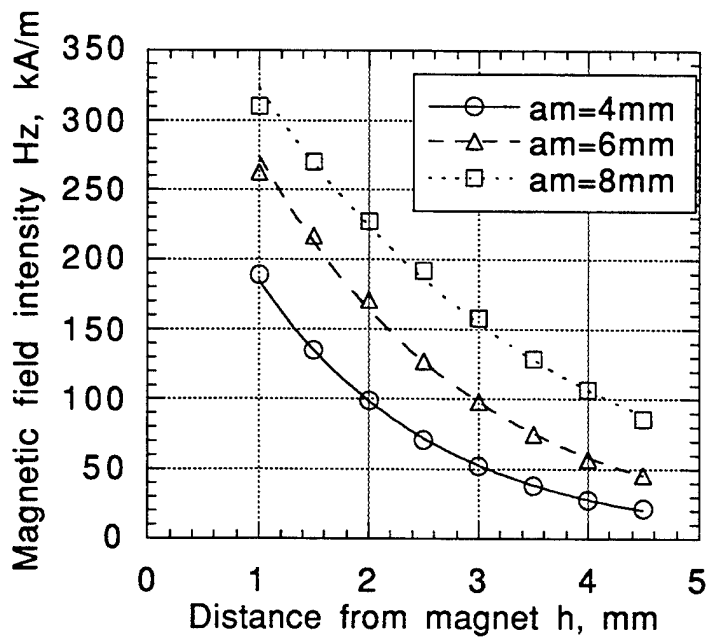(ANSYS Simulation) a_m = width of magnet

Figure 9   Variation of the Magnetic Field Intensity, H_z with the Distance from
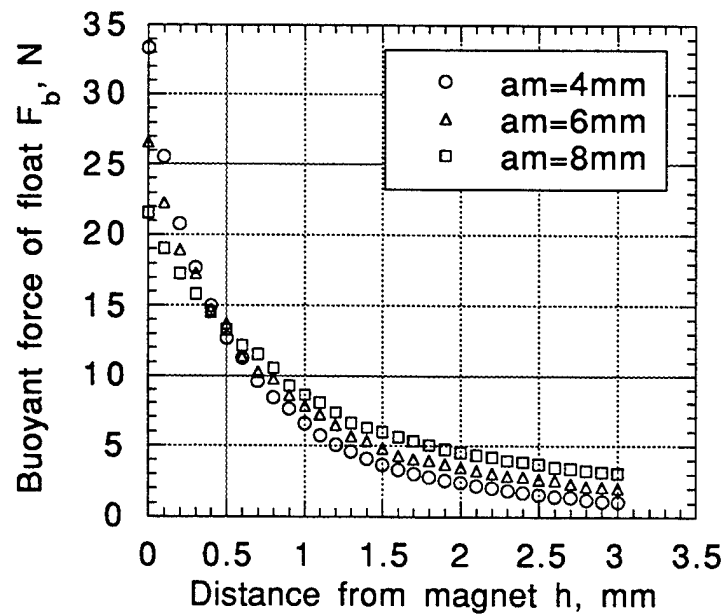the Magnet, h (Experimental Results) a_m = width of magnet

Figure 10 Variation of the Buoyant Force on the Float, F_b with the Gap between the Magnet and the Float, h (Experimental Results) a_m = width of magnet

Figure 11 Variation of Stiffness of the Float with Buoyant Force on the Float, F_b (Experimental Results) a_m = width of magnet

Figure 14   Variation of Ball Circulation Speed, Ω_b with Drive Shaft Speed, Ω_s
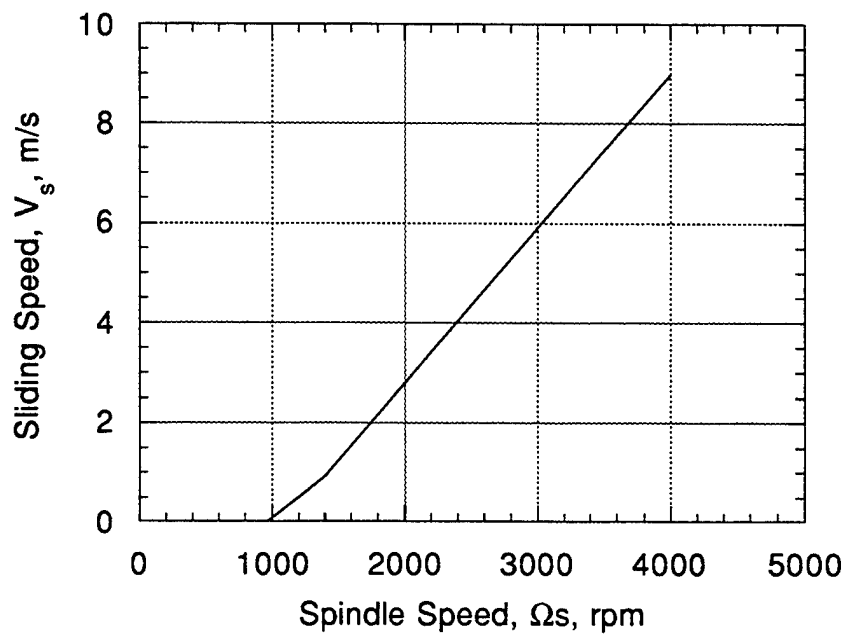
Figure 15   Variation Between Sliding Speed, V_s with Drive Shaft Speed, Ω_s

Figure 12 Schematic showing the Velocity and Geometric Components of the
Float Polishing Apparatus [17]

Figure 13 Apparatus for Measuring the Ball Circulation Speed

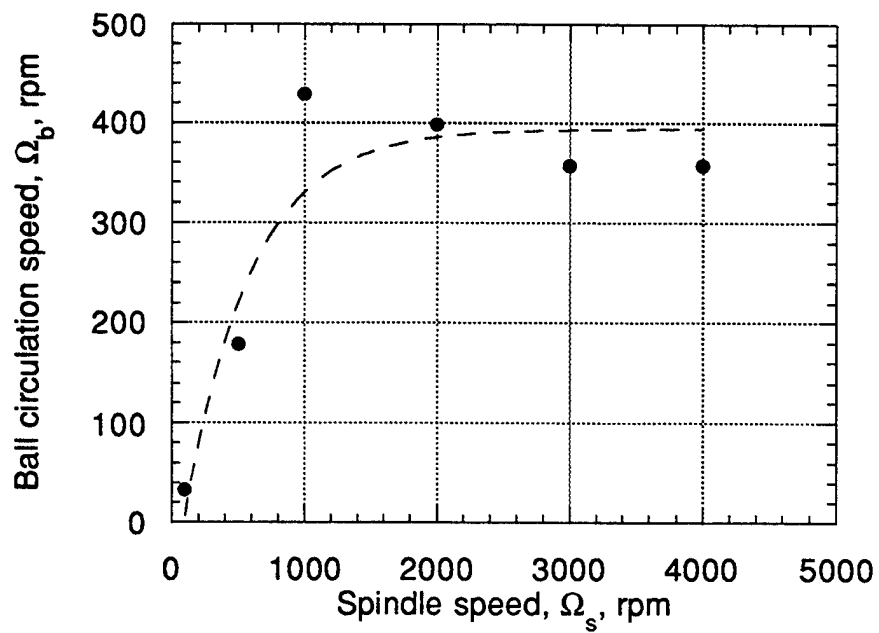| Large Surface Roughness		Moderate Surface Roughness	Small Surface Roughness	
Small Sphericity			Moderate Sphericity	No-Ball-Shape
Small Removal Rate	Moderate Removal Rate		High Removal Rate	Small Removal Rate
Micro-Sliding		Macro-Sliding		
Rolling		Rolling-Sliding		Sliding

Driving Shaft Speed Ω_s
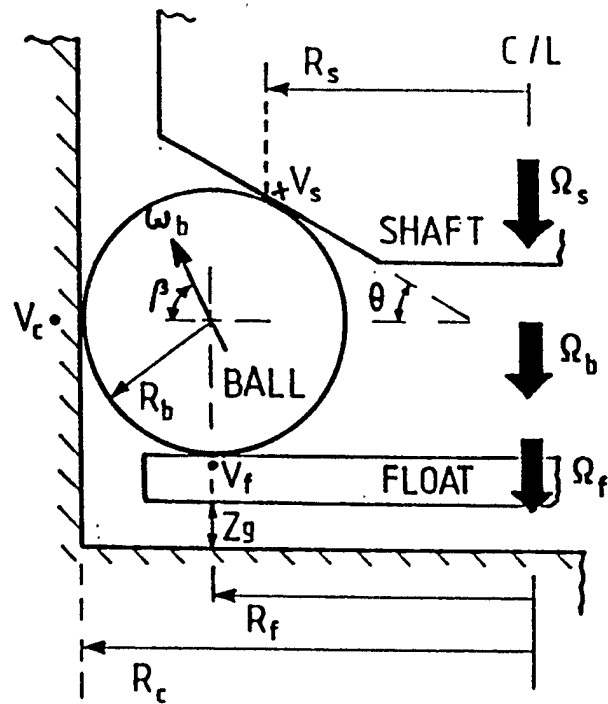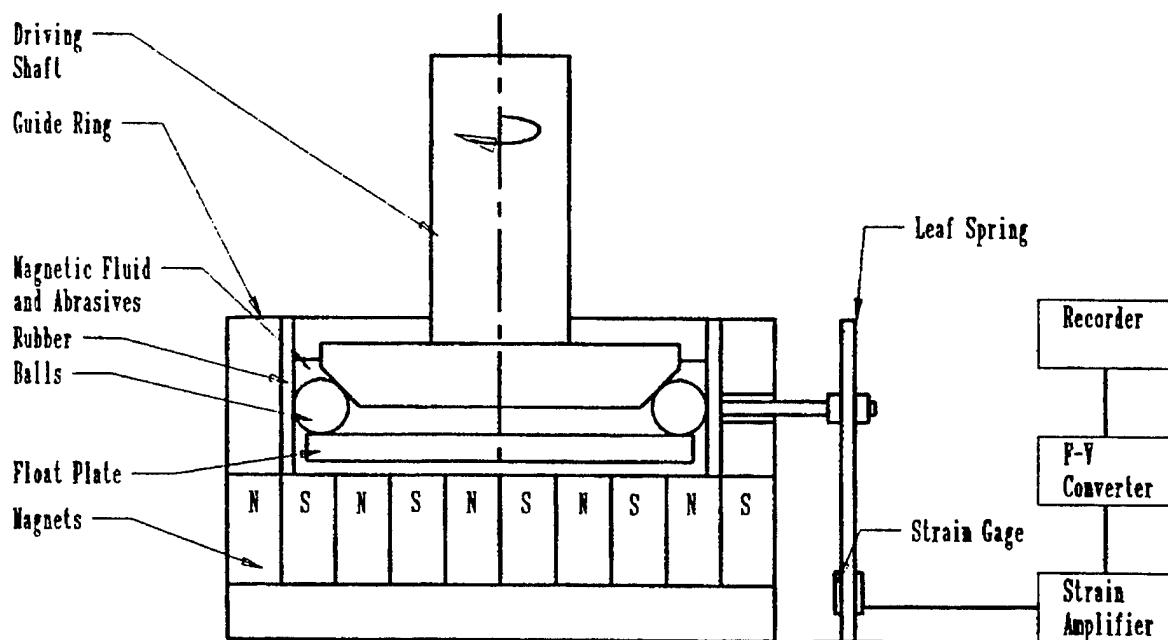
Ball Circulation Speed Ω_b

Figure 16   Schematic of a Typical Optimum Operating Conditions Map

APPENDIX C

MAGNETIC FLUID GRINDING - A NEW TECHNIQUE FOR

FINISHING ADVANCED CERAMICS

N. Umehara

Magnetic Fluid Grinding – a New Technique for Finishing Advanced Ceramics

N. Umehara, Oklahoma State University, Stillwater, OK, USA – Submitted by S. Kalpakjian (1)
Received on January 12, 1994

SUMMARY :

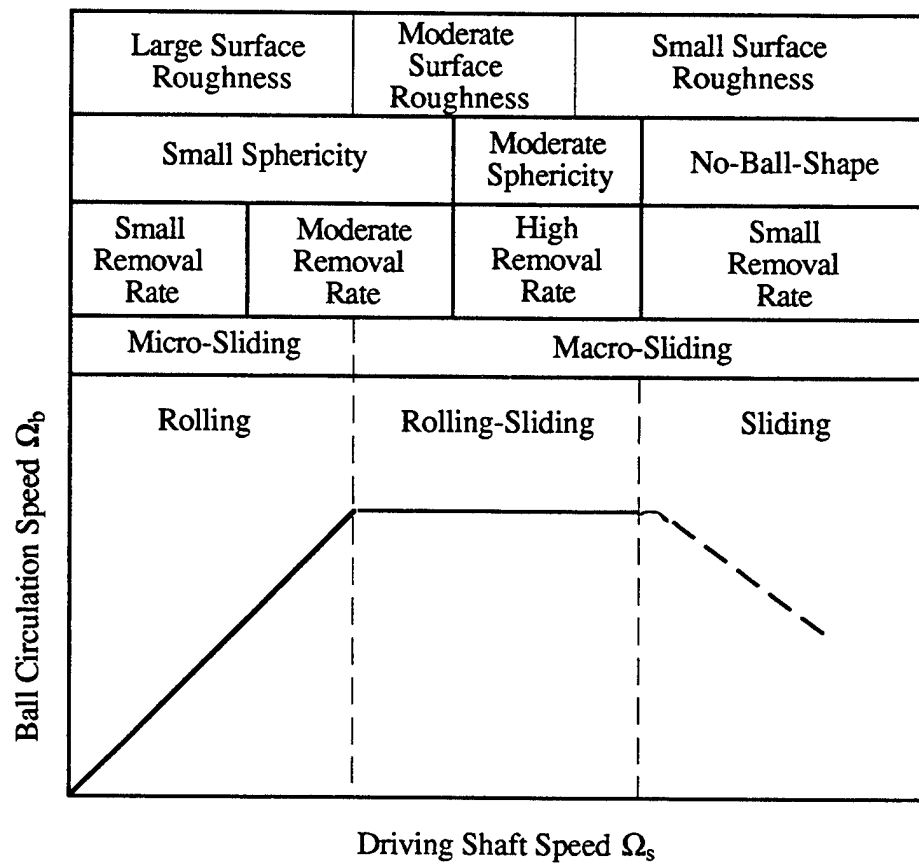Most advanced ceramics are finished by conventional grinding followed by polishing. However, due to the brittle nature of these materials, the grinding process introduces surface defects, such as cracks which can significantly reduce the strength and reliability of the parts in service. Also expensive diamond abrasives and long polishing times add significantly to the cost of manufacture.

To address these concerns, a new polishing technique, known as magnetic fluid grinding, was developed that uses controlled low level force during polishing. The process is found to produce more accurate surfaces at significantly less time than conventional polishing. The paper presents the principles of this technique, design of magnetic fluid grinding cell, salient features of the process, and results of finishing balls, rollers, and plates using this technique.

Key words: Polishing , Ceramics, Ferromagnetic materials

1. Introduction

In traditional mechanical surface finishing operations, such as grinding, lapping, honing, polishing, or buffing a shaped solid tool such as a grinding wheel, a lapping plate or a hone is used. These solid tools are pressed mechanically by a screw, oil pressure or spring against the workpiece. However, when grinding advanced ceramics which are brittle, these processes introduce surface defects such as cracks which can significantly reduce the strength and reliability of the parts in service. To overcome these problems and against these traditional finishing methods, magnetic field assisted finishing process was developed. This new finishing method can be classified to two types. The first one is magnetic abrasive finishing which uses a brush of magnetic abrasives for finishing [1]. The polishing characteristics of the magnetic abrasive brush can be altered by varying the magnetic field. The second type, termed, magnetic fluid grinding uses magnetic fluid which is a colloidal suspension of subdomain magnetic particles in a liquid carrier [2]. Magnetic fluid grinding can also be expected to produce salient finishing properties of advanced ceramics by optimum combination of magnetic fluid, abrasive grains, and magnetic field.

Application of magnetic fluid to surface finishing has been investigated originally by Imanaka et al. [3], followed by Tani et al. [4]. They used magnetic buoyant force of abrasive grains in a magnetic fluid as the grinding force. However, the magnetic buoyant force of abrasive grains was too low to give effective removal rate, and shape accuracy was poorly controlled.

To overcome these problems, a special element named 'float' was introduced by Umehara and Kato [5] to increase the grinding force and improve the shape accuracy. As a result, the combination of magnetic fluid, a float, abrasive grains, and magnetic field showed to form a new practical grinding method named "Magnetic Fluid Grinding."

This magnetic fluid grinding has been shown to be effective in grinding of ceramic balls [5], a metal cylinder end, a ceramic cylinder, ceramic rollers [6], ceramic plates [7] and a metal pipe.

In the following sections, the principle of the magnetic fluid grinding, design of the grinding apparatus for obtaining optimum grinding conditions, and several examples of application of this method for finishing advanced ceramics are presented.

2. Principle of Magnetic Fluid Grinding

The starting point of the development of the magnetic fluid grinding process is the theory of ferrohydrodynamics developed by Rosensweig [8]. According to this theory, a buoyant force F_b acts on a non-magnetic body immersed in a magnetic fluid and subjected to a magnetic field as shown in Fig.1.

According to this principle, non-magnetic abrasive grains can be dispersed at a certain position in a magnetic fluid under specially designed magnetic field. Figure 2 shows an example where abrasive grains are floated at a certain height.

If a workpiece is submerged and rotated in the layer of abrasive grains as shown in Fig.3(a), the surface is ground by free abrasive grains. But the removal rate is found to be very low [3,4] since the total buoyant force of abrasive grains is too small to accomplish large removal rates.

If a float is introduced to this system as shown in Fig.3(b), larger grinding pressure can be produced since large buoyant force near the magnet pole surface is transmitted to the grinding surface of a workpiece.

Figure 4 shows an example of grinding pressure P as a function of distance h of abrasive grain layer or a float from magnet. Solid lines in this figure show the theoretical values of grinding pressure calculated using the following equation developed by Rosensweig [8],

$$F_b = -\iint_s \left(\mu_0 \frac{Mn^2}{2} + \int_0^H M dH \right) n \cdot dS \qquad (1)$$

where F_b is buoyant force of the non-magnetic body, 's' area of non-magnetic body, μ_0 permeability of free space, 'M' magnetization of magnetic fluid, 'M_n' normal component of M to non-magnetic body, 'H' the strength of magnetic field, and 'n' normal unit vector to non-magnetic body.
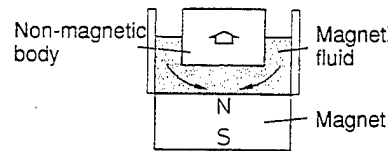

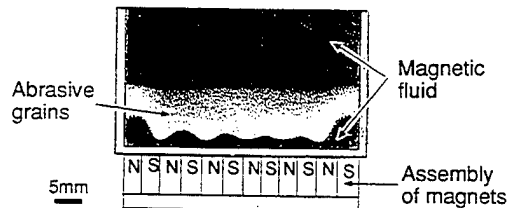Fig.1 Buoyant force acting on a non-magnetic body in magnetic fluid with magnetic field

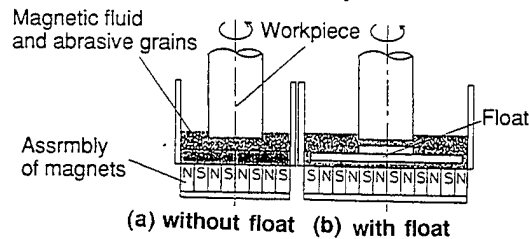Fig.2 Floating of abrasive grains in a magnetic fluid under the action of a magnetic field

(a) without float (b) with float

Fig.3 The principle of magnetic fluid grinding with and without a float
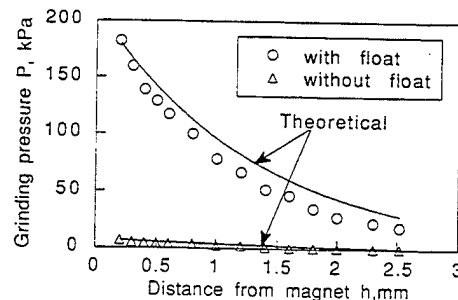
Fig.4 Grinding pressure P as a function of distances 'h' of floating abrasive grain layer and a float from magnet

The lower theoretical and experimental values show the grinding pressure caused by abrasive grains only and the higher values show the pressure caused by abrasive grains and a float. The float has a square shape (38mm×20mm) and its thickness is 1mm. It has a step of 1mm thickness and a contact area of 30mm² with the workpiece. The volume concentration of abrasive grains is 30vol%. Magnet is SmCo₅ whose residual flux density is 0.75 T. A water-based magnetic fluid whose saturated magnetization was 0.4 T at 637kA/m was used.

From Figure 4, it is clear that the estimated grinding pressure agrees reasonably well with the measured grinding pressure. Also, the grinding pressure with a float at h=1mm is 20 times larger than that without a float. It is obvious from these results that a float can easily produce large grinding pressure.

The contact stiffness, which is defined as the grinding load divided by

58

the elastic displacement of the contact surface, can be calculated from Fig.4 to be 3.5x10³N/m at h=0.6mm. In contrast, the contact stiffness of a standard grinding wheel of 5mm width and polyurethane polisher of 1mm thickness are 5-50x10⁶N/m [9] and 9-12x10³N/m, respectively. These results show that the contact stiffness in magnetic fluid grinding is smaller than that of the grinding wheel or the polyurethane polisher. Therefore, it is considered that such low contact stiffness in loading with a float can prevent the workpiece surface from severe damage or generation of cracks in finishing of ceramics.

The salient features of magnetic fluid grinding are the following.

(1) Vibration and impact that are produced between the workpiece and the tool at high grinding speeds can be reduced by the float which is flexibly supported by the magnetic fluid. So, the system can operate at high speeds (more than 10,000rpm) for accomplishing high removal rates.
(2) If the workpiece is placed in the floating abrasive grain layer, abrasive grains in a magnetic fluid can be supplied to the workpiece surface continuously from outside.
(3) Wear of abrasive grains is decreased by the cooling effect of the magnetic fluid. As a result, abrasive grains have longer life.
(4) All sharp edges of abrasive grains have an opportunity to contact with the surface of the workpiece in grinding. Hence, one abrasive grain can work more effectively than that fixed in a standard hard grinding wheel.

3. Design of the apparatus for optimal grinding load, stiffness, and distribution of abrasive grains

3.1 Magnetic field

Childs et al. [10] have calculated magnetic field and magnetic buoyant force of a float using a finite difference method. However, in their method, the physical meaning of each effect of magnetic fluid properties, magnet properties, and geometry of the apparatus on the magnetic field and magnetic buoyant force of a float could not be understood easily. So, in this study, magnetic field and magnetic buoyant force of a float are analyzed theoretically.

In order to obtain a large buoyant force of the float as grinding load, large magnetic field gradient as well as large magnetic field are necessary. Most simple magnetic assembly for satisfying such conditions is the assembly of magnets with opposite polarity in adjacent magnets as shown in Fig.5. In the following, the magnetic field above such a magnet assembly is analyzed. Since ordinary magnetic fluid is a nonconductor, the current density is zero in a magnetic fluid and a potential function ϕ_1 above the magnet exists. Such a potential function above a magnet should satisfy the following Laplace's Equation.

$$\nabla^2 \phi_1 = 0 \qquad (2)$$

Other potential function ϕ_2 should be given in the magnet by the following Laplace's Equation.

$$\nabla^2 \phi_2 = 0 \qquad (3)$$

Trial solutions for each equation may be written as follows;

$$\phi_1 = \left(be^{\frac{\pi}{a}z} + ce^{\frac{-\pi}{a}z} \right) \sin\left(\frac{\pi}{a}x\right) \qquad \phi_2 = \left(de^{\frac{\pi}{a}z} + fe^{\frac{-\pi}{a}z} \right) \sin\left(\frac{\pi}{a}x\right) \qquad (4),(5)$$

where 'a' is width of magnet.

The boundary conditions are given as follows,

1. $z = 0$ $\qquad H_z = \frac{\pi}{2}B_r\sin\left(\frac{\pi}{a}x\right)$ (6.a)
2. $z = +\infty \rightarrow \phi_1 = 0, \qquad z = -\infty \rightarrow \phi_2 = 0$ (6.b), (6.c)
3. $\phi_1 = \phi_2 \; at \; z = 0$ (6.d)
4. $(B_1 - B_2) \bullet n = 0$ (6.e)

where B_r is residual flux density of the magnet.

Using these boundary conditions (6.a)-(6.e), both potential functions can be written as follows :

$$\phi_1 = -\frac{a}{4}B_r e^{-\frac{\pi}{a}z}\sin\left(\frac{\pi}{a}x\right), \qquad \phi_2 = -\frac{a}{4}B_r e^{\frac{\pi}{a}z}\sin\left(\frac{\pi}{a}x\right) \qquad (7),(8)$$

The two components of the magnetic field intensity can be written as follows :

$$H_z = \frac{\partial \phi_1}{\partial z} = \frac{\pi}{4}B_r e^{-\frac{\pi}{a}z}\sin\left(\frac{\pi}{a}x\right), \qquad H_x = \frac{\partial \phi_1}{\partial x} = -\frac{\pi}{4}B_r e^{-\frac{\pi}{a}z}\cos\left(\frac{\pi}{a}x\right) \qquad (9),(10)$$

Measured values using a Hall element and calculated values from Equation (9) above magnet assemblies for 4mm, 6mm and 8mm of magnet width are shown in Fig.6. It is obvious that, when residual flux density B_r of the magnet is 0.75T, the calculated values agree well with experimental values.

3.2 Magnetic buoyant force of a float (Grinding Load)

The magnetic buoyant force F_b of a non-magnetic body can be calculated using Equation (1). Magnetization M of a magnetic fluid can be given by Langevin's function [2]. It means M is nonlinear related to magnetic field. However, in order to calculate F_b analytically, it was assumed that magnetization of the magnetic fluid is constant at the saturated magnetization M_s of the magnetic fluid. This is reasonable since magnetic
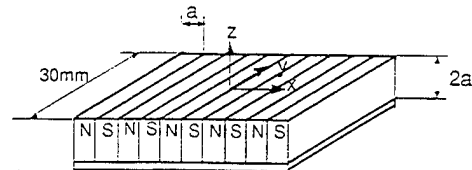
Fig.5 The size and shape of permanent magnet assembly
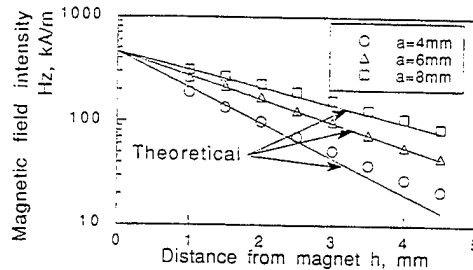
Fig.6 Variations of magnetic field intensity H_z with distance from magnet 'h' as a function of magnet width 'a'
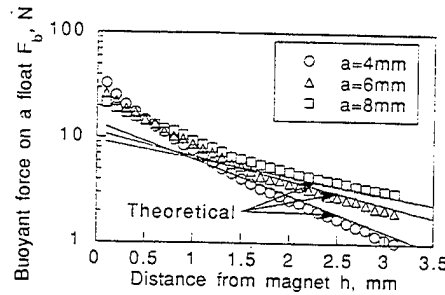
Fig.7 Variation of the magnetic buoyant force of the float with distance from the magnet 'h' as a function of magnet width 'a'
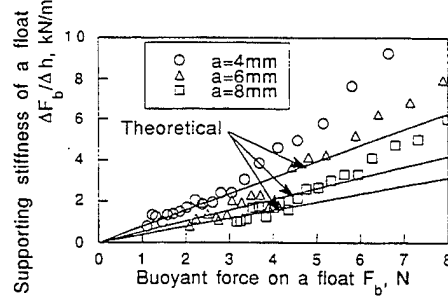
Fig.8 Variation of the supporting stiffness of the float with the magnetic buoyant force of the float as a function of the magnet width 'a'
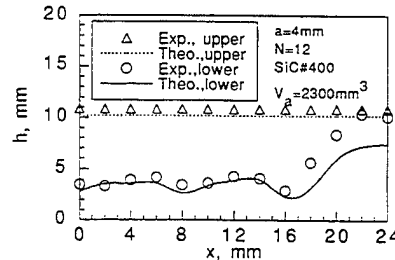
Fig.9 Floating distribution of abrasive grains in a magnetic fluid with a magnetic field

field close to the magnet is sufficiently strong for the saturation of magnetic fluid.

Magnetic buoyant force F_b can be given by the following equations;

$$F_b = -\iint_S (\mu_0 M_s H)n \bullet dS \qquad (11)$$

$$F_b = \mu_0 M_s A\left(\frac{\pi}{4}B_r\right)e^{-\frac{\pi}{a}h}\left(1 - e^{-\frac{\pi}{a}t}\right) \qquad (12)$$

where M_s is saturated magnetization of the magnetic fluid, 'A' area of a float, and 't' thickness of the float

59

From Equation (12), the effect of saturated magnetization M_s of the magnetic fluid, area of the float 'A', residual flux density B_r of the magnet, width of magnets 'a' and thickness of a float 't' on the buoyant force of the float can be found. Equation (12) is very convenient for the design of magnetic fluid grinding apparatus. A comparison between calculated values using Equation (12) and the measured values is shown in Fig.7. It shows the calculated values agree well with the measured values over 1.5mm of distance h. Under 1.5mm of distance h, measured values are larger than calculated values on magnets. Saturated magnetization M_s of magnetic fluid depends on the concentration of the magnetic particles in a magnetic fluid. Under weak magnetic field, the concentration is uniform throughout the magnetic fluid. But, under high magnetic fields, agglomeration of magnetic particles can occur and this should be considered [2]. In this study, the agglomeration of magnetic particles is considered as the reason for the difference between the calculated and measured values in Fig.9 close to the magnet.

3.3 Supporting stiffness of the float (Grinding Stiffness)

Supporting stiffness of a float can be obtained from Equation (12) as follows,

$$\frac{\partial F_b}{\partial h} = \mu_0 M_s A \left(\frac{\pi}{4} B_r \right)\left(-\frac{\pi}{a} \right) e^{-\frac{\pi}{a}h}\left(1 - e^{-\frac{\pi}{a}t} \right) \quad (13)$$

Calculated values from Equation(13) and measured values are shown in Fig.8. This figure shows the proportional relationship between the buoyant force and the supporting stiffness of a float. Also the gradient of the supporting stiffness of the float to buoyant force depends on the magnet width. This means a change in magnet width can result in change only of the supporting stiffness of the float under the same grinding load.

3.4 Floating distribution of abrasive grains

Without the magnetic field, abrasive grains sink to the bottom of the vessel and form an abrasive grain layer. Magnetic field can cause the abrasive grain layer float in a magnetic fluid. In magnetic fluid grinding, whole workpiece or main grinding part of the workpiece should be placed in the floating abrasive grains layer for obtaining optimal grinding conditions. Hence calculation of the height of the floating abrasive grain layer is necessary for design of the apparatus.

To avoid consideration of the internal forces among abrasive grains, abrasive grain layer is treated as a porous block made of abrasive grains. It means that buoyant force of the non-magnetic body, which has the same apparent volume as the floating abrasive grains layer, is calculated. The floating height is determined by the balance between the magnetic buoyant force and the gravity force. The abrasive floating layer is divided into small segments for the calculation of buoyant force corresponding to a magnetic field and position in the x-direction. The height of each segment is calculated using Equation (1). The floating abrasive grain layer is observed in a transparent glass vessel from the side. Calculated and observed heights of lower surface of the floating abrasive layer is shown in Fig.9. Height of the upper surface of the abrasive grain layer is calculated from the condition of constant volume of abrasive grain layer. Figure 9 shows the calculated values agree well with the measured values. This means floating distribution of abrasive grains can be estimated theoretically by this calculation method.

4. Application of magnetic fluid grinding

4.1 Silicon nitride balls

Figure 10 shows a schematic diagram of the grinding apparatus for finishing ceramic balls used for ceramic ball bearing application [5]. Magnetic fluid, float, abrasive grains, as-sintered ceramic balls, and permanent magnets are arranged as shown in Fig.10. A float, abrasive grains, and ceramic balls which are all non-magnetic materials are floated in the magnetic fluid by magnetic buoyant force. Balls are rotated and revolved along the inner wall of the guide ring by the driving shaft, they are ground by the abrasive grains in the magnetic fluid.

The removal rate of the silicon nitride balls (made by pressureless sintering) increases with the grinding load and the rotational speed of the driving shaft. Maximum removal rate of silicon nitride balls was 12.4 μm/min with SiC abrasive grains. This removal rate is about 40 times larger than that by traditional V-groove lapping method. Surface roughness decreased with the decrease in the mean grain size of the abrasive grains. Minimum surface roughness was 0.1 μm R_{max}.

Figure 11 shows the relationship between the sphericity and the grinding time for cases with and without a float. In Fig.11, sphericity is given by the difference between the maximum and the minimum diameters of a ball, and L is the mean grinding load. In the case without a float, sphericity of the balls increase gradually with grinding time. In contrast, the sphericity of a ball with a float decreases rapidly with grinding time and reaches 2 μm after 120 min of grinding. It is clear from this that a float is indispensable for finishing balls by this method [5].

Figures 12 and 13 show the effect of supporting stiffness of a float on ball diameter and sphericity of silicon nitride balls made by hot isostatic pressing, respectively. It can be seen from Figs.12 and 13 that larger stiffness provides higher removal rate and quick decreasing rate of sphericity, and the smaller stiffness provides smaller minimum sphericity. From these results, the importance of the design of supporting stiffness of a
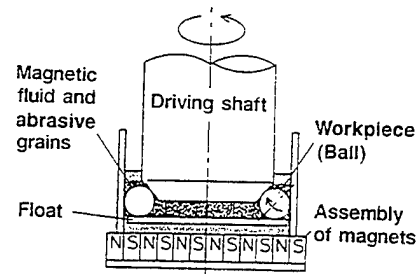
Fig.10 Schematic diagram of the magnetic fluid grinding apparatus for finishing advanced ceramic balls
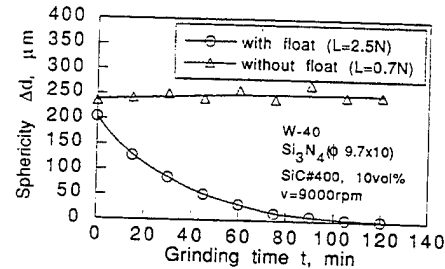
Fig.11 The relationship between grinding time and the sphericity of silicon nitride balls in magnetic fluid grinding with or without a float
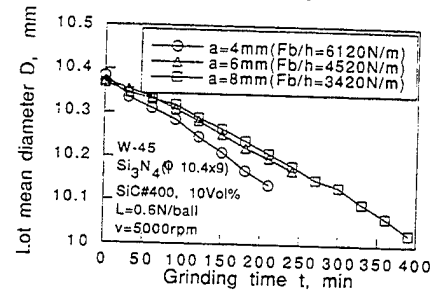
Fig.12 Variation of the lot mean diameter of balls with grinding time as a function of supporting stiffness of the float
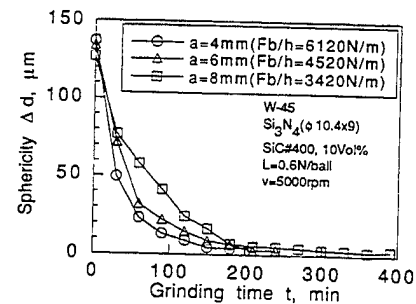
Fig.13 Variation of the mean volume diameter variation of balls with grinding time as a function of supporting stiffness of the float

Table 1 Surface roughness and sphericity of an as-sintered ball and a ground ball of silicon nitride under optimum grinding condition

	As-sintered	Ground
Optical view of Si₃N₄ balls		
Ball diameter	7.7mm	7.1mm
Roughness	10 μm R_{max}	0.1 μm R_{max}
Sphericity	500 μm	0.14 μm
Grinding time : 180min		

float can be realized.

Table 1 shows grinding properties under optimum grinding conditions. The sphericity of the as-sintered balls was reduced from 500μm to 0.14μm and its original rough surface looks shiny after 180 min of grinding.

4.2 Silicon nitride rollers

Figure 14 is a schematic diagram of the grinding apparatus for finishing ceramic rollers [6]. These rollers are as-sintered silicon nitride made under hot isostatic pressure. The rollers are pressed against a driving shaft by a cylindrical float which is pushed by the magnetic buoyant force. As the rollers are rotated by the driving shaft, they are ground by abrasive grains in the magnetic fluid. The revolution of the rollers is prevented by a roller holder.

Figure 15 shows the change in shape of the roller with the grinding time. Grinding of a roller surface starts from its edge and spreads over its whole surface. Traditional centerless grinding can not grind such a roller of irregular shape. But in this method, such rollers can be ground from initial stage because of its flexible support with a float.

The cylindricity and circularity of the as-sintered silicon nitride rollers were reduced to one tenth of their initial values within three hours. Maximum removal rate was 0.76μm/min. Minimum cylindricity was 22 μm. Minimum circularity was 3.18μm around the center of the roller. The removal rate was found to be increased with the grinding load and the rotational speed. Cylindricity showed a minimum value at a certain grinding time.

4.3 Alumina plates

Figure 16 is a schematic diagram of the grinding apparatus for finishing ceramic plates (25.4 mm width and 5mm thickness) [7]. The plates are aluminium oxide made by pressureless sintering and are bonded on three planetary disks which are rotated at the same rotational speed as the sun disk but in opposite direction for obtaining uniform sliding distance on the alumina plates. The float has a step as shown in Fig. 17.

Figure 18 shows the effect of the step width of the float on the mean flatness of the plates. Optimum step width of the float provides minimum flatness. A minimum flatness of 0.5 μm is obtained in the case of the float with a 18mm step width. The flatness is thus a function of the step width of the float.

Optimum grinding load and abrasive grain size exist for the removal rate and flatness. Observed values of maximum removal rate, minimum flatness, and minimum surface roughness were 6.4μm/min, 0.5 μm and 0.06 μmRa, respectively.

5. Conclusions

(1) A new method of finishing advanced ceramics, namely, magnetic fluid grinding with a float was developed and applied to a variety of geometry (balls, rollers, and flat surfaces) and work materials (alumina and silicon nitride).

(2) The magnetic fluid grinding apparatus consists of a combination of magnetic fluid, a float, abrasive grains, and suitable arrangement of magnets. The driving shaft, the float and the guide ring provide the three point contact for the balls.

(3) Magnetic fluid grinding has several advantages in finishing over traditional mechanical methods including grinding and lapping .

(4) Design of the float, namely, buoyant force on the float and supporting stiffness of the float, is especially important for application to various shapes of workpieces with high removal rate, good finish, and accurate shape control.

(5) Under optimal finishing conditions the sphericity of the as-sintered silicon nitride balls was reduced from 500μm to 0.14μm and its rough surface appears shiny after 3 hours of grinding. The minimum surface roughness and maximum removal rate are found to be 0.1μmRmax and 12.4 μm/min, respectively. The cylindricity and circularity of the as-sintered silicon nitride rollers were reduced to one tenth of their initial values within three hours. Maximum removal rate was 0.76μm/min, minimum cylindricity was 22 μm, and minimum circularity around the center of the roller was 3.18μm. In finishing alumina plates the observed values of maximum removal rate, minimum flatness, and minimum surface roughness were 6.4μm/min, 0.5 μm and 0.06 μmRa, respectively.

References

[1] Shinmura,T., Takazawa,K., Hatano,E., Matsunaga,M., 1990, Study of Magnetic Abrasive Finishing, Annals of CIRP, 39:325-328.

[2] Rosensweig,R.E., 1985, Ferrohydrodynamics, Cambridge University Press, New York.

[3] Imanaka,O., Kurobe,T., Matsushima,K., 1981, A Study on Field Assisted Finishing Using Magnetic Fluid , Proc. of The JSPE Spring Conf.:774-777.(In Japanese)

[4] Tani, Y., Kawata,K., 1984, Development of High-Efficient Fine Finishing Process Using Magnetic Fluid, Annals of CIRP, 33:217-220.

[5] Umehara, N., Kato,K., 1990,Principles of Magnetic Fluid Grinding of Ceramic Balls, International Journal of Applied Electromagnetics in Materials, 1:37-43.

[6] Umehara, N. Kato, K. ,Nakano,H., 1992, Magnetic Fluid Grinding of Ceramic Rollers, Supplement to Volume 2 of the International Journal of Electromagnetics in Materials:139-142.

[7] Umehara, N. Kato, K., Kanagawa.I., 1992, Magnetic Fluid Grinding of Ceramic Flat Surfaces, Supplement to Volume 2 of the International Journal of Electromagnetics in Materials :143-146.

[8] Rosensweig,R.E., 1966, Fluidmagnetic Buoyancy, AIAA Journal, 4, 10:1751-1758.

[9] Fukuda, R, Tokiwa,T., 1974, A Study on the Contact Stiffness between Grinding Wheel and Workpiece, Journal of the Japan Society of Precision Engineering, 40,10:809-814.

[10] Childs,T.,H.,C., Yoon,H., J., 1992, Magnetic Fluid Grinding Cell Design, Annals of the CIRP, 41:343-346.

Fig.14 Schematic diagram of the magnetic fluid grinding apparatus for finishing advanced ceramic rollers
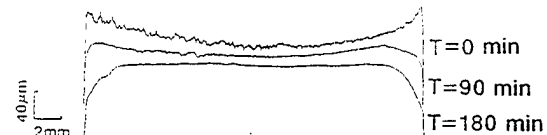
Fig.15 The profile change of a roller of silicon nitride in grinding process (Grinding load : 0.9N, Revolution speed : 600rpm, Abrasive grain : CBN#320, Concentration : 6Vol%)

Fig.16 Schematic diagram of the magnetic fluid grinding apparatus for finishing advanced ceramic plates

Fig.17 A float with a step (left)
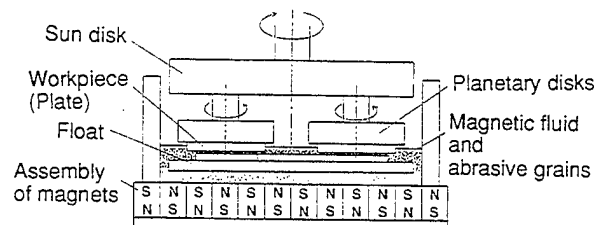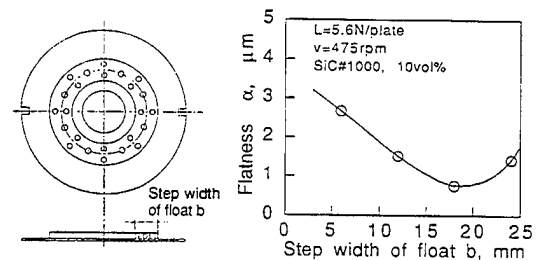Fig.18 Effects of step width of a float on the mean flatness of workpieces (right)

APPENDIX D

MAGNETIC FLUID GRINDING OF HIP-Si$_3$N$_4$ ROLLERS

N. Umehara and R. Komanduri

Magnetic Fluid Grinding of HIP-Si$_3$N$_4$ Rollers

N. Umehara[1] and R. Komanduri[2]

[1]School of Mechanical Engineering, Tohoku University, Aramaki-aza-aoba, Sendai 980 (Japan)
[2]Mechanical & Aerospace Engineering ,Oklahoma State University, Stillwater OK, 74078 (USA)

ABSTRACT

Hot pressed silicon nitride (Si$_3$N$_4$) rollers were finished by magnetic fluid grinding yielding a surface finish, R_a of about 5 nm. Three types of abrasives (B$_4$C, SiC, and Cr$_2$O$_3$) in the 30 to 50 μm size range and three grain sizes of one of the abrasives, namely, Cr$_2$O$_3$ (3, 6, and 30 μm) were used to investigate the effect of abrasive and grain size on the removal rates and surface finish. High removal rate (1.1 μm/min) was obtained with B$_4$C abrasive and high surface finish (R_a of 5 nm) with Cr$_2$O$_3$ abrasive. Magnetic fluid grinding process enables finishing of the rollers with rounded edges (crowns) which may be ideal for roller bearing applications.

1. INTRODUCTION

Hot isostatically pressed (HIP'ed) silicon nitride ceramic material (HIP-Si$_3$N$_4$) offers many interesting properties for high-speed/high temperature bearing applications. They include: 1) High hardness (twice that of a conventional bearing steel), 2) Hardness not significantly affected by temperature upto about 1000 °C, 3) Good corrosion resistance with no sacrifice in bearing performance, 4) Low density (about 40% of a conventional bearing steel) resulting in reduced centrifugal loading at high rotational speeds. Hence, silicon nitride bearings can be used at higher speeds (DN value of 3 to 10 x 10^6 depending on whether it is used as a hybrid bearing or as an all ceramic bearing) as compared to a maximum of 1x 10^6 with an all steel bearings), 5) Good fatigue life. Silicon nitride, fails generally by spalling due to higher toughness, similar to steels, while other ceramics fail catastrophically due to lower toughness, 6) High Youngs Modulus (E) (about 50% more than a conventional bearing steel). This together with lower density results in higher specific stiffness than conventional bearing steel, 7) Non-magnetic. Hence, can be used in magnetic sensitive instruments that require non-magnetic bearings, 8) Low friction and high wear properties, and 9) Requires, in many cases, practically no lubrication which is very valuable for sealed bearings.

Unfortunately, silicon nitride, like the other advanced ceramics, is hard and brittle. Hence, it is rather difficult to polish by conventional methods of grinding, lapping, polishing etc. and requires considerable processing time (from several days to a few weeks) to finish. Centerless grinding can also generate lobes on the ground rollers. Because of the high hardness of these ceramics diamond abrasive is used invariably as the grinding media. However, diamond grinding wheels are very expensive. Further, in view of the high hardness of diamond, the material removal mechanism with diamond abrasive is predominantly by abrasion with the result the surfaces of the finished ceramics are left with defects, such as scratches, pitting (due to dislodgement of grains) which can affect the reliability and service life of the parts made by this technique. Wide usage or acceptance of advanced ceramics for bearing and other structural applications has been somewhat limited because of the high cost of processing, lack of reliability due to unknown defect structure generated during conventional grinding and finishing, and sometimes limited service life. For increasing the applications of ceramics for bearing and structural applications need, therefore, arises for new processing technologies that address these limitations.

To overcome some of these problems, Kato and Umehara [1-8] have developed a new technique known as magnetic fluid grinding (also termed magnetic float polishing). Magnetic fluid grinding utilizes magnetic buoyant force of a non-magnetic body in a magnetic fluid effectively. In this method, grinding load is applied to the ceramic workpieces (balls or rollers) by the magnetic buoyant force of a float via the abrasives in the magnetic fluid. Hence, the forces applied by the abrasives on the workpiece are extremely small (1N per ball or roller) and highly controllable. Umehara and Kato [3,4] polished PLS-Si_3N_4 (PLS: pressure-less sintering) balls by magnetic fluid grinding and reported some 40 times higher removal rate than by traditional ball lapping, quick reduction of sphericity of the balls from 500 μm to 0.14 μm in about 180 min of polishing, and comparable surface finish on the balls (about 0.1 μm Rmax). Following this, they applied this technique to different types of workpieces (geometry and materials) such as Si_3N_4 rollers [4], Al_2O_3 plates [5], Si_3N_4 rings [6], aluminum alloy ring [4], and internal surface of a steel pipe [7] using different magnetic fluid grinding equipment specifically developed for each of these applications on the principle of magnetic buoyancy [8]. Their results showed that in all cases the float plays an important role on the material removal mechanism in general and the removal rate in particular. While much of the research on magnetic fluid grinding was concentrated on finishing of balls [1-13], very little effort was expended on finishing of

rollers [4]. While significant work is being conducted in the finishing of silicon nitride rollers by magnetic abrasive finishing using *magnetic abrasives* [14-15], the focus of this paper is on finishing of silicon nitride rollers using *magnetic fluid* grinding technique.

Umehara, Kato, and Nakano [4] developed a magnetic fluid grinding apparatus for finishing rollers based on their experience with the apparatus for finishing balls. They attempted to polish the as-sintered Si_3N_4 rollers whose initial straightness was more than 50 μm. It may be noted that it would be rather difficult to grind rollers of such irregular shape directly by conventional centerless grinding process. But, such irregular shaped rollers can be easily accommodated in magnetic fluid grinding because of the flexible support of the float. Using this apparatus, Umehara et al [4] reduced the straightness and out-of-roundness of the as-sintered silicon nitride rollers to one tenth of their initial values within three hours. Maximum removal rate was 0.76 μm/min, minimum straightness was 22 μm, and minimum out-of-roundness at the center of the roller was around 3.18 μm. These results established the feasibility of this method for rough polishing but they could not obtain good finish.

With the objective of obtaining good finish (5-10 nm Ra) on Si_3N_4 rollers (with practically no scratches) and at the same time aim for high removal rates, different abrasive materials (and grain sizes) were used in this investigation to study their effect on the surface roughness and removal rates. A harder abrasive, B_4C was selected for obtaining higher removal rates and a softer abrasive, Cr_2O_3 was selected for chemo-mechanical polishing as well as for the elimination of the scratch marks on the polishing surface. SiC abrasive was chosen as an intermediate between B_4C and Cr_2O_3 in terms of hardness.

2. EXPERIMENTAL APPARATUS AND TEST PROCEDURE

Description of the Experimental Apparatus:

Figure 1 is a schematic of the magnetic fluid grinding apparatus used for finishing ceramic rollers [4]. Figures 2 (a) and (b) show the top and side sectional views of the apparatus, respectively. Figure 3 is an exploded view showing the assemblage of magnetic ring B, float, rollers, roller holder, and drive shaft in the hole of the magnetic ring A. Figure 4 is a photograph of the magnetic grinding apparatus for finishing ceramic rollers. As can be seen from Figures 1 and 2, there are two magnetic rings A and B. The magnets in both magnetic rings are made of $SmCo_5$ (Residual magnetization: 1.2 T). Magnetic ring A comprises of 30 individual magnets assembled

65

into one hollow cylindrical magnet (inner diameter: 95 mm, outer diameter: 145 mm, length: 60 mm). Each magnet was magnetized in the radial direction. The polarity of adjacent magnets is alternate N and S. Magnetic ring A is fixed to the chamber [as shown in Figures 2 (a) and 3] and has two functions; one, to support the float in place like a static hydrodynamic bearing, and the other, to facilitate in concentrating the abrasives around the center of the chamber. Magnetic ring B comprises of 16 individual magnets assembled into a ring magnet (inner diameter: 70 mm, outer diameter: 90 mm, and thickness: 18 mm). Each magnet in this ring is magnetized in the longitudinal direction. The polarity of the adjacent magnets in this ring is again alternate N and S. Magnetic ring B is fixed to the cover plate and pushes the float in the longitudinal direction as the magnetic buoyant force is applied. The float then follows the inner 10-degree-tapered surface and presses it against rollers.

Test Procedure:

Table I gives details of the workmaterial, magnetic fluid, and test conditions used in this investigation. Eight HIP-Si_3N_4 rollers (diameter: 19 mm and length: 26 mm) were located on the roller holder (Figure 3) which acts like a cage in a bearing. The assembly was then placed in the polishing chamber filled with the magnetic fluid (water-based) and appropriate abrasive (see Table I for details) . The drive shaft is connected to the spindle of a Bridgeport CNC milling machine which is capable of operating in the speed range of 60 - 6,000 rpm. The rotation of the rollers along the axis of the shaft is prevented by the roller holder in order to obtain high sliding velocity between the roller and the drive shaft and consequently higher removal rates. However, the rotation of the rollers along their own axes is facilitated by providing fingers in the roller holder. This apparatus enables finishing of eight silicon nitride rollers simultaneously. Depending on the size of the rollers, different roller holders need to be used.

In an earlier work by Umehara et al [4], only SiC abrasive was used to demonstrate the feasibility of the new finishing method for ceramic rollers. In the present study, three different abrasives, namely, B_4C, SiC, and Cr_2O_3 were used. As pointed out earlier, B_4C was selected as a hard abrasive against HIP-Si_3N_4 rollers for obtaining larger removal rates. Cr_2O_3, on the other hand, was selected as a soft abrasive against the HIP-Si_3N_4 rollers so that the rollers can be finished without any scratch marks. Also, chemo-mechanical action between the Cr_2O_3 abrasive and the Si_3N_4 roller can be accomplished resulting in a smooth surface on the rollers based

on earlier work [16-17]. The polishing load depends on the gap between the float and the magnetic ring B as shown in Figure 5. It shows that a smaller gap provides larger polishing load. In the present study, we selected very small load (0.084 N/roller) with the objective of obtaining very good surface (Ra 5-10 nm). Based on the previous work [4], rotational speed of the spindle and volume concentration of the abrasive in the magnetic fluid were fixed at 1500 rpm and 6 vol.%, respectively as they seem to provide optimum conditions for polishing. Furthermore, in the present study, in order to polish ceramic rollers uniformly in the longitudinal direction, the drive shaft was given a sinusoidal oscillation (frequency: 0.2 Hz and amplitude: 5 mm) during polishing through the NC control of the machine tool.

Removal volume and removal depth were calculated from the difference in weights of the roller before and after polishing. Surface profiles in the longitudinal direction of the eight rollers were obtained using a Form TalySurf surface profilometer. From the surface profiles, surface roughness Ra of the eight rollers were measured and the average value of their Ra was used as a representative value of surface roughness, Ra. Straightness and out-of-roundness of the rollers were measured before and after polishing using Form TalySurf and TalyRond, respectively. Straightness is defined as the difference in height between the peak (or highest point and the valley (lowest point) of the entire surface profile in the longitudinal direction of the roller.

3. EXPERIMENTAL RESULTS

3.1 Variation of the Removal Volume and Surface Roughness With Polishing Time:

Figure 6 shows the variation of removal volume (or removal depth) with polishing time. It may be noted that the polishing conditions used are also given in the figures. It can be seen from Figure 6 that the removal volume (or removal depth) increases linearly with polishing time up to about 60 min of polishing time and further increase in the polishing time leads to a decrease in the removal rate (lesser slope) perhaps due to the breakdown of the abrasive.

Figure 7 shows the variation of surface roughness, Ra (average values for eight rollers) with polishing time. The scatter bands of surface roughness are also shown for the eight rollers at each polishing time to show the statistical nature of the polishing process. It can be seen from Figure 7 that initially the average value of surface roughness of the eight rollers decreases rapidly with polishing time followed by a

gradual decrease with further increase in polishing time reaching a value of 0.029 μm (Ra). Also, the size of the scatter band of the surface roughness also decreases with increase in polishing time.

3.2 Effect of the Abrasive Materials on Removal Rate and Surface Roughness

Three abrasives, namely, Cr_2O_3, SiC, and B_4C in the 30-50 μm range were used for comparison in magnetic fluid grinding of silicon nitride rollers. Figures 8 (a) and (b) show the effect of abrasive material on the removal rate and surface roughness, respectively. It may be noted that the grain size of the three abrasives is slightly different. Figure 8 (a) shows that the removal rate is influenced by the type of abrasive material used. The removal rate increases in the order of increasing hardness of the abrasive used, namely, Cr_2O_3, SiC, and B_4C. Also, a fraction of this increase can be attributed to larger grain size used in the case of B_4C. Also, from Figure 8 (b) it can be seen that Cr_2O_3 generates the best finish (lowest surface roughness) compared to B_4C and SiC. This improvement in surface roughness with Cr_2O_3 can be attributed to the lower hardness of the abrasive as well as chemo-mechanical polishing ability of this abrasive when finishing silicon nitride [16-17].

3.3 Effect of the Abrasive Size on the Removal Rate and Surface Roughness

In the previous section, we showed that among the three abrasives used, Cr_2O_3 gave the best finish. Since we are interested in obtaining the best finish, we investigated the effect of Cr_2O_3 abrasive size on the removal rate and surface finish. Figure 9 shows the effect of the abrasive size on the removal rate and surface roughness after polishing for 30 minutes. It can be seen from Figure 9 that removal rate increases linearly with increase in grain size. However, the surface finish improves rapidly with a decrease in grain size [for small grain size (3-10 μm)] with a gradual deterioration of surface finish with further increase in grain size. Figures 10 (a) to (c) show the surface profiles (TalySurf traces) of the silicon nitride rollers form the as-received condition to the finished state. It can be seen that the surface roughness, Ra, has improved from 1.6 μm to 4.9 nm with the Cr_2O_3 abrasive (7 and 3 μm grain sizes) after a total polishing time of 90 minutes.

3.4 Variation of Straightness Before and After Polishing

Figures 11 (a) and (b) show profiles in the longitudinal direction of a roller before and after polishing. Similar results were obtained with the other seven rollers

polished in this batch by magnetic fluid grinding technique. We have also polished another batch of rollers yielding similar results. It can be seen from Figure 11 that the rollers polished by this technique provide slightly rounded edges with a minimum value of straightness of about 10 μm over its length. A similar feature was observed in an earlier study [4] where a minimum value of straightness was found for a certain grinding time. This feature seems to be a characteristic of the process as this process polishes both the face as well as the sides leading to rounded edges. This, however, may be considered as an advantage (and not a limitation) with this process as most rollers for bearing applications have similar geometries imposed by the designer to prevent stress concentrations at the contact surface. So, a secondary operation is needed to provide this crown on the rollers by conventional grinding technique.

Figure 12 is a section of a roller bearing along with details of the crown for a silicon nitride (7.5 mm x 7.5 mm) rolling element and Table 2 is a summary of the design features of a silicon nitride bearing after Miner et al [18]. The shape of the crown, however, depends on the size of the roller as well on the application of the bearings. In magnetic fluid grinding such a crown can be incorporated on the roller in the polishing stage without the need for a separate operation.

3.5   Variation of Out-of-Roundness Before and After Polishing

Figures 13 (a) and (b) show the roundness profiles before and after polishing. It can be seen from Figure 13 that the out-of-roundness of the roller has improved from 16.65 μm before polishing to 4.25 μm after polishing. Improvement in out-of-roundness appears to be partly responsible for the improvement in surface roughness obtained in this investigation.

4.   DISCUSSION

4.1.   Effect of Hardness Ratio (H_a/H_m) of Abrasive to the Roller (Workpiece) on Removal Rate

To further analyze the effect of abrasives on the removal rate and surface roughness, the data in Figures 8 (a) and (b) was rearranged using the hardness ratio of the abrasive to the roller workpiece (H_a/H_m) as a basis. It may be noted that in many studies on abrasive wear, the hardness ratio is considered as an important parameter [19-21]. Figure 14 shows the effect of hardness ratio of abrasive to the roller workpiece (H_a/H_m) on the removal rate and surface roughness. It can be seen from Figure 14, the removal rate increases with the hardness ratio (H_a/H_m). Based on experimental data, Rabinowicz [11] has shown that the wear coefficient (defined as the

wear volume multiplied by the hardness of the specimen and divided by the product of load and the sliding distance) is strongly influenced by the hardness ratio (H_a/H_m). The wear coefficients are shown (a) for values of H_a/H_m larger than 1.25 to be a constant; (b) .for values of H_a/H_m in the range of 0.8 to 1.25 to be proportional to $(H_a/H_m)^{2.5}$; and for values of H_a/H_m less than 0.8 to be proportional to $(H_a/H_m)^6$, respectively. In the present investigation, since the hardness ratios (H_a/H_m) of both B_4C and SiC are larger than 1.25, both wear coefficients should have the same value based on Rabinowicz's theory. In the present study, the removal rate was used as an indicator of the polishing ability of each abrasive. Because of small removal depth (compared with the radius of roller), it can be considered that the removal rate (μm/min) is proportional to the volumetric removal rate (mm^3/min). If the contact load and sliding velocity of the roller (between the driving shaft and roller) under different abrasives are assumed to have the same value, then the removal rate (μm/min) can be considered to be proportional to the wear coefficient. As can be seen from Figure 12, the removal rate with B_4C is much larger than that with SiC. Plausible reasons for the observed differences in the removal rates between B_4C and SiC can be attributed to (a) the use of larger size B_4C abrasiveand (b) higher hardness of B_4C than SiC. For the case of Cr_2O_3 abrasive, as the hardness ratio (H_a/H_m) is about 1.1, the scratching ability (abrasion) of Cr_2O_3 abrasive can be considered relatively low. This means the tips of the Cr_2O_3 abrasives would be worn by attrition or microchipping when Cr_2O_3 was used as a polishing media for finishing Si_3N_4.

4.2. Effectiveness of Cr_2O_3 Abrasive to Produce Good Finish on Si_3N_4

In an earlier study on magnetic fluid grinding of silicon nitride roller polishing [4], a surface roughness of 0.2 μm (Ra) was obtained with a SiC abrasive (grain size 38 μm). In this investigation, we were able to improve the surface finish to 5 nm Ra with Cr_2O_3 abrasive (grain size 3 μm). The surfaces generated on the silicon nitride rollers were practically scratch-free. From this, Cr_2O_3 abrasive can be considered as an ideal abrasive for polishing HIP-Si_3N_4 rollers. It can be argued that the effectiveness of Cr_2O_3 is related to the chemo-mechanical reaction possible between the Cr_2O_3 abrasive and Si_3N_4 roller material based on several previous literature [16-17].

4.3. Comparison of Roller Characteristics

Table 3 gives a comparison of results obtained from an earlier study [4] with those of the present investigation. It may be noted that the rollers used in the earlier investigation were sintered material while in the present investigation we have used

HIP-Si$_3$N$_4$ which is much denser and hence harder to finish. On examining Table 3, it can be noted that (a) the removal rate obtained in the present study is higher, (b) there is a significant improvement in straightness, and (c) more importantly a significant improvement on the finish. While the Rmax is the previous study was 2 μm, in the present study it was brought down to 0.091 μm with a minimum R$_a$ of 5 nm. For bearing applications it is desirable to obtain finish of this magnitude on the rollers.

5. CONCLUSIONS

HIP-Si$_3$N$_4$ rollers were polished successfully using the magnetic fluid grinding technique. In order to improve the surface finish over what was obtained in an earlier investigation and of acceptable quality for bearing applications different abrasives (SiC, Cr$_2$O$_3$ and B$_4$C) in the size range of 30-50 μm were investigated. Based on this investigation the following specific conclusions can be reached.

1. Cr$_2$O$_3$ abrasive (grain size:3 μm) gave a surface finish Ra of 5 nm on HIP'ed Si$_3$N$_4$ rollers.

2. The surface finish improved with decrease in grain size of Cr$_2$O$_3$ abrasive.

3. Surface finish Ra improved in the order of B$_4$C, SiC and Cr$_2$O$_3$ abrasives.

4. B$_4$C abrasive (grain size:50μm) gave the largest removal rate of 1.1 μm/min.

5. Rollers polished by this technique provides slightly rounded edges on the rollers. This, however, may be considered as an advantage (not a limitation) with this process as most rollers for bearing applications have similar geometries imposed by the designer to prevent stress concentrations at the contact surface. There is hence no need for a secondary operation to provide the crowns on the rollers.

REFERENCES

[1]   Umehara, N. "Study on Magnetic Fluid Grinding," Ph.D. Thesis, Tohoku University, Sendai, Japan (1988) (in Japanese)

[2]   Kato, K.,"Tribology of Ceramics," Wear, 136 (1990) 117-133

[3]   Umehara, N. and K. Kato, "Principles of Magnetic Fluid Grinding of Ceramic Balls," International Journal of Applied Electromagnetics in Materials, 1, (1990) 37-43

[4]   Umehara, N. Kato, K. and H. Nakano, "Magnetic Fluid Grinding of Ceramic Flat Surfaces," Electromagnetic Foces and Applications,Supplement to Volume 2 of the International Journal of Electromagnetics in Materials, (1992) 139-142

[5]   Umehara, N. Kato, K. and I. Kanagawa, "Magnetic Fluid Grinding of Ceramic Flat Surfaces," Electromagnetic Foces and Applications, Supplement to Volume 2 of the International Journal of Electromagnetics in Materials., (1992) 143-146

[6]   Umehara, N. Kato, K. and J. Watanabe, "A Study of Magnetic Fluid Grinding - Grinding Properties with of Cylinder with a Float," (3rd Report) Journal of Japan Society of   Mechanical Engineers, 55, 519, (1989) 2879-2884 (in Japanese)

[7]   Yamamoto, T., Umehara, N. Kato, K., Ataka, M. and K. Watanabe, "Magnetic Fluid Grinding for Innersurface of Pipe of Which Crosss-Sectional Area is Hexagonal Circle," Journal of Japan Society of Mechanical Engineers, 58, 553 C (1992) 2767-2772 (in Japanese)

[8]   N.Umehara, "Magnetic Fluid Grinding - a New Technique for Finishing Advanced Ceramics," Annals of CIRP, 42/1(1994) 185-188

[9]   Tani, Y., and Kawata, K., "Development of High-Efficient Fine Finishing Process Using Magnetic Fluid," Annals of CIRP, 33/1 (1984) 217-220

[10]   Childs, T. H. C., and H. J. Yoon, "Magnetic Fluid Cell Design," Annals of CIRP, 41/1 (1992) 343-346

[11]   Childs, T.H.C., Jones, D.A., Mahmood, S., Kato, K., Zhang, B , and N. Umehara, "Magnetic Fluid Grinding Mechanics," Wear 175 (1994) 189-198

[12]   Childs, T.H.C., Mahmood, S., and Yoon, H. J. " The Material Removal Mechanism in Magnetic Fluid Grinding of Ceramic Ball Bearings," Proc. of I. Mech. E.(Lon), 208, B1 (1994b) 47-59

[13]   Raghunandan, M., Umehara, N., Noori-khajavi, N., and R. Komanduri, "Magnetic Float Polishing of Advanced Ceramics," paper submitted for publication (1994)

TABLE I : SPECIFICATION OF MATERIALS AND EXPERIMENTAL CONDITIONS

Magnetic fluid	W-40 (Water-based) Saturated magnetization: 400 G at 8 KOe Density: 1.4 g/cm^3 Viscosity: 0.014 Pas Carrier Fluid: water
Workpiece	HIP-Si$_3$N$_4$ (ϕ19 x 26) rollers Density: 3.2 g/cm^3 Strength: 100 kgf/mm^2 Youngs Modulus: 290 GPA Hv: 1677 Kgf/mm^2 K$_{1c}$: 7.9 MN/m$^{3/2}$ No of rollers: 8
Abrasives	B$_4$C(#320) SiC(#400, #2000) Cr$_2$O$_3$ (15-45 μm, 2-12 μm, 1-5 μm)
Concentration	6 vol% abrasive + 94 vol% magnetic fluid
Polishing load	0.084 N/roller
Spindle speed	1500 rpm
Linear oscillation of the shaft	Stroke: 5 mm Frequency: 0.2 Hz
Magnets	SmCo$_5$(12.7 mm wide x 25.4 mm thick) (Residual magnetization: 1.2 T)

TABLE II- BEARING DESIGN FEATURES FOR A
CERAMIC (SILICON NITRIDE) ROLLER
BEARING [18]

Bore diameter, mm (in)	35(1.3780)
Outer diameter, mm (in)	62(2.4408)
Width, mm (in)	17
Element size, mm	7.5006 x 7.5006
Number of Elements	14
Inner Raceway Radius, mm	- -
Outer Raceway Radius, mm	- -
Contact Angle, deg	- -
Diametral Clearance, mm	0.1270
Raceway Roughness, m x 10^{-8}	15
Element Roughness, m x 10^{-8}	7.6-10.2
Tolerance Specification	RBEC 5
Raceway Material	AMS 6490
Cage Material	AMS 6414
Element Material	NC 132

TABLE III. MAGNETIC FLUID GRINDING OF Si_3N_4 ROLLERS

Roller Charactristics	Earlier Work [4]	This Work
Workmaterial: Si3N4	Sintered	HIP'ed
Removal rate, $\mu m/min$	0.76	1.1
Straightness, μm	22	10
Roundness, μm	3.18	4.25
Surface Roughness, μm	2.0(R_{max})	0.091 (R_{max})
		0.029 (R_a)
		0.005 (R_a,min)
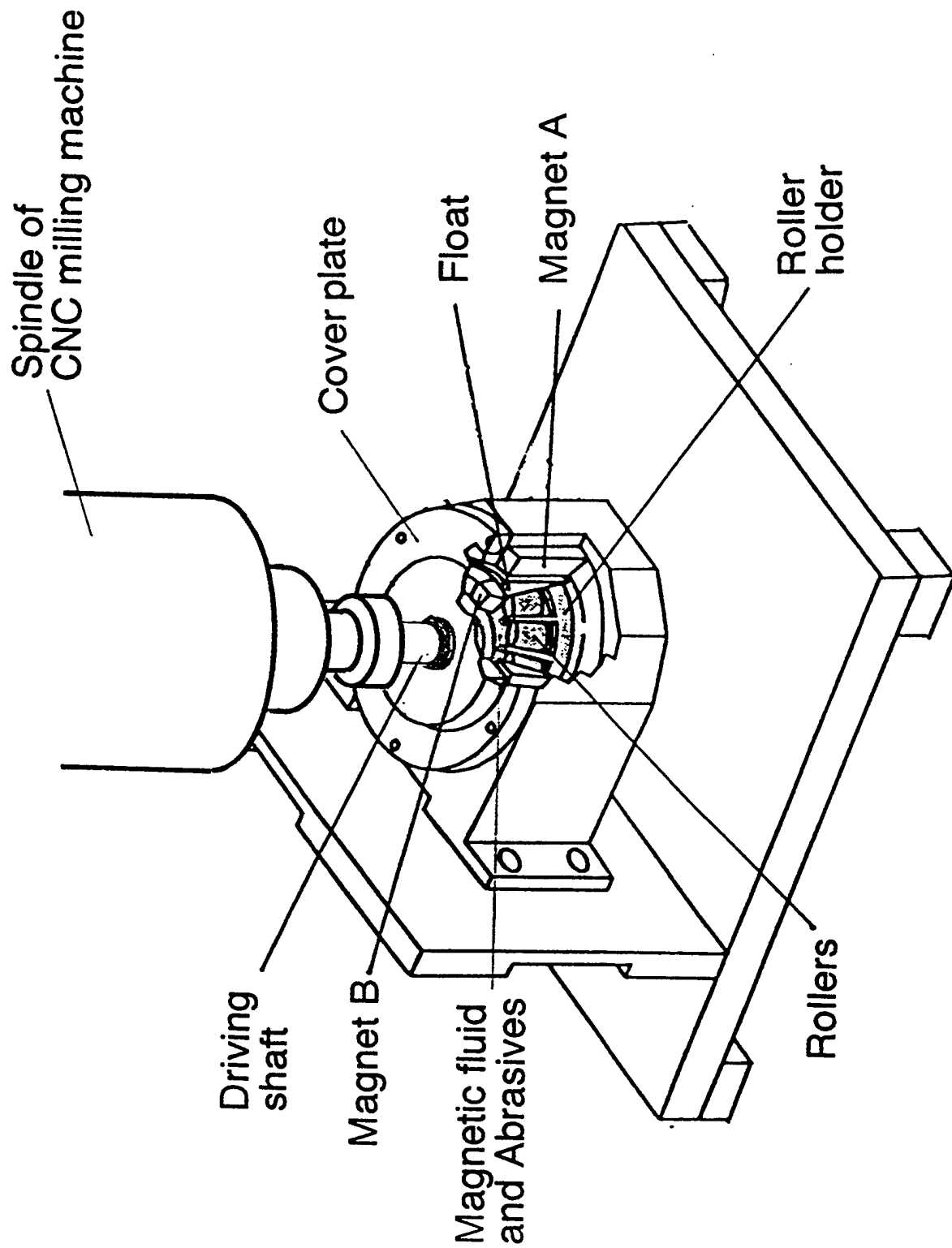
Figure 1 Schematic diagram of magnetic fluid grinding equipment for ceramic rollers

Magnet A

Rollers

Roller
holder

A -

Float

Driving
shaft

Magnetic fluid
and Abrasives

A'
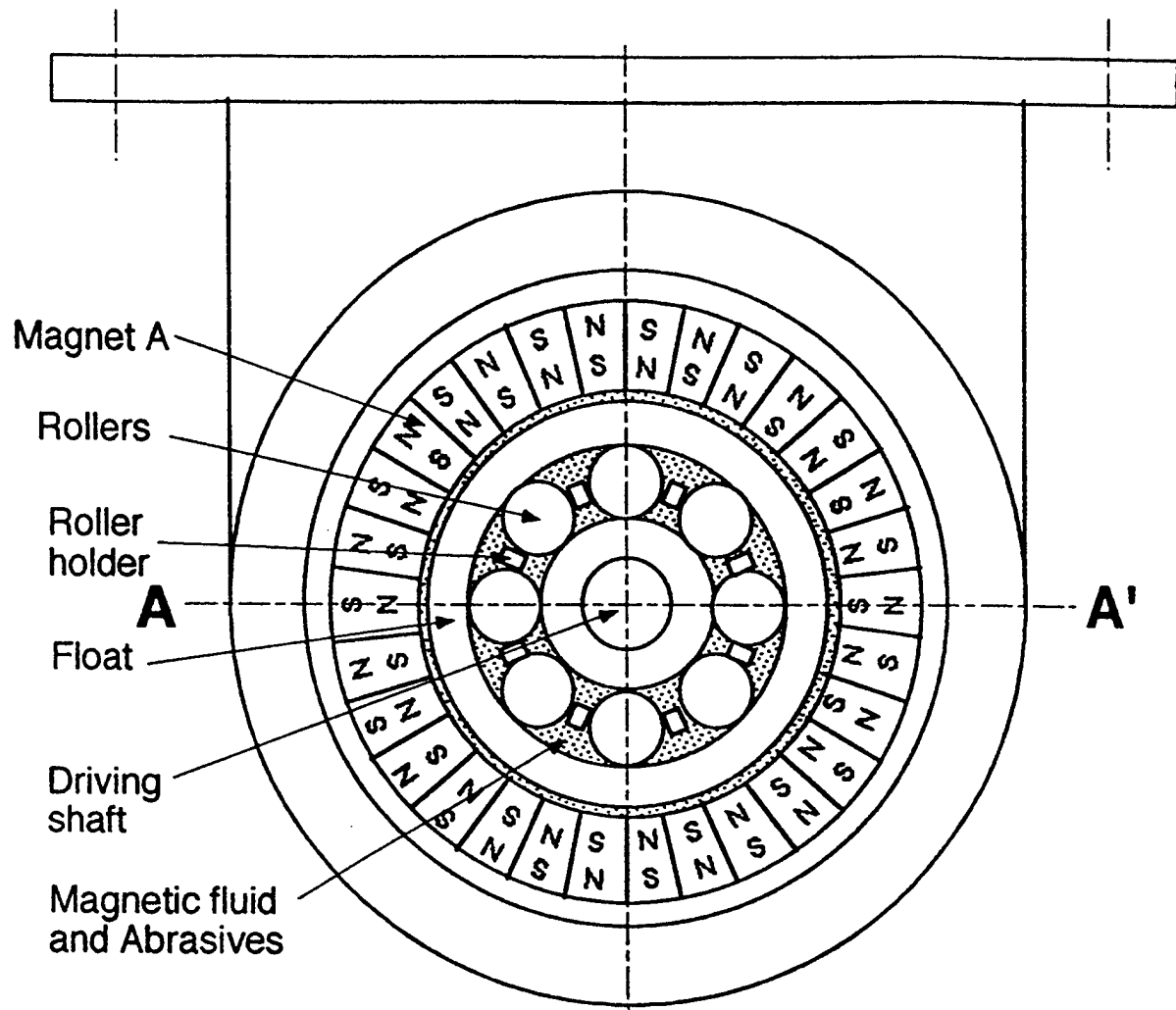
Figure 2(a) A top view of magnetic fluid grinding equipment
for ceramic rollers
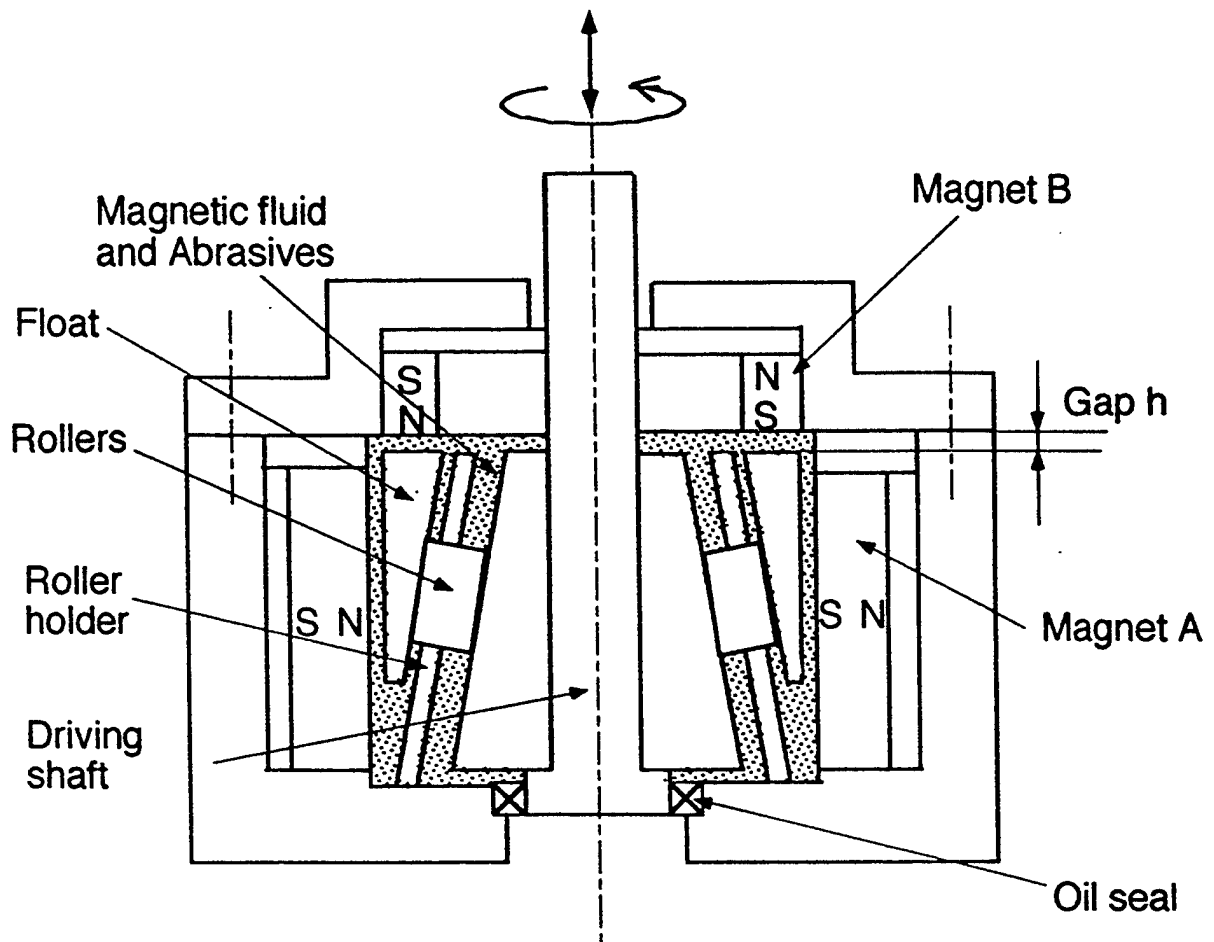
Figure 2 (b) A side section view of magnetic fluid grinding
 for ceramic rollers
(Section plane is through A-A' line in Fig. 2(a))
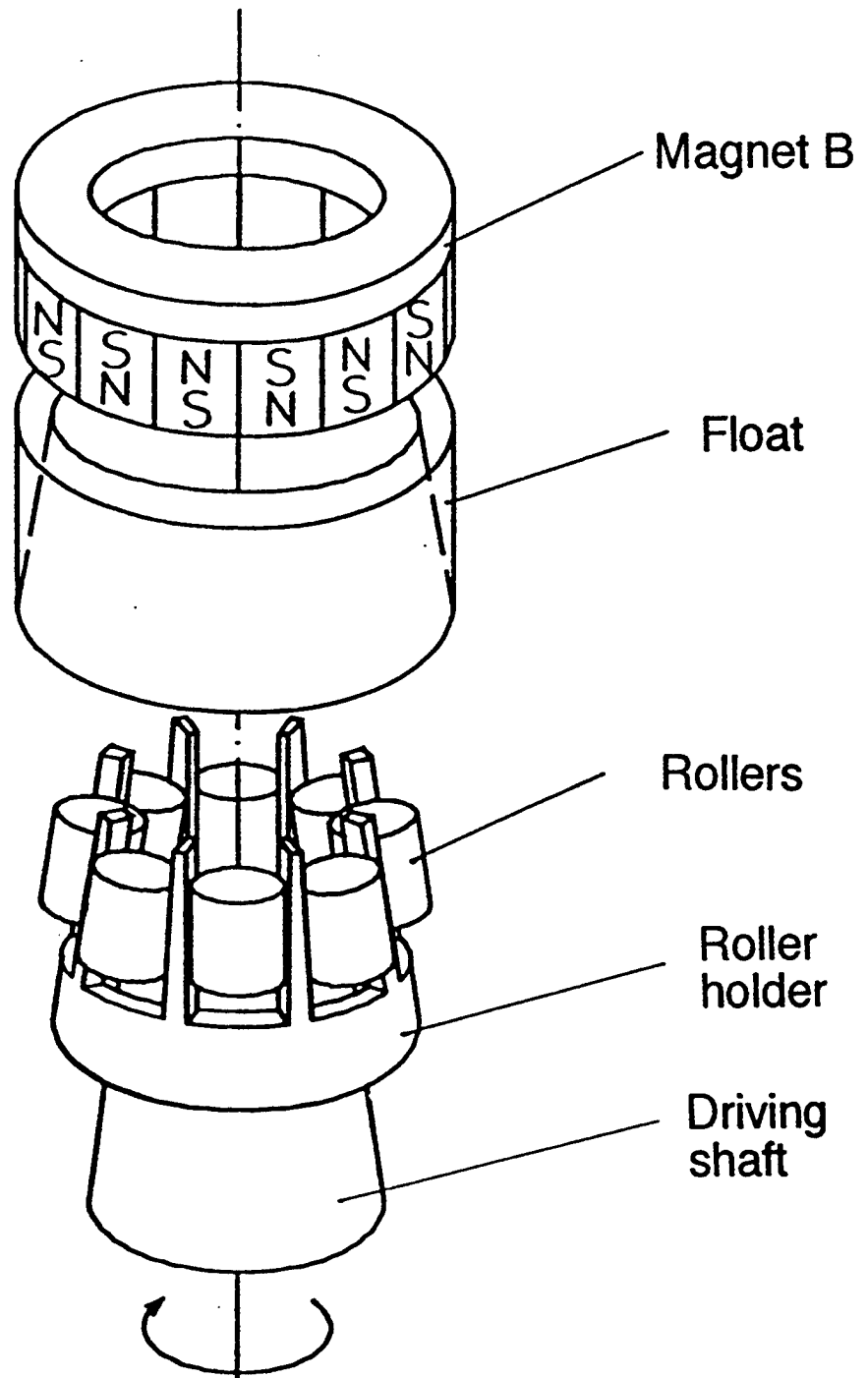
Figure 3 Assembly way of Magnet B, Float, Rollers, Roller holder and Driving shaft
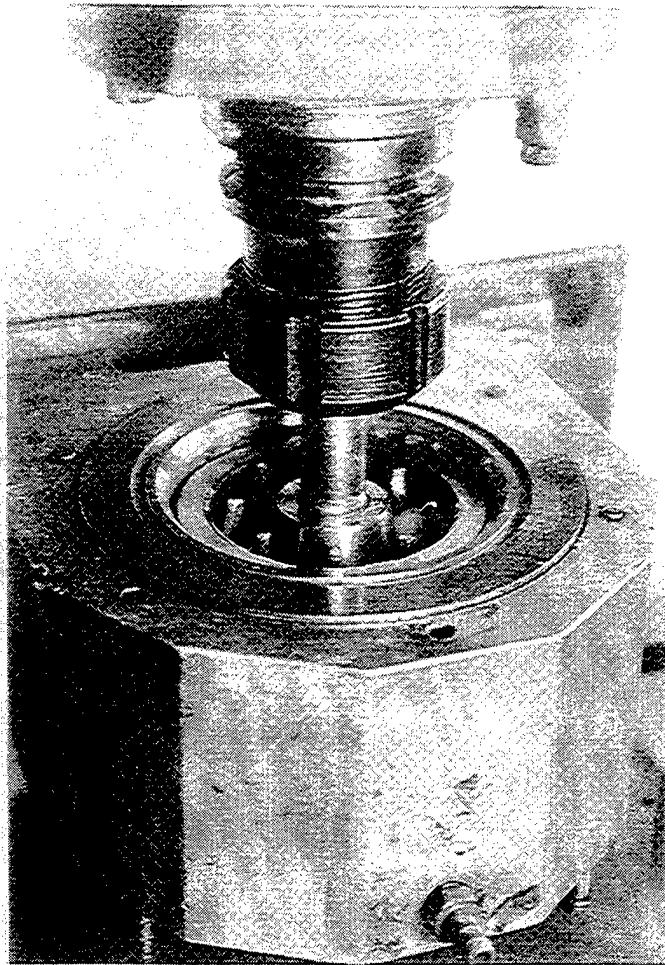
Figure 4   Photograph of the magnetic fluid grinding equipment for ceramic rollers showing the drive shaft, the cage (roller holder), rollers, float, and the float chamber
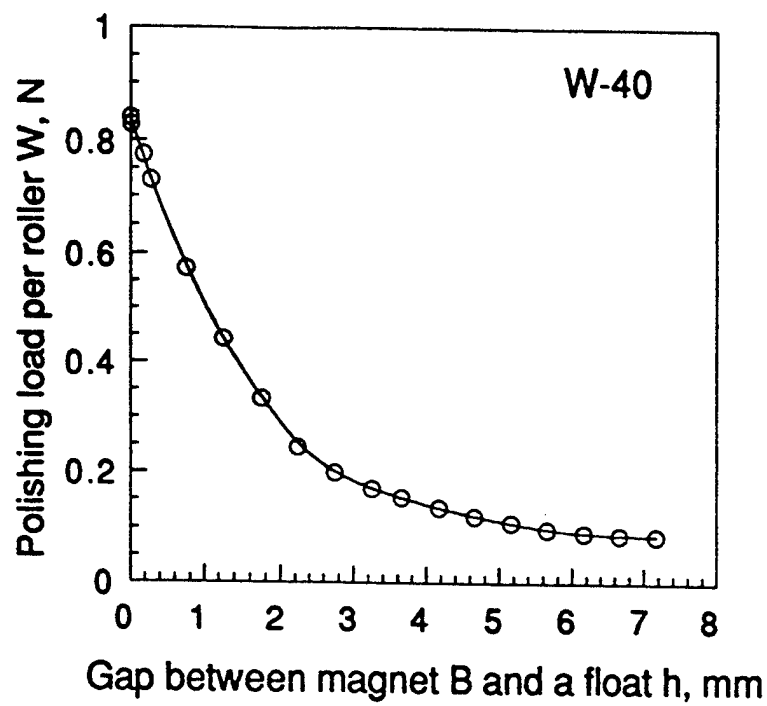
Figure 5   Relationship between polishing load and the gap
between magnet B and the float
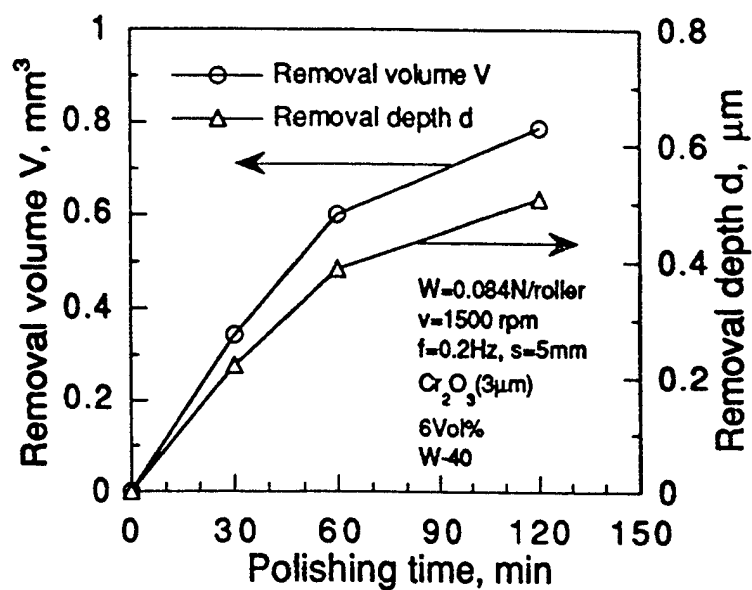
Figure 6 Variation of removal volume and removal depth
with polishing time
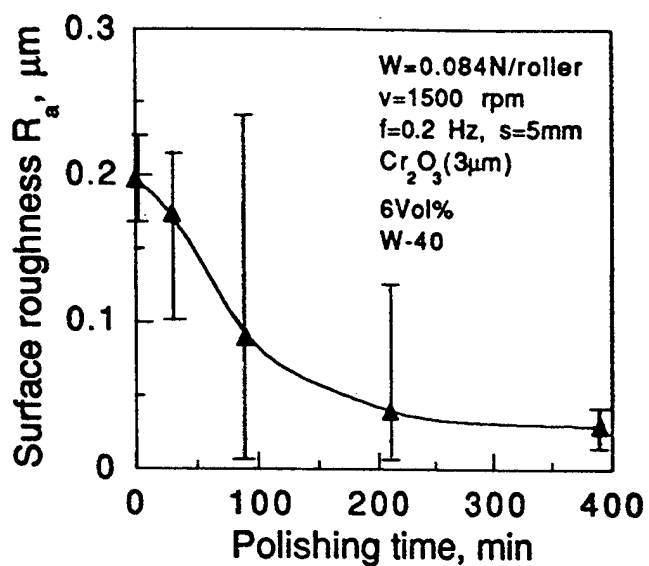
Figure 7 Variation of surface roughness Ra with polishing time
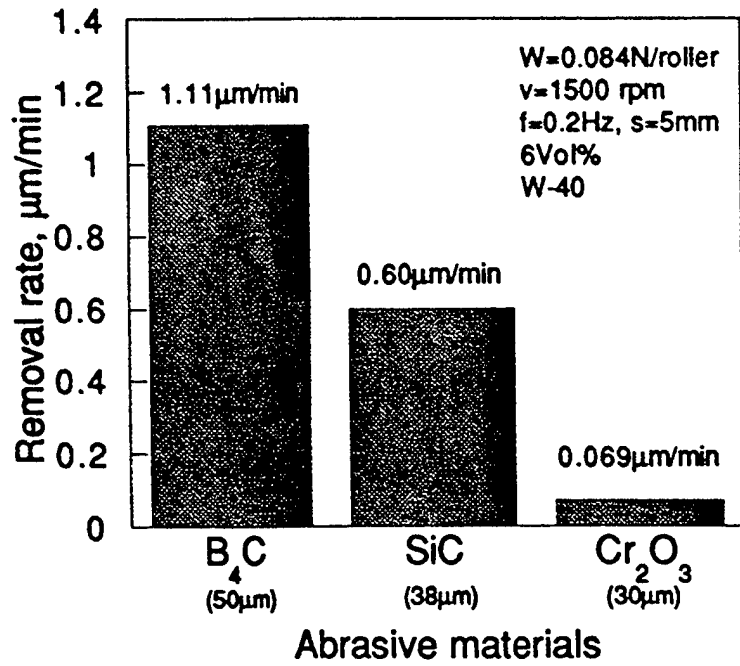
Figure 8 (a) Effect of abrasive material on removal rate
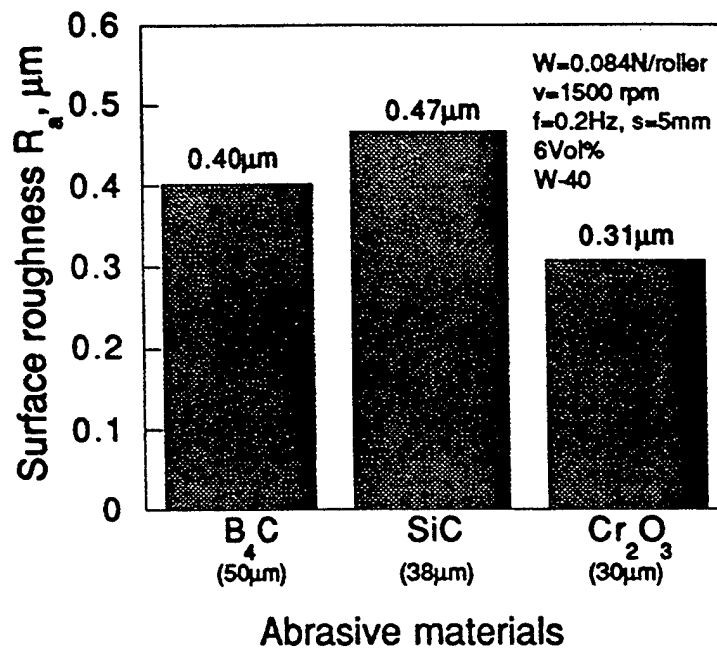
Figure 8 (b) Effect of abrasive material on surface roughness
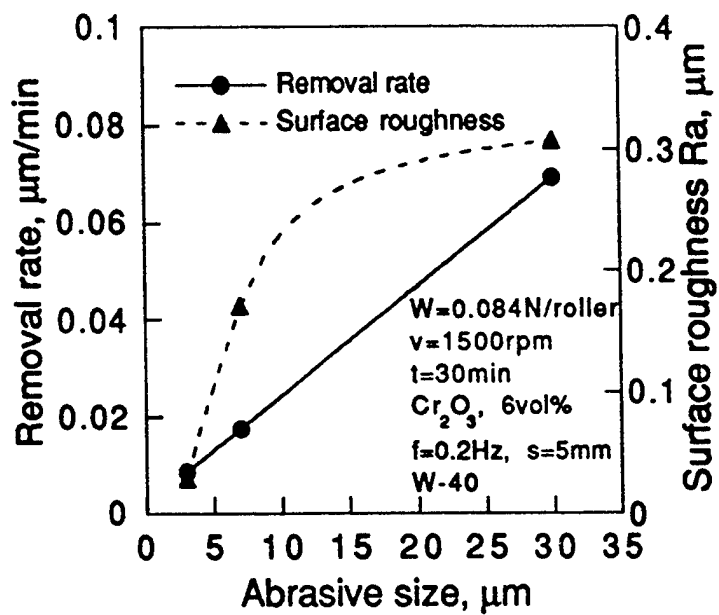
Figure 9   Effect of abrasive size of Cr_2O_3 on removal rate
and surface roughness

2μm
0.5mm

| Ra | 1.6861 um | Rq | 2.0760 um | Rp | 5.7435 um |
| Rv | 7.3358 um | Rt | 13.0785 um | | |

As-received

0.2μm
0.1mm

| Ra | 0.1717 um | Rq | 0.2279 um | Rp | 0.3433 um |
| Rv | 1.0045 um | Rt | 1.4278 um | | |

Polished with Cr_2O_3 (7 μm)

0.2μm
0.1mm

| Ra | 0.0049 um | Rq | 0.0074 um | Rp | 0.0133 um |
| Rv | 0.0771 um | Rt | 0.0905 um | | |
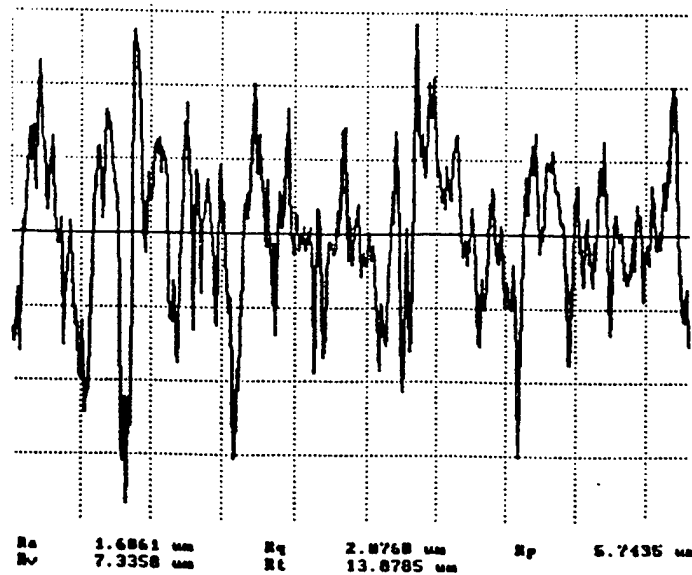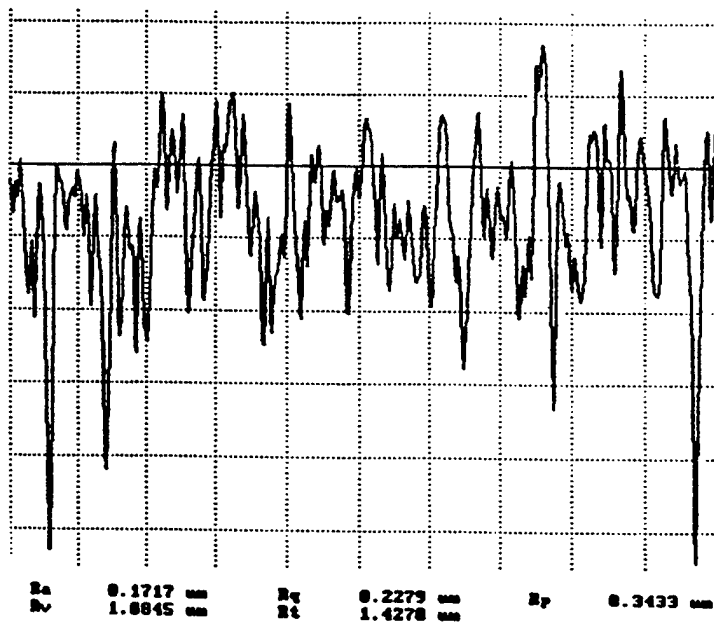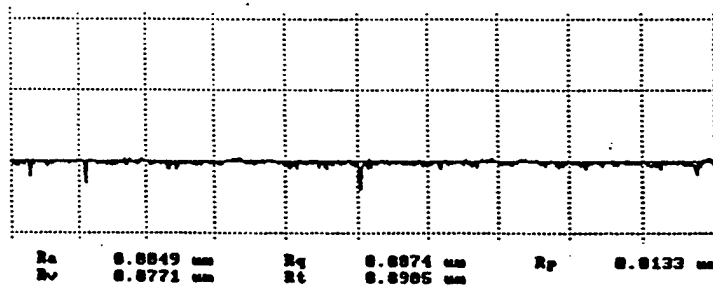
Polished with Cr_2O_3 (3 μm)

Figure10   Surface roughness profiles before and after polishing with Cr_2O_3 (7 μm) and Cr_2O_3 (3 μm)   84

As-received

Polished

10μm

1mm

Peak to valley   36.28 um

Peak to valley   45.75 um
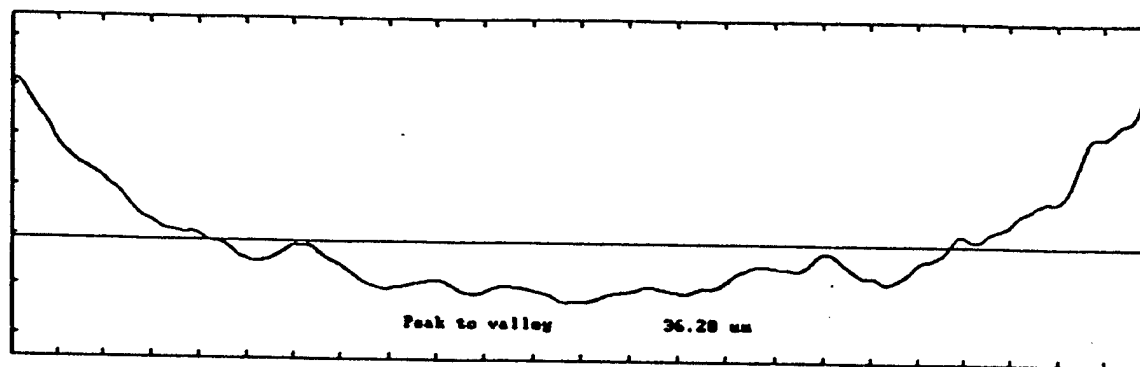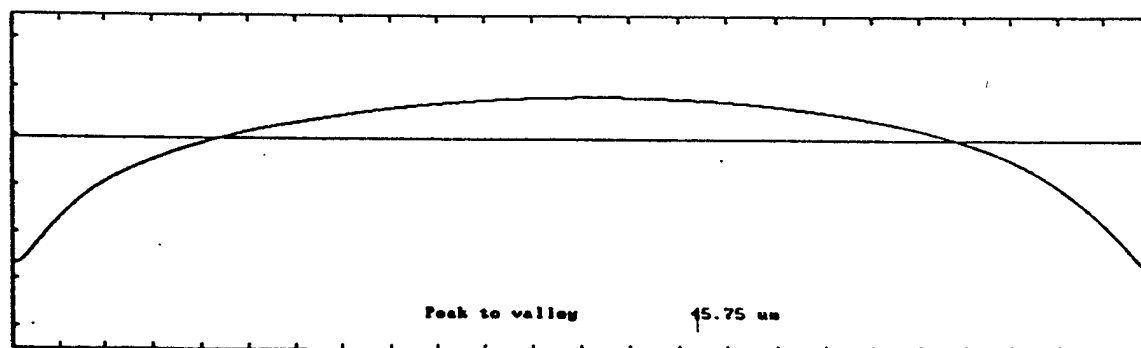
Figure 11   Surface profiles of a roller in the longitudinal direction
(a) as received and (b) after polishing

85

1.016
Gage

0.0106
0.0081

(2.4408)
61.9988 Dia
61.9937

35.0012 Dia
34.9961
(1.3779)

17.0002
16.8732
(0.6668)

DIMENSIONS: mm (in.)
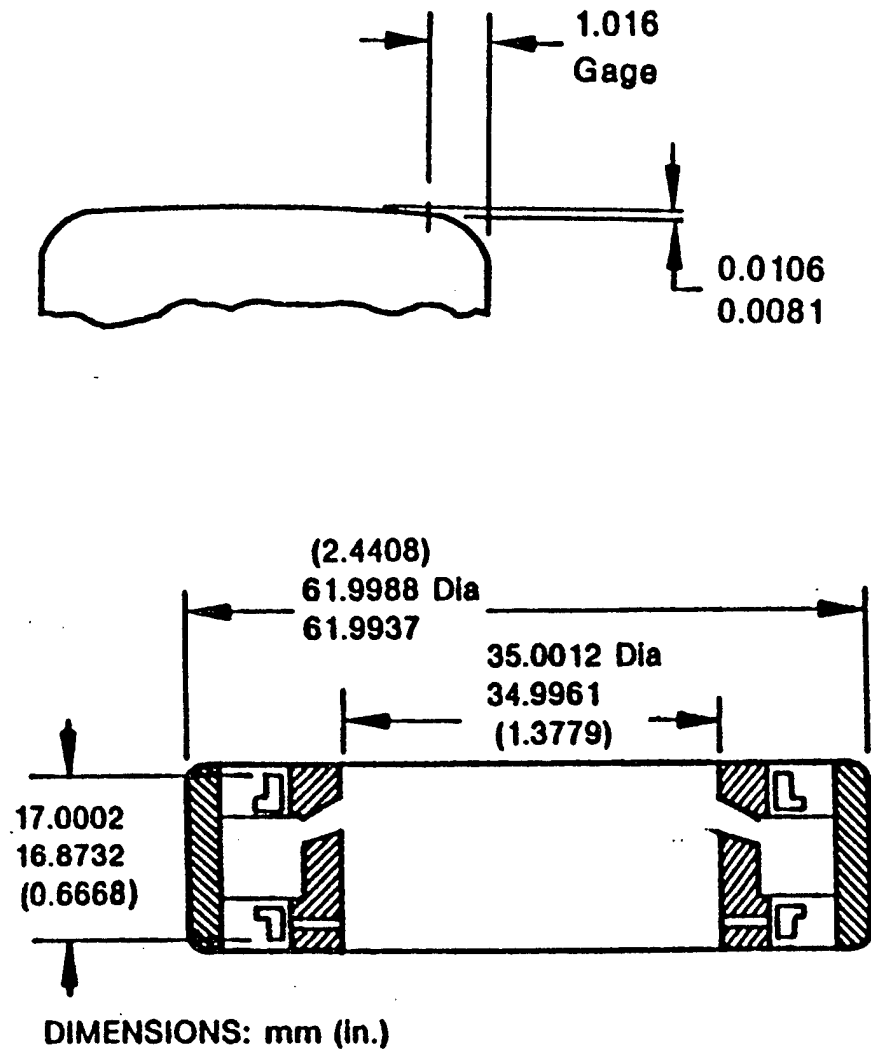
Figure 12.   Partial view of the roller crown and separable roller bearing design
            for silicon nitride bearing (after Miner et al [18])

86
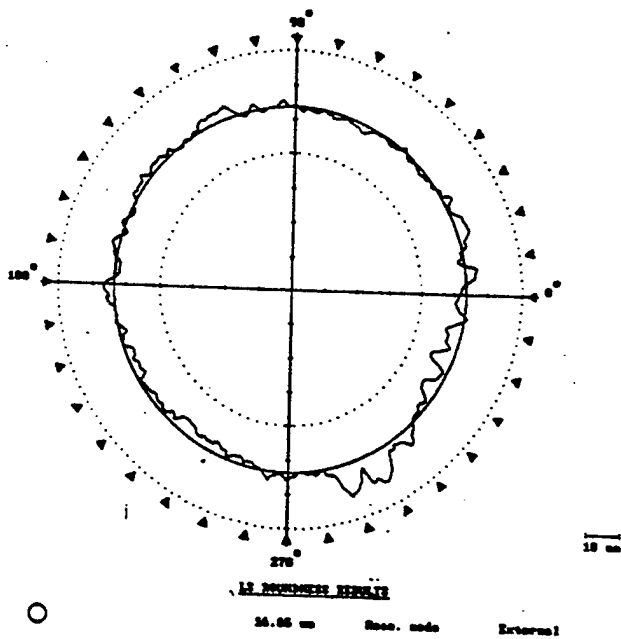
As-received
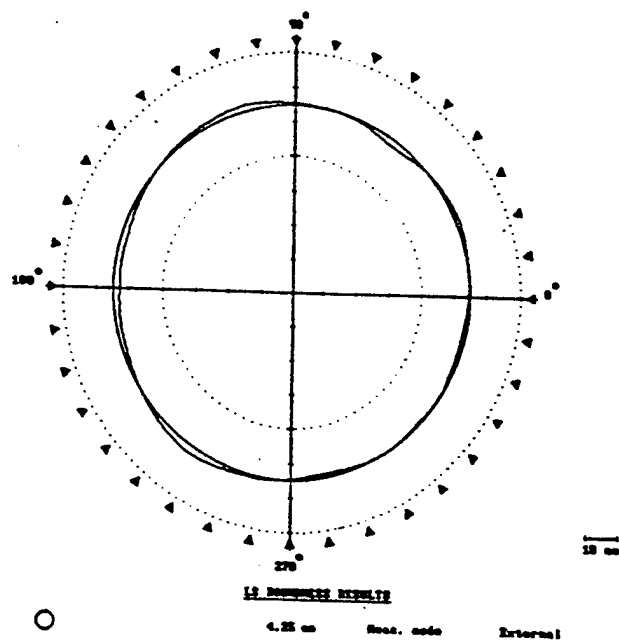
Polished

Figure 13 Roundness profiles (a) before and (b) after polishing
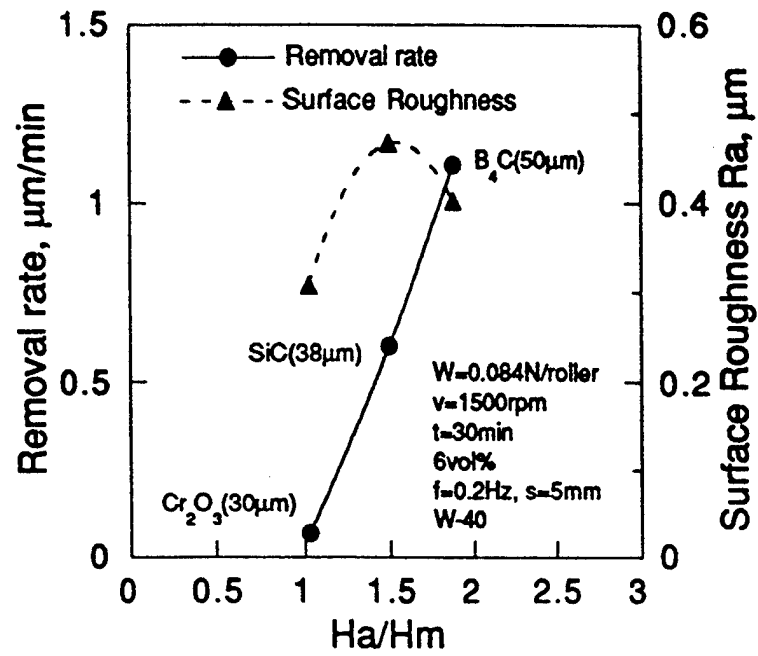
Figure 14   Effect of hardness ratio H_a/H_m of abrasive
to workpiece material

APPENDIX E

MAGNETIC ABRASIVE FINISHING OF ROLLERS

M. Fox, K. Agrawal, T. Shinmura, and R. Komanduri

Magnetic Abrasive Finishing of Rollers

M. Fox, K. Agrawal, T. Shinmura, R. Komanduri (1), Oklahoma State University, Stillwater, OK, USA
Received on January 11, 1994

Summary

Advanced ceramics, such as silicon nitride are increasingly being considered for structural applications, such as ceramic bearings for high speed spindles. The requirements of high finish and accuracy and minimal surface defects, such as cracks, combined with the difficulty of finishing them by conventional methods of grinding and polishing cost effectively, necessitated the investigation of alternate manufacturing technologies. Magnetic field assisted polishing is one such technology which is capable of generating (a) very high finish and accuracy, (b) very little or no surface damage, such as microcracks to the components during the finishing operation due to extremely low level of forces, and (c) the finishing operation can be significantly faster than by conventional techniques due to the possibility of using higher spindle speeds. In this paper, this technique will be briefly reviewed followed by an experimental investigation of the application of this technology for finishing of stainless steel (non-magnetic) rollers to simulate non-magnetic silicon nitride. Surface finish (Ra) of the order of 10 nm can be obtained. Some of the parameters of the process that effect the finish and material removal rate are discussed.

Key Words: Superfinishing, roller, polishing

1. Introduction

Finish, accuracy, and surface integrity of parts produced by conventional machining (i.e. tool harder than the workpiece) depend on the machine tool system which comprises the machine tool, cutting tool, workpiece, cutting conditions, and cutting fluid. For accomplishing higher removal rates or higher finishes, the machine tools need to be rigid, free from quasi-static errors (deflections) as well as dynamic errors (chatter or vibration), and workpiece and tooling errors. Often it is difficult to economically build machine tools that are extremely rigid, vibration free, and error free. With the introduction of many difficult-to-machine materials, such as hardened steels, nickel-, cobalt- and titanium-based superalloys oscillations in the cutting process (cyclic variation of forces) become inherent to the cutting process (cyclic chip formation) and can not be modified significantly by the machine tool system. Also, with the advent of advanced materials, such as ceramics and glasses very few cutting tool materials (including diamond and cubic boron nitride) with geometrically defined edges are capable of material removal effectively. Ceramics and glass are inherently brittle and failure of parts made from these materials are initiated by cracks formed during machining as well as by other defects.

To minimize the damage due to machining, it is necessary to process advanced ceramics under gentle conditions, i.e. very low forces. While improved machine tools will certainly facilitate in reducing deflections and chatter, need arises for controlling the force level. Also, the finishing operation has to be economically attractive. This led to the introduction of non-traditional machining where the cutting process is aided by a secondary source. For example, in ultrasonic grinding, the material removal operation is facilitated by the vibratory action. Similarly, in laser assisted machining, a laser compliments the cutting action. Magnetic field assisted polishing is one such non-conventional machining technology in which the cutting force is controlled by the magnetic field. Finish polishing is essentially accomplished without the need for designing expensive, rigid, ultra-precision, vibration free, and error free machine tools by incorporating the magnetic polishing elements necessary into the existing conventional machine tools, thereby minimizing the cost of new equipment. The process can thus be very effective and economical.

2. Magnetic Abrasive Finishing of Rollers

It is difficult to cost effectively finish advanced ceramics, such as silicon nitride, silicon carbide, and aluminum oxide by conventional grinding and polishing techniques, and also meet the requirements of high finish, accuracy, and minimal surface defects, such as microcracks. This has necessitated the development of an alternate manufacturing technology, namely, magnetic field assisted polishing. This new technique can be classified into two types. The first one is the magnetic abrasive finishing which uses a brush of magnetic abrasives for finishing [10]. The second type is the magnetic float polishing (also termed magnetic fluid grinding) uses a magnetic fluid which is a colloidal dispersion of subdomain magnetic particles in a liquid carrier and abrasives [12]. In this paper magnetic abrasive finishing of non-magnetic stainless steel rollers will be covered briefly. Other details are covered elsewhere [3].

Figure 1 is a schematic of the magnetic abrasive finishing apparatus. A cylindrical workpiece, such as a ceramic roller is clamped in the chuck of the spindle providing the rotary motion. The rollers can be magnetic or non-magnetic. Hence, this technique is applicable to both steel and ceramic rollers. For non-magnetic work materials, the magnetic field lines go around the workpiece through the magnetic abrasive while for magnetic materials they pass through the workpiece. Axial vibratory motion is introduced in the magnetic field by oscillating motion of the magnetic poles relative to the workpiece. Magnetic-abrasive conglomerate which is a mixture of fine abrasives held in a ferromagnetic material is introduced between the workpiece and the magnetic heads where the

finishing pressure is exerted by the magnetic field. Typically the size of the magnetic abrasive conglomerate is 50 to 400 μm and the abrasives are in the 1 to 10 μm range. Figure 2 is a SEM micrograph of a magnetic abrasive (KMX 80) whose mean diameter is about 80 mm and the size of the abrasive is 2-3 mm. With non-magnetic work materials, the magnetic abrasives are linked to each other magnetically between the magnetic poles N and S along the lines of magnetic force, forming flexible magnetic abrasive brushes as shown in Figure 3. Finishing action takes place predominantly in this region. To achieve uniform circulation of the abrasives, the magnetic abrasives should be stirred periodically. Both surface and edge finishing can be accomplished by the magnetic abrasive brushes. The process is highly efficient and the removal rate and finish depend on the workpiece circumferential speed, magnetic flux density, working clearance, workpiece material, size of the magnetic abrasive conglomerate including the type of abrasive used, its grain size and volume fraction in the conglomerate. The recent understanding of the tribo-chemical wear of silicon nitride suggests additional possibility of finishing ceramic rollers based on mechano-chemical action.

Figure 4 is a schematic of the magnetic field polishing showing the two-dimensional magnetic field distribution in the finishing zone of the process. The magnetic abrasive particles form a brush around the workpiece linking the N and S poles. The magnetic flux density is stronger around the non-magnetic workpiece (along the magnetic brushes) than through the workpiece. The magnetic abrasive at position "A" in Figure 4 is affected by the magnetic forces represented by the following equations [10]:

$$F_x = V c H \partial H / \partial x \qquad F_y = V c H \partial H / \partial y \qquad (1)$$

where, V is the volume of the magnetic abrasive particles,
c is the susceptibility of the particle,
H is the magnitude of the magnetic field strength at point A,
x, and y are coordinate points fixed at A,
and $\partial H / \partial x$, $\partial H / \partial y$ are gradients of the magnetic field strengths in the x and y directions

It is evident from Eq. 1 that the magnetic forces F_x and F_y are proportional to the volume of the magnetic abrasive particles, the susceptibility of the particles, the magnetic field strength, and its gradient. If the gradients are not equal to zero then magnetic abrasive particles are pushed toward the work surface. The magnetic force F_y actuates the magnetic abrasive particles to take part in the surface finishing of the workpiece. In addition, the force F_x is acting on the abrasive grain in the rotating tangential direction of the work surface by the cutting and frictional actions. The runoff of the abrasive grains from the working zone is prevented by the force F_y. It is also clear from Eq. 1 that, even if x is nonzero, the magnetic force will not act, if $\partial H / \partial x$, $\partial H / \partial y$ are equal to zero. Thus both susceptibility and magnetic field gradients are important in this operation. The larger values of magnetic strength gradients forces the abrasive grains to move towards the working zone thus preventing separation and splashing of the abrasive grains from the working zone.

3. Brief Review of Magnetic Abrasive polishing

Although the magnetic abrasive finishing process was originated in the U.S. in the 40's, it was in the former U.S.S.R. (Baron and his associates [2,5-8]) and Bulgaria (Mekedonski and his associates [6]) that much of the development took place in the late 50's and '60s. These researchers have shown that the technique can be applied to a wide range of products. In the 80's Japanese researchers (chiefly Professor Kato and his associates at Tohoku University [13], Professor Nakagawa and his associates at Tokyo University [1] and Dr. Shinmura and his associates at Utsunomia University [9-12]) followed this work and conducted research for finish polishing applications. For example, Takazawa, Shinmura, and

Hatano[9-10] have conducted extensive research on the magnetic abrasive finishing of rollers and the associated equipment. They studied the principles of operation, finishing characteristics under different conditions, and variousapplications of magnetic abrasive finishing. Shinmura et al [10] later extended these studies and designed various equipment for internal finishing of tubes, external finishing of rods, finishing of flat surfaces etc. However, all of Shinmura's work deals with ferromagnetic materials. In this paper we report resutls on a non-ferromagnetic material, namely, austenitic stainless steel.

4. Experimental Set-Up and Test Conditions

Figure 5 is a photograph of the experimental set-up of the magnetic polishing apparatus mounted on a Hardinge precision lathe. Figure 6 is a close-up of the apparatus showing key elements. The equipment consists of an electromagnet used for the generation of the magnetic field, magnetic heads, vibrator for axial motion of the magnetic heads, and a lathe chuck to hold and rotate the workpiece, and magnetic abrasives. A copper coil wound in the form of a solenoid is used for generating the magnetic field in the core. A low carbon (0.16%) steel is used as the magnetic core material. Current in the range of 0.5-2 A is passed through the copper coil. This corresponding to a magnetic flux density of 0.17 to 0.35 T with a non-magnetic workmaterial. The values of the magnetic flux density would be at least four times with a magnetic workmaterial. The magnetic heads are designed in such form that the magnetic field is concentrated with minimum leakage of the field taking place surrounding the air gap between the magnetic heads. A pneumatic air vibrator is used for providing the axial vibratory motion to the magnetic head. Typical frequency of vibration of the head is 15-25 Hz. The magnetic finishing equipment is mounted on a 1.5 hp Hardinge precision lathe with continuous speed capability from 500 up to 3000 rpm.

In the following the specifications of the equipment and test conditions used in this investigation are given.

Machine capacities	: 1.5 hp Hardinge Precision Lathe,
Roller speed	: 500, 1,000, and 2,000 rpm (corresponding to 0.32, 0.65, and 1.3 m/sec.)
Work material	:Non-magnetic stainless steel rods
Workpiece size	: 5-15 mm diameter x 120 mm long cylindrical roller
Polishing capacity	: 45 mm long
Current density	: 0 -2 A
Magnetic field density	: 0 -0.35 T
Magnetic pressure	: 0-30 KPa
Magnetic core	: 0.16% carbon steel
Magnetic abrasives	: Al₂O₃ abrasive (2-10 mm) in a matrix of iron particles (50-400 mm) (KMX80, M5), SiC, 400 mm Fe)
Lubricant	: Dry, oil, and zinc stearate

The workpiece is examined periodically for surface characterization using Form Talysurf, Talyrond, ZYGO laser interference microscope, and scanning electron microscope.

5. Test Results and discussion

Figure 7 shows the Talysurf traces of the as-received, ground stainless steel rod and the same rod finished by magnetic field assisted polishing. The roughness of the ground surface (Ra) is about 220 nm while that of the polished surface is about 7.6 nm. While it is possible to polish the surface of the stainless steel roller to a surface finish (Ra) close to 10 nm, the finish that can be obtained rapidly is in the 15 nm range.

In the following effects of some of the parameters in the magnetic abrasive finishing on the finish and material removal rates will be discussed. They include effect of bonded vs unbonded magnetic abrasive type, effect of lubricant, effect of magnetic flux density, and combined effect of rotational speed and axial vibration.

(a) Effect of Bonded and Unbonded Magnetic Abrasive Type With an Oil Lubricant

Magnetic abrasive can be used in the form of either a mechanical mixture (unbonded) of ferromagnetic material and abrasive or abrasives held in a ferromagnetic matrix (bonded) formed by sintering or other techniques. In the first case, under the influence of the magnetic field, the abrasives are loose and may move around freely within the constraints of the magnetic material adjacent to them. In the later case the abrasives are integral with the magnetic material and hence the movement of the abrasive is somewhat constrained. To examine the effect of bonded versus unbonded type abrasive mixtures on the material removal rate and finish tests were conducted with an oil based lubricant. In the bonded case, magnetic abrasive consisting of 40# iron and KMX80 was used. In the unbonded case abrasives consisting of 40# iron and 400# SiC (which is not physically bonded to iron) was used.

Figure 8 shows the variation of the surface finish (Ra) and material removal rate with finishing time for bonded and unbonded magnetic abrasives. Initially the material removal rates are high in both cases but drop to steady state levels with time. It can be seen that the removal rate with unbonded material is much higher than with the bonded material (the steady state value is about 15-20 times higher for the unbonded case). The higher removal rate is attributed to the availability of free abrasives that can scratch much deeper than the bonded abrasive. However, this results in much rougher surface with the unbonded abrasive (Ra of about 300 nm with unbonded magnetic abrasive compared to 20 nm with bonded abrasive). The material removal mechanism also appears to be different for these two cases.

As a strategy of using this technique for finishing, one should use unbonded abrasive if the initial finish is rough (say fine turned). This will enable higher removal rate which can be followed by finishing using bonded magnetic abrasives. However, if the initial surface is semifinished (say a ground surface) then bonded abrasive would be preferable for finishing.

(b) Effect of Lubricant:

Solid lubricant such as zinc stearate can be used to enhance the surface finishing efficiency of the process. The lubricant causes the abrasive brush to be more flexible and enhances its ability to produce better finish. Figure 9 shows the variation of finish with 0 w % (dry), 2 w %, 5 w % and 8 w % of zinc stearate. It can be seen that the finish increases with increasing zinc stearate content up to about 5 w % after which the finish decreases. Also, the time required to reach the best finish also decreases with increasing zinc stearate content. It also appears with increasing the amount of lubricant up to 5 w %, the surface finishing action is enhanced and same surface finish can be achieved in lesser time.

(c) Effect of Magnetic Flux Density

In the magnetic abrasive finishing process, the magnetic field is generated by an electromagnet. The source current density generates the magnetic field between the magnetic poles which in turn controls the magnetic force exerted by the abrasives on the rollers. The source current density can effect both the metal removal and the surface finish. Figure 10 shows the variation of surface finish (Ra) with finishing time for various magnetic flux densities. It can be seen that increasing the flux density from 0.17 to 0.37 T results in improvement in the surface finish. Also the surface finish improves rapidly with time and reaches a saturation level. It is also observed that increasing the magnetic flux density (current density) increases the removal rate up to certain extent beyond which it reaches a saturation value. In the experiments conducted with unbonded abrasives (40# Fe mixed with 1200# SiC), the source current used is 0.5, 1, and 2 A corresponding to the magnetic flux density of 0.17, 0.25 and 0.37 T respectively. Better surface finish (Ra less than 50 nm) and higher removal rate was observed in the case of 2A source current density.

(d) Combined Effect of Rotational Speed and Axial Vibration

The removal rate and the finish generated depend on both the rotational speed and the axial vibration (both amplitude and frequency). Without axial vibration and with only rotation of the workpiece, circumferential grooves will form. By introducing axial vibration, the resultant velocity will be changed which will result in cross hatching. The rotational velocity is given by p D w, where D is the diameter of the workpiece and w is the rotational speed; the vibrational velocity can be represented by 2 p a f Cos (2 p f t) where a is the amplitude and f is the frequency of the axial vibration. For maximum velocity Cos (2 p f t) would be unity and if one were to use an rms value it would be 0.707. By varying the rotational speed and axial vibration, one can generate different cross hatched patterns. Figure 11 shows the variation of removal rate and surface finish after 5 minutes of polishing with half included angle of the cross hatched pattern calculated from the resultant velocity. It can be seen that the removal rate is lowest with no axial vibration and increases with increase in axial vibration. At a given half included angle, higher the vibrational frequency, the higher the removal rate. So for higher removal rate one needs to increase the frequency/amplitude of axial vibration. It can also be seen from Figure 11 that maximum removal rates as well as the best finish occur at half included angle between 25 to 35 deg. Low (close to 0 deg.) and high (close to 90 deg.) half included angles result in low removal rate and poor finish. Figure 12 shows the theoretical variation of the half included angle with workpiece rotational speed for various pole vibration frequencies. It can be seen that at low pole frequency of vibration the workpiece rotational speed is low and the range of workpiece rotational speed is rather narrow to obtain half included angle in the 15 to 35 deg. range. To enable the use of higher workpiece rotational speeds and hence higher removal rates, one needs to increase both the pole vibration frequency and amplitude significantly.

91

6. Conclusions

1. Magnetic field assisted polishing apparatus can be incorporated on a conventional lathe and used for finishing non-magnetic stainless steels rollers. Consequently this process can be economical and cost effective.

2. The surface finish (Ra) of a ground rod can be finished to about 10 nm

3. While unbonded magnetic abrasives are found to yield higher removal rates, bonded magnetic abrasives are found to give better finish.

4. Increasing the weight percentage of zinc stearate in the magnetic abrasive was found to yield better surface finish up to a certain w % of zinc stearate. Also the time required for best finish was shorter with higher zinc stearate concentration.

5. Increasing the magnetic flux density was found to increase the rate of finishing as well as the best finish attainable.

6. Axial vibration of the magnetic heads was found to be critical for finishing by magnetic field assisted polishing. High removal rates and best finish were obtained with increase in the axial vibration (frequency as well as amplitude). Both axial vibration and rotational speed of the workpiece has to be taken into consideration for obtaining the best cross pattern that would give best finish as well as high removal rates. Half included angles between 15 and 35 deg. are found to be optimum for best finish and high removal rates.

7. Although stainless steel (non-magnetic) meets the requirements as far as simulation of non-magnetic silicon nitride rollers, there are significant other differences. The first among them is the nature of failure of these materials (plastic deformation is the primary mode in the case of stainless steel while brittle fracture, dislodgement of grains, microcracks, and viscous flow of the glassy phase in the case of silicon nitride). Also, work hardening of the stainless during polishing leads to fatigue cracks and removal of flakes of stainless steel material.

References

1. Anzai, M., Kawashima, E., Otaki, H., and T. Nakagawa," 1994, "Magnetic Abrasive Finishing of WC-Co Curved Surfaces," NIST Special Publication No. 847:415-424

2. Baron, J. M. 1975, "Technology of Abrasive Machining in a Magnetic Field," Masino-strojenije, Leningrad (in Russian).

3. Fox, M., Agrawal, K., Shinmura, T. and R. Komanduri, 1994, "Magnetic Field Assisted Polishing of Austenetic Stainless Steel Rollers," to be submitted for publication.

4. Konovalov, E. G. and G. S. Sulev, 1967 "Finishing Machining of part by Ferromagnetic Powder in Magnetic Field." Naukaitechnika, (in Russian)

5. Konovalov, E. G. and F. J. Sakulevich,1974, "Principles of Electro-Ferromagnetic Machining," Naukaitechnika, (in Russian).

6 Makedonski,. B. G. and A. D. Kotshemidov, 1974, "Schleifen im Magnetfeld," Fertigungstechnik und Betrieb, 24, H.4 230 - 235

7. Sakulevich, F. J. and L. M. Kozuro, 1978, "Magneto-Abrasive Machining," Naukaitechnika, Minsk (in Russian).

8. Sakulevich, F. J. and L. M. Kozuro, 1977, "Magneto-Abrasive Machining of Fine Parts," Vyssaja Skola, Minsk (in Russian).

9. Shinmura, T., Yamaguchi, H. and T. Aizawa, 1994, "A New Internal Finishing Process for Non-Ferromagnetic Tubing by the Application of a Magnetic Field - The Development of a Unit Type Finishing Apparatus Using Permanent Magnets," to be submitted to Trans.NAMRC -XXII

10. Shinmura, T., Takazawa, K., and E. Hatano, 1990, "Study of Magnetic Abrasive Finishing," Annals of CIRP, 39/1:325-328

11. Takazawa, K., Shinmura, and E. Hatano, 1983, "Development of Magnetic Abrasive Finishing and Its Equipment," MR 83-678. Proc. of the SME'S 12th Deburring and Surface Conditioning Conference, Orlando , Nov 8-10, 1983

12. Takazawa, K., Shinmura, and E. Hatano, 1985, "Advanced Development of Magnetic Abrasive Finishing and Its Equipment," Proc. of the SME'S Deburring and Surface Conditioning Conference '85, Orlando , (Sept 23-26, 1985) 30-46

13. Umehara, N. and K. Kato, 1990, " Principles of Magnetic Fluid Grinding of Ceramic Balls," Int. J. of Applied Electro-magnetics in Materials, 1 : 37-43.
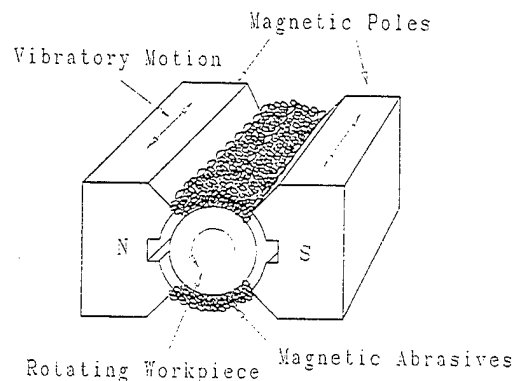
Figure 1 Schematic of the magnetic abrasive finishing apparatus.
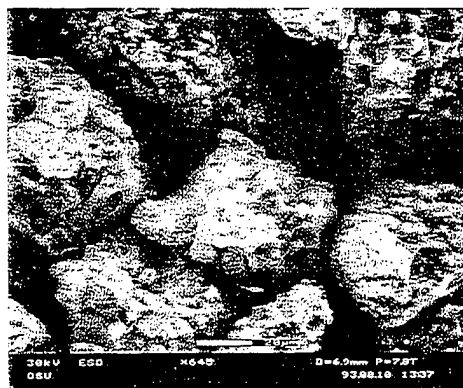
Figure 2 SEM micrograph of a magnetic abrasive (KMX 80)

Figure 3 Photograph showing flexible magnetic abrasive brushes formed by linking magnetic abrasives between the magnetic poles N and S with non-magnetic work materials
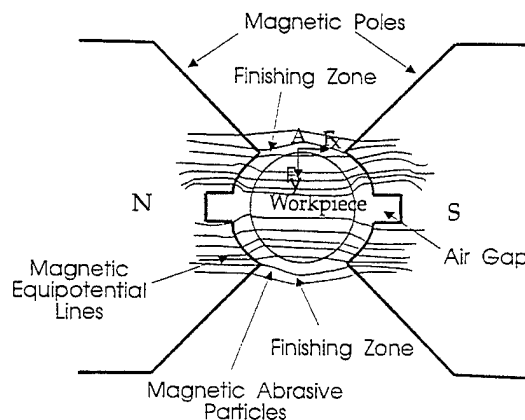
Figure 4 Diagram showing two-dimensional magnetic field distribution in the working zone of the polishing process [1].
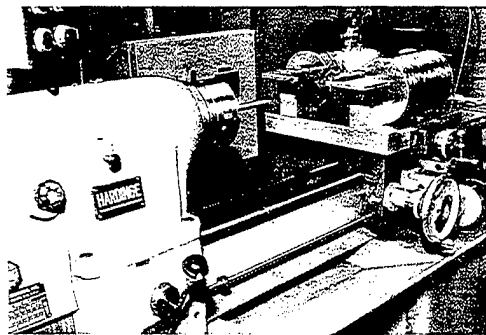
Figure 5 Photograph of the experimental set-up of the magnetic polishing apparatus mounted on a Hardinge precision lathe
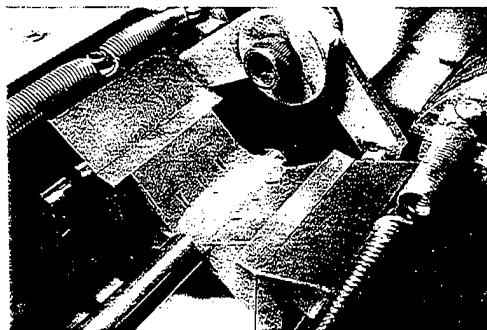
Figure 6 Close-up of the magnetic abrasive finishing apparatus
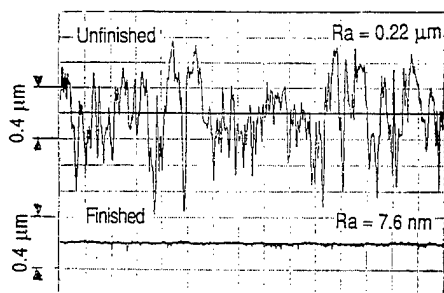
Figure 7 Talysurf traces of the as-received (ground) stainless steel rod and the same finished by magnetic filed assisted polishing
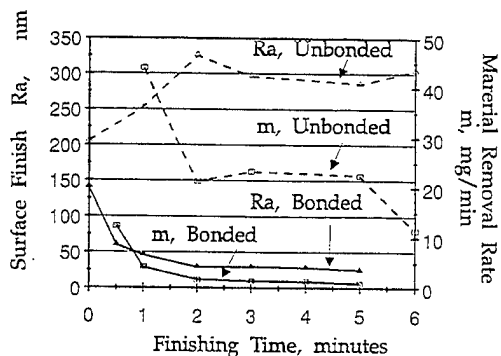
Test Conditions:
Surface Speed: 1.3 m/sec   Bonded Abrasive:
Flux Density: 0.37 T   80 w% Fe (40#) + 20 w% KMX 80
Lubricant: oil (SAE 30)   Unbonded Abrasive:
                              80 w% Fe (40#) + 20 w% SiC (400#)

Figure 8 Variation of the surface finish (Ra) and material removal rate with finishing time for bonded and unbonded magnetic abrasive
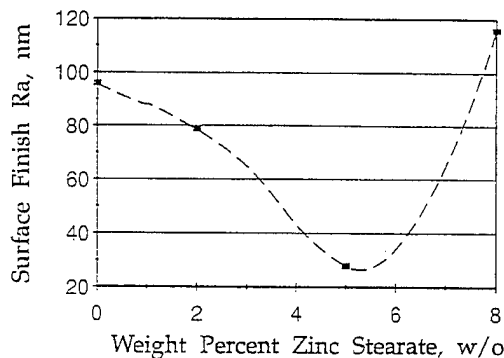
Test Conditions:
Surface Speed: 1.3 m/sec   Abrasive: KMX 80
Flux Density: 0.37 T   Lubricant: Zinc stearate

Figure 9 Variation of surface finish (Ra) with 0 w % (dry), 2 w %,5 w % and 8 w % of zinc stearate
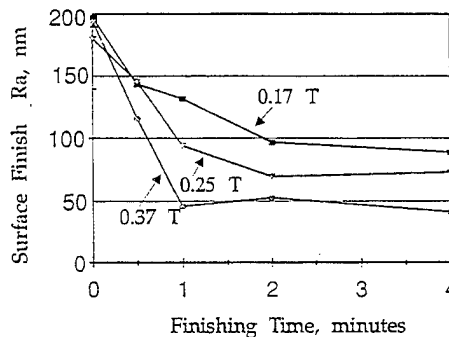
Test Conditions:
Surface Speed: 1.3 m/sec   Abrasive Type: 80 w% Fe (40#)
Lubricant: 3 w% Zinc stearate   + 20 w% SiC (1200#)

Figure 10 Variation of surface finish (Ra) with finishing time for various magnetic flux densities
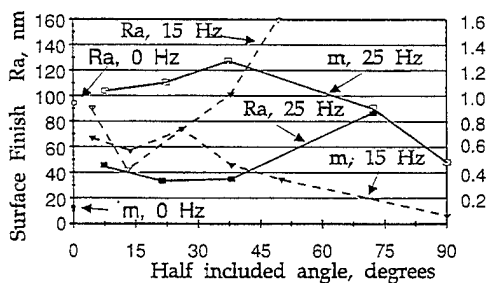
Test Conditions:
Surface Speed: 1.3 m/sec   Abrasive: 80 w% Fe (40#) + 20 w% M5
Flux Density: 0.37 T   Lubricant: 3 w% Zinc stearate

Figure 11 Variation of removal rate and surface finish after finishing for 5 min. with half included angle
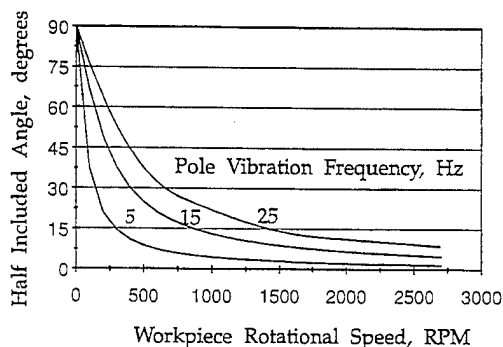
Figure 12 Theoretical variation of the half included angle with workpiece rotational speed for various pole vibration frequencies

93

APPENDIX F

ON THE MECHANISMS OF MATERIAL REMOVAL IN FINE

GRINDING AND POLISHING OF ADVANCED CERAMICS

R. Komanduri and T. R. Ramamohan

◆

Advancement
of Intelligent
Production

7TH INTERNATIONAL CONFERENCE ON PRODUCTION/
PRECISION ENGINEERING

◆

4TH INTERNATIONAL CONFERENCE ON HIGH TECHNOLOGY

◆

CHIBA, JAPAN, SEPTEMBER 15-17, 1994

◆

Edited by

Eiji Usui
Tokyo Denki University
Tokyo, Japan

ON THE MECHANISMS OF MATERIAL REMOVAL IN FINE GRINDING AND POLISHING OF ADVANCED CERAMICS AND GLASSES

R. Komanduri and T. R. Ramamohan

School of Mechanical and Aerospace Engineering
218 Engineering North, Oklahoma State University, Stillwater, OK 74078, U.S.A.

This paper deals with the fundamental considerations on the interactions between the abrasive and the work material as well as the micro-mechanisms of material removal and surface generation process in 'gentle' grinding and polishing (surface roughness in the range of a few nanometers rms) of advanced ceramics and glasses. In developing plausible mechanisms, an attempt is made to delineate the failure mechanisms operable in polycrystalline ceramics and glasses versus the metals. This is necessary because of the significant differences in the nature of bonding, microstructure and the tribochemistry, and, flaws generated during processing of these materials and their consequent effect on the failure mechanisms associated. For example, metals are fully dense crystalline materials with an orderly arrangement (both long and short range) of atoms in all directions. Plastic deformation, instead of brittle fracture, is by far the predominant mode of failure in these materials. Glasses, in contrast, are non-crystalline (or amorphous) and respond intermediate between a liquid and a solid, i.e. at room temperature they behave in a brittle manner but above the glass transition temperature in a viscous manner. Ceramics, though mostly crystalline, are different in the nature of bonding. For example, metallic bonding in the case of metals, no long range order in the case of glasses, and ionic and/or covalent bonding in ceramics.

Since ceramics are processed from powders using sintering, hot-pressing, or hot-isostatic pressing, they are less than theoretically dense. This results in some inherent porosity in the microstructure. Also, the grain boundaries generally consist of a weak, glassy phase. All these factors affect the strength and failure (deformation/fracture) behavior of these materials. Grain dislodgement, viscous flow at the grain boundaries, and microfracture of the crystals may be the predominant modes of failure than plastic deformation in this case. Also, under the high pressures and temperatures generated at the contacting points during polishing, mechano-chemical effects can play an important role in the material removal. In this investigation, effect of these factors are carefully considered in the development of a mechanistic model of the process. While plastic deformation is feasible at high temperatures and/or under high hydrostatic pressures, the wide range of defect structures present at various levels in most ceramics tend to favor microfracture, grain dislodgement etc. Further, in ceramics containing a glassy phase at temperatures higher than the glass transition temperature, viscous flow of the glassy phase takes place. Since the glassy phase is present at the grain boundaries, this can cause grain boundary sliding.

1. INTRODUCTION

High technology applications of advanced ceramics depend heavily on their superior strength at elevated temperature, chemical stability, and electronic properties of the components made from these materials. The application of glasses similarly depend on the optical properties. However, the conventional manufacturing and finishing processes (involving grinding followed by polishing) employed in the production of these components generate defects which adversely affect the properties and performance of components in service. Finishing, or more specifically, 'gentle' grinding and polishing are processes which involve the generation of a useful surface by intimate contact (generally sliding contact) of two surfaces (work material and abrasive) under the conditions of polishing and 'gentle' grinding. Depending on the atomic, chemical, and physical structure of the surfaces of the work material and the abrasive particles, the micromechanisms of material

failure differ. Tribological interactions are center to the polishing process. A fundamental understanding of the process can facilitate improvements in finishing practices and the efficiency of polishing or grinding. The following sections give brief introductions on the various topics of interests. They include a brief review of the polishing mechanisms for metals, 'gentle'/ 'ductile' grinding and polishing of advanced ceramics and glasses, the nature of bonding in various classes of materials, work materials (silicon nitride and glasses), abrasives, conventional polishing, advanced ceramics and glasses as work materials, and methods of finishing advanced ceramics.

2. POLISHING MECHANISMS FOR METALS

Polishing of metals and glasses has been of great interest for centuries in the production of optical components chiefly for mirror and lens applications. Consequently, the underlying mechanisms of material removal and finish generation were of obvious interest since then. The conventional technique of polishing involves the use of fine abrasive in a liquid carrier (usually oil) on a polishing scaife. By this process, a rough surface having visible irregularities is transformed into practically smooth surface to the naked eye. If the surface gives specular reflection, the height of these irregularities will be less than half a wave-length of visible light. Based on these observations several celebrated scientists formulated mechanisms of polishing. For example, Hooke, Newton, Rayleigh, and Herschel formulated polishing mechanisms for metals based on abrasive particles cutting away the asperities on an abraded surface, replacing them by a set of very much finer ones. The classical but controversial work on polishing was that of Sir George Beilby [1] who reported that the top surface of the polished material is different in structure from that of the underlying material. According to him, the polished surface has lost its crystalline nature and has apparently flowed over the surface filling the valleys on the surface. This can be demonstrated by metallographic polishing a metal specimen and etching it to reveal the microstructure, a procedure commonly practiced by metallurgists. It will be interesting to note that in addition to the microstructural details, the original pre-

polished scratches can be seen. This thin surface layer removed by etching is considered amorphous and commonly known as the Beilby layer. It is without doubt that such a layer exits on the surface of a polished surface. Whether or not this is an amorphous layer, or a highly strained layer, or an oxide layer is under intense debate even to day. The structure of the Beilby layer was examined by several researchers by electron diffraction. It showed that crystals near the surface have been broken down in size and reached the crystal size of the bulk metal only at a depth of several atom layers. The surface layer itself consisted either of very fine crystals or of an amorphous layer. It is, however, somewhat difficult to distinguish unambiguously between these two states by electron diffraction technique. Of course, the possibility of an oxide layer formation exits very much, however small the thickness may be. This can also be so, particularly with non-oxide ceramics, such as silicon nitride which is known to form such an oxide layer. Also, grain boundary phase consisting of magnesium silicate can smear on the surface due to viscous flow of the glassy layer at the grain boundaries and grain boundary sliding during polishing.

Samules and his associates [2] conducted extensive studies on polishing of metals and showed that mechanical polishing of metals with very fine abrasive is essentially the same as that of abrasion, i.e. microcutting is involved rather than surface flow. This is in marked contrast to the view of Beilby and others. Samules also pointed out that the striking piece of evidence (which many other researchers have acknowledged) in favor of Beilby's theory was that when a polished surface is etched the subsurface scratches reappear, suggesting that they were covered by a smeared polished layer. Samules suggested that the scratches are revealed because in an earlier stage of surface preparation, the scratches left intense local deformation which are not entirely removed by later polishing. He, thus, concluded that polishing involves removal of material by abrasion except at a finer scale. Samules, however, agrees that the abraded surfaces (i.e. polished surfaces) contain a damaged layer. It is clear that Samules made a subtle distinction by saying that a Beilby layer does not form but a

97

characteristic damaged layer of plastically deformed material does.

Bowden and Hughes [3] conducted extensive studies on polishing and concluded that polishing at high speeds is due to a high temperature softening or melting at the points of rubbing contact. They pointed out that at high speeds, surface softening followed by surface flow undoubtedly plays a major part. The rate of polishing will depend on the relative mechanical properties of the polisher (abrasive) and the work material at the temperature generated during the polishing process. Bowden and Tabor [4] pointed out that at low sliding speeds, microcutting or microabrasion may well be the dominant mechanism, as Samules suggested, while at high speeds, surface softening followed by surface flow undoubtedly play a major role. The mechano-chemical action that can take place at high polishing speeds between a given abrasive-work material combination and in the presence of a suitable polishing fluid will be an additional mechanism of polishing especially in the case of some ceramics.

Rabinowicz [5] conducted careful studies on polishing and based on that proposed an alternate hypothesis. Since the size of the abrasive as well as the force on each abrasive particle during polishing is rather small, Rabinowicz pointed out that this is generally below the minimum size needed for the formation of wear particles. Accordingly, material is removed from high spots to low spots on the surface by some mechanism not yet understood, but which appears to involve lateral displacement along the surface without the formation of a free surface, thus leaving a relatively smooth surface. Rabinowicz considered that it is probably because of the presence of the minimum load effect, rather than surface melting or softening effects, that polished surfaces are produced whose surface roughness is so much smaller than the average roughness normally attained during sliding.

3. 'GENTLE' / 'DUCTILE' GRINDING AND POLISHING OF ADVANCED CERAMICS AND GLASSES

Material removal in *conventional* grinding of hard, brittle materials, such as advanced ceramics and glasses is generally characterized by brittle fracture of the work material. Consequently, many brittle materials after grinding are finished by polishing to remove the damage caused in the previous operations. The development and use of very rigid, high precision machine tools (e.g. Nanocentre 600) are enabling finishing of hard, brittle materials without the need for subsequent polishing. Surface finish in the nanorange is being accomplished. As is well known, the performance of ceramic components will be strongly dependent on the processing technique used in their manufacture. It is hoped that ultraprecision grinding at fine depths of cut would produce nearly defect free surfaces that can result in improved performance and reliability of components.

While the technological advances are taking place, the mechanism of material removal is still not well understood and the evidence available has not been clearly established as to the mechanisms responsible for the material removal and the finish generated on these parts. For example, one sees long stringy chips when grinding glass. Are they due to viscous flow of glass above the glass transition temperature? Similarly, some plastic deformation is observed in the indentation of brittle materials. The plastic deformation, in this case, is it due to the presence of high hydrostatic component of stress underneath the indenter ? Different researchers have advanced different hypotheses and it is the objective of this paper is to present some evidence which will facilitate in a better understanding of this process.

It should be realized at the outset that although various glasses and advanced ceramics are brittle materials, they may respond differently under load. For example, glass can deform viscoplastically above the glass transition temperature. Ceramics containing the glassy phase may also deform viscoplastically this phase above the glass transition temperature Also, most of the ceramics are polycrystalline in nature and dislodgement of the grains and formation of pits may also occur in addition to any micro (and , macro-) cracks and plausible plastic deformation. Also, some porosity may be present in some of these ceramics.

The mechanics of material removal in grinding of ceramics and glasses can be

classified into two categories -- brittle fracture and plastic deformation. The former is analogous to indentation on a brittle material by a hard indenter, which involves two principal crack systems with lateral cracks responsible for material removal, and radial/median cracks for strength degradation. The latter is similar to the chip formation process in metal grinding, which involves scratching, plowing, and formation of chips. It is not clear if these polycrystalline, sintered materials ever deform plastically under the conditions of grinding or polishing. The loading on the individual grits (i.e. the state of stress at the cutting point), as well as the strength and fracture toughness of the work material are the governing factors that control the extent of brittle fracture. The radial/median cracks that initiate during loading of the indenter, and the elastic recovery and residual stresses during unloading are the driving forces for lateral cracks and the propagation of radial/median cracks. The lateral cracks at the bottom of the irreversibly deformed zone below the indenter propagate parallel to the surface of the specimen. The location and extent of the radial cracks depend on the geometry of the indenter.

There is one hypothesis recently advanced involving 'ductile' grinding of brittle materials. According to this hypothesis, all materials, regardless of their hardness and brittleness, will undergo a transition from a brittle to a ductile machining region below a critical grinding infeed rate. Below this threshold depth of cut, the energy required to propagate cracks is believed to be larger than the energy required for plastic deformation, so that plastic deformation is the predominant mechanism of material removal in grinding these materials. Hence, the term 'ductile' grinding of brittle materials.

There is an alternate hypothesis, known as 'gentle' grinding wherein plastic deformation is not involved in the material removal. According to this hypothesis, since the mode of deformation (plastic or brittle) depends on the state of stress and not on the magnitude of the stress, it is hard to comprehend that it will change (i.e. the mode of deformation) merely by changing the depth of cut, all other parameters remaining constant. Late Professor P.W. Bridgman of Harvard University had conducted extensive investigations and shown

convincingly that in order for a brittle material to deform in a ductile manner (at room temperature) a considerable hydrostatic stress component is required. Merely decreasing the depth of cut (scale effect) will only reduce the magnitude of the stresses without changing the stress state. It, therefore, follows that as the depth of cut in grinding is reduced, the superior surface obtained at light depths of cut are due to this effect and not necessarily due to plastic deformation. In other words, at light loads, microcracks may be forming but they may not propagate to form larger cracks. Consequently, grinding at extremely small depths of cut is termed as 'gentle' grinding' rather than 'ductile' grinding.

In the case of polycrystalline ceramics, the material removal mechanism in fine grinding or polishing may involve the dislodgement of grains(s) by fracture at the grain boundaries resulting in the formation of pits. Subsequent polishing involves removal of material till the pits are removed. However, many finished surfaces acceptable for optical applications, such as lenses contain multitude of pits. In the case of silicon nitride, in addition to the polycrystalline nature, one finds significant amounts of the glassy phase at the grain boundaries which will respond in a different manner than the bulk of the material. These factors have to be considered in the development of mechanistic model of the material removal.

Recent molecular dynamics modelling of the machining of silicon by researchers at Lawrence Livermore National Laboratory indicates that amorphization of the surface layers are possible due to chemical interactions between diamond and the silicon surface. Is this the age old Bilby Layer ? To address these issues, we need supporting evidence, new ideas, and new approaches.

4. ON THE NATURE OF BONDING

In bonding of materials the unfilled outermost electron shells are involved [6]. Elements that have eight electrons in the outer most shell (stable octet) are stable and do not form bonds with other elements easily. Elements with unfilled electron shells are not as stable and interact with other atoms in a controlled manner such that the electrons are shared or exchanged between the atoms to

achieve stable octet. This results in the three primary interatomic bonds exhibited by most solids, namely, *metallic, ionic, and covalent.*

Metallic bonding is the predominant bond mechanism for metals. It is also referred to as electronic bonding because of the valency electrons that are freely shared by all the atoms in the structure. Mutual electrostatic repulsion of the negative charges of the electrons keeps their distribution statistically uniform throughout the structure. It is the mutual attraction of all the nuclei in the structure for this same cloud of shared electrons that results in the metallic bond. As the valence electrons in a metal distribute themselves uniformly and since all atoms are of the same size, closed packed structures result. Since close packed structures contain numerous slip planes along which movement can occur during polishing, plastic deformation will be the predominant mode of material removal in the case of metals.

Ionic bonding occurs when one atom gives up one or more electrons and another atom or atoms accept these electrons such that electrical neutrality is maintained and each atom achieves a stable octet. Ceramic materials are either ionic or covalent bonded although many of them possess a combination of ionic and covalent bonding. The crystal structure of an ionically bonded material is determined by the number of atoms of each element required for electrical neutrality and the optimum packing based on the relative sizes (ionic radius) of the ions. Most of the ionic structures appear close packed and the bonding is nondirectional. The degree of ionic character can be estimated using the electronegativity scale developed by Pauling. The larger the electronegativity difference between atoms in a compound, the larger the degree of ionic character. Ionic compounds with more highly charged ions have stronger bonds and thus have higher strength, higher melting temperature, and higher hardness, e.g. alumina, zirconia. Material removal by microcleavage or microfracture may be the predominant mode of failure than by plastic deformation. In the case of polycrystalline materials, fracture and grain dislodgement may account for most of the material removal in polishing.

Covalent bonding occurs when two or more atoms share electrons such that each achieves a stable octet. Unlike metallic or ionic bonds, covalent bonds are directional. Each covalent bond consists of a pair of electrons shared between two atoms which produces directionality of the bond. Bonding of carbon atoms in diamond is an example of classical 100 % covalent bond. Silicon carbide (90 %) and silicon nitride (75 %) have significant fractions of covalent bonding while SiO_2 is 50 % ionic and 50 % covalent. Covalent bonded ceramics, depending on the strength of the bond and the nature of the structure, typically are hard, strong, and have high melting temperatures. Microcleavage and microchipping are the predominant modes of failure in these materials rather than plastic deformation. In the case of silicon nitride, due to strong covalent bonding, plastic deformation may not be the preferred mode, instead microchipping would be the mode of failure. However, the flow in this material, reported by many researchers, may in fact be due to the viscous flow of the glassy phase at the grain boundaries. In the case of polishing diamond, Tolkowsky [7] conducted extensive studies and concluded that material is removed during the process by micro-cleavage and that the abrasion resistance of the diamond is dependent on the position of the cleavage planes relative to the surface being polished. Wilks and Wilks [8] developed a block model illustrating the mechanism of material removal in polishing diamond. Accordingly, the polished surface of diamond is formed by a process of brittle fracture on a microscopic scale. Hence, the surface left by the removal of material will be rough and jaggered on a microscale with rugosites delineated at least to some extent by [111] cleavage planes.

From the above discussion on the nature of bonding in different materials, it is clear that metals should behave differently than ceramics during polishing. The former fails predominantly by plastic deformation while the latter by microchipping or microcleavage, grain boundary cracking, and grain dislodgements, etc. The presence of grain boundary glassy phase in some ceramics, as in the case of silicon nitride with an MgO sintering aid, should not be overlooked in formulating the mechanism of failure. Similarly, glasses, though brittle like ceramics, should behave entirely different than

either metals or ceramics as the structure in the former case is amorphous. At room temperature, failure should occur predominantly by brittle fracture and above the glass transition temperature by viscous flow. Thus many of the models advanced on polishing of glass and ceramics based on the application of polishing of metals should be viewed with skepticism and need to be rectified. It is the objective of the proposed investigation to address this problem in detail and present evidence to the micromechanisms of material removal in polishing of advanced ceramics and glasses before proposing a mechanism of polishing.

5. THEORETICAL CONSIDERATIONS

Fine polishing is essentially an interfacial phenomenon involving mating surfaces in sliding contact under the conditions of high contact pressures and high spot temperatures. Since ceramics are polycrystalline materials processed from powders using sintering or hot-pressing techniques, there can be flaws present in them at various levels with associated effects as follows:1) Stress concentrations in the lattice -- movement of atoms, microvoids, and crack nucleation; 2) Grain boundary interactions -- grain boundary sliding, wedge shaped crack formation, cavities, grain dislodgement, intergranular fracture, and flow of glassy phases; 3) Surface defects -- surface atoms, surface roughness, adsorbed species, surface reactivity and mechano-chemical reactions; 4) Indentation by abrasives -- brittle fracture and viscous flow. In crystalline solids, at high temperature, plastic flow is a possibility

The first mechanism which was not given enough attention in the literature is responsible for the failure of the solid at atomic and crystal lattice levels. These can be theoretically simulated by molecular dynamics modelling and experimentally verified using AFM/STM. The next mechanism operates at the microstructural level and indirectly accounts for major part of the material removal. The severity of the damage created depends upon whether the material is single crystal or polycrystalline and also on the amorphous (or glassy) phases contained in it. Surface defects and mechano-chemical action operate at the interface between the abrasive and the workpiece and can result in very smooth surfaces of the order of a few nanometers. Finally, indentation scratching is the process which is primarily responsible for material removal by the generation of lateral and ring cracks in the material (both surface and sub-surface). When these cracks meet at the surface of the workpiece wear fragment results which accounts for the material removal. At the macroscopic level this can be regarded as the principle mode of material removal under roughing and semifinishing conditions.

<u>Stress Concentrations at the Atomic Level</u> : Ionic solids contain point defects, and substitutional and interstitial impurities which introduce localized stress concentrations. As compared to the regular lattice constituents the activities and chemical potentials of atoms as well as electrons in these stressed regions are high which is responsible for diffusional mass transfer at moderate temperatures causing viscous/ plastic flow. However, when the solid is subjected to stresses, these localized stress concentrations act as discontinuities in the stress field, there by nucleating microvoids which can grow and coalesce leading to material removal by ductile transgranular fracture. Pure covalent solids can only fail by brittle cleavage fracture which occurs due to tearing of atoms on either side of the cleavage plane.

The absence of plasticity in crystalline ceramics can also be traced to the nature of their bindings. The mechanism of plastic flow in materials is due to the movement of the line faults in the crystal structure (dislocations) over certain crystal planes (slip planes). In metals because of non-directional metallic bonding, extensive movement of dislocations can take place even at low stresses. In covalent ceramics, the directional bond is between specific atoms, leading to a narrow dislocation and a high resistance to movement. In terms of microscopic parameters, it can be shown that the dislocation width is given by a function of the ratio of G/K where G is the shear modulus and K the bulk modulus [16]. This ratio is given by $G / K = 3 (1- 2v) / 2 (1 + 2 v)$, where n is the Poisson's ratio. For metals v is about 0.3 and G/K = 0.37, whereas in ceramics v = 0.1 and G/K = 1. Consequently, the yield stress, at which dislocation moves, is much higher for ceramics

than for metals, and approaches the fracture stress. Thus, covalent ceramics are brittle in the single and polycrystalline state. This should be the case with silicon nitride ceramic which is predominantly covalent.

In polycrystalline ionic materials, the adjacent grains are compelled to change their shape in the same manner, if voids are not to be formed at the boundaries. von Mises showed that this requires five independent slip systems. A slip system is the combination of a slip plane and a slip direction and an independent system is one that produces a deformation that cannot be produced by a combination of the others. Whereas metals have many slip systems, ionic crystals are only able to slip on a limited number of slip planes, due to the restriction that similarly charged ions must not be forced into near-neighbor positions such that cohesion would be lost. Consequently, polycrystalline ionic materials are brittle with cracks forming at the grain boundaries instead of plastic deformation.

Grain boundary Effects:

Grain boundaries constitute weak links in polycrystalline solids. While they are more cohesive in metallic and to some extent in ionic solids, they are very weak in covalent solids. A grain boundary can be considered as an interface and hence the tribological considerations applicable to free surfaces can be applied to them.

Glassy Grain boundary Phases: Presence of a glassy phase at the grain boundaries, even if it is in a few volume percent, can have a dominant influence on the deformation behavior of polycrystalline ceramics due to one or more of the following reasons: I) Above the glass transition temperature the glassy phase can flow in a viscous manner between the grain junctions promoting grain boundary sliding, 2). Since the liquid phase is often constrained in pockets at triple grain junctions, it can become stressed in hydrostatic tension and cause cavitation. 3) Grain boundaries can become separated by the lateral growth of penny shaped bubbles in the liquid film when a tensile stress is applied across the interface, and 4) The liquid may lead to accelerated crack growth along the interface if the meniscus along the

crack front becomes unstable and breaks into finger-like morphology.

Glassy liquid phases, although in minor amounts, are always present at the grain boundaries in hot pressed silicon nitride. It is possible that the temperatures and stresses associated with the machining process cause grain boundary sliding. The latter can produce large tensile stresses at triple junctions which will produce cavities [17] as shown in Figure 4. The arrow C shows the initiation of a cavity at a triple junction, and the other pair of arrows show the stress concentration arising from grain boundary sliding. The absence of dislocations indicates that all inelastic deformation is localized to the glassy liquid phase region.

Grain Pullout : Typically cracks formed during conventional grinding followed by polishing deteriorate the strength of ceramics. Some of these cracks are so deep that they can not be removed easily during further finishing operations. The situation becomes further complex in the case of silicon nitride or silicon carbide ceramics which are processed either by reaction bonding or by hot pressing. Presence of porosity in these materials gives rise to flaws whose size can be larger than critical dimensions. In such a case, even moderate stresses associated with the grinding and polishing can nucleate cracks at pore surfaces making it tear shaped. Further grinding propagates the crack which eventually links the various pores causing intergranular fracture. If, during this process, sub-surface cracks are also generated, possibly along the cleavage plane (0001), then the entire grain itself will be scooped off the surface of the particle, causing the appearance of a highly porous surface with large and irregular pores (actually pits) due to grain pullout.

Surface Interactions: Ceramics are ionically and/or covalently bonded solids. The ionic bonds are nondirectional similar to metallic bonds, but the absence of free electrons give ionic solids a brittle nature. The strength of the ionic bond is dependent on the polarizing power of the metallic ions. While these ions are well coordinated inside the lattice, their charges are not screened on the surfaces. Thus, the surface of any ionic compound contains firmly adherent chemisorbed films. Similar situation

exists in covalent compounds excepting that the chemisorbed films are more firmly held.

Metal ion sites on the surfaces of an ionic solid chemisorb oxygen from the surround-ing atmosphere. This results in a vacant metal site on the surface. Over a period of time the surface will be full of metal vacancies, and due to the concentration gradient metal ions diffuse to the surface. Thus a defective surface layer exists, the thickness of which depends on the extent of interdiffusion of oxygen and metal ions through it. In any case, the outermost surface layers of oxide formed will still have metal vacancies. The oxide layer on covalent ceramics will be thin, and firmly adherent to the surface, as diffusion through covalent solids is extremely difficult.

When a ceramic abrasive particle collides with ceramic workpiece, as in polishing, it is really the defective surfaces that come into contact, and any of the following situations can result:

Ionic Abrasive and Ionic Work Material: If the workpiece is harder than the abrasive, then the metal ions in the workpiece have more polarizing power, smaller radius, and higher charge as compared to metal ions in the abrasive. Therefore, diffusion proceeds towards the abrasive particle and eventually metal ions of the work piece are likely to be found in solid solution in the abrasive particles when the wear debris is analyzed. Smaller size of the abrasive and higher temperatures at the contact points will favor the material removal by solid solution formation. If there is no compatibility between both the metal ions then a compound formation is likely to take place at the interface and the material removal is possible only when the interface between the workpiece and the compound is weak and therefore, is fractured. Finally, if the abrasive can collide with the work piece with a very high energy, it can nucleate a crack on the surface which on further propagation can cause material removal.

If silica or glass is involved either as the work piece or as an abrasive, then a special situation arises. If there is sufficient force to break the more highly stressed bonds, fracture and deformation can occur at stress concentrations in directions perpendicular to the resolved tensile stresses, and viscous deformation can occur in the direction of maximum resolved shear stress. The cations within a glass are subject to diffusion and exchange just as they are in a crystalline silicate, more so when the surface to volume ratio is large (fine abrasive particles). The most common exchange is between sodium ions in the glass and other monovalent ions such as hydrogen ions from water or moisture. This exchange leads to stress concentrations and nucleates microcracks. The heat generated at the contact point during polishing can result in a chemical reaction between the abrasive and the glass. While the anions of the abrasive enter the glass and break up the network, the cations will occupy the interstices. There will be local viscosity changes which can result in material removal.

Covalent Abrasive and Ionic Work Material: Hard covalent abrasives such as diamond and silicon carbide are often used to polish the relatively softer ceramics and glasses. If the workpiece does not contain any flaws or stress concentrations (which is highly unlikely), and if the applied stresses are primarily compressive which are resolved into shear stresses superimposed with high hydrostatic pressures, it is possible to observe plastic deformation by slip. Tensile stresses on the other hand cause brittle fracture.

Heat generated at the contact point between the abrasive and the work piece can cause diffusion of the metal ions of the abrasive into the work piece. Depending on the charge difference of both the metal ions, compensating defects are likely to be formed in the surface layers of the work piece giving rise to stress concentrations. These stress concentrations can nucleate voids which eventually coalesce leading to material removal from the work piece. Also, if the polishing conditions are gentle and if the abrasives are ultrafine, it is possible to remove the material by chemo-mechanical reactions.

Covalent Abrasive and Covalent Work Material: There are only two possibilities. Either of the materials fracture by crack propagation, or if the polishing conditions are gentle and the abrasive is fine,resulting in the surfaces interaction by chemo-mechanical action results, leading to material removal.

103

It is by now evident that indentation by abrasives is the primary cause which leads to such effects as brittle failure by crack propagation, or plastic deformation. The real responsibility for the material removal rests with the defects at the surface or near-surface, microstructural, and substructural levels. In the proposed investigation an attempt will be made to link these aspects and arrive at a unified mechanistic model to explain the observed material removal during polishing.

If the solid that is being fine finished contains preexisting cracks or pits from the abrasive machining process, which is usually the case, then the polishing technique can only result in smoother surface but with the original pits enlarged and the cracks expanded. The polished surface is most likely to reveal huge pits some times linked by wide cracks. Further removal of the material by polishing can only worsen the situation. Therefore, it is proposed to use polishing techniques with less mechanical force, such as chemo-mechanical polishing, or use of magnetic fluids dispersed with active abrasive powders that can cause chemo-mechanical action which can yield better finish.

6. ADVANCED CERAMICS AND GLASSES AS WORK MATERIALS

Advanced ceramics and glasses of interest include alumina, silicon nitride, silicon carbide, zirconia, and representative glasses. The nature of some of these materials will be briefly discussed in the following:

Silicon Nitride

Silicon nitride, has for some time been at the forefront of developments in high-strength, high-temperature materials because of the possibility of using it in the development of more efficient, ceramic gas turbine able to run at temperatures far beyond the capability of conventional superalloys currently used. In addition, silicon nitride is also being used as balls and rollers in hybrid bearing applications.

Silicon nitride is predominantly a covalent (75 %) solid built up of Si_3N_4-tetrahedra joined in a three dimensional network by sharing corners β-Si_3N_4 has a hexagonal structure. Although it was originally believed that an α-form exists that form was found to be a defective silicon nitride containing one oxygen for every 30 nitrogen atoms, and is therefore regarded as an oxynitride. Silicon nitride can be processed by sintering, reaction bonding, hot-pressing, and HIP'ing. Yttria or magnesia are the common sintering aids. During the high-temperature hot-pressing of silicon nitride with small amounts of MgO addition, a complex glassy phase is found to form at the grain boundaries. It is primarily a magnesium silicate modified by Ca, Fe, Al, and other impurities initially present in Si_3N_4. At temperatures around 1100 ^oC grain boundary sliding occurs under loading. Additions of yttria to Si_3N_4, generally leads to a crystallization in the glassy phase at the grain boundaries instead of pure glassy phase with MgO. However, the oxidation resistance of this material was found to be inferior to those with MgO additions [9]. For this reason, MgO added Si_3N_4 is increasingly used in high temperature applications.

Hot-pressed Si_3N_4 is produced either by conventional uniaxial hot-pressing or HIP'ing. One starts with an α-Si_3N_4 powder and adds a densification aid, such as MgO, Y_2O_3 or $SiBeN_2$. Under pressures of 14 MPa and temperature in the range of 1650 ^oC to 1750 ^oC some of the α-Si_3N_4 reacts with the additive and the thin layer of SiO_2 that coats each particle of Si_3N_4, producing a liquid silicate in which the remaining α-Si_3N_4 dissolves and re-precipitates as elongated β-Si_3N_4 grains. On completion of the α to β transformation, the elongated β-grains are surrounded with residual silicate oxynitride grain boundary phase. The elongated nature of these grains, that are typically 0.5 to 4 μm, gives hot-pressed Si_3N_4 its high strength.

The apparent limitations of the hot-pressed Si_3N_4 are due to the nature of the grain boundary phase and not intrinsic to the Si_3N_4 [10]. So, attention was focussed on controlled modification of the grain boundary , such as grain boundary crystallization in hot-pressed Si_3N_4 with Y_2O_3 additions. While such a modification was found to provide higher strength at both room and elevated temperature (1400 ^oC) as well as better creep and oxidation resistance, this material was

found to suffer from an intermediate temperature oxidation (1000 °C) problem. This material is also found to be difficult to finish by grinding and polishing. Consequently, complex parts made of this material are rather expensive, once again shifting the emphasis to Si_3N_4 with MgO additions.

Relatively pure Si_3N_4 material was found to be elastic to fracture exhibiting practically no plasticity. This is understandable in view of the predominantly non-ionic nature of bonding in this material. Impurities in the material seem to enter into the grain boundary glassy phase and lower its viscosity. Thus the high-temperature mechanical properties of hot-pressed Si_3N_4 appear to be controlled by the viscous grain boundary phase, the viscosity at a particular temperature being controlled by impurities, and more than likely, the hot-pressing aid. Grain boundary sliding is the suggested mechanism for subcritical crack growth, plasticity, and creep.

Glasses

Glasses are a class of inorganic materials whose physical state is intermediate between a liquid and a solid. They are mainly silicates or borates containing metallic ions. In contrast with other solid materials, which are crystalline, glasses are non-crystalline (amorphous or vitreous). Glasses can be distinguished from a supercooled liquid in that the latter has nearest neighbor atoms that are randomly organized. In other words, there is a short range order in glass but no long range order (or periodicity) as in other crystalline materials. On cooling a liquid to the glassy state there is no crystallization and no continuous change in specific volume and mechanical properties. However, a transition at the glass transition temperature, does occur in some properties. Rigidity in a glass is achieved by a steady state increase of viscosity with falling temperature. The glassy state is a non-equilibrium one and is only achieved because crystallization is prevented by rapid cooling through a temperature range just below the thermodynamic freezing point, i.e., the temperature at which crystalline phases would start to form if time were allowed for equilibrium. The basis unit of the glasses is a tetrahedron with the small silicon ion surrounded by four oxygen anions. In the glassy state adjacent tetrahedra share corner oxygen atoms to form an irregular three-dimensional network. Glass is a Hookean solid if loaded quickly and a Newtonian liquid under slow rates of deformation. Whether a glass is behaving predominantly elastically or viscously depends on the duration of the loading in relation to the relaxation time. At room temperature under short term loading glass is elastic to fracture. Because of the inability of glass to deform plastically the high local stress at the tip of the crack causes it to propagate at a very rapid rate, the small energy of the fracture surfaces being obtained entirely from the elastic energy surrounding the material. Above the glass transition temperatures (400-600 °C) the viscosity is reduced significantly and glass behaves as a viscous fluid at normal rates of straining.

7. METHODS OF FINISHING ADVANCED CERAMICS

Conventional Polishing

Conventionally, ceramic and glass components are finished using diamond abrasive grinding and diamond lapping. These operations, although give smooth surface finish, result in several flaws such as pits, subsurface cracks which affect the intended performance of the components. The last decade has seen the emergence of new manufacturing techniques for the finishing of ceramics and glasses to a mirror finish, particularly in Japan. To day, considerable work is in progress on the magnetic field assisted polishing and mechano-chemical polishing which are all employed for the finish polishing of ceramics and glasses.

Ultra Fine Polishing Techniques.

Mirror finish on a component is achieved by the progressive removal of the surface undulations using abrasive grains. The traditional polishing methods employ large abrasive grains (a few micrometers in diameter) and high polishing forces which generate flaws and deep scratches affecting the performance of the glass and ceramic components. As a solution to this problem, novel precision

polishing techniques using abrasives in a magnetic fluid, or soft abrasives in mechano-chemical polishing, highly active fine abrasives under gentle forces in 'gentle' grinding were developed. The latter, presumably takes place due to mechano-chemical reactions at the contacting surfaces between the abrasive and the work material.

Mechano-Chemical Polishing

In order to avoid scratches or grinding damage in brittle materials, a novel polishing principle based on the use of abrasives softer than the workpiece was developed [10]. In this technique, a hard brittle material (e.g. most ceramics and some semiconducting materials, such as silicon) is polished with a softer abrasive. Since such an abrasive cannot damage or scratch the workpiece, the technique yields damage free and scratch free surfaces. Even though the abrasive used in this method is soft, the rate of material removal is often comparable to that achieved with the harder abrasives. One proposed explanation is that chemical reactions activated by mechanical action occur at the points of contact between the abrasives and workpiece because such contact points are subjected to high contact temperatures and pressures. This new method has been named as mechano-chemical polishing or chemo-mechanical polishing [11].

Mechano-chemical polishing method combines chemical and mechanical actions between soft abrasive grains and harder work material for providing smooth surface finish. A typical model of the mechano-chemical reaction is shown in Figure 1. It shows the activation of chemical reaction between a soft abrasive and a hard work material at the contacting points (i.e. in the micro-reaction zone) where high temperatures and high pressures are generated. After the reaction, the reaction product is removed along with the soft abrasive grain due to mechanical forces. Therefore, this mechanism can be controlled by controlling the mechano-chemical reaction rates,i.e., by selecting a proper combination of soft abrasive grains and hard work material, and sliding conditions such as polishing pressure, contact temperature and sliding speed.

Chemo-mechanical polishing was demonstrated for the polishing of single crystals of silicon, quartz, alumina, silicon nitride, and silicon carbide [12-15]. Vora et al.[12] reported a damage and scratch-free polishing method for silicon nitride using iron oxides (Fe_2O_3 and Fe_3O_4). Suga et al.[14,15] made a survey of other oxides and discovered that Cr_2O_3 is a more suitable abrasive for chemo-mechanical polishing of silicon nitride.

8. RESULTS

As pointed out earlier, some researchers consider the mechanism of material removal in grinding at low depths of cut due to plastic deformation of the ceramic. However, the arguments are somewhat circuitous and the evidence is far from direct. With this in view we have examined a range of glasses and ceramic materials to investigate the mechanism of material removal. Figure 2 (a) is a glass surface ground on a Rank-Pneumo sub-micron diamond grinding machine (ASG 2500) using a diamond grinding wheel. The surface finish is considered excellent and of optical quality. To the naked eye, the surface appears highly polished and smooth. The surface roughness is 32.23 nm (rms). However, on careful examination in the environmental scanning electron microscope (ESEM) which neither requires the sample to be conductive nor a conducting coating for non-conducting materials, we find the surface to be far from smooth. We observed several pits and parallel grooves corresponding to the feed marks of the grinding wheel made during the cross feed of the diamond wheel past the glass surface [Figure 2 (a)]. At higher magnification, it appears that some of the pits are filled by material [Figure 2 (b)] smeared over them. The visco-plastic nature of the glass may play an important role in the material removal mechanism. We have then examined the surface using a ZYGO laser interference microscope using a 20 x Fizeau lens. The peak to valley distance is about 306 nm and the rms finish is about 32.23 nm.

Figure 3 (a) is a scanning electron micrograph of a glass ball polished by magnetic float polishing. The surfaces of these balls are very smooth but in some areas pits are formed by microfracture [Figure 3 (b)]. Note also the fine scratches, the nature of which would be of interest in the analysis. Figure 4 (a) is a scanning electron micrograph of an aluminum

oxide ball polished by conventional methods. It can be seen that the finished surface contains several pits. Figure 4(b) is a scanning electron micro-graph of a pit at higher magnification showing dislodgement of individual crystallites. In addition, submicron sized scratches in random directions can be seen. These appear to be responsible for the finishing of the balls while the formation of large pits appear to be responsible for material removal. However, once these pits are formed, the polishing process for finishing requires that all these pits be removed which would be a time consuming process involving several hundred hours as currently experienced. It may be necessary to investigate alternate strategies for obtaining the required finish by not damaging the surfaces so severely by the formation of multitude of pits during rough polishing.

The smooth surfaces obtained in grinding Si_3N_4 with fine diamond abrasive is interpreted by some researchers as the change in the mechanism of material removal from brittle to ductile. It should, however, be noted that Si_3N_4 ceramics have a glassy phase and the smooth surface can be due to viscous flow of the glassy phase on the surface of the ceramic. In fact, when examined in the electron microscope, this layer appears as a transparent layer.

ACKNOWLEDGMENTS

REFERENCES

1. Beilby, G, "Aggregation and Flow of Solids," Macmillan and Co, London (1921)

2. Samules, L.E., "Metallographic Polishing by Mechanical Methods," American Elsevier, New York, NY, 2nd Edition (1971)

3. Bowden, F. P., and T. P. Hughes, Nature, 139 (1937) 152

4. Bowden, F. P., and D. Tabor, "The Friction and Lubrication of Solids," Parts I & 2, Oxford University Press, Oxford, U.K. (1964)

5. Rabinowicz, E.,"Friction and wear of Materials,"John Wiley & Sons, New York, NY (1965)

6. Richerson, D. W., "Modern Ceramic Engineer ing Marcel Dekker, Inc., New York, NY (1982)

7. Tolkowsky, M., D.Sc Thesis, University of London (1920)

8. Wilks, J., and E. Wilks, "Properties and Applications of Diamond," Butterworth-Heinemann Ltd., Oxford, U.K. (1991)

9. Lange, F. F. "Strong, High Temperature Ceramics,"Annual Review of Materials Science, 4 (1974) 365-390

10. Leatherman, G. L., and R. Nathan Katz, " Structural Ceramics: Processing and Properties,"in Superalloys, Super Compo sites, and Super Ceramics, Academic Press Inc. (1989) 671-696

11. Yasunaga,N.,Ohara,A and O, Imanaka, " Study of Mechano-chemical Effect on Wear and Its Application to Surface Finishing," J. of JSPE, 44,(1978)77-83. (in Japanese).

12. Vora,H.,Orent,T.W. and R.J. Stokes, " Mechano-chemical Polishing of Silicon Nitride," J.   Amer. Ceram. Soc. 65, No. 9,(1982) C140-C141.

13. Suga,T.,Suzuki,S. and K, Miyazawa," Mechano-chemical polishing of Sintered Silicon Nitride," J.JSPE, 55, No.12,(1989) 2247-2253.

14. Kikuchi,M.,Takahashi,Y.,Suga,T., Suzuki, S. and Y. Bando, " Mechano-chemical polishing of Silicon Carbide Single Crystal with Chromium(III) Oxide Abrasive," J. Amer. Ceram.Soc., 75, No.1,(1992)189-195.

15. Suzuki,K., Uematsu,T., Ohashi,H. ,Kitajima,K., Suga,T. and O,Imanaka, " Development of a New Mechano-chemical Polishing Method with a Polishing Film for Ceramic Round Bar," Annals of the CIRP, 41/1,(1992) 339-342.

16. Wyatt, O. H., and D. Deew-Hughes, "Metals, Ceramics, and Polymers," Cambridge University Press, Cambridge, U. K. (1974)

17. Tsai.R.L, and R. Raj, "Creep fracture in ceramics containing small amounts of a liquid phase.",in " Perspectives in Creep Fracture.", Ed. M.F. Ashby and Brown.L.M, Pergamon Press, Oxford, (1983) 33-70.

18. Kayaba,T.,Kato,K. and Y. Nagasawa,." Abrasive Wear in Stick-slip Motion," Proc. Int. Conf. on Wear of Materials, San Francisco, California, ASME (1981) 439-446.

19. Kayaba,T. and K, Kato, " The Adhesive Transfer of the Slip-Tongue and the Wedge," ASLE Transactions, 24, 2(1983) 164-174.

20. Kayaba,T.,Hokkirigawa,K. and K. Kato, " Analysis of Abrasive Wear Mechanism by Successive Observations of Wear Processes in a Scanning Electron Microscope," Wear, 110,(1986) 419-430

21. Kato,K.,Hokkirigawa,K.,Kayaba,T., and Y. Endo, " Three Dimensional Shape Effect on Abrasive Wear," Transaction of ASME, J. Tribology, 108,(1986) 364-351.

22. Hokkirigawa,K.and K. Kato," An Experimental and Theoretical Investigation -- Ploughing, Cutting and Wedge Formation During Abrasive Wear,"Tribology International, 21,(1988)51-57.

23. Hokkirigawa,K., Kato,K. and Z.Z. Li, " The Effect of Hardness on Transition of Abrasive Wear Mechanism of Steels," Wear, 123 (1988) 281-288.

24. Hokkirigawa,K.,Kato,K. and S. Araya, " The Transition of Microscopic Wear Mode of SiC during Repeat Pass Sliding in SEM," Proc. Japan Int. Trib. Conf., Nagoya (1990) 1425-1430.

25. Hokkirigawa,K.,Kato,K.,Kitsunai,H. and M. Mizumoto, "Microscopic Wear Mechanism of Alumina and Silicon Nitride Observed in the FE-SEM Tribosystem," Proc. Japan Int. Trib. Conf., Nagoya,(1990)1413-1418.

26. Doy-Karaki,T., Optical Technology Contact, 29, 12 (1991) 674. (in Japanese)
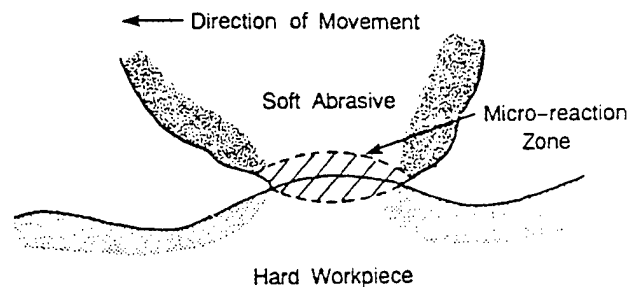
Fig. 1   Model of the mechano-chemical process (after Yasunaga et al [11])
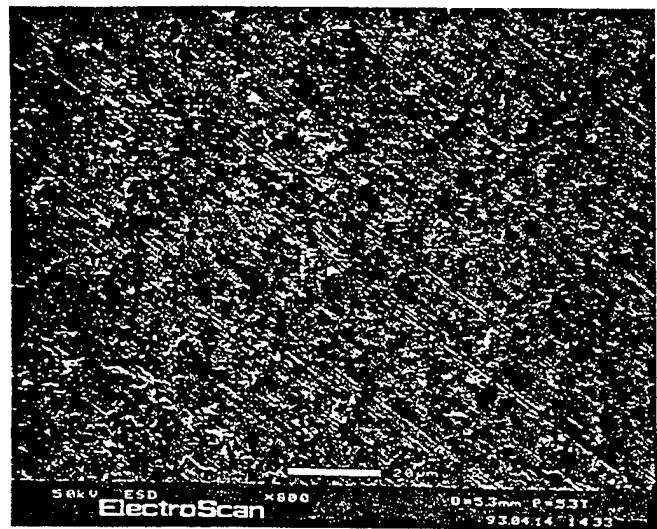

Fig. 2 (a)   Scanning electron micrograph of a glass surface finished by ultra-precision grinding
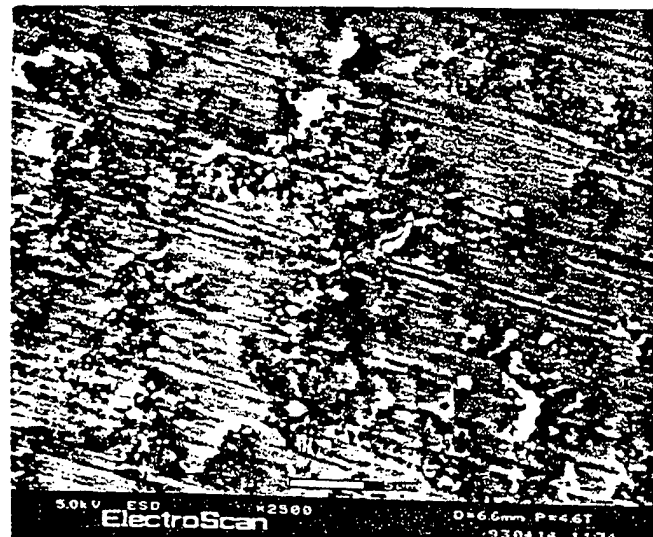
Fig. 2 (b)   Scanning electron micrograph at higher magnification of a glass surface finished by ultra-precision grinding showing filling of some pits.
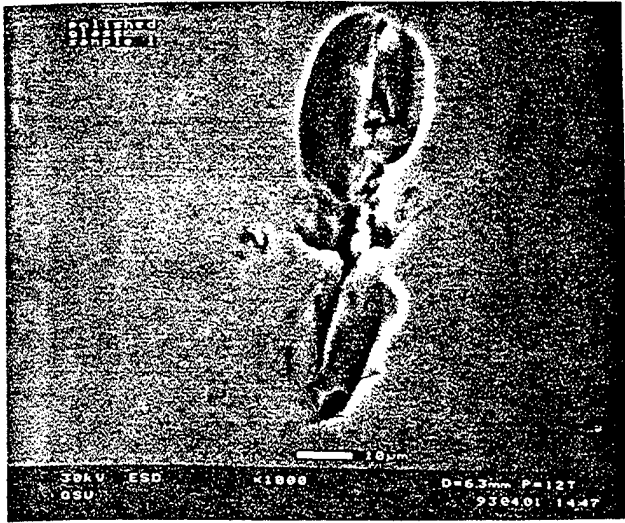
Fig. 3 (a)   Scanning electron micrograph of a glass ball polished by magnetic float polishing showing pits formed by fracture.
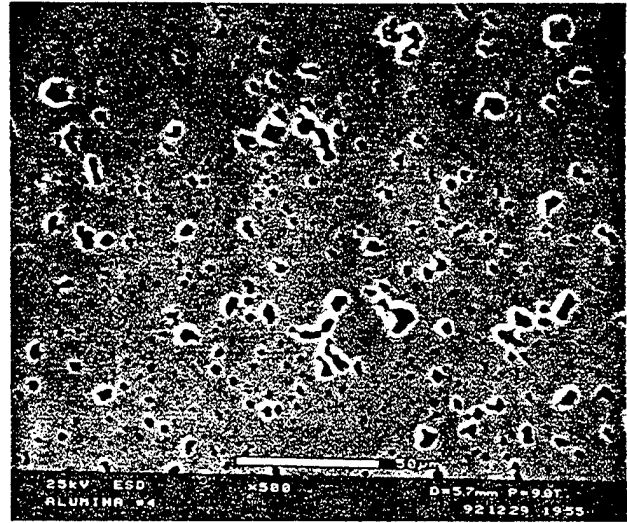
Fig. 4 (a)   Scanning electron micrograph of an alumina ceramic polished by conventional techniques showing numerous pits

Fig. 3 (b)   Scanning electron micrograph of a glass ball at higher magnification showing random scratches formed during polishing.

Fig. 4 (b)   Scanning electron micrograph at high magnification showing dislodgment of individual crystallites

109

APPENDIX G

ON THE MATERIAL REMOVAL MECHANISMS IN
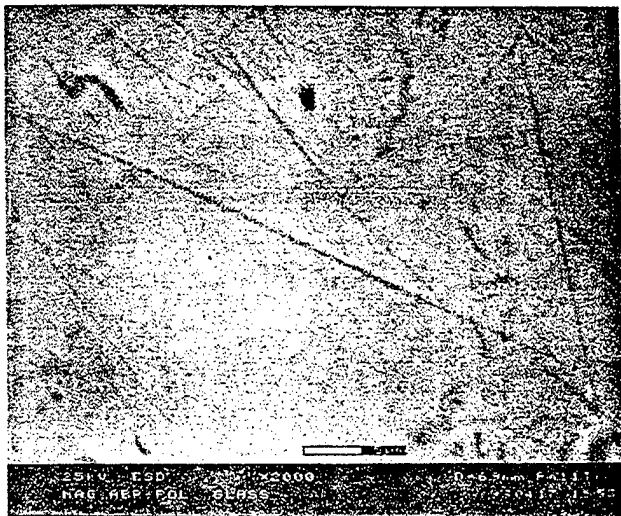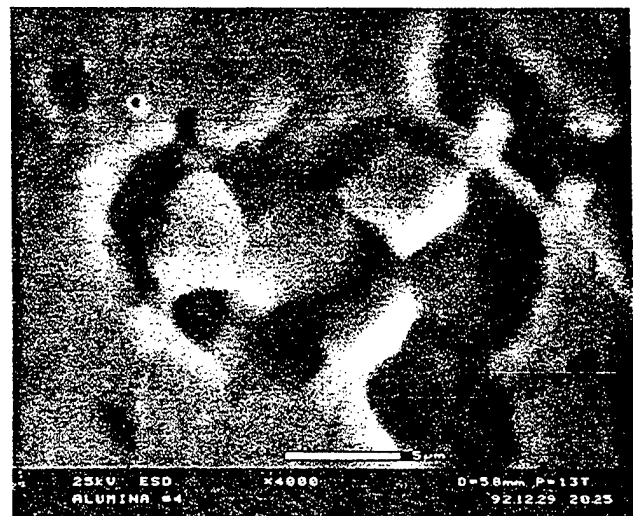
POLISHING OF ADVANCED CERAMICS

N. Umehara and R. Komanduri

セラミック球の磁性流体研磨における材料除去機構

東北大工　　　　正会員※梅原　徳次

オクラホマ州立大　　ASME会員　Ranga Komanduri

1. 緒　言

近年，超高速及び超精密軸受用転動体として，セラミック球の使用が期待されている．しかし，セラミックスは，加工損傷を少なくするため，ダイアモンド等の高価な超砥粒を用いてゆっくりと研削及び研磨されなければならないため，その加工コストは非常に高く，セラミック玉軸受を広く利用するための障害となっている．この問題を解決するため，著者の一人と加藤は，磁性流体研磨を開発し，これをセラミック球の研磨に応用した．その結果，窒化ケイ素球の研磨において，安価な炭化ケイ素砥粒により，従来法と同程度の真球度（0.1μm）の球を，約40倍の研磨率で仕上げることに成功した[1]．また，我々は種々の材料及び形状の加工物に応用し，優れた研磨特性を得た[2]-[4]．しかし，未だにその研磨機構は不明であり，更に高精度高能率の研磨を望む場合，その研磨機構を明らかにする必要がある．

近年，Childsらは，セラミック球の磁性流体研磨における駆動軸とセラミック球の転がりすべり運動に注目し，研磨体積が，駆動軸と球のすべり距離に比例することを示し，砥粒が2体アブレシブ摩耗と同様の役割であることを示した[5]．しかし，材料除去機構については，言及していない．また，Gardasらは，窒化ケイ素球のラッピングの研磨機構を明らかにするために，機械的特性値（ビッカース硬さ，破壊じん性値）の異なる窒化ケイ素球を用意し，その研磨体積が，Evansらにより提案されたパラメーターに大きく影響を受けることを示し，セラミックの従来のラッピングによる材料除去機構が連続したラテラルクラックの連結によるものであることを示唆した[6]．セラミック球の磁性流体研磨も，球と工具との転がりすべり条件下における研磨であり，同様の材料除去機構であることが考えられる．

そこで，本研究では，機械的特性の異なるセラミック材料として，一般的に構造用材料として用いられるジルコニア，窒化ケイ素及びアルミナにおいて磁性流体研磨を行い，その材料除去機構について検討した．

2. 実験装置及び実験条件

セラミック球の磁性流体研磨装置の概略図を図1に示す．図1において，ガイドリングは，短冊型組み合せ磁石の上に置かれ，その中に浮子，セラミック球，砥粒を含む磁性流体が図の様に入っている．セラミック球は浮子上にガイドリングの内周に沿って並べられている．上部の駆動軸は上下に移動する事ができ，所定の位置まで下げることで，浮子と球の磁気浮揚力より与えられる加工荷重が決定される．この荷重はロードセルにより測定され，研磨時には一定に制御される．また，駆動軸は，NCフライス盤のチャックに取り付けられ，回転させられる．その結果，セラミック球は，ガイドリングに沿って

図1　セラミック球の
磁性流体研磨装置概略図

表1　セラミック球の諸特性

Materials	PSZ	Si3N4(J)	Si3N4(N)	Al2O3
Sintering process	PLS	HIP	HIP	PLS
Initial diameter,mm	10.81	10.29	13.45	9.46
Density, g/cm³	6.0	3.2	3.2	3.9
Hv, GPa	11.8	16.7	19.6	17.6
K1c, MN/m^{1/2}	10	5.5	5.4	4.0
E, GPa	220	305	310	400

(a)PSZ   (b)Si3N4(J)

(c)Si3N4(N)   (d)Al2O3

1μm

0.1mm
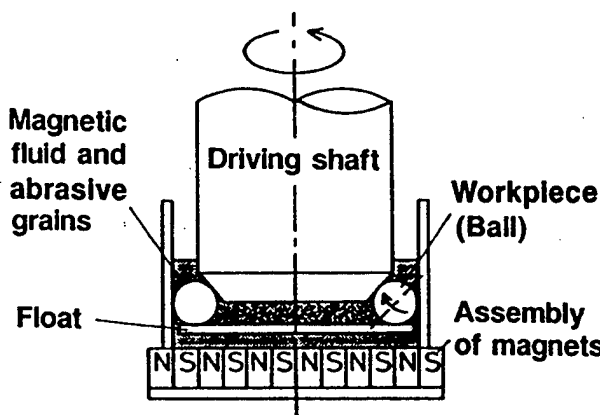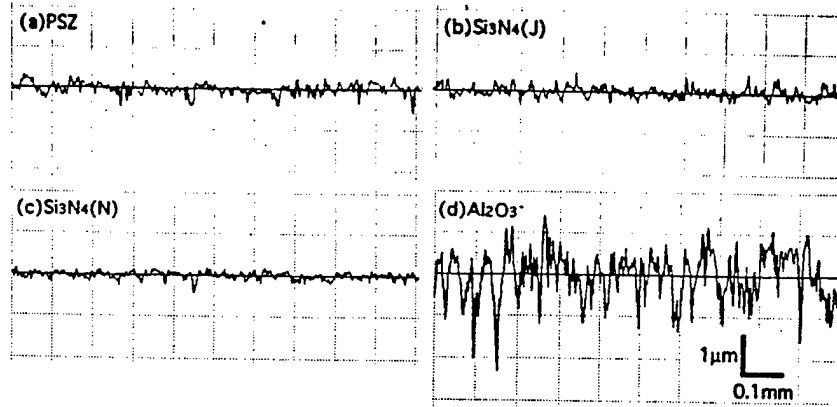
図2　研磨後の各セラミック球の粗さ曲線

図3　研磨率と表面粗さ

自転，公転し，その際研磨される．異なる機械的特性を有するセラミックス材料として，部分安定化ジルコニア（PSZ），窒化ケイ素2種類(Si3N4(J),Si3N4(N))及びアルミナ(Al2O3)が用いられた．それぞれの球に対し，1N/ballの荷重，2000rpmの回転速度で，研磨時間は1回90分とし，砥粒GC#400を用いて研磨した．磁性流体は，水ベースのW－45である．研磨が終わる毎に磁性流体と砥粒は新しいものと取り替えられた．研磨終了後，球を水により超音波洗浄し，マイクロメーターで1個の球に対して任意の10カ所の直径を測定し，平均値をその球の平均直径とした．各セラミック球に対し，直径不同が減少しなくなったところで研磨を終了し，駆動軸，ガイドリング，浮子を新しいものと取り替えた．

3．実験結果

3.1　平均直径と研磨時間の関係

　各セラミック球の直径不同は，研磨の進行に従い減少し，ある一定値となるが，その際，研磨率は，直径不同が変化しても，平均直径の研磨時間に対する変化量はほぼ等しかった．そこで，本研究では，平均直径の研磨時間に対する減少量を研磨率（μm/min）として表わす．ここで，研磨の進行にともなう直径の減少量は，球の直径に比べて著しく小さいことから，この研磨率（μm/min）は，体積減少量より表わす研磨率(mm³/min)にほぼ比例する．

3.2　表面粗さ曲線

　図2に，直径不同が一定となり，実験を終了した際の，各セラミック球の表面粗さ曲線を示す．図より，アルミナの表面粗さが，他の3つのセラミック球に比べて，著しく大きいことがわかる．

3.3　研磨率及び表面粗さ

　図3に，各セラミック球の研磨率と，図3より得られた研磨後の各セラミック球の最大高さ粗さ Rmax を示す．図において，横軸の材料は硬さの順に並べてあるが，Al2O3を除き，PSZ，Si3N4(J)，Si3N4(N)と硬くなるにつれて，研磨率が減少することがわかる．また，図より，アルミナの研磨率及び表面粗さがが，他のセラミック球に比べて約2倍以上大きいことがわかる．

3.4　SEMによる表面観察

　図4に，各セラミック球の実験終了後のSEM写真を示す．PSZにおいては幅が1～3μm程度の砥粒によると思われる引っ掻き傷が無数に見られた．Si3N4(N)及びSi3N4(J)においては，幅が1～5μm程度の引っ掻き傷と，砥粒が転動した際，砥粒の角により押し込まれたと思われる傷が見られた．一方，Al2O3においては，引っ掻き傷は見られず，無数の粒子の脱落が見られた．

図4　研磨後のセラミック球のSEM写真

図5　研磨率と各パラメーターの関係

4. 考察

4.1 研磨率と各パラメーターの関係

一般にアブレシブ摩耗の様な材料に主にせん断応力が作用する事で摩耗する摩耗形態のときには, 単位荷重, 単位すべり距離当たりの研磨体積は, 1/Hvに比例する[7]. また, エロージョンなどの接触応
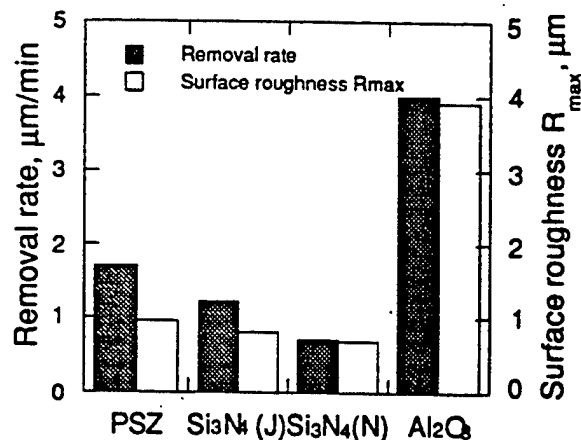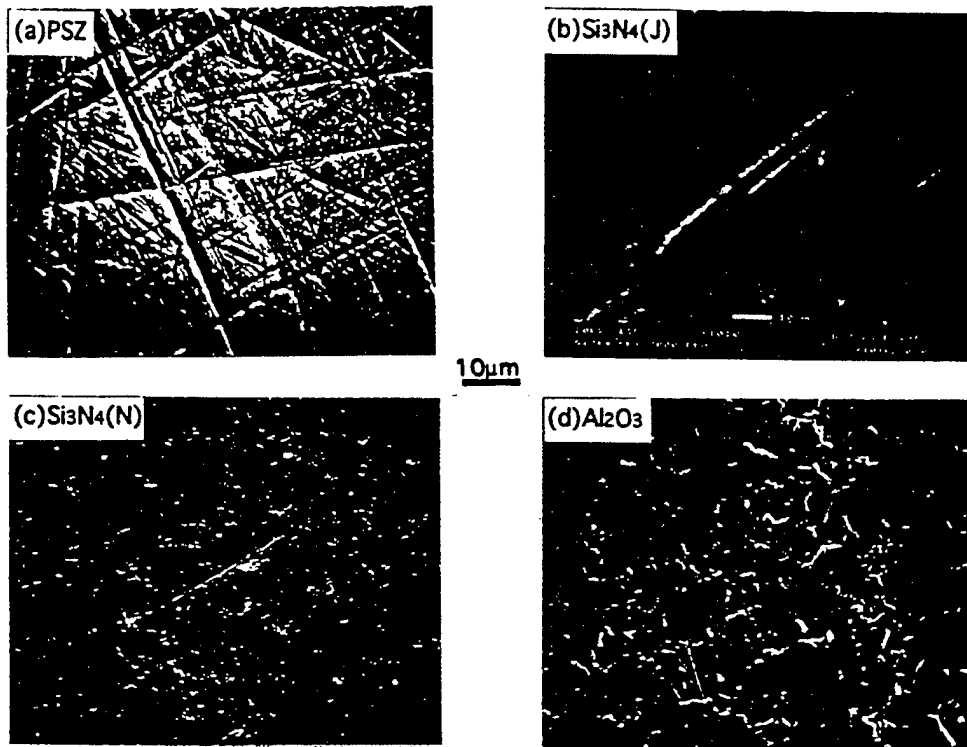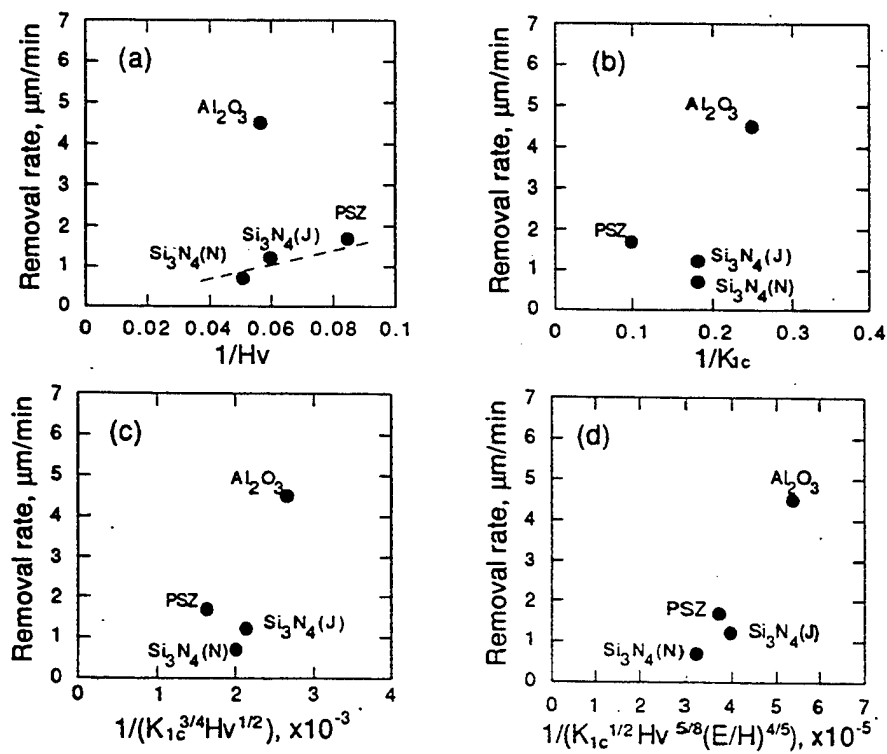
力が主に垂直方向に作用するときは，K1cが重要なパラメーターとなる[4]．そこで，各セラミック球の材料除去機構を明らかにするために，まず，セラミック球の機械的特性値の中からビッカース硬さHv及び破壊靱性値K1cを用いて研磨率のデータ整理を行った．図5(a)及び(b)に，研磨率とパラメーター1/Hv及び1/K1cの関係を示す．図5(a)より，PSZ，Si3N4(J)，Si3N4(N)の研磨率は，ほぼ一直線上にあるが，Al2O3のみこの直線上からはずれ，硬い割に研磨率が大きいことがわかる．この結果より，PSZ，Si3N4(J)，Si3N4(N)の材料除去機構は硬さに大きく支配されることがわかる．また，図5(b)からは，研磨率と破壊靱性値の間には，全ての材料に共通する関係が無い事がわかる．また，セラミックスの研磨率に比例する材料パラメーターとしてEvansらにより，2つのパラメーターが提案されている[8][9]．それらは，隣接した圧子間のラテラルクラックの干渉により材料が除去されることを仮定して得られたらたパラメーター$1/(K1c^{3/4}Hv^{1/2})$と，一つの圧子のラテラルクラックにより材料が除去されることを仮定して得られたパラメーター$1/(K1c^{1/2}H^{5/8})(E/H)^{4/5}$である．そこで，それらのパラメーターにより，本研磨率を整理した結果を，それぞれ図6(c)と(d)に示す．しかし，いずれの図においても研磨率は，それぞれのパラメーターに比例していないことがわかる．

4.2 各セラミック材料の磁性流体研磨における材料除去機構

SEM観察では，PSZ，Si3N4(J)，Si3N4(N)において，無数の引っ掻き傷が見られた．また，4.1項の考察より，この3種類の研磨率が硬さに大きく支配されていることがわかった．これらの結果より，この3種類のセラミックスの磁性流体研磨における材料除去機構は，砥粒による球表面の引っ掻きによる塑性変形によるものと考えられる，ただし，窒化ケイ素の結晶は，共有結合性が高く，すべり系の数が少ないため，結晶内で塑性変形したとは考えづらく，各粒界のガラス相が粒界すべりを起こしたためと考えられる．一方，Al2O3においては，SEM観察より，粒子の脱落が見られ，かつ4.1項で考察したように，硬い割に，研磨率が大きいことから，粒子間の亀裂の伝播により，材料が除去したと考えられる．

最後に，Gardosらにより，従来のラッピングによる窒化ケイ素のラッピングの材料除去機構は，ラテラルクラックの伝播によるものであることが示唆れている[6]．それに対し，本研究によって窒化ケイ素球の磁性流体研磨の材料除去機構が塑性変形によるものであるが示されたことから，磁性流体研磨の方が，従来のラッピングに比べて加工損傷が少ないことが期待できる．

5. 結言

セラミック球の磁性流体研磨の材料除去機構を調べるために，異なる機械的特性を有する材料として，ジルコニア，窒化ケイ素（2種類）及びアルミナを選び，それらの材料除去機構を検討した．その結果，ジルコニア及び窒化ケイ素の研磨率は，硬さに支配され，それらの材料除去機構が塑性変形によるものである事，及びアルミナの除去機構が，粒界の亀裂伝播に伴う粒子の脱落によるものである事を明らかにした．

<参考文献>

(1)梅原・加藤, 日本機械学会論文集(C編),54,503(1988)1599.
(2)梅原・加藤・渡辺,日本機械学会論文集(C編),55,519(1989),2879.
(3)山本・梅原・加藤・阿高・渡辺,日本機械学会論文集(C編),58,553,(1992)2767.
(4)N.Umehara, Annals of CIRP, 43/1(1994)185.
(5)T.H.C.Childs, S.Mahmood and H.J.Yoon, Proc. I.M.E.,208,B1(1994)47.
(6)M.N.Gardos and R.G.Hardisty, STLE Trans., 36,4(1993)652.
(7)E.Rabinowicz, MIT Industrial Liason Program Report No.2-40-88, MIT, Camb, (1988)
(8)A.G.Evans and T.R.Wilshaw, Acta. Metall., 24(1976)939.
(9)A.G.Evans and D.B.Marshall, Fundamental Friction and Wear of Materials, ASM, (1980)439.

APPENDIX H

ON THE POSSIBILITY OF CHEMO-MECHANICAL

POLISHING OF SILICON NITRIDE

M. Raghunandan, N. Umehara and R. Komanduri,

ON THE POSSIBILITY OF CHEMO-MECHANICAL ACTION IN MAGNETIC FLOAT POLISHING OF SILICON NITRIDE

M. Raghunandan, N. Umehara, and R. Komanduri
Mechanical & Aerospace Engineering
Oklahoma State University
Stillwater, OK 74074

ABSTRACT

Chromium oxide abrasive has been reported in the literature to provide efficient chemo-mechanical polishing action for silicon nitride ceramic. Since aluminum oxide and chromium oxide abrasives are nearly of the same hardness, magnetic float polishing tests were conducted on silicon nitride balls with these two abrasives to investigate mechanical versus chemo-mechanical aspects of polishing. Tests results show higher removal rates and smoother surface texture (with fewer pits) with chromium oxide abrasive compared to aluminum oxide abrasive. Formation of pits due to brittle fracture seems to be the more predominant mode of material removal with aluminum oxide abrasive than with chromium oxide abrasive. While there may be some mechanical action (abrasion) with chromium oxide abrasive initially, subsequent removal is believed to be due to chemo-mechanical action. This could be due to degeneration of the chromium oxide abrasive (both mechanical and chemical) during polishing. Various hypotheses for the material removal mechanism (both mechanical and chemo-mechanical) were considered. Based on that, the higher removal rates and smoother surface texture on the silicon nitride balls with chromium oxide abrasive in semifinish polishing is interpreted here as possibly due to chemo-mechanical action. Higher chemical stability of aluminum oxide abrasive (compared to chromium oxide abrasive) and the known role of chromium oxide as a catalyst for the oxidation of silicon nitride are some of the reasons attributed for this action.

1. INTRODUCTION

Advanced ceramics, such as aluminum oxide, zirconia, silicon nitride, and silicon carbide are difficult materials to finish by conventional grinding and polishing in view of their high hardness and low fracture toughness. Brittle fracture rather than plastic deformation would be the dominant mode of material removal under normal grinding conditions. Unfortunately, the failure of these materials is generally initiated from the surface and the defects on the surface play a significant role on the life and reliability of parts made of these materials. However, the extent of damage due to brittle fracture can be minimized significantly by 'gentle' grinding and polishing using submicron abrasives where the material removal is limited to low depths of cut (a few nanometers or less) and consequently low levels of force (on the order of 1 N or less per ball).

2. FACTORS AFFECTING FINE MATERIAL REMOVAL IN ADVANCED CERAMICS

In finishing of advanced ceramics, the material response to the process is an important factor that affects the quality of the surface generated. The material response in turn depends on the magnitude and size of the stress field as well as the response of the work material-abrasive-environment combina-tion under the conditions of the operation. Kim et al [1986] investigated the wear mechanisms of various ceramics in dry rolling friction and found the brittle fracture to dominate in the wear process. The wear process under these conditions can be considered to be similar to the material removal during polish-ing or 'gentle' grinding in many respects including the loads, Hertzian contact area, chemo-mechanical effects, size of the debris etc. Yoshikawa [1967] conducted pioneering studies on the brittle-ductile behavior of crystal surfaces in finishing. Since then, many researchers have been addressing this issue in ultraprecision machining, 'gentle' or 'ductile' grinding, and polishing [Xu and Jahanmir, 1994; Subramanian and Ramanath, 1992; Bifano et al, 1991; Jahanmir et al, 1992].

Yoshikawa [1967] considered the size of the stress field in terms of 'working units' and classified it into four domains as shown in Figure 1. Each domain is characterized by the defect structure which either preexists or has been generated by the processing method.

According to Yoshikawa in domain I, the material removal is considered only on the order of a few atoms or molecules. Material removal of this order could not possibly

117

occur by pure mechanical action. Chemical action enhanced by mechanical stress and temperature may play an important role in the material removal process in this domain.

In domain II, where no dislocations or cracks exist, a crystal should behave mechanically as an ideal crystal. Theoretical considerations indicate that under a given load the crystal surface in this domain should give rise to the generation of dislocations prior to brittle fracture. After the generation of dislocations, the crystal is assumed to behave as in domain III.

In domain III, with only dislocations present, plastic deformation occurs first, some amount of which will allow cracks to nucleate in the deformation zone.

In domain IV, the defects due to cracks is the dominant factor.

Of course, this classification is for an ideal single phase material with no preexisting defect structure, such as point defects, dislocations, grain boundaries, presence of a second phase, microcracks, or voids. The presence of these defects will no doubt alter the mode of material removal in all the domains. However, it appears reasonable to assume that at fine depths of removal, chemo-mechanical action may play a dominant role in 'gentle' grinding and polishing, followed by plastic deformation/microfracture depending on the conditions of polishing. This is especially so when proper choice is made of the abrasive and the environment for a given work material and the conditions of fine material removal, such as pressure and temperature which are conducive to this action.

3. CHEMO-MECHANICAL POLISHING

The mechanical removal rate of advanced ceramics in grinding and polishing is dependent on one hand on the type and hardness of the abrasive, its grain size etc. and on the other on the force per grain of the abrasive on work material. Thus, rough grinding with a hard abrasive can yield high removal rates by extensive brittle fracture at the expense of surface quality. 'Gentle' grinding or polishing with submicron super abrasive may yield superior surface quality at the expense of the removal rate. The removal rate when polishing silicon nitride work material will be much lower with conventional abrasives (such as aluminum oxide, silicon carbide) which are much softer than super-abrasives (e.g. diamond) but considerably less expensive. Alternately, the material removal rate can be increased to some extent without causing significant damage to the finished component by combining mechanical action with chemical action. Such a process is called tribo-chemical polishing [Heinicke, 1984]. It is also termed mechano-chemical or chemo-mechanical

118

polishing [Fischer, 1988]. In this paper these terms are used somewhat interchangeably with preference to the term 'chemo-mechanical' at the begining of the term to emphasize the chemical effect. The material removal by this process is believed to be at the molecular level thereby yielding a smooth surface instead of the classical removal (by mechanical action) of entire particles by brittle fracture resulting in pitting on the surface with most ceramics. Often, the formation of a reaction layer and its removal controls the process. Also, the dissolution of the reaction products in the carrier fluid plays a role.

Chemo-mechanical action depends on the availability for a short duration of time certain threshold pressure and temperature at the contact zone of the polishing process provided a chemical reaction layer can form by the interaction of the abrasive, work material, and the environment (Figure 2 [Yasunaga et al, 1978]). The exact values of pressure and temperature depend on the type of reaction product that can form which is subsequently removed by the mechanical action. This way higher removal rate can be accomplished without causing damage due to brittle fracture to the ceramic work material. Also, softer abrasives (softer than the work material) can be used in cases where a reaction product can be formed between the abrasive and the work material. This method is expected to overcome many problems of surface damage, such as pitting due to brittle fracture, dislodgment of grains, scratching due to abrasion etc. associated with harder abrasives resulting in smooth, damage-free surfaces on ceramics. However, if chemo-mechanical reaction products remain on the surface or diffuse into the work material, they may affect the performance and reliability of the product in subsequent use. So, it is necessary to ensure that chemo-mechanical action generates the reaction product but this reaction product is completely removed from the ceramic work material, i.e., at the surface as well as subsurface.

Mechano-chemical polishing was first demonstrated by Yasunaga et al [1977, 1978, 1979] for polishing of single crystals of sapphire, silicon, and quartz using soft abrasives. They used SiO_2 for polishing sapphire; $BaCO_3$, CeO_2, and $CaCO_3$ for polishing Si single crystals; and Fe_3O_4 and MgO for polishing quartz crystals and demonstrated that damage-free, smooth surfaces can be generated by this technique. Chemo-mechanical action is used to advantage in polishing without causing any detrimental effect to a range of work materials including sapphire, silicon, quartz, gallium arsenide, and various ferrites [Namba and Tsuwa, 1977, 1978; Karaki-Doy, 1993; Kashiwagura et al, 1983; Kawata and Tani, 1993; Kikuchi et al, 1983, 1992].

119

4. CHEMO-MECHANICAL POLISHING OF SILICON NITRIDE

Vora et al [1982, 1983] demonstrated the feasibility of polishing silicon nitride to a high level of finish by mechano-chemical polishing with iron oxides (both Fe_2O_3 and Fe_3O_4). A chemical reaction between iron oxide and silicon nitride at the contacting points was assumed which is promoted by a local mechanical effect associated with non equilibrium conditions, such as high temperature and high pressure, although the nature of this reaction was not investigated. Suga et al [1989] also investigated polishing of Si_3N_4 using several abrasives including $CaCO_3$, MgO, SiO_2, Fe_2O_3, Fe_3O_4, and Cr_2O_3 and concluded that Cr_2O_3 is a more suitable abrasive for the mechano-chemical polishing of Si_3N_4. In a later investigation, Kikuchi et al [1983, 1992] found Cr_2O_3 to be a suitable abrasive for mechano-chemical polishing of silicon carbide as well. They proposed that chromium oxide may be operating catalytically thereby enhancing the surface oxidation during polishing. It may also lower the activation energy and/or the starting temperature for the reaction. The tribo-chemical form of wear mentioned earlier is interpreted as due the removal of material, molecule by molecule, instead of the classical removal of entire particles by brittle fracture [Fischer, 1988].

Singhal [1975] studied the effect of water vapor on the oxidation of hot pressed silicon nitride and interpreted its formation as due to the following reactions:

$$Si_3N_4 + 6\,H_2O \rightarrow 3\,SiO_2 + 4\,NH_3$$
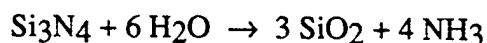
The dissolution of SiO_2 in water is given by :

$$SiO_2 + 2\,H_2O \rightarrow Si(OH)_4$$

Kanno et al [1983] found the formation of NH_3 in milling of silicon nitride powder in water conforming Singhal's interpretation. Fischer and Tomizawa [1985] and Tomizawa and Fischer [1986] studied wear of silicon nitride in water and concluded that wear is due to tribochemical dissolution of the material via the formation of SiO_2 and the dissolution of that SiO_2 in water to form silcilic acid, i.e., no solid wear particles are generated. Thus SiO_2 is dissolved in water more rapidly than amorphous SiO_2 particles. Fischer and Tomizawa also found the debris to be white in dry sliding of silicon nitride (NBD 200, which is black in color) indicating the formation of SiO_2 particles but found no wear debris

in sliding in water. However, when the water was evaporated, particles of SiO_2 were found to be precipitated.

Sugita et al [1984] studied the mechanism of material removal during rubbing of silicon nitride in water. They found the wear debris in water to be amorphous. They interpreted the results as due to oxidation of silicon nitride which subsequently changed to amorphous hydrate $SiO_2:xH_2O$ during rubbing in water. The amorphous hydrate was removed from the rubbing interface as a result of sliding.

Akazawa and Kato [1988] and Akazawa et al [1986] investigated the wear properties of silicon nitride in rolling contact and rolling-sliding contact. They identified one type of wear debris to be glassy film with SiO_2 structure. Similar results were reported by Jahanmir and Fischer [1987], Kapsa and Kanemura [1988], Gee [1992], Fischer and Mullins [1993], Danyluk et al [1993], Kennedy et al [1993], Jahanmir [1993], and Dong and Jahanmir [1993].

Although, it is widely believed that advanced ceramics can be finished by chemo-mechanical action by proper choice of the abrasive and the environment, the exact mechanism of its action is not well established. However, some plausible explanations were offered including the formation of silicates, spinals, oxidation of silicon nitride with/without catalytic action of chromium oxide, and less chemical stability of chromium oxide compared to aluminum oxide.

5. MAGNETIC FLOAT POLISHING

The magnetic float polishing technique for finishing ceramic balls was initiated in Japan chiefly by Umehara [1988], Kato [1990], Umehara and Kato [1990]. They termed it magnetic fluid grinding. We prefer to use the term magnetic float polishing, as originally introduced by Tani [1984] as this is more a polishing (3-body) process than a grinding (2-body, fixed abrasive) operation. However, one would find in the literature use of both terms to describe the process.

The magnetic fluid is a colloidal dispersion of extremely fine (100 to 150 A) sub-domain ferro-magnetic particles, usually magnetite (Fe_3O_4), in various carrier fluids, such as water or kerosene. The ferrofluids are made stable against particle agglomeration by the addition of surfactants. When a magnetic fluid is placed in a magnetic field gradient, it is attracted towards the higher magnetic field side. If a non-magnetic substance (e.g., abrasives in this case) is mixed in the magnetic fluid, they are discharged towards the lower

side. When the field gradient is set in the gravitational direction, the non magnetic material is made to float on the fluid surface by the action of the magnetic levitational force.

The polishing operation in this process occurs due to the magnetic levitational force. The process works on the basis of the magneto-hydrodynamic behavior of a magnetic fluid that can float non-magnetic abrasives suspended in it. The process is considered highly effective for finish polishing because a levitational force is applied to the abrasives in a controlled manner. The forces applied by the abrasives to the part in this process are extremely small (about 1 N or less). The time required to finish the balls to the same accuracy or better by this technique is at least an order of magnitude faster than by conventional polishing techniques. Consequently, this technique can be extremely cost effective and viable for the manufacture of ceramic balls.

6. EXPERIMENTAL SETUP AND TEST CONDITIONS

Experimental Setup

Figure 3(a) is a schematic diagram and Figure 3 (b) is a photograph of the magnetic float polishing apparatus showing permanent magnets located at the base of the apparatus. The magnets are located with alternate N and S poles underneath the float chamber. A guide ring is mounted on top of the float vessel to contain the magnetic fluid. Magnetic fluid containing fine abrasive particles is filled into the chamber. The silicon nitride ball blanks are held in 3-point contact between the float at the bottom, chamber wall on the side, and a shaft at the top. The shaft is connected to the spindle of the Bridgeport CNC milling machine which is capable of operating in the speed range of 60 - 6000 rpm. The balls and float are pushed upwards against the shaft by the magnetic buoyancy force. This force increases at an exponential rate as the float moves closer to the magnets [Raghunandan et al, 1994]. When a magnetic field is applied, the ceramic balls, abrasive grains, and the float of non-magnetic material all float and are pushed upwards by the magnetic fluid. Silicon nitride balls are pressed against the drive shaft and are finished by the rotation of the drive shaft.

Test Conditions

In the present investigation the drive shaft is made of austenitic stainless steel (non-magnetic) with a 30° chamfer at the edge. The chamfer angle is measured from a plane perpendicular to the axis of the shaft. The chamber wall was covered with urethane rubber and the float material used was acrylic resin. The materials for the shaft, float, and

chamber wall were selected based on the results of an earlier investigation [Umehara, 1988] where it was shown that this combination gives the largest removal rate. Table 1 lists the test conditions used.

Neodinium-iron-boron permanent magnets [12.7 mm squares] (with 10,500 G residual magnetization) were used in this investigation. The thickness of the float was kept at half the width of magnets. Water based magnetic fluid (W-40) with 400 G saturation magnetization was used. The silicon nitride balls were separated by spacer balls (nylon balls) thus preventing collision between neighboring silicon nitride balls and consequent surface damage. A total of ten balls were polished during each run. After each run, the material removal was measured as the change in weight. The diameter of balls (10 points per ball on all balls) were also measured. The surface topography of the samples was analyzed using a stylus based device (TalySurf) and a non-contact measuring device (ZYGO optical interference microscope) after some of the tests. Since there is no one to one correspondence of the data from TalySurf and ZYGO one would invariably find different values of Ra depending on the technique used. Hence, we can only use average values.

7. EXPERIMENTAL RESULTS

Figure 4 shows the variation of the material removal rate (MRR in mg/min and μm/min) with spindle speed on silicon nitride balls using aluminum oxide and chromium oxide abrasives respectively. It can be seen that the removal rate is higher on the average by about 80% with chromium oxide than with aluminum oxide although both are nominally of the same hardness (chromium oxide is estimated to be about 5-10 % harder than aluminum oxide). This difference in removal rate increases with increase in spindle speed upto 4,000 rpm and decreases with further increase in speed. Since, the removal rates by the abrasive action with both abrasives should be about the same, in view of similar hardness level, the higher removal rates with chromium oxide has to be accounted for by reasons other than mechanical action. We believe, that this could be due to chemo-mechanical action. We should also recognize that aluminum oxide and chromium oxide abrasives may have different shape and friability which can influence the removal rate. Figures 5 (a) and (b) are scanning electron micrographs of the balls finished for 90 minutes by aluminum oxide and chromium oxide abrasive (1-5 μm) respectively at 2,000 rpm spindle speed. These photographs were obtained by examining the silicon nitride balls inside an environmental scanning electron microscope (ESEM). The instrument enables the examination of surfaces of non-conducting materials without the need for a conductive coating, such as Au-Pd. It can be seen from the figure that silicon nitride balls polished

with aluminum oxide abrasive has several pits while the surface polished with chromium oxide appears rather smooth. However, some pits can be seen with chromium oxide abrasive indicating some mechanical action. Similar effects are found using ZYGO laser interference microscope (Figures 6 and 7). It should be noted, however, the objective of this investigation is to compare the removal rates and not necessarily to obtain the best finish. In fact, we have obtained smooth surfaces with Ra in the range of 10 nm [Figure 8 9a)] on silicon nitride balls using the chromium oxide abrasive.

Figures 6 (a) and (b) are surface profile data of the silicon nitride balls polished using aluminum oxide and chromium oxide abrasive respectively. They are obtained using ZYGO laser interference microscope. The smoother finish with chromium oxide is clear not only from the 3-D plot of the surface roughness but also from the values of R_a. Also, the 2-D plots of the surface (picture on the top hand side) clearly show the presence of numerous pits formed with aluminum oxide abrasive (possibly due to abrasive action) and rather smooth surface with chromium oxide abrasive. The formation of pits in a silicon nitride ball with aluminum oxide abrasive can more clearly be seen at higher magnification (100 x Fizeau) [Figure 7]. Figure 8 (a) and (b) show the surface roughness profile obtained using the Form TalySurf on silicon nitride balls using aluminum oxide and chromium oxide abrasives. The smooth surface with chromium oxide and formation of deep pits in the case of aluminum oxide is again evident.

8. DISCUSSION

Let us consider for the sake of discussion the following six plausible hypotheses for the material removal mechanisms in semifinishing of silicon nitride balls with aluminum oxide and chromium oxide abrasives.

Hypothesis 1:   Material removal in both cases is predominantly mechanical (abrasion) with very little chemo-mechanical action,

Hypothesis 2:   Material removal in the case of chromium oxide is predominantly by chemo-mechanical action,

Hypothesis 3:   Material removal in the case of aluminum oxide is predominantly by chemo-mechanical action,

Hypothesis 4:   Oxidation of silicon nitride and formation of amorphous hydrate ($SiO_2:xH_2O$) during polishing in the presence of a water based magnetic fluid, and

124

Hypothesis 5: Lower transition speed for sliding with chromium oxide abrasive compared to aluminum oxide abrasive and consequent higher removal rates (this is specific to the magnetic float polishing process).

What we have found in the present study is higher removal rates and smoother surface texture with chromium oxide abrasive than with aluminum oxide abrasive. It is entirely possible that the higher removal rate with chromium oxide abrasive is purely mechanical (abrasion) in nature with very little or no chemo-mechanical action (Hypothesis 1). But then, the differences in both the removal rates and the surface texture cannot be explained by this argument alone since the hardness of both the abrasives is nearly the same (about 10 % difference, the exact values are not quoted here as they vary depending on the crystallographic orientation, load etc.). However, the differences in hardness between the work material (silicon nitride) and the abrasives (chromium oxide and aluminum oxide) is not significant. Hence, small difference in the hardness between the abrasives may account for the differences in the material removal rates. But it is difficult to explain by Hypothesis I, the difference in the surface texture (several large pits in the case of aluminum oxide abrasive and fewer pits with smoother surface texture with chromium oxide abrasive). This together with the reported claim in the literature that chromium oxide is a superior abrasive for chemo-mechanical polishing of silicon nitride [Suga et al , 1989; Suzuki et al , 1992; Uematsu et al , 1993] leads us to discount this hypothesis as solely responsible for the material removal.

Hypothesis 2, namely, material removal in the case of chromium oxide is predominantly by chemo-mechanical action appears reasonable based on the experimental observations. Chromium oxide is also well known as a catalyst for oxidation of other materials. It is, therefore, possible for chromium oxide to act in this role by oxidizing silicon nitride and form SiO_2 surface. This may be the reason for the smooth texture on the silicon nitride balls polished with chromium oxide and not with aluminum oxide.

Similarly, one could argue that aluminum oxide abrasive can also polish silicon nitride by chemo-mechanical action (Hypothesis 3). For example, aluminum oxide abrasive can react with silicon nitride to form aluminum silicate or act as a catalyst in oxidizing silicon to form SiO_2 (a role possibly similar to chromium oxide). However, the present findings, namely, lower removal rates and presence of pits on the surface with aluminum oxide abrasive do not lend support to this hypothesis. If there is chemo-mechanical action with aluminum oxide abrasive, then the lower removal rates could be interpreted as the degradation of aluminum oxide (chemical wear of the abrasives) to form

125

aluminum silicate. This would not aid the material removal process; instead it would hinder it due to wear of the abrasive.

It is possible that in the presence of a water based magnetic fluid used in this investigation, oxidation of silicon nitride and formation of amorphous hydrate (SiO_2::x H_2O) can both take place during polishing. However, in polishing with aluminum oxide and chromium oxide a water base magnetic fluid is used. So, whatever happens with chromium oxide should also happen with aluminum oxide. Hence, this hypothesis even though is possible cannot explain for the difference.

Another possible reason for the difference in the material removal rates on silicon nitride with Cr_2O_3 and Al_2O_3 is different sliding speeds between the driving shaft and the balls at the same drive shaft speed (Hypothesis 5). As pointed out earlier, this is specific to the magnetic polishing technique. The sliding speed between the driving shaft and the balls during polishing is estimated as follows. It is assumed that sliding begins at the drive shaft speed where the material removal rate (MRR) is zero. It can be found from Figure 4 that the drive shaft speeds with Cr_2O_3 and Al_2O_3 when the MRR is zero are 650 rpm and 1214 rpm respectively. For the condition where the balls just roll on the surface of the driving shaft without sliding Childs et al [1994a] developed a relationship between the drive shaft speed Ω_s and the ball circulation speed Ω_b as follows:

$$\frac{\Omega_b}{\Omega_s} = \frac{1}{1 + \cos\theta + \sin\theta} \frac{R_s}{R_f} \left(1 + \frac{R_f}{R_s} \frac{\Omega_f}{\Omega_s} \cos\theta \right) \tag{1}$$

where R_s is the radius at the contact point between ball and the driving shaft, R_f is the radius at the contact point between ball and the float, θ is the taper angle of the driving shaft and Ω_f is the float rotational speed.

From the results of Childs et al [1994b], Ω_f/Ω_s is assumed as 0.05. In the present investigation the values of R_s, R_f, and θ are 32.8 mm, 29.2 mm, and 30 deg respectively. Using equation (1), Ω_b with Cr_2O_3 and Al_2O_3 can be calculated as 257 rpm and 479 rpm respectively.

If the ball circulation speed Ω_b remains constant after occurrence of sliding between the balls and the driving shaft, the sliding speed V_s between the balls and the shaft can be calculated using the following equation [1994a]

$$\frac{V_s}{R_s\Omega_s} = 1 - \frac{R_f}{R_s} \frac{\Omega_b}{\Omega_s} (1 + \cos\theta + \sin\theta) + \frac{R_f}{R_s} \frac{\Omega_f}{\Omega_s} \cos\theta \tag{2}$$

Figure 9 shows the variation of sliding speed with the driving shaft speed obtained from equation 2. It can be seen that the sliding speed with Cr_2O_3 is larger than that with Al_2O_3 even if at the same drive shaft speed. Figure 10 shows the variation of the MRR with the sliding speed. It can be seen that the MRR's are proportional to the sliding speed and the gradient for Cr_2O_3 is larger than that for Al_2O_3 by about 20 %. Although, some scatter in the data is noted in the case of aluminum oxide abrasive, we have used the best fit to compare the slopes. Thus, the higher removal rates associated with Cr_2O_3 abrasive in polishing silicon nitride can be accounted partially on the basis of lower transition speed for sliding with Cr_2O_3 than with Al_2O_3 abrasive.

In addition to the five hypotheses presented here, there may be other possibilities not considered here responsible for the difference . For example, the shape of the abrasives can be different. Similarly, the friability of the abrasives can be different. Thus shape and size changes during the polishing process can possibly explain for some of the difference. One cannot totally rule this or other factors out at this stage till a conclusive evidence is available.

Whether or not chemo-mechanical action occurs in polishing of silicon nitride with chromium oxide or aluminum oxide, it is clear from this study that chromium oxide is a superior abrasive to aluminum oxide in finishing of silicon nitride in view of higher removal rate and better surface finish. It is also clear that further studies are needed to delineate the micromechanisms of polishing of silicon nitride with these abrasives. Examination of the wear debris in the SEM and TEM, and characterization of the surface and near-surface using Auger Electron Spectroscope (AES), μ-Raman Spectroscope, low-angle X-ray diffraction, and FTIR may throw more light on this subject. Similarly, it is necessary to measure the ball circulation speed W_b and the sliding speed V_s between the balls and the shaft. Work is currently underway along these lines and it is hoped that the results of this work will be communicated in the not too distinct future.

9. CONCLUSIONS

1. Chromium oxide abrasive is found to be a good abrasive for polishing silicon nitride. Surface finish (R_a) of less than 10 nm can be obtained using this material.

2. Material removal with chromium oxide at these fine levels of polishing appears to be at the molecular level although some pits were also observed. These could have been generated during the early stages of polishing.

3.   Although both aluminum oxide and chromium oxide are nearly of the same hardness, the material removal rate (MRR) on silicon nitride balls with these two abrasives was found to be different. The higher removal rate with chromium oxide over aluminum oxide is attributed here as due to possible chemo-mechanical action of chromium oxide with silicon nitride. It appears that chromium oxide may be serving as a catalyst in the oxidation of silicon nitride and the formation of SiO_2.

4.   Observation of the semifinished silicon nitride balls shows pits, possibly formed by abrasion, brittle fracture, and dislodgment of grains with aluminum oxide abrasive and relatively smooth surface (with fewer pits) possibly formed by chemo-mechanical action with chromium oxide.

ACKNOWLEDGMENTS

REFERENCES

Akazawa, M. and Kato, K. "Wear Properties of Si3N4 in Rolling-Sliding Contact," Wear, 124 (1988) 123-132

Akazawa, M., Kato, K., and Umeya, K. "Wear Properties of Silicon Nitride in Rolling Contact," Wear 110 (1986) 285-293

Bifano, T. G., Dow, T. A., and Scattergood, R. O. "Ductile Regime Grinding: A New Technology for Machining Brittle Materials," Trans ASME 113 (1991) 184-189

Childs, T.H.C., Jones, D.A., Mahmood, S., Kato, K., Zhang, B and Umehara, N. "Magnetic Fluid Grinding Mechanics," Wear, 175 (1994a) 189-198

Childs, T.H.C., Mahmood, S., and Yoon, H. J. " The Material Removal Mechanism in Magnetic Fluid Grinding of Ceramic Ball Bearings," Proc. of the I. Mech. E., 208, B1 (1994b) 47-59

Danyuluk, S., Park, D. S., and McNallan, M. " Friction and wear of Silicon Nitride Exposed to Moisture at High Temperatures," in "Friction and Wear of Ceramics," (Ed. S. Jahanmir) Marcel Dekker, Inc., New York (1993)

Dong, X., and Jahanmir, S. "Wear Transition Diagram of Silicon Nitride," Wear 165, (1993) 169-180

Fischer, T. E. and Tomizawa, H. "Interaction of Tribo-chemistry and Microfracture in the Friction and Wear of Silicon Nitride," Wear, 105 (1985) 29-45

Fischer, T. E., and Mullins, W. M. "Relation Between Surface Chemistry and Tribology of Ceramics," in "Friction and Wear of Ceramics," (Ed. S. Jahanmir) Marcel Dekker, Inc., New York (1993)

Fischer, T. E. "Tribochemistry," Ann. Rev. Mater. Sci. 18, (1988) 303-323

Gee, M. G. "The Formation of Glass in the Wear of Reaction-Bonded Silicon Nitride," J. Phys. D. App. Phy. 25 (1992) A182- A188

Heinicke, G. "Tribochemistry," Carl Hanswe Verlag, Munich (1984)

Jahanmir, S. "Friction and Wear of Ceramics," Marcel Dekker, Inc., New York (1993)

Jahanmir, S. and Fischer, T. E., "Friction and Wear of Silicon Nitride Lubricated by Humid Air, Water, Hexadecane and Hexadecane + 0.5 percent Stearic Acid," Trans STLE, 31, 1 (1987) 32-43

Jahanmir, S., Ives, L.K., Ruff, W. A., and Peterson, M. B. " Ceramic Machining: Assessment of Current Practice and Research Needs in the United States," NIST Special Publication No. 834, U. S. Government Printing Office, Washington, D.C. (1992)

Kanno, Y., Suzuki, K., and Kuwahara, Y. "NH_3 Formation Caused by the presence of H_2O in the Wet Grinding of Silicon Nitride Powder," Yog Yo-K yokai-Shi, 91 (1983) 386

Kapsa, P. and Kanemura, Y. "Sliding Damage on Hot-Pressed and Sintered Silicon Nitride Caused by a Diamond Tip Under Controlled Humidity," Wear, 127 (1988) 65-83

Karaki-Doy, T. "Study on Mechanism of Mechano-chemical Polishing and its Application - An Instance of Silicon Wafers," J. of Saitama Univ., Faculty of Education (Mathematical and Natural Science) 42 (1), (1993) 33-47

Kashiwagura. N, Harada. J, and Ogino, M. "Characterization of Mechanochemically Polished (111) Surface of Silicon by Diffuse X-Ray Scattering," J. Appl. Phys., 54, [5], (1983) 2706-2710

Kato, K. "Tribology of Ceramics," Wear 136 (1990) 117-133

Kawata, K. and Tani, Y." Development of High-Concentration Lapping Discs with Low Bonding Strength and Their Application to Mirror Finishing of Brittle Materials," JSME Int. Journal, Series C, 36, 2, (1993) 264-270

Kikuchi, M., Takahashi, Y. , Suga, T., Suzuki, S., and Bando, Y. "Mechanochemical Polishing of Silicon Carbide Single Crystal with Chromium(III) Oxide Abrasive," J. Amer. Ceram. Soc., 75,1, (1992) 189-195

Kikuchi, M., Takahashi, Y., Suga, T., Suzuki, S., and Yasunaga, N. "Mechanochemical Polishing of Silicon Carbide," Proc. Fall Meeting of JSPE, (1990) 327-328 (in Japanese)

Kim, S. S., Kato, K., Hokkirigawa, K. and Abe, H. "Wear Mechanism of Ceramic Materials in Dry Rolling Friction," Trans ASME, J of Tribology, 108 (Oct. 1986) 522-526

Namba, Y and Tsuwa, H. "Mechanisms and Some Applications of Ultrafine Finishing," Annals of the CIRP, 27/1, (1978) 511-516

Namba, Y and Tsuwa, H. "Ultrafine Finishing of Sapphire Single Crystal," Annals of the CIRP, 26/1, 1977, 325

Raghunandan, M., Umehara, N., Noori-khajavi, N., and Komanduri, R. "Magnetic Float Polishing of Advanced Ceramics," paper to be submitted for publication (1994)

Singhal, S. C. "Effect of Water Vapor on the Oxidation of Hot-Pressed Silicon Nitride and Silicon Carbide, " J. Am. Cer, Soc. 58, (1975) 17

Subramanian, K. and Ramanath, S. "Mechanisms of Material Removal in the Grinding of Ceramics," Proc. of the Symposium on Precision Machining, ASME Publication PED-58 (1992)

Suga, T., Suzuki, S. and Miyazawa, K. "Mechanochemical Polishing of Sintered Silicon Nitride," J. JSPE, 55, 12 (1989) 2247-2253 (in Japanese)

Sugita, T., Ueda, K. and Kanemura, Y. "Material Removal Mechanism of Silicon Nitride During Rubbing in Water," Wear 97 (1984) 1-8

Suzuki, K., Uematsu, T., Ohashi, H., Kitajima, K., Suga, T. and Imanaka, O. "Development of a New Mechanochemical Polishing Method with a Polishing Film for Ceramic Round Bar, " Annals of the CIRP, 41/1, (1992) 339-342.

Tani, Y., and Kawata, K. "Development of High-Efficient Fine Finishing Process Using Magnetic Fluid," Annals of CIRP, 33/1 (1984) 217-220

Tomizawa, H. and Fischer, T. E. "Friction and Wear of Silicon Nitride and Silicon Carbide in Water: Hydrodynamic Lubrication at Low Sliding Speeds Obtained by Tribochemical Wear," Trans ASLE 30, (1) (1986) 41-46

Uematsu, T., Suzuki, K., Wu, M. H., Suzuki, K. and Imanaka, O. "Efficient Mechanochemical Polishing for Silicon Nitride Ceramics," Machining of Advanced Materials, NIST Special Publication No. 847 (edited by S. Jahanmir) (1993) 409-413

Umehara, N., and Kato, K. "Principles of Magnetic Fluid Grinding of Ceramic Balls," Applied Electromagnetics in Materials, 1 (1990) 37-43

Umehara, N. "Study on Magnetic Fluid Grinding," Ph.D. Thesis, Tohoku University, Sendai, Japan (1988) (in Japanese)

Vora, H., Orent, T.W. and Stokes, R. J. "Mechano-Chemical Polishing of Silicon Nitride.", J. Amer. Ceram. Soc. 65, 9, (1982) C140-C141

Vora. H, and Stokes, R. J. "Study of Mechano-Chemical Machining of Ceramics and the Effect on Thin Film Behavior," Rept. No. N00014-80-C-0437-2 (1983)

Whittledon, E. P., Ives, L. K., and Peterson, M. B. "Surface Damage and Mechanics of Fretting Wear in Ceramics," in Friction and Wear of Ceramics (Ed. S. Jahanmir), Marcel Dekker, Inc. New York (1993)

Xu, H. K. K., and Jahanmir, S. "Simple Technique for Observing Subsurface Damage in Machining Ceramics," J. Amer. Cer. Soc. 77 [5] (1994) 1388-90

Yasunaga, N, Tarumi, N, Obara, A., and Imanaka, O. "Mechanism and Application of the Mechanochemical Polishing Method Using Soft Powder," in the Science of Ceramic Machining and Surface Finishing II, Ed. B. J. Hockey, and R. W. Rice, NBS Special Publication No. 562 (1979) 171

Yasunaga, N., Obara, A., and Imanaka, O. "Study of Mechanochemical Effect on Wear and Its Application to Surface Finishing," J. of JSPE, 44, (1978) 77-83 (in Japanese)

Yasunaga. N, Obara, A, and Tarumi, N. "Study of Mechanochemical Effect on Wear and Its Application to Surface Finishing," Res. Electrotech. Lab, 776 (1977) 50-134 (in Japanese)

Yoshikawa, H. "Brittle-Ductile Behavior of Crystal Surface in Finishing," J. Japan Society for Precision Engineering (JSPE), 35, (10) (Oct. 1967) 662-667 (in Japanese)

TABLE 1 EXPERIMENTAL CONDITIONS

Work material	HIP'ed Silicon nitride balls from Japan; 10.2 mm dia.
Ferrofluid	water based (W-40) Density: 1.4 kg/mm^3; Viscosity: 2.25 Pa.s. (25°C); Magnetization: 400 G at 8 KOe
Abrasive types	Cr_2O_3 and Al_2O_3
Abrasive size, μm	1-5
Abrasive concentration	10% by volume
Spindle speed, rpm	1000, 2000, 4000, and 6000
Working load/ball, N	1 N

TABLE 2 PROPERTIES OF THE SILICON NITRIDE BALLS USED

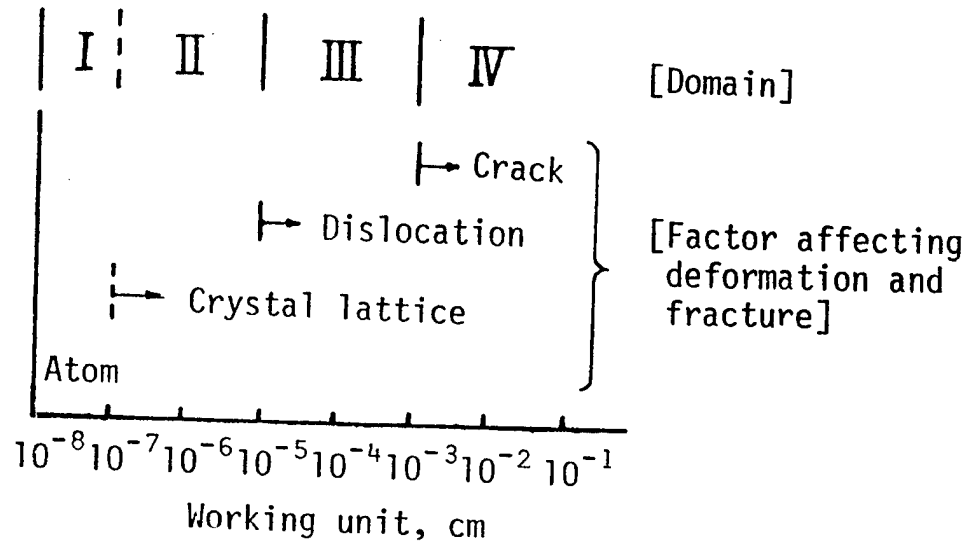|	
Chemical Composition	Si_3N_4 : 94 wt.%; Al_2O_3: 4 wt. %; and Y_2O_3: 2 wt %
Density, g/cm^3	3.228
Bending Strength, ,MPa	980
Hardness, kg/mm^2	1600-1800
Fracture Toughness, K_{IC}, MN/m $^{3/2}$	5-6

Figure 1   Classification of the stress field into four domains in
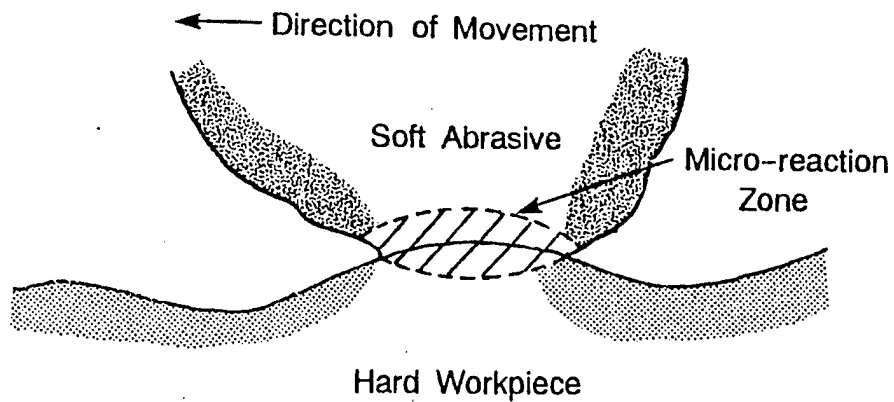terms of "Working Units" (after Yoshikawa, 1967)

Figure 2   Schematic of the chemo-mechanical polishing process
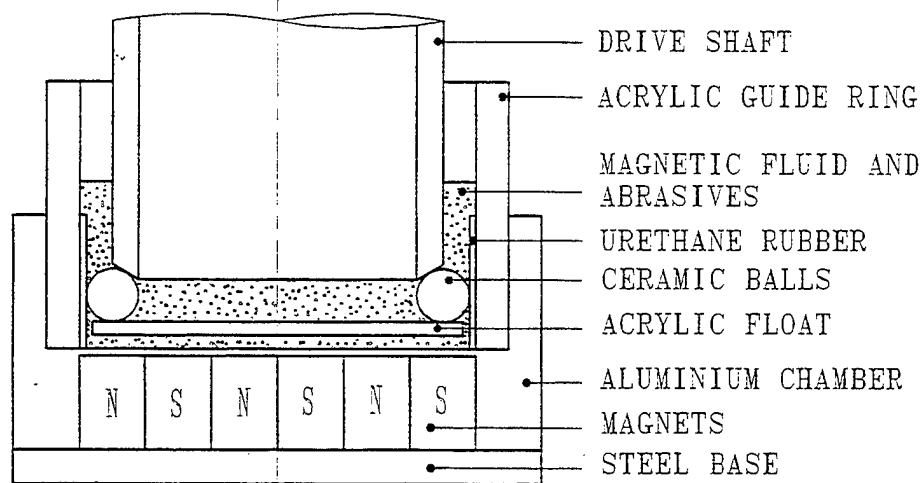(after Yasunaga et al, 1978)

133

Figure3(a) Schematic diagram of the magnetic float polishing apparatus showing permanent magnets located at the base of the apparatus

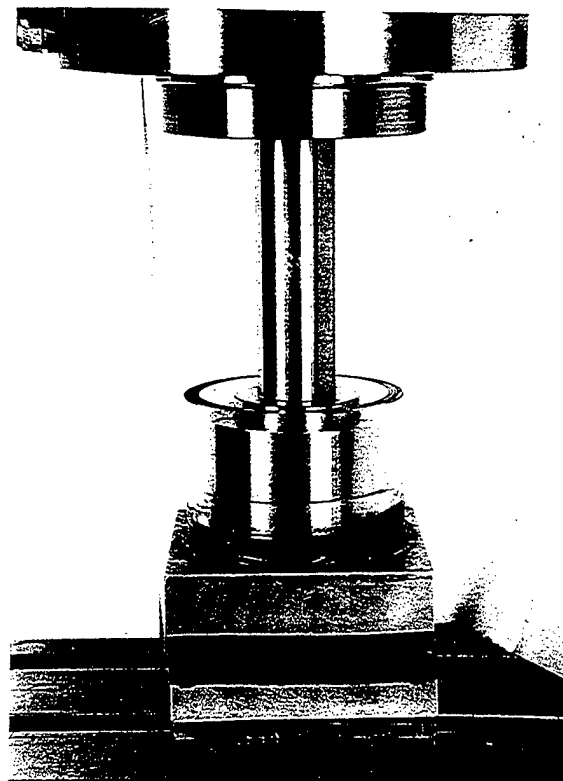Figure 3(b) Photograph of the magnetic float polishing apparatus
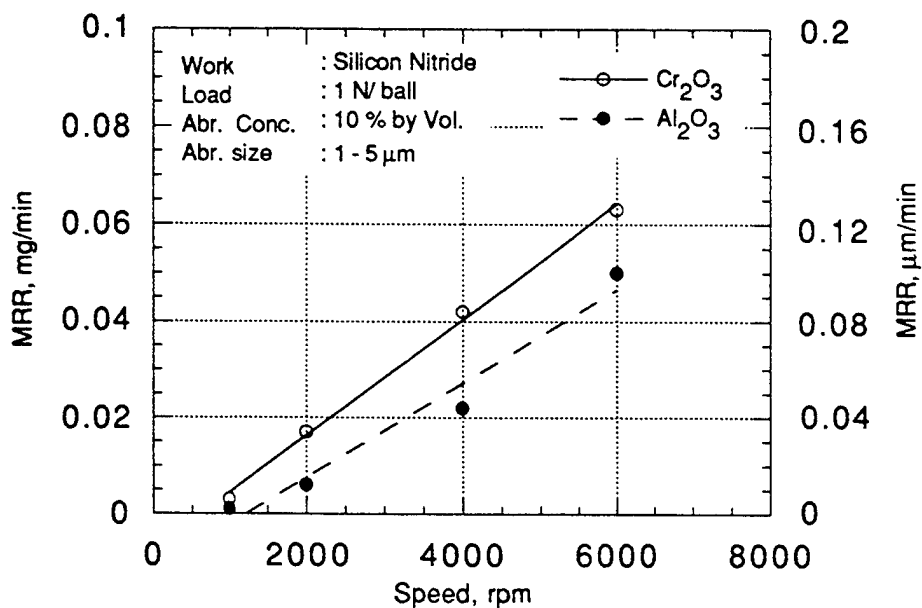
Figure 4 Variation of the material removal rate (MRR in mg/min or μm/min) on silicon nitride balls with the spindle speed using Al₂O₃ and Cr₂O₃ abrasives
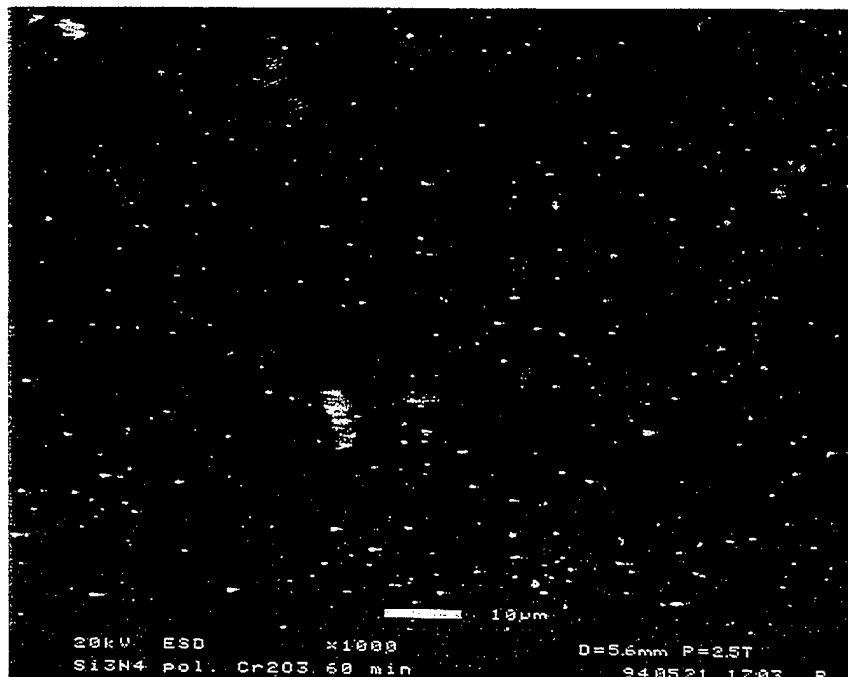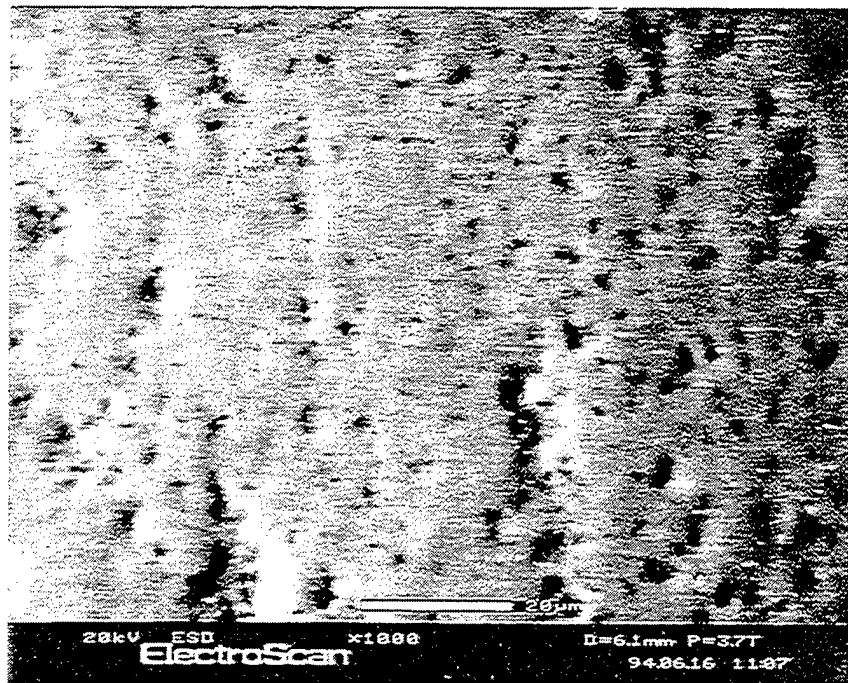
Figure 5(a) Scanning electron micrographs of the silicon nitride balls
     & (b) finished for 90 minutes by Al_2O_3 and Cr_2O_3 abrasives
        (1-5 μm) at 2000 rpm spindle speed

Figure 6 (a) Surface roughness profiles (using zygo laser interference microscope) of the silicon nitride ball polished using Al₂O₃ abrasive

137
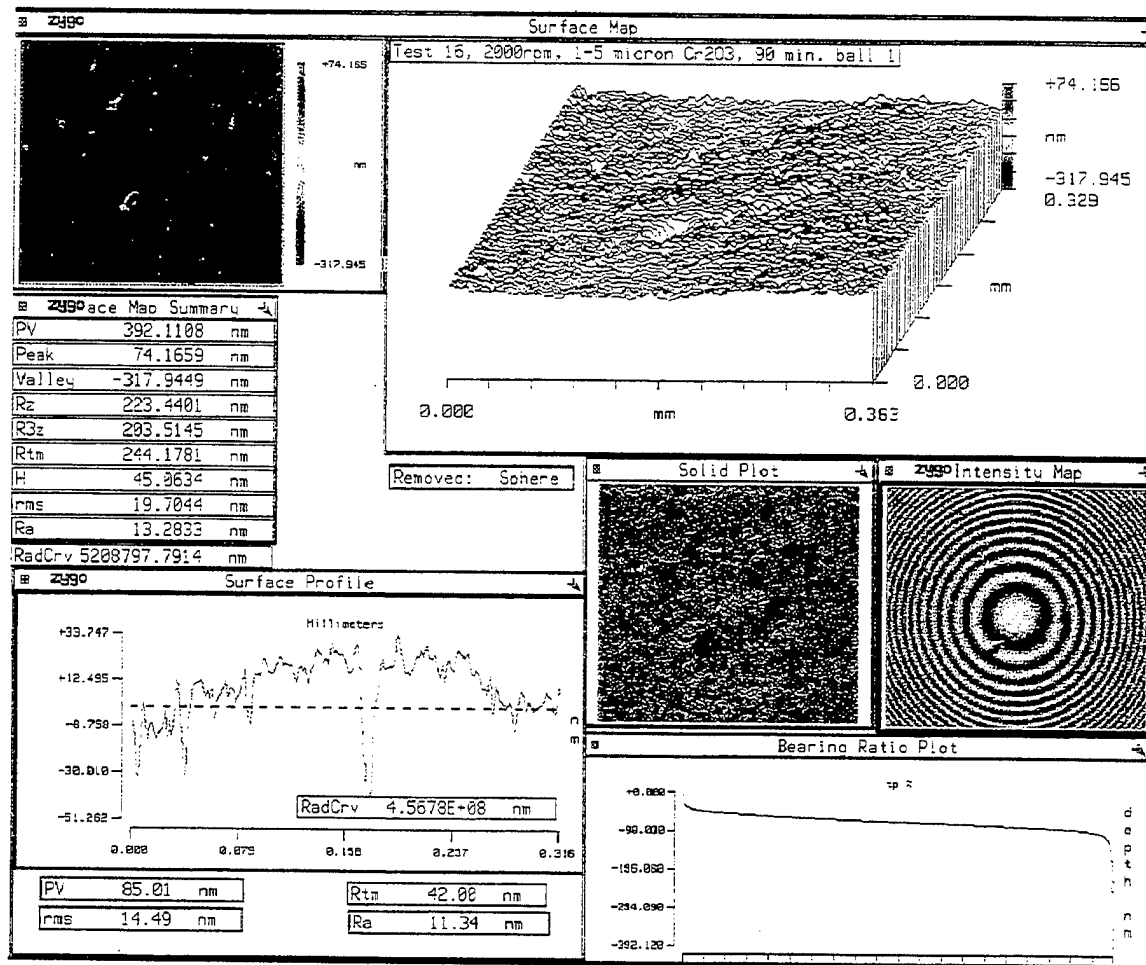
Figure 6(b) Surface roughness profiles (using zygo laser interference microscope) of the silicon nitride ball polished using Cr_2O_3 abrasive
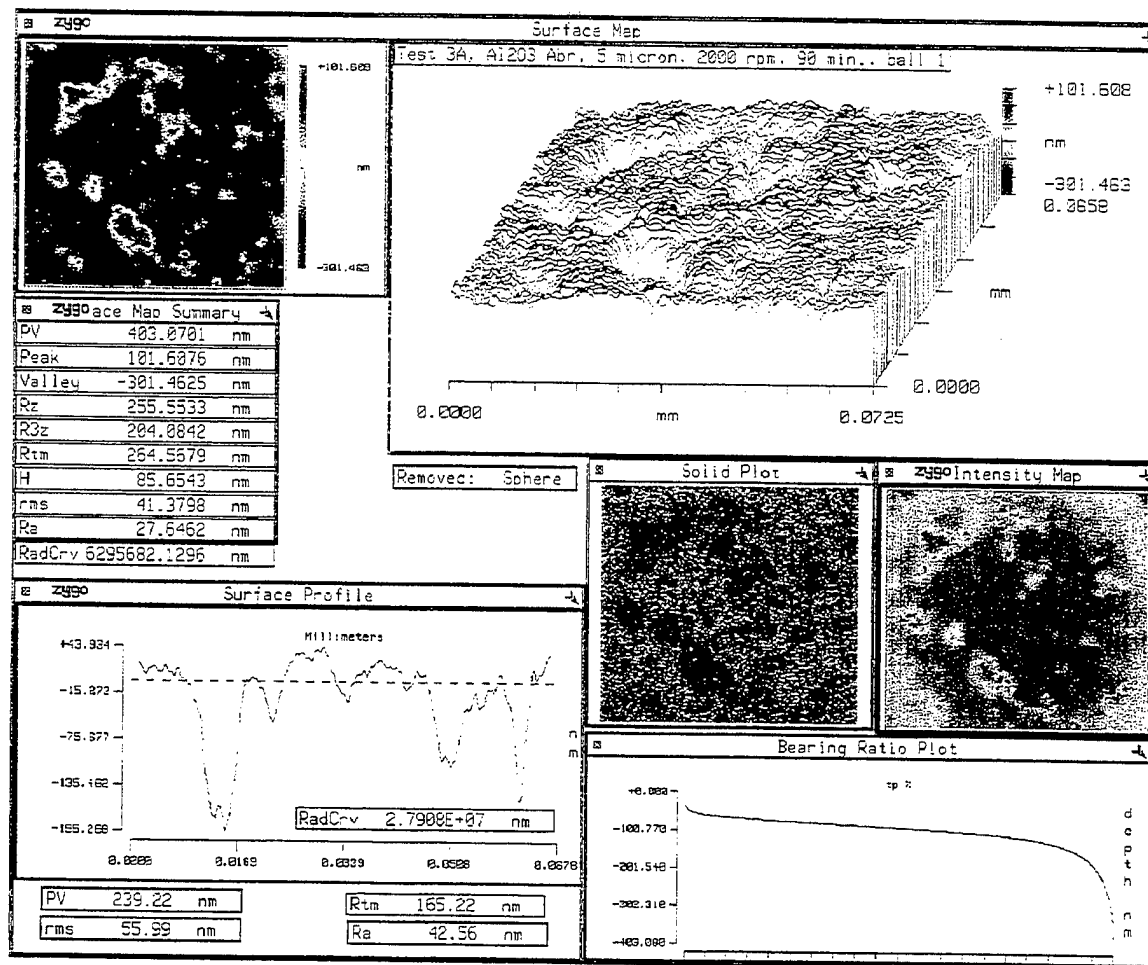
Figure 7   Surface roughness profiles (using ZYGO laser interference
microscope) at higher magnification (100x fizeau) of the
silicon nitride ball polished using Al_2O_3 abrasive showing
pits due to dislodgement of grains by brittle fracture

a)   Polished with Al_2O_3 abrasive

R_a 35.8 nm R_t 492.5 nm R_p 116.2 nm

R_v 376.4 nm   RMS   58.5 nm

200 nm

100μm

b)   Polished with Cr_2O_3 abrasive
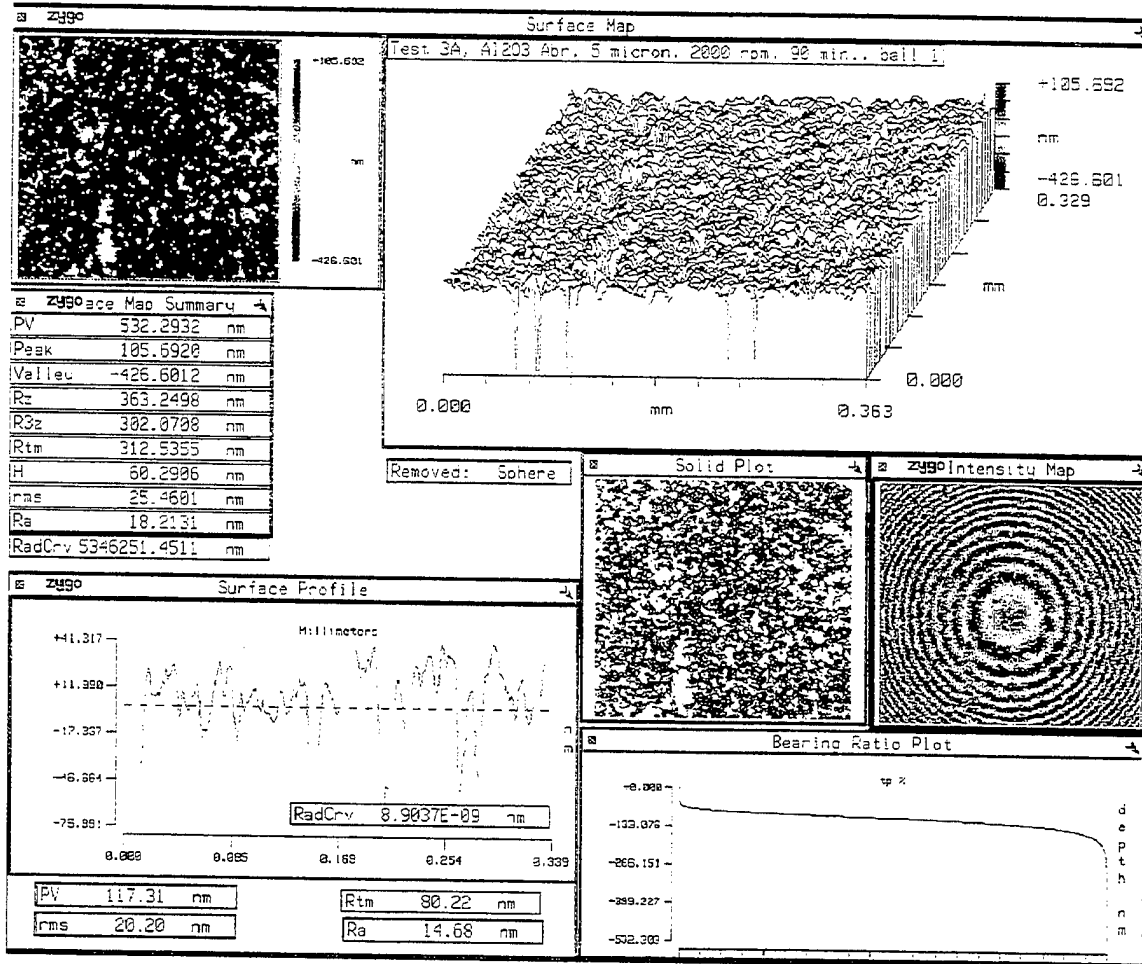
R_a 9.1 nm R_t 146.4 nm R_p 33.2 nm

R_v 113.2 nm   RMS   13.6 nm

200 nm

100μm
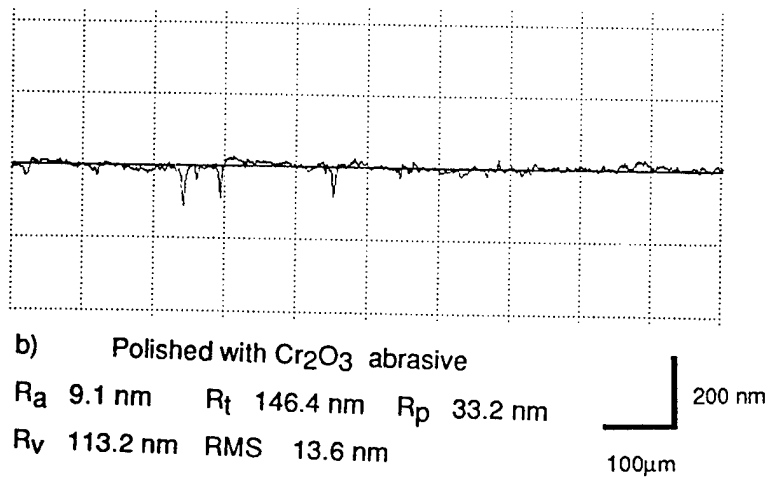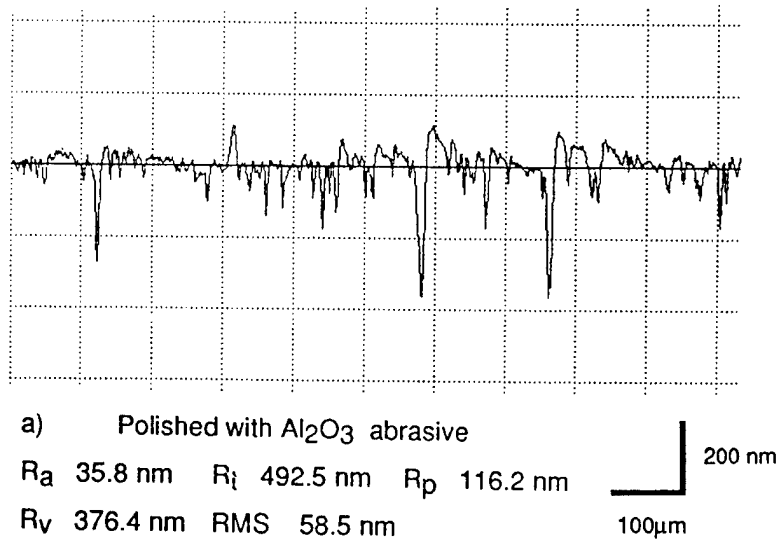
Figures 8(a) Surface roughness profiles obtained (using the Form
& (b) Talysurf) on silicon nitride balls polished using Al_2O_3
and Cr_2O_3 abrasives Respectively.The smoother surface
with Cr_2O_3 and the formation of deep pits in the case of
Al_2O_3 abrasive are evident
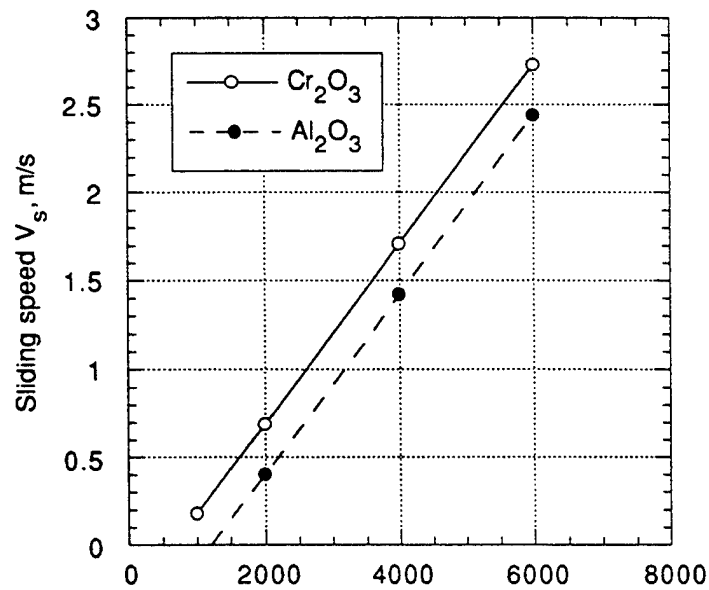
Figure 9 Variation of sliding speed with drive shaft speed (from Equation 2). It can be seen that the sliding speed with Cr_2O_3 is larger than with Al_2O_3 at the same shaft speed
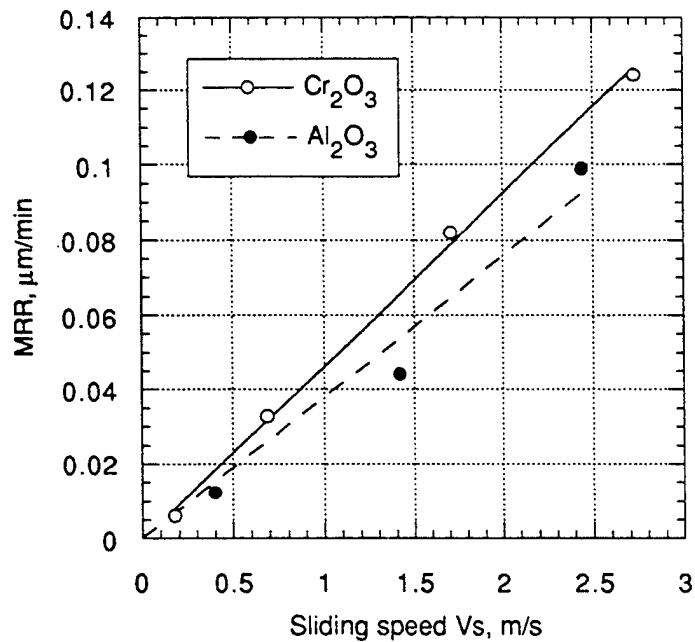
Figure 10 Variation of the MRR with sliding speed showing that MRR's are proportional to the sliding speed and the gradient for Cr_2O_3 is larger than that of Al_2O_3 by approximately 20%

APPENDIX I

ON CHEMO-MECHANICAL POLISHING OF SILICON

NITRIDE WITH CHROMIUM OXIDE ABRASIVE

S. R. Bhagavatula and R. Komanduri

FINISHING OF ADVANCED CERAMICS

Part I : on chemo-mechanical polishing of Si_3N_4 with Cr_2O_3 abrasive

S. R. Bhagavatula and R. Komanduri

Mechanical and Aerospace Engineering, Oklahoma State University

Stillwater, OK 74078, U.S.A.

ABSTRACT

Chromium oxide (Cr_2O_3) is an excellent abrasive for the polishing of silicon nitride (Si_3N_4) work material. As the hardness of Cr_2O_3 is nearly the same as that of Si_3N_4, the mechanism of material removal is believed to be chemo-mechanical rather than mechanical abrasion. However, no evidence of any compound formation of Si_3N_4 with Cr_2O_3 abrasive was reported. Consequently, the role of Cr_2O_3 was considered to be one of a *catalyst* , in view of its well known role as a catalyst, rather than its direct involvement in the chemical reactions with Si_3N_4. In this letter, we report new evidence using an SEM with an X-ray microanalyzer and a low angle X-ray diffraction that shows conclusively that Cr_2O_3 does participate in chemo-mechanical polishing of Si_3N_4 forming chromium nitride and chromium silicate, thus establishing the role of Cr_2O_3 not as a *mere catalyst* but one actively taking part in the chemical reactions during chemo-mechanical polishing.

1. INTRODUCTION

The development of high performance ceramics (or advanced ceramics) is stimulating major advances in a large spectrum of industries including machine tools, electronics, manufacturing engineering, and chemical and metallurgical processing. Alumina (Al_2O_3), zirconia (Zr_2O), silicon carbide (SiC), and silicon nitride (Si_3N_4) are the most important advanced ceramic materials among high performance ceramics and Si_3N_4 is the most promising material in this category for structural and bearing applications. This is in view of silicon nitride's high fracture toughness and failure mode amongst advanced ceramics in addition to its other desirable properties (Katz and Hanoosh 1985).

Most of the advanced ceramic materials, unfortunately, are difficult to shape and finish, in general, owing to their high hardness and brittleness. Unlike with metals, plastic deformation is not the preferred mode of material removal. Instead material removal is by brittle fracture. Consequently, with conventional grinding and polishing techniques, surface damage is inherently present on the workpiece in the form of pits and scratches, and subsurface damage in the form of lateral and median cracks (Marshall et al 1983). These defects affect the performance and reliability of the products in service. Diamond abrasive is invariably used for grinding as well as for polishing of

advanced ceramics. Consequently, the cost of finishing is high and the time taken for finishing is also significantly long, sometimes of the order of several weeks. To address this problem, need arises for an alternate technique that minimizes the defects associated with conventional material removal processes. Chemo-mechanical polishing is one such technique suitable for hard, brittle workmaterials that have good chemical affinity with the abrasive under the conditions of polishing and in a given environment.

Conventional material removal of advanced ceramics using abrasives harder than the work material involves indentation and abrasion leaving scratches, pitting, and fine cracks on the surface (Marshall et al 1983). In contrast, chemo-mechanical polishing (also termed mechano-chemical polishing) depends on the chemical interaction between the abrasive, the workmaterial, and the environment (Yasunaga 1979). Oftentimes, the abrasive used is of the same hardness or even softer than the workmaterial since hardness is really of no consequence in this type of material removal but chemical activity. Consequently, no scratching or groove formation is expected with these abrasives leading to a very smooth surface. Hence, for finishing advanced ceramics, chemo-mechanical action is rather an attractive alternate proposition especially during the final stages of polishing.

The chemo-mechanical process initiates a chemical reaction between a given abrasive and the work material. The process produces a weaker reaction product compared to either the abrasive or the workmaterial. The environment used can facilitate the chemical action. The reaction product thus formed is brittle and subsequently removed by the abrasive action. This results in producing a smooth surface. However, the presence of defects, such as pits, grooves from an earlier semifinishing operation can still exist in the final operation unless all the defects are removed by this operation. Or, alternately, these defects should be gradually minimized as one progresses from roughing to semifinishing to finishing. Hence, the history of polishing is a very important consideration in the final finishing condition of advanced ceramics.

Several studies were reported in the literature on the various aspects of finishing Si_3N_4 in view of this material's potential for advanced structural applications, such as parts of gas turbine, bearings for high-speed and high-precision spindles. These studies include oxidation of Si_3N_4 (Singhal 1976, Clarke and Lange 1980, Cubicciotti and Lau 1978, Kiehle et al 1975) in air; hydrothermal oxidation of Si_3N_4 (Contet et al 1987), mechano-chemical polishing of Si_3N_4 using fine, softer abrasives, such as Fe_2O_3 (Yasunaga 1979, Uematsu et al 1993, Vora et al 1982), grinding of Si_3N_4 powder in water (Kanno et al 1983), tribochemical studies of Si_3N_4 on Si_3N_4 in different gaseous and liquid media (Fischer and Tomizawa 1985, Fischer 1988, Cranmer 1989), sliding

wear of Si_3N_4 on Si_3N_4 in air and in water (Cranmer 1989), wear of Si_3N_4 on Si_3N_4 in water under rolling contact (Kato 1990, Akazawa et al 1986, Akazawa and Kato 1988), tribological studies of Si_3N_4 in various environments (Jahanmir and Fisher 1988, Dong and Jahanmir 1993), combined effect of speed and humidity on wear and friction of Si_3N_4 (Gee and Butterfield 1993), corrosion of Si_3N_4 (Munro and Dapkunas 1993), Sato et al 1991), material removal mechanism of Si_3N_4 during rubbing in water (Sugita et al 1984), fracture toughness and hardness dependent polishing wear of Si_3N_4 ceramics (Gardos and Hardisty 1993), and the wear behavior of Si_3N_4 sliding on Si_3N_4 in the presence of water at high temperatures and pressures (Xu et al 1994). The possibility of chemo-mechanical action is polishing of Si_3N_4 with Cr_2O_3 abrasive was investigated by Raghunandan et al (1994).

The above studies have indicated that oxidation of Si_3N_4 as the crucial step in the tribological and tribochemical behavior of this material. The results also indicate the formation of an amorphous silica on the surface when Si_3N_4 was polished in air and the formation of a hydrated silica layer when polished in water. However, no evidence of compound formation of Si_3N_4 with Cr_2O_3 abrasive was reported. Consequently, the role of Cr_2O_3 was considered as one of a catalyst rather than direct involvement in the chemical reactions. This is reasonable in view of the well known role of Cr_2O_3, in general, as a catalyst for chemical reactions and the absence of any evidence to prove otherwise. In this letter, we report new evidence that shows conclusively that Cr_2O_3 does participate in the chemo-mechanical polishing of Si_3N_4 forming chromium nitride and chromium silicate, thus establishing the role of Cr_2O_3 not as a mere *catalyst* but one actively taking part in the chemical reactions during chemo-mechanical polishing.

2. EXPERIMENTAL PROCEDURE

Chemo-mechanical polishing studies were conducted using hot isostatically pressed Si_3N_4 workmaterial (CERBEC 200 made by Norton Advanced Ceramics) (balls and rollers) with Cr_2O_3 abrasive. MgO was used as the sintering aid. It may be noted that Cr_2O_3 abrasive is about the same hardness as Si_3N_4 work material. Hence, very little of the material removal, if any, should occur by mechanical abrasion. Magnetic float polishing technique (with a water based magnetic fluid) was used for finishing Si_3N_4 balls (Fox et al 1994) and magnetic abrasive finishing technique with magnetic abrasive agglomerate (iron particles with about 10 % Cr_2O_3 abrasive) was used for finishing Si_3N_4 rollers (Umehara 1994).

The magnetic float polishing technique is based on the magneto-hydrodynamic behavior of a magnetic fluid that can float non-magnetic abrasives suspended in it by a magnetic fluid. The forces applied by the abrasive to the part are extremely small

(1N/ball) and highly controllable. The magnetic fluid is a colloidal dispersion of extremely fine (100 to 150 A) subdomain ferromagnetic particles, usually magnetite (Fe_3O_4), in a carrier fluid, such as water or kerosene. In this investigation a water base ferrofluid is used. The ferrofluids are made stable against particle agglomeration by the addition of surfactants. When a magnetic fluid is placed in a magnetic field gradient, it is attracted towards the higher magnetic field side. If a non magnetic substance (abrasives in this case) is mixed with the magnetic fluid, they are discharged towards the lower side. When the field gradient is set in the gravitational direction, the non magnetic material is made to float on the fluid surface by the action of the magnetic levitational forces. Thus, the polishing operation in this process is facilitated by the magnetic buoyant levitational force.

In magnetic abrasive finishing an agglomerate of ferromagnetic particles (iron power) and fine abrasive is used as the magnetic abrasive. The magnetic abrasive conglomerates are about 50 to 400 μm and the abrasives are in the 1 to 10 μm range. The magnetic abrasive is charged into the gap between the magnetic poles to form a magnetic brush. When a cylindrical workpiece, such as a ceramic roller with rotary and vibratory motions, is placed in the magnetic field, surface and edge finishing operations are performed by these magnetic abrasive brushes. The process is highly efficient and the removal rate and finish depend on the workpiece circumferential speed, magnetic flux density, working clearance, workpiece material, size of the magnetic abrasive conglomerate including the type of abrasive used, grain size, and volume fractions of the abrasive and magnetic material in the conglomerate.

Wear debris generated during polishing was collected, separated, and analyzed using an ABT 32 scanning electron microscope (SEM) with a Kevex energy dispersive X-ray microanalyzer (EDX) and a Seimens low angle X-ray diffractometer (XRD). Similarly, the finished balls and rollers were examined in the SEM for surface characterization and a stylus based TalySurf for surface roughness measurements.

3. RESULTS AND DISCUSSION

Figure 1(a) is a SEM micrograph of a portion of the polished Si_3N_4 ball showing an extremely smooth surface generated during polishing and Figure 1(b) is a TalySurf trace showing surface profile (Ra of the order of 16.6 nm). Energy dispersive X-ray (EDX) analysis (i.e. Si and Cr maps) with the SEM images of some individual wear particles generated during polishing of Si_3N_4 with Cr_2O_3 abrasive showed the presence of both chromium and silicon in the same area as the wear particle suggesting the possibility of chromium silicate formation (Figure 2). Similarly, EDX analysis of other wear particles showed the presence of silicon but absence of magnesium in some cases

and presence of magnesium in the other. The later was identified as due to brittle fracture of Si_3N_4 wear particles and the former as chemo-mechanical reaction product possibly of chromium nitride. Unfortunately, the X-ray dispersive microanalyzer of the SEM is not capable of detecting light elements including nitrogen. However, the analysis of the wear debris using the X-ray diffractometer (XRD) clearly showed the formation of chromium nitride and chromium silicate in addition to SiO_2 and Cr_2O_3 (Figure 3) thus lending support to the EDX analysis. The brittle reaction product that is formed during chemo-mechanical polishing is then expected to be removed during subsequent mechanical action by the abrasive. In addition to chromium silicate and chromium nitride, magnesium silicate was also identified. This is the glassy grain boundary phase that forms with the sintering aid, MgO, and which flow towards the surface.

4. CONCLUSIONS

In conclusion, it may be noted that polishing of Si_3N_4 workmaterial with Cr_2O_3 abrasive yields excellent surface finish with minimal surface and subsurface defects (R_a 16.6 nm). Since material removal by abrasion is not possible with Cr_2O_3 (in view of small difference, if any, in the hardness between Cr_2O_3 abrasive and Si3N4 workmaterial) chemo-mechanical action between the abrasive-workmaterial -environment is generally offered as the alternate mechanism of polishing. In chemo-mechanical polishing, material removal is accomplished by a solid phase chemical reaction caused by the high temperatures and high pressures generated due to frictional energy at the contacting points between the abrasive and the workpiece. Very small amounts of material is removed from the surface of the ceramic workpiece as a reaction product due to chemical reaction between the abrasive particles and the workpiece at the contact points. The reaction product is removed by the mechanical action of the abrasive. It is therefore necessary to examine the wear debris (and not the finished part) to identify the mechano-chemical action. Instead of the exclusive role of catalytic action of Cr_2O_3 postulated by other researchers, we have identified by X-ray diffraction and SEM EDX analysis, the formation of chromium nitride and chromium silicate during chemo-mechanical polishing. Thus, the role of Cr_2O_3 abrasive in chemo-mechanical polishing is more than a catalyst. It, in fact, participates actively in the chemical reactions forming reaction products with the work material and the environment. A similar approach can be adopted in polishing other advanced ceramics by properly selecting the abrasive that is conducive to chemo-mechanical polishing. Part II presents a model of the chemo-mechanical polishing of Si_3N_4 workmaterial with Cr_2O_3 abrasive in air and in water environments based on the chemical reactions that can be formed

thermodynamically during the process and the experimental evidence presented in this letter (Bhagavatula, 1995).

ACKNOWLEDGMENTS

REFERENCES

Akazawa, M., Kato, K., and K. Umeya, 1986, Wear **110**, 285-293
Akazawa, M. and K. Kato, 1988, Wear **112**, 123-132
Bhagavatula, S. R., 1995, M.S. Thesis, Oklahoma State University, Stillwater,OK
Clarke, D. R. and F. F. Lange, 1980, J. Am. Cer. Soc., **63**, 586-593
Contet, C., Kase, Noma, J.I., Yoshimura, T. M., and S. Somiya, 1987,
J. Mater. Sci. Lett. **6**, 963-964
Cranmer, D. N., 1989, STLE Lubrication Engineering **44** , 975-980
Cubicciotti, D. and K. H. Lau, 1978, J Am. Cer. Soc., **61**, 512-517
Dong, X. and S. Jahanmir, 1993, Wear **165**, 169-180
Fischer, T.E. and H. Tomizawa, 1985, Wear **105** , 29-45
Fischer, T.E., 1988, Ann. Rev. of Mat. Sci., **18**, 303-323
Gee, M. G. and D. B. Butterfield, 1993, Wear **162-164**, 234 -245
Jahanmir, S. and T. E. Fisher, 1988, STLE Trans., **31**, 32 -43
Kanno, Y., et al., 1983, Yogyo-Kyokai-Shi, **91**, 386
Kato, K., Wear **136**, 117-133 (1990)
Katz, R. N., and J. G. Hanoosh, 1985, Int.J. High.Tech. Cer. **1**, 68-79
Kiehle, A. J. , L. K. Heung, P. J. Gielisse, and T. J. Rockett, 1975, J. Am. Cer. Soc.
58, 17-20
Marshall, D.B., Evans, A.G., Khuri-Yakub, B. T., Tien, J. W., and G. S. Kino, (1983,
Proc. Roy. Soc. (Lond) A385, 461-475
Munro R. G. and S. J. Dapkunas, 1993, J. Research of the NIST **98**, 607-631
Raghunandan, M., Umehara, N., and R. Komanduri, 1994, Proc. of the Sym. on Tribology in Manufacturing, ASME/STLE Triblology Conference, Lahaina, Maui, Hawaii, 81-89. Sato, T., Murakami, T., Endo, T., Shimada, M., Komeya, K., Kameda, T., and M. Komatsu, 1991, J. Material Sci., **10**, 1749-1754
Singhal, S. C., 1976, J. Am. Cer. Soc. **59**, 81
Sugita, T., Veda, K., and Y. Kanemura, 1984, Wear, **97**, 1-8
Tomizawa, H and T.E. Fischer, 1987, ASLE Trans. **30** , 41-46
Uematsu, T., Wu, M. H., Suzuki, K., and O. Imanaka, Jan 1993, Machining of Advanced Ceramics, NIST Special Publication No. 847, 409-413
Umehara, N, 1994, Annals of CIRP 43/1,185-188

Vora. H., Orent, T. W., and R.J. Stokes, 1982 Commn. of Am. Cer. Soc., C140 -C141
Yasunaga, N., Tasuni, N. and A. Ohara, 1979, NBS Publication No. 562, 171-183
Xu, J. G. , K. Kato, and N. Umehara, 1994, Personal Communication
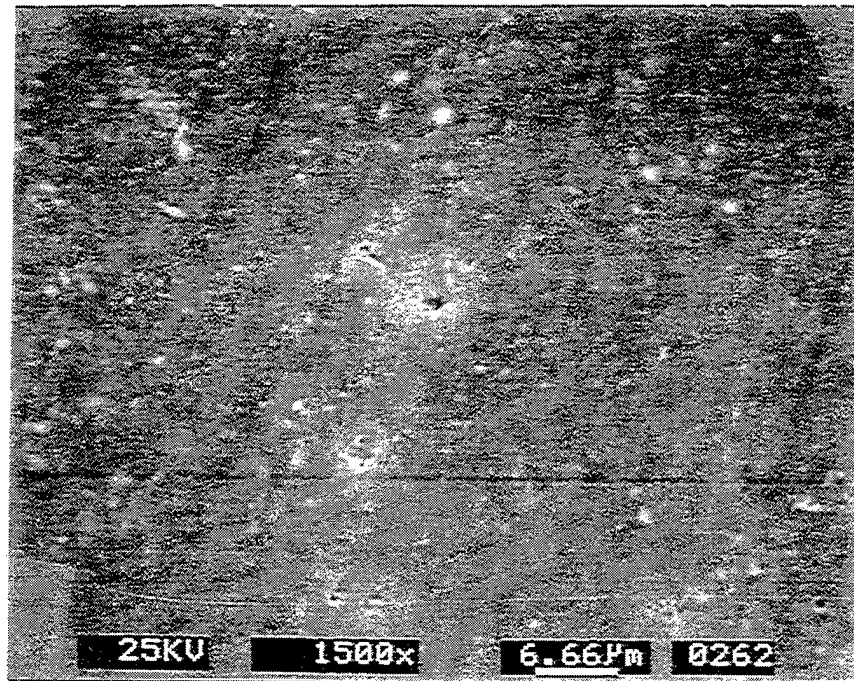
Figure 1 (a)   SEM micrograph of a chemo-mechanically polished Si_3N_4 work material with Cr_2O_3 abrasive showing smooth surface.

R_a 16.6 nm R_t 0.54 μm
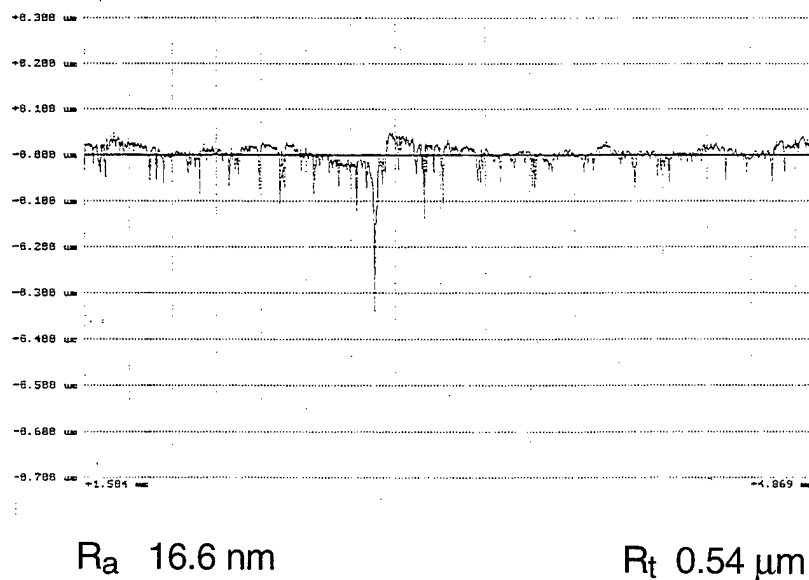
Figure 1 (b)   Surface profile (obtained using Talysurf) on Si_3N_4 work material showing a surface finish (R_a) of about 16.6 nm.
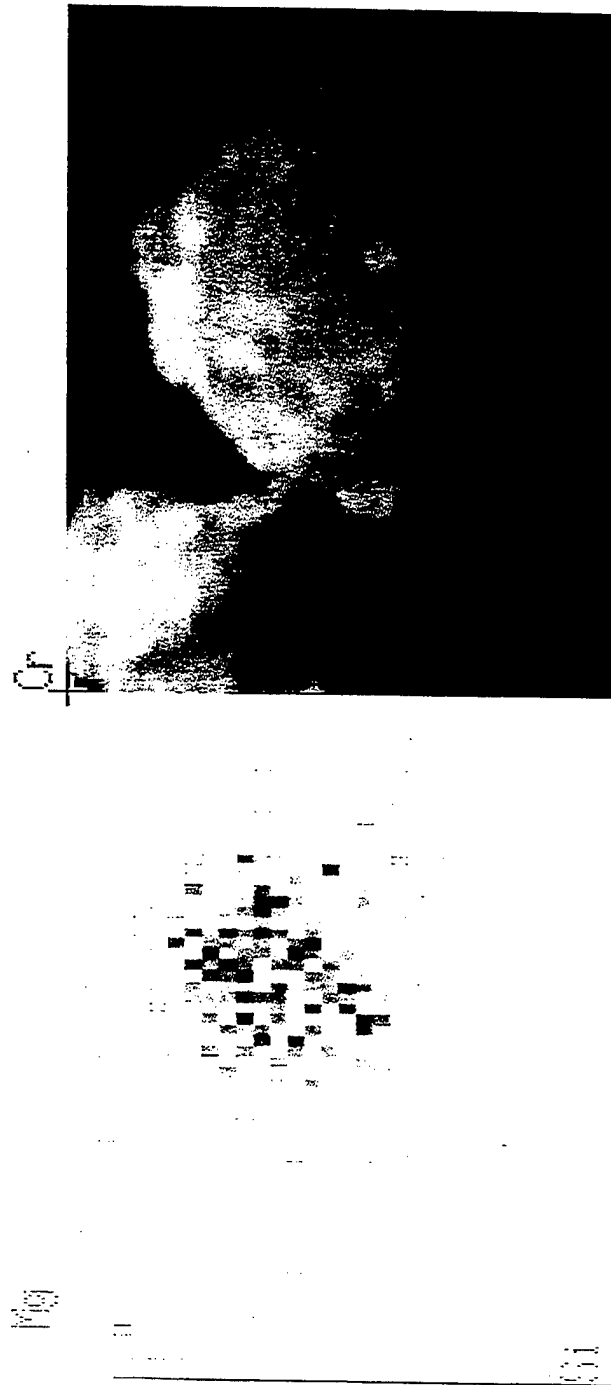
Figure 2   SEM micrograph and EDX analysis of Cr and Si of a typical
particle from the wear debris showing simultaneous existance of
Cr and Si (suggesting the formation of Cr_2SiO_4). Compare the
morphology of the wear particle with that of Cr and Si mapping.

Figure 3. X-ray diffraction analysis of the wear debris showing the
presence of chromium nitride and chromium silicate
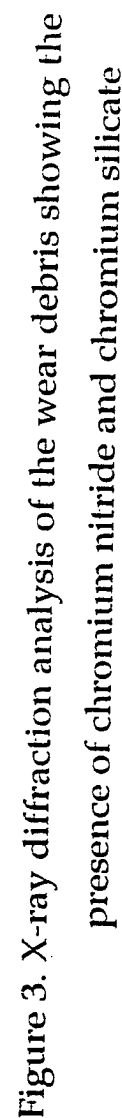
APPENDIX J

ON THE MECHANISM OF CHEMO-MECHANICAL

POLISHING OF SILICON NITRIDE WITH CHROMIUM OXIDE

ABRASIVE

S. R. Bhagavatula and R. Komanduri

FINISHING OF ADVANCED CERAMICS

Part II: on the mechanism of chemo-mechanical polishing

of Si_3N_4 with Cr_2O_3 abrasive

S. R. Bhagavatula and R. Komanduri
Mechanical and Aerospace Engineering, Oklahoma State University
Stillwater, OK 74078, U.S.A.

ABSTRACT

Based on the experimental evidence presented in Part I (Bhagavatula and Komanduri 1995) a new model of chemo-mechanical polishing of Si_3N_4 in air and in water environments with Cr_2O_3 abrasive is presented. This model is based on the formation of such reaction products as chromium silicate and chromium nitride in addition to the formation of silica layer on Si_3N_4 surface as well as the gaseous reaction products, such as ammonia (in water) and nitrogen (in air). For the chemo-mechanical polishing Si_3N_4 work material with Cr_2O_3 abrasive in air, the reactions that are formed include oxidation of Si_3N_4 to form a silica layer on the surface and the evolution of nitrogen gas. Other reaction products include the formation of chromium nitride and chromium silicate. For the chemo-mechanical polishing in water, the reactions are essentially the same except in this case, the adsorption of hydroxyl ions to the surface of Si_3N_4 and oxidation of the surface takes place, which forms initially a silica layer which further gets oxidized to form a hydrated silica ($SiOH_4$) layer. When the nitrogen ions get an opportunity to pair up with hydrogen ions present in water, they form ammonia gas (instead of nitrogen gas, as in the case of air). The other reaction products are the same, namely, chromium nitride and chromium silicate. The implication of gaseous reaction products in the generation of pore-free surface in finishing is also pointed out.

1. INTRODUCTION

As pointed out in Part I (Bhagavatula and Komanduri 1995), several studies were reported in the literature on the various aspects of finishing Si_3N_4. This is in view of this material's potential for advanced structural applications, such as parts of gas turbine, bearings for high-speed and high-precision spindles. These studies have indicated that oxidation of Si_3N_4 as a crucial step in the tribochemical behavior of this material. The results also indicate the formation of an amorphous silica on the surface when Si_3N_4 was polished in air and the formation of a hydrated silica layer when polished in water. However, no evidence of compound formation of Si_3N_4 with Cr_2O_3 abrasive was reported. Consequently, the role of Cr_2O_3 was considered as one of a catalyst rather than direct involvement in the chemical reactions. This conclusion

appears reasonable in view of the well known role of Cr_2O_3 as a catalyst, in general, for initiating chemical reactions and the absence of any evidence thus far to support an alternate mechanism. However, new evidence that was reported in Part I (Bhagavatula and Komanduri 1995) showed conclusively that Cr_2O_3 does participate in the chemo-mechanical polishing of Si_3N_4 forming chromium nitride and chromium silicate. This establishes the role of Cr_2O_3 not as a mere catalyst but one actively taking part in the chemical reactions during chemo-mechanical polishing. In this letter we present a mechanism of chemo-mechanical polishing of Si_3N_4 work material with Cr_2O_3 abrasive both in air and in water environments.

2. MECHANISM OF CHEMO-MECHANICAL POLISHING

Chemo-Mechanical Polishing in Air

During polishing, depending on the depth of cut, the abrasive encounters a thin layer of silica on the surface as well as the underlying material, namely, Si_3N_4 parent material. Chemo-mechanical action takes place at the real areas of contact under the conditions of polishing. Figure 1 is a schematic of the chemo-mechanical polishing model for Si_3N_4 workmaterial with Cr_2O_3 abrasive in air showing the various reactions occurring during the process (Bhagavatula 1995). During polishing, the flash temperatures at the real areas of contact can be relatively high. Using Carslaw and Jaeger's solutions (Carslaw and Jaeger 1959) for a moving disk heat source, we have estimated the flash temperatures to be in the range of 1200-2000°C when polishing in air (magnetic abrasive finishing) (Hou and Komanduri 1995). At these conditions, oxygen from the surrounding atmosphere can react with Si_3N_4 to form a thin layer of silica on the surface. This has to be balanced by the evolution of nitride ions through the bulk material. When two nitride ions combine, a molecule of nitrogen gas is formed in the bulk of Si_3N_4 and is evolved from the silica layer giving rise to porosity on the surface. For obtaining near defect free surface this should be minimized. The oxidation of Si_3N_4 in air can thus be represented by the following equation:

$$Si_3N_4 + 3\ O_2 \rightarrow 3\ SiO_2 + 2\ N_2\uparrow \qquad (1)$$

Also, the nitride ions can react with the chromium ions provided by the Cr_2O_3 abrasive to form chromium nitride. Chromium in its 3^+ state forms a large number of complexes, particularly when nitrogen is the donor atom, virtually all being six co-ordinate and octahedral (Earnshaw and Harrington 1973). The effect of Cr_2O_3 alone on the oxidation of Si_3N_4 can be represented by the following equation:

$$Si_3N_4 + 2\ Cr_2O_3 \rightarrow 3\ SiO_2 + 4\ CrN \qquad (2)$$

155

The combined effect of Cr_2O_3 and oxygen can be obtained by adding and balancing Equations 1 and 2 which is represented by the following equation:

$$4 Si_3N_4 + 2 Cr_2O_3 + 9 O_2 \rightarrow 12 SiO_2 + 4 CrN + 6 N_2 \qquad (3)$$
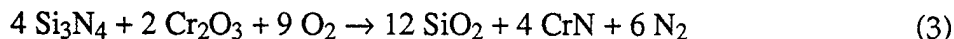
Further, the action of Cr_2O_3 on the formation of silicate phase can be represented by the following equation:

$$2 Cr_2O_3 + 2 SiO_2 \rightarrow 2 Cr_2 SiO_4 + O_2 \uparrow \qquad (4)$$
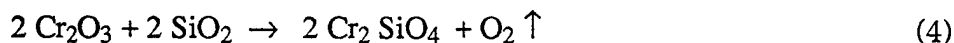
Thus, the reaction product consists of both chromium nitride and chromium silicate. The material removal occurs largely by this process and the brittle reaction product that is formed is removed by subsequent mechanical action of the abrasive.

Chemo-Mechanical Polishing in Water

Figure 2 is a schematic of the chemo-mechanical polishing model for Si_3N_4 work material with Cr_2O_3 abrasive in water showing the various reactions occurring during the process (Bhagavatula 1995). During polishing, the flash temperatures at the real areas of contact can be relatively high. Using Carslaw and Jaeger's solutions (Carslaw and Jaeger 1959) for a moving disk heat source, we have estimated the flash temperatures to be in the range of 500-800°C when polishing in water (magnetic float polishing of balls) (Hou and Komanduri 1995). Here, the reactions are essentially the adsorption of hydroxyl ions to the surface of Si_3N_4 and oxidation of the surface, which forms initially a silica layer which further gets oxidized to form hydrated silica layer. When the nitrogen ions get an opportunity to pair up with hydrogen ions present in water, it forms ammonia gas. Generation of ammonia gas was detected by previous investigators (Kanno et al 1983) thus lending support to this hypothesis. Thus, the oxidation of Si_3N_4 in water proceeds by the following equation:

$$Si_3N_4 + 6 H_2O \rightarrow 3 SiO_2 + 4 NH_3 \uparrow \qquad (5)$$

The thermodynamic arguments given above for the dry case is equally applicable here for the wet case, except that instead of the nitrogen gas, ammonia gas is produced. The action of chromium in Cr_2O_3 in its 3^+ state alone on Si_3N_4 can be again represented by Equation 2, thus

$$Si_3N_4 + 2 Cr_2O_3 \rightarrow 3 SiO_2 + 4 CrN \qquad (2)$$

The combined action of Cr_2O_3 and water can be represented by the following equation:

$$Si_3N_4 + Cr_2O_3 + 3 H_2O \rightarrow 3 SiO_2 + 2 CrN + 2 NH_3 \uparrow \qquad (6)$$

156
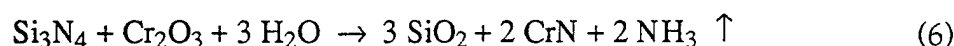
Further, Cr_2O_3, with chromium in its 2^+ oxidation state, can react with silica in the presence of water to form chromium silicate.

$$2\ Cr_2O_3 + 2\ SiO_2\ \rightarrow\ 2\ Cr_2\ SiO_4\ + O_2 \uparrow \tag{7}$$
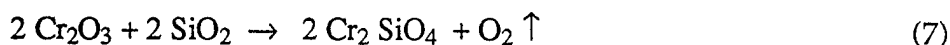
This equation is similar to the above case for air. Chromium in Cr_2O_3 in its 2^+ oxidation state reacts with silica, forming chromium silicate as a reaction product (Earnshaw and Harrington 1973). This reaction also evolves oxygen, partly replenishing the amount that was spent during the previous reactions. Therefore, oxygen is made continuously available even in water for oxidation. Consequently, these reactions are almost identical. However, the important difference in polishing Si_3N_4 with Cr_2O_3 in water and in air is that water forms an additional reaction with silica which is represented by the following equation:

$$3SiO_2 + 6H_2O \rightarrow 3Si(OH)_4 \tag{8}$$

This reaction produces a hydrated layer of silica forming silicic acid (H_2SiO_3) as a reaction product. Since the hydrated silica layer is amorphous, the reaction products, such as chromium silicate and chromium nitride generated during the chemo-mechanical polishing with Cr_2O_3 in water could not be detected by X-ray diffraction in higher amounts as was the case in polishing in air. Also, the flash temperatures generated during polishing of Si_3N_4 in water are in the range of 500 to 800 °C where as in the case of polishing in air, they are much higher, in the range of 1200 to 2000 °C. This enables chromium silicate (the reaction product) and chromium nitride (the oxidation product) to increase in their crystallinity and to achieve higher order arrangement of the lattices as observed in the X-ray diffraction of the wear debris (Bhagavatula 1995).

3. DISCUSSION

It can be seen that the flash temperatures are higher (estimated to be in the range of 1200-2000°C) when polishing in air (magnetic abrasive finishing) than when polishing in water (magnetic float polishing of balls) (estimated to be in the range of 500-800°C (Hou and Komanduri 1995). A thermodynamic analysis of the oxidation of Si_3N_4 in air and hydrothermal oxidation of Si_3N_4 was carried out in this investitgation. Based on the calculated values of Gibbs free energy of formation, it was found that water is more effective below 700 °K ($\Delta G^O\ _{700\ °K}$ = -113 kcal/mole) and air is effective at higher temperatures ($\Delta G^O\ _{700\ °K}$ = -131 kcal/mole).

The effect of air on the oxidation of Si_3N_4 is represented by Eqn. 1 This reaction generates four nitride ions which combine to form two molecules of nitrogen gas. The

effect of Cr_2O_3 alone on oxidation of Si_3N_4 is represented by Eqn. 2. The attraction of chromium ions towards nitride ions and the presence of three oxygen molecules of gas in Cr_2O_3 plus the high flash temperatures that are generated in polishing can result in the dissociation of Si-N bonds from Si_3N_4 to form silica. All the 4 nitride ions released from this reaction can combine to form chromium nitride. Hence, there is no nitrogen gas formation in this case. It can also be seen that the amount of nitrogen gas production is effectively reduced because of chromium nitride formation (or in other words due to the presence of Cr_2O_3). In the absence of Cr_2O_3, 4 Si_3N_4 atoms would require 12 oxygen molecules to produce 8 molecules of nitrogen, giving rise to 12 molecules of silica (Eqn. 1). But the presence of 2 molecules of Cr_2O_3 will facilitate in all 12 atoms of silica formation, even though only 9 oxygen molecules are present, while limiting the nitrogen gas generation to only 6 molecules (Eqn. 3). This implies that the activation energy required for the silica formation is being reduced and the generation of nitrogen gas is not favoured. Both these issues are favorable and critical in the ultimate polishing characteristics of Si_3N_4. Also, chromium in its 2^+ state reacts with the silica layer to form chromium silicate as the reaction product evolving oxygen as a byproduct (Earnshaw and Harrington 1973). This oxygen in turn is made available for subsequent oxidation of Si_3N_4.

Thus, Cr_2O_3 abrasive in chemo-mechanical polishing of Si_3N_4 performs three functions: 1. It promotes oxidation of Si_3N_4 by directly reacting with the nitride ions released during the initial oxidation to form chromium nitride. The reaction causes a reduction in the release of nitride ions, 2. Oxidation of Si_3N_4 in the presence of Cr_2O_3 increases the residence time of the nitride ions and promotes the release of nitride ions from the bulk material which would otherwise get released as nitrogen gas from the bulk material. The activation energy required for oxidation in the presence of Cr_2O_3 is reduced considerably owing to the strong attraction of nitride ions towards chromium ions (3^+) oxidation state. Thus, it reduces the generation of surface porosity during the oxidation of Si_3N_4, and 3. Cr_2O_3 also takes part in the chemical reaction with the silica layer on the Si_3N_4 and forms a brittle reaction product, chromium silicate, which is removed during subsequent mechanical action by the abrasive. Chemo-mechanical polishing in water results in reduced gas generation (ammonia) which is advantageous in the production of defect free or pore free surfaces.

It is interesting to note that the chemo-mechanical action in air and in water is very similar. The main difference being the degree of crystallinity of the reaction products which increases in air due to the generation of higher temperatures at the real area of contact. Water causes hydrolization of the silica layer making it amorphous. X-

ray diffraction analysis of the wear debris collected from samples polished in air and water confirmed these findings (Bhagavatula 1995).

Based on the above descriptions, the main differences in the chemical reactions in chemo-mechanical polishing of Si_3N_4 with Cr_2O_3 in air and in water are the following: 1. Formation of nitride (N^{-3}) ions due to oxidation of Si_3N_4 which combine among themselves to form nitrogen gas in air and formation of nitride (N^{-3}) ions which combine with H^+ ions to form ammonia gas in water, 2. formation of oxygen 2^- ions in air and OH^- and H^+ ions in water, and 3. formation of hydrated silica layer in water in addition to silica layer in both cases.

It may be noted that in this simple analysis of chemo-mechanical polishing presented here, we have only considered the reactions between Si_3N_4 and Cr_2O_3 in air and water environments. For a more complete picture, we should also consider the role of the sintering aid, namely, MgO in this case, which forms magnesium silicate. During polishing, the high temperatures generated at the contact points can result in grain boundary sliding and viscous flow of the glassy phase. This can affect the reaction kinetics.

4. CONCLUSIONS

In summary, the function of Cr_2O_3 in chemo-mechanical polishing of Si_3N_4 may be considered as three fold. First, it enhances the oxidation kinetics by forming chromium nitride which facilitates the formation of the silica layer. Second, it increases the nitrogen ion residence time, which ultimately reduces the formation of surface porosity which is crucial in achieving a good surface without stress concentrations. Third, it reacts with the silica layer to form chromium silicate, which gets removed during the subsequent mechanical abrasion. Though, silica does not provide a protective layer, physical removal of the surface film increases the diffusional characteristics which again facilitates the oxidation process. This may be termed as an autocatalytic action of the abrasive, which removes material from the workmaterial while reacting with it, and the mere action of material removal again forms the same material which will be removed in the next instant. Cr_2O_3 can still provide the catalytic effect as identified by the earlier researchers but not exclusively.

ACKNOWLEDGMENTS

Coblenz of ARPA for their interest in this work. Thanks are also due to Mr. M. Raghunandan and Mr. M. Fox, graduate students at OSU, for generating the samples used in this investigation.

REFERENCES

Bhagavatula, S. R. , 1995, M.S. Thesis, Oklahoma State University, Stillwater, OK

Bhagavatula, S. R. and R. Komanduri, 1995, Part I submitted for publication

Carslaw, H. S. and J. C. Jaeger, 1959, "Conduction of Heat in Solids," Oxford University Press, Oxford, U.K.

Earnshaw, A. and T. J. Harrington, 1973, "The Chemistry of Transition Metals," Clarendon Press, Oxford, U.K.

Hou, Z. B., and R. Komanduri, 1995, to be submitted for publication

Kanno, Y., Suzuki, K., and Y. Kuwahara, 1983, Yogyo-Kyokai-Shi, 31, 386
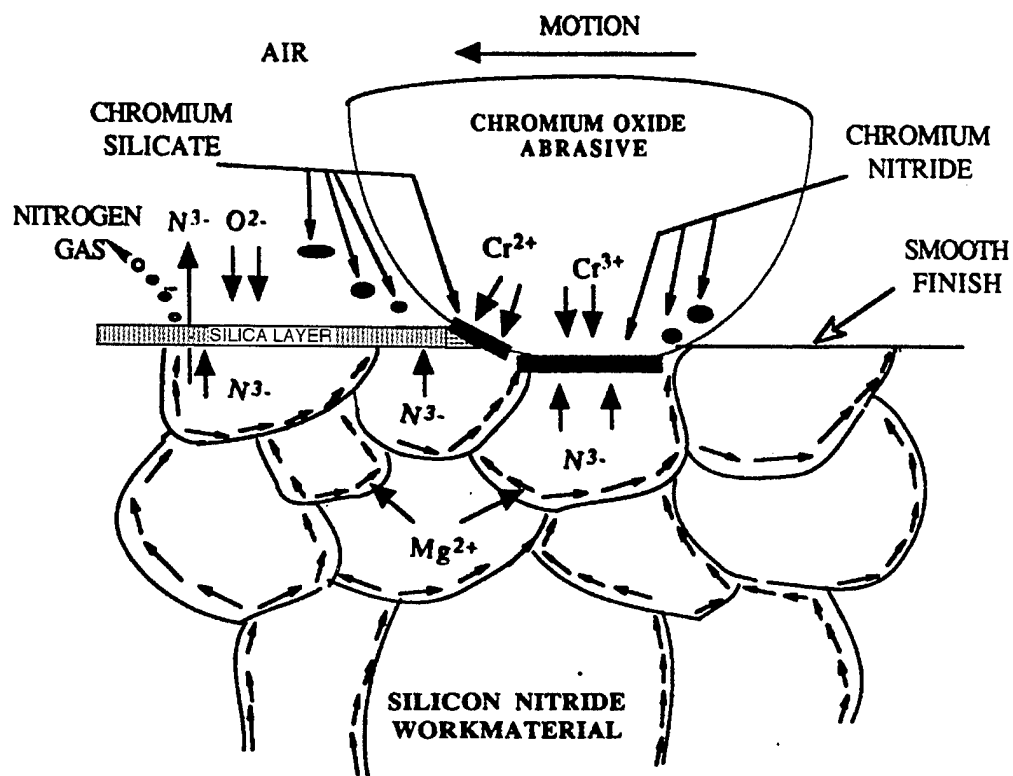
Reactions occuring in the chemo-mechanical polishing of silicon nitride with chromium oxide abrasive in air
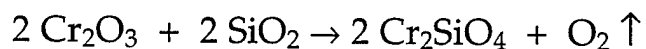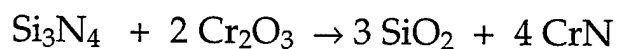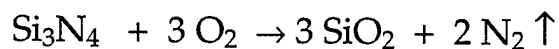
$$Si_3N_4 \ + \ 3\,O_2 \rightarrow 3\,SiO_2 \ + \ 2\,N_2 \uparrow$$

$$Si_3N_4 \ + \ 2\,Cr_2O_3 \rightarrow 3\,SiO_2 \ + \ 4\,CrN$$

$$4\,Si_3N_4 \ + \ 2\,Cr_2O_3 \ + \ 9\,O_2 \rightarrow 12\,SiO_2 \ + \ 4\,CrN + N_2 \uparrow$$

$$2\,Cr_2O_3 \ + \ 2\,SiO_2 \rightarrow 2\,Cr_2SiO_4 \ + \ O_2 \uparrow$$

Figure 1   Schematic of the model for chemo-mechanical polishing Si3N4 work material with Cr2O3 abrasive in air

Reactions occuring in the chemo-mechanical polishing of silicon nitride with chromium oxide abrasive in water

$$Si_3N_4 + 6 H_2O \rightarrow 3 SiO_2 + 4 NH_3 \uparrow$$

$$3 SiO_2 + 6 H_2O \rightarrow 3 Si(OH)_4$$

$$Si_3N_4 + 2 Cr_2O_3 \rightarrow 3 SiO_2 + 4 CrN$$

$$Si_3N_4 + Cr_2O_3 + 3 H_2O \rightarrow 3 SiO_2 + 2 CrN + 2 NH_3 \uparrow$$

$$2 Cr_2O_3 + 2 SiO_2 \rightarrow 2 Cr_2SiO_4 + O_2 \uparrow$$
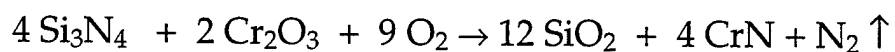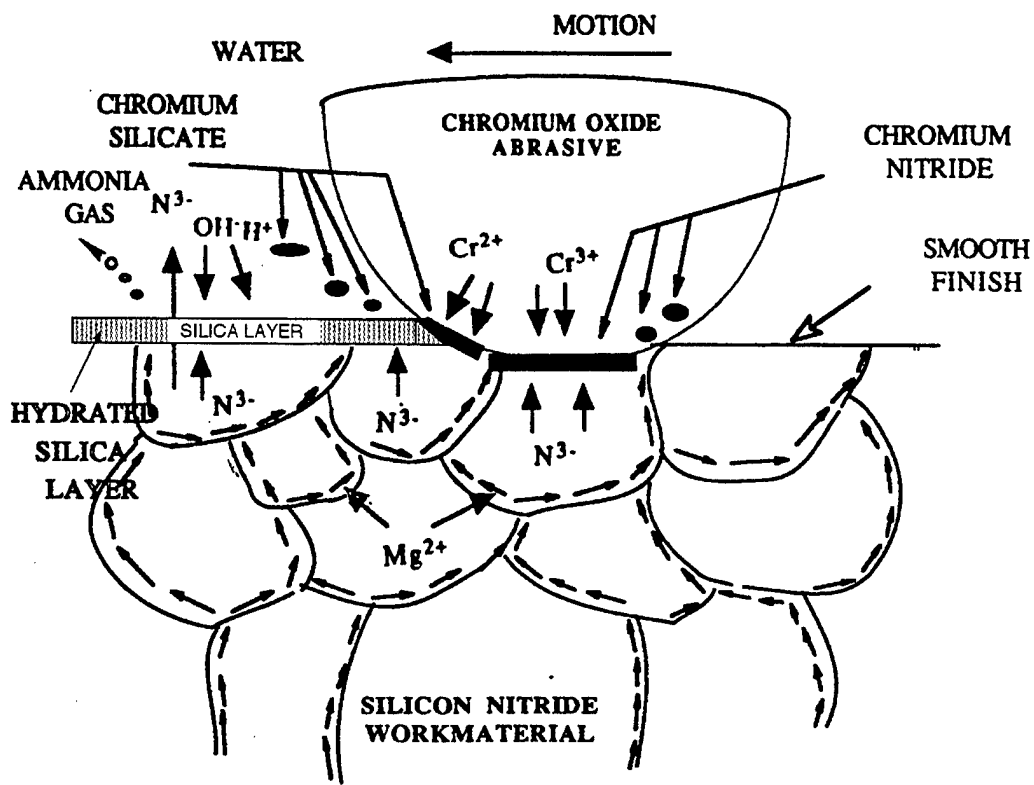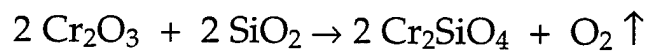
Figure 2   Schematic of the model for chemo-mechanical polishing Si3N4 work material with Cr2O3 abrasive in water

APPENDIX K

A THERMAL MODEL OF MAGNETIC FLOAT POLISHING OF
CERAMICS

Zhen Bing Hou and R. Komanduri

ON THE THERMAL ASPECTS OF MAGNETIC FLOAT POLISHING (MFP) OF CERAMIC BALLS

Hou Zhen-Bing and R. Komanduri
Mechanical and Aerospace Engineering
Oklahoma State University
Stillwater, OK 74078, USA

ABSTRACT

A thermal model for the calculation of flash temperatures generated at the contact points in the magnetic float polishing (MFP) process is presented. The heat source at the contact area between the ball and the shaft in magnetic float polishing where much of the material removal takes place was approximated as a disc. The disc plane heat source was considered as a combination of a series of concentric circular ring heat sources with different radii. Each ring in turn was considered as a combination of a series of infinitely small arc segments and each arc segment as a point heat source. Starting with the instantaneous point heat s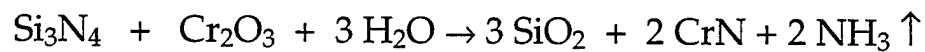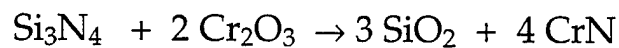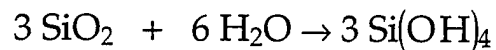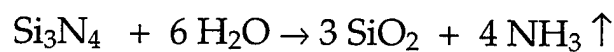ource, Carlsaw and Jaeger's classical moving heat source theory was used to solve the circular ring heat source problem and finally the disc heat source problem. The flash temperatures, flash times, and temperature distribution at the interface between the balls and the shaft of the polishing apparatus were calculated using this technique.

1. INTRODUCTION

Advanced ceramics, such as silicon nitride, alumina, silicon carbide are difficult-to-machine materials because of their high hardness and brittleness. They are currently finished by conventional grinding followed by polishing. Unfortunately, these processes remove material mostly by brittle fracture leaving behind several pits, microcracks, and other defects. Since ceramics are sensitive to surface flaws, the performance and reliability of parts fabricated by this process depends on the quality of the surface (or near surface) generated. Also, conventional polishing takes considerable time, on the order of several weeks. To overcome some of the problems, a new polishing technique known as Magnetic Fluid Grinding (MFG) was recently introduced [1,2]. The present authors, however, prefer the use of the term Magnetic Float Polishing (MFP) instead of Magnetic Fluid Grinding (MFG) to describe the process, as grinding connotes the use of

164

fixed abrasive (grinding wheel) while in MFP process one uses loose abrasives. In MFP, the load on the polishing balls is kept low (about 1 N/ball) and controlled during the process so that material removal by brittle fracture is minimized. In addition, by proper selection of the abrasive, polishing conditions, and the environment for a given work material, chemo-mechanical action can be initiated [3]. Material removal by chemo-mechanical action is caused by the formation of reaction products between the abrasive and the work material and the environment under the conditions of polishing thereby yielding an extremely smooth surface with minimal amount of defects. In addition, the polishing speeds can be significantly higher (3000-9000 rpm) instead of a few hundred rpm in conventional polishing.

The chemo-mechanical action, however, depends on the flash temperatures generated at the contact zone of the polishing process as well as the duration that enable chemical reaction products to form by the interaction of the abrasive, work material, and the environment. The type of reaction product that can form depends on the choice of the abrasive for a given workmaterial, the temperature generated and the duration. The reaction product (wear debris) is subsequently removed by the mechanical action of the abrasive. In this way higher removal rates can be accomplished without causing damage due to brittle fracture of the ceramic workmaterial. Also, since material removal mechanism depends mainly on the formation of reaction products, softer abrasives (softer than the work material) can be used. This method, thus, is expected to overcome many problems of surface damage, such as pitting due to brittle fracture, dislodgment of grains, and scratching due to abrasion associated with the use of harder abrasives. The resulting surface on ceramics is smooth and damage-free.

In this paper thermal aspects of the magnetic float polishing (MFP) are presented for the first time. They include a heat transfer model of the process, temperature field calculation assuming the contact area to be a moving disc source, and the calculation of the area of expected flash temperature and related flash time. The contact between the ball and the shaft is assumed to be disc shaped. The model is illustrated with an example of magnetic float polishing of ceramic balls.

2. MAGNETIC FLOAT POLISHING OF CERAMIC BALLS

The magnetic float polishing technique was developed on the principle of the magneto-hydrodynamic behavior of a magnetic fluid that can float non-magnetic abrasives suspended in it under the action of a magnetic field. The process is considered highly effective for finish polishing because a low level levitational force can be applied to the abrasives in a controlled manner. Hence, the forces applied by the abrasives to the part are extremely small (1 N/ball or lower) and highly controllable. The magnetic fluid is a colloidal dispersion of extremely fine (100 to 150 A) sub-domain ferromagnetic particles, usually magnetite (Fe_3O_4), in various carrier fluids, such as water or kerosene. The ferrofluids are made stable against particle agglomeration by the addition of surfactants. When a magnetic fluid is placed in a magnetic field gradient, it is attracted towards the higher magnetic field side. If non-magnetic substances (e.g., abrasives in this case) are mixed in the magnetic fluid, they are discharged towards the lower side. When the field gradient is set in the gravitational direction, the non-magnetic material is made to float on the fluid surface by the action of the magnetic levitational forces. The polishing operation in this process occurs due to the magnetic levitational force.

Figures 1 (a) and (b) are schematic and photograph of the magnetic float polishing apparatus, respectively, showing permanent magnets located at the base of the apparatus [4]. The float vessel is placed on top of the magnets with alternate N and S poles. A guide ring is provided on top of the float vessel to contain the magnetic fluid. Magnetic fluid containing fine abrasive particles is filled into the chamber. Balls to be polished are located between the drive shaft and the float around the periphery of the float vessel. The silicon nitride ball blanks are held in a 3-point contact between the float at the bottom, chamber wall on the side, and a shaft at the top. When a magnetic field is applied, the balls, abrasive grains, and the float of non-magnetic material all are pushed upwards by the magnetic fluid. The balls are pressed against the drive shaft and are finished by the rotation of the drive shaft. The material of the shaft is selected from an appropriate non-magnetic material. In this study, a stainless steel shaft and water-based magnetic fluid are used. It has been reported that sliding of silicon nitride on stainless steel in the presence of a water-based magnetic fluid results in the formation of a layer of chemical reaction products [5] and use of chromium oxide abrasive in polishing silicon nitride [6-8] promotes chemo-mechanical action. These conditions are assumed in the present analysis.

3. THERMAL ASPECTS OF MAGNETIC FLOAT POLISHING

Heat Transfer Model

In magnetic float polishing, the contact area between the ball and the shaft is approximated to a circular disc with a diameter in the range of ~10 to 20 μm depending on the hardness of the ball and the shaft as well as the contact load. Typically a load of 1 N/ball is used in MFP. Hence this value is used in the present analysis. The contact area is estimated using the hardness of the ball (or the shaft) material and the load acting on each ball. The sliding velocity of the ball (v m/sec) is generally in the range of 1 to 6 m/sec. Therefore, the heat generated on the contact area, q is given by:

$$q = 0.2388 \cdot P \cdot \mu \cdot v \ \text{cal/sec}$$

where μ is the coefficient of friction (in the presence of a water based magnetic fluid, μ between a Si$_3$N$_4$ ball and the shaft material is assumed to be 0.25 [9]), and P is the load applied on the ball in Newtons.

Figure 2 shows schematically the model used for simulating the heat transfer process during magnetic float polishing of ceramic balls. For convenience, as well as, for the choice of a model closer to practice, a normal distribution of the heat generation from the center to the periphery is considered. A moving disc heat source with a radius of r_0 cm and heat generation intensity of q cal/sec, moves on the ceramic surface with a velocity of v m/sec. In this initial analysis, the variation of thermal properties with temperature of the ball and the shaft materials are not considered. The objective of this analysis is to determine the temperature rise at any point nearby and at the heat source, including on the surface as well as in the subsurface.

In order to solve the moving heat source problem, it is convenient to change it from an unsteady to a quasi-steady state along the lines originally proposed by Rosenthal [10]. Carlsaw and Jaeger [11,12] gave a complete analyses of the various moving heat source problems. They suggested the use of *instantaneous point heat source* as the basis for analysis which can then be applied to various configurations of interest. We found this method to be very convenient in solving the problem of moving disc plane heat source with normal distribution of heat generation, for the problem considered here. While many researchers have considered the flash temperatures (maximum and mean values) [13-15], for the study of chemo-mechanical reactions, one

should consider not only the maximum temperature but also the distribution of temperature at and around the heat source. This will enable the calculation of flash times at any given temperature.

The disc plane heat source can be considered as a combination of a series of concentric circular ring heat sources with different radii (from r=0 to r_0). Each ring can be regarded as a combination of a series of infinitely small arc segments and each segment as a point heat sources. Based on the solution of the instantaneous point heat source, we can solve the instantaneous circular ring heat source problem.

Instantaneous Ring Heat Source Problem

Figure 3 is an illustration of the instantaneous ring heat source problem. The origin of the coordinate system coincides with the center of the instantaneous ring heat source with radius, r_0. Consider a small segment of the ring heat source ($r_0 \, d\alpha$) as an instantaneous point heat source.

Using the solution for the instantaneous point heat source [11,12], the temperature rise caused by the ring segment of the heat source at any point M and at any instant τ (the time after the initiation of the instantaneous ring segment heat source) can be calculated as:

$$d\theta_M = \frac{Q_{rg} \, d\alpha}{c\rho(4\pi a\tau)^{3/2} \cdot 2\pi} \cdot \exp\left(-\frac{R^2}{4a\tau}\right)$$

where Q_{rg} is the heat released by the instantaneous ring heat source in calories, $Q_{rg}/2\pi r_0$ is the heat released by the ring heat source per unit length, and $Q_{rg} d\alpha/2\pi$ is the heat released by the segment $r_0 d\alpha$, where $R^2 = r'^2 + z^2$, r' is the projection of R on x-o-y plane, $r'^2 = r_0^2 + r^2 - 2rr_0\cos\alpha$, $R^2 = r_0^2 + r^2 + z^2 - 2 r r_0 \cos\alpha$, and r is the projection of distance vector between the center of ring heat source o and any point M on plane x-o-y of interest.

The total temperature rise at any point M, caused by the whole ring heat source is given by:

$$\theta_M = \frac{Q_{rg}}{c\rho(4\pi a\tau)^{3/2}} \cdot \frac{1}{2\pi} \cdot \exp\left(-\frac{r_0^2 + r^2 + z^2}{4a\tau}\right) \int_0^{2\pi} \exp\left(\frac{r r_0}{2a\tau}\cos\alpha\right) d\alpha$$

Here, $\dfrac{1}{2\pi}\displaystyle\int_0^{2\pi} \exp(p\cos\alpha)d\alpha$ is the modified Bessel function of the first kind

order zero and designated as $I_0(p)$, where $p = \dfrac{rr_0}{2a\tau}$

Hence,

$$\theta_M = \frac{Qrg}{c\rho(4\pi a\tau)^{3/2}} \cdot \exp\left(-\frac{r_0^2 + r^2 + z^2}{4a\tau}\right) \cdot I_0\left(\frac{rr_0}{2a\tau}\right) \tag{1}$$

For the case shown in Figure 2, Eq. (1) can also be written as:

$$\theta_M = \frac{Qrg}{c\rho(4\pi a\tau)^{3/2}} \cdot \exp\left(-\frac{r_0^2 + x^2 + y^2 + z^2}{4a\tau}\right) \cdot I_0\left(\frac{r_0}{2a\tau}\sqrt{x^2 + y^2}\right) \tag{2}$$

For ease of later derivations for a moving ring heat source problem, the function $I_0(p)$ can be replaced by the following approximate exponential functions with error less than 5%.

when $p < 1.6$ $\qquad$ $I_0(p) = 0.935 \cdot \exp(.352p)$

when $1.6 <= p <= 3$ $\qquad$ $I_0(p) = 0.529 \cdot \exp(.735p)$

when $p > 3$ $\qquad$ $I_0(p) = \exp(p)/(2\pi p)^{.5}$

Moving Ring Heat Source Problem

Figure 4 illustrates the moving ring heat source problem. x-, y-, z- axes are the absolute coordinate system while X, y, z axes are the corresponding moving coordinate system which has its origin coinciding with the center of the moving ring heat source and moving with it with the same velocity along the X-axis. Figure 4 gives the relationships between the spatial and temporal parameters. As shown in the upper part of Figure 4, a moving ring heat source continuously liberates heat q_{rg} (cal/sec) and moves along the X-axis with a velocity v (cm/sec). It is intended to determine the temperature rise at any point M(x,y,z) and at t sec after the initiation of the heat source.

Consider a small time interval $d\tau_i$ at time τ_i [refer to Figure 4]:

1. In this time interval, the heat liberated by the ring heat source which can be considered as liberated instantaneously is given by $q_{rg} \cdot d\tau_i$, cal.

2. At instant τ_i, the ring heat source has moved a distance $v\tau_i$, [see Figure 4]. So the location of M relative to the heat source center has changed. The projection of the distance vector between the center of the ring heat source and point M on plane x-o-y has changed from r to r_i, where $r_i^2 = (x-v\tau_i)^2 + y^2$

3. At time τ_i, the heat liberated in the small time interval $d\tau_i$ will cause a certain temperature rise at point M at time t:

$$d\theta_M = \frac{q_{rg}\, d\tau_i}{c\rho(4\pi a\tau)^{3/2}} \cdot$$
$$\exp\left(-\frac{r_0^2 + (x - v\tau_i)^2 + y^2 + z^2}{4a\tau}\right) \cdot I_0\left[\frac{r_0}{2a\tau}\sqrt{(x - v\tau_i)^2 + y^2}\right] \quad (3)$$

To solve this moving heat source problem, we need to convert the unsteady state problem into a quasi-steady state problem to facilitate mathematical analysis. For this, we have to use moving coordinate system and find a way to eliminate the time variables (τ_i, τ) in Equation 3.

For changing the coordinate system, we should consider the case of a moving coordinate system having its origin coinciding with the center of the moving ring heat source and moving with the same velocity as the heat source.

From Figure 4, it can be seen, that the X-direction component of the distance vector between the center of the heat source and point M (which is of interest) is changing with time. At the instant τ_i, it is given by:

$$x - v\tau_i = x - v(t - \tau) = x - vt + v\tau$$

Here, the term (x-vt) is just the location of point M in a moving coordinate system in the X-direction as shown in Figure 4, designated as X, that is:

$$x - v\tau_i = X + v\tau$$

170

where $\tau_i = t - \tau,$ and $d\tau_i = -d\tau$

The total temperature rise of point M at time t, caused by the moving ring heat source from $\tau_i = 0$ to $\tau_i = t$ is given by:

$$\theta_M = \frac{q_{rg}}{c\rho(4\pi a)^{3/2}} \int_{\tau_i=0}^{\tau_i=t} \frac{d\tau_i}{\tau^{3/2}} \exp\left(-\frac{r_0^2 + (X + v\tau)^2 + y^2 + z^2}{4a\tau}\right) \cdot$$

$$I_0\left[\frac{r_0\sqrt{(X + v\tau)^2 + y^2}}{2a\tau}\right] \tag{4}$$

Here $(X + v\tau)^2 = X^2 + 2Xv\tau + v^2\tau^2,$

Hence, $\exp\left(-\frac{r_0^2 + (X + v\tau)^2 + y^2 + z^2}{4a\tau}\right)$

$$= \exp\left(-\frac{r_0^2 + X^2 + y^2 + z^2}{4a\tau}\right) \cdot \exp\left(-\frac{Xv}{2a}\right) \cdot \exp\left(-\frac{v^2\tau}{4a}\right)$$

Thus, Eq. (4) can be written as:

$$\theta_M = \frac{q_{rg}}{c\rho(4\pi a)^{3/2}} \cdot \exp\left(-\frac{Xv}{2a}\right) \int_{\tau=0}^{\tau=t} \frac{d\tau}{\tau^{3/2}} \cdot \exp\left(-\frac{r_0^2 + X^2 + y^2 + z^2}{4a\tau}\right) \cdot$$

$$\exp\left(-\frac{v^2\tau}{4a}\right) \cdot I_0\left[\frac{r_0\sqrt{(X + v\tau)^2 + y^2}}{2a\tau}\right]$$

Let $\dfrac{v^2\tau}{4a} = \omega;$ $R_h^2 = r_0^2 + X^2 + y^2 + z^2;$ $\dfrac{v}{2a} = V;$ $R_h V = u;$ $v\tau = \dfrac{2\omega}{V}$

171

Substituting these values, we get

$$\theta_M = \frac{q_{rg}\,v}{16\lambda a\pi^{3/2}} \cdot \exp(-XV) \int_0^{\frac{v^2 t}{4a}} \frac{d\omega}{\omega^{3/2}} \cdot \exp\left(-\omega - \frac{u^2}{4\omega}\right) \cdot$$

$$I_0\left[\frac{r_0 V^2}{2\omega}\sqrt{\left(X + \frac{2\omega}{V}\right)^2 + y^2}\right] \qquad (5)$$

Figure 5 shows the variation of the function $f(\omega)$ with ω, where $f(\omega)$ is given by,

$$f(\omega) = \frac{1}{\omega^{3/2}} \cdot \exp\left(-\omega - \frac{u^2}{4\omega}\right) \cdot I_0\left[\frac{r_0 V^2}{2\omega}\sqrt{\left(X + \frac{2\omega}{V}\right)^2 + y^2}\right]$$

It can be seen that for different values of X, the form of the curve is different but is always convergent when $\omega \to 0$ and $\omega \to 10$ (Figure 5). Also note that the function $f(\omega)$ increases initially for x= 1, 3, 4.8 μm and then decreases with further increase of x to 7, 9 μm. Since, in practice, the upper limit of integration of Equation 5 is always much larger than 10, we can consider the upper limit as ∞. Once the integration is from zero to infinity, the variable ω becomes merely a dimensionless real number. Thus in Equation 5 the time variables disappear. The temperature rise, therefore, will no longer be dependent on time. This means, at all those points in the moving coordinate system, the temperature rise reaches a steady state, i.e. $\left(\frac{d\theta}{d\tau} = 0\right)$. This is the so called quasi-steady state. Of course, if the locations of those points are designated by the absolute coordinate system, their distances relative to the heat source will be changing with time. Thus, their temperature rises will still be time dependent, i.e. they are in unsteady state.

When the approximate equations for the special function $I_0(p)$ are used, Eq. 5 can be written as:

$$\theta M = \frac{q_{rg}\ v}{16\lambda a\pi^{3/2}} \cdot \exp(-XV) \int_0^{\frac{v^2 t}{4a}} \frac{d\omega}{\omega^{3/2}} \cdot \exp\left(-\omega - \frac{u^2}{4\omega}\right) \cdot I_0(p) \tag{6}$$

where,

q_{rg}	the heat generated by a ring heat source, cal/sec.
v	sliding velocity, cm/sec.
λ	thermal conductivity of silicon nitride, cal/cm.sec. $^\circ$C.
a	thermal diffusivity of silicon nitride, cm^2/sec.
X,y	co-ordinate of the point of interest,
V	V= v/2a
ω	a dimensionless number which has its maximum value equals to the upper limit of the integration,
r_0	the radius of the ring, cm.
$I_0(p)$	a modified Bessel function of first kind order zero,

$$p = \frac{r_0 V^2}{2\omega}\sqrt{\left(X + \frac{2\omega}{V}\right)^2 + y^2}\ ;$$

$$u = \frac{R_h v}{2a};$$

$$R_h^2 = r_0^2 + X^2 + y^2 + z^2$$

when $\quad p < 1.6 \qquad\qquad I_0(p) = 0.935 \cdot \exp(.352p)$

when $\quad 1.6 <= p <= 3 \qquad I_0(p) = 0.529 \cdot \exp(.735p)$

when $\quad p > 3 \qquad\qquad I_0(p) = \exp(p)/(2\pi p)^{.5}$

Using Eq. 6, we can calculate the temperature rise at any point near by and on the moving ring heat source. Thus we can obtain a complete picture of the temperature distribution around the moving ring heat source. Eq. 6 is for an infinitely large conduction medium. For semi-infinite solid, the temperature rise on the surface and under the surface is given by :

$$\theta_M = \frac{q_{rg}\, V}{8\lambda a \pi^{3/2}} \cdot \exp(-XV) \int_0^{\frac{v^2 t}{4a}} \frac{d\omega}{\omega^{3/2}} \cdot \exp\left(-\omega - \frac{u^2}{4\omega}\right) \cdot I_0(p) \qquad (7)$$

The disc heat source can be considered as a combination of a series of concentric ring heat sources with different radii from zero to r_0 (here r_0 is the radius of the disc heat source). Usually the intensity of heat liberation is not uniformly distributed from the center to the periphery. A reasonable assumption would be to consider it as distributed normally.

Based upon the above considerations the solution for the moving disc heat source for a semi-infinite body, as in the present case, is given by the following equation:

$$\theta_M = \frac{9 q_{dc} \cdot V}{4\lambda a \pi^{3/2} r_0^2} \cdot \exp(-XV) \int_0^{r_0} r_i \cdot \exp\left(-\left(\frac{3 r_i}{r_0}\right)^2\right) \cdot dr_i \cdot$$

$$\int_0^{\frac{v^2 t}{4a}} \frac{d\omega}{\omega^{3/2}} \cdot \exp\left(-\omega - \frac{u^2}{4\omega}\right) \cdot I_0(p) \qquad (8)$$

where

$$p = \frac{r_i V^2}{2\omega} \sqrt{\left(X + \frac{2\omega}{V}\right)^2 + y^2} \, ; \, V = \frac{v}{2a} \, ; \, u = R_h \cdot V$$

$$R_h^2 = r_i^2 + X^2 + y^2 + z^2$$

when $p < 1.6$ $I_0(p) = 0.935 \cdot \exp(.352 p)$

when $1.6 <= p <= 3$ $I_0(p) = 0.529 \cdot \exp(.735 p)$

when $p > 3$ $I_0(p) = \exp(p)/(2\pi p)^{.5}$

Calculation of the Temperature Field of a Moving Disc Shaped Heat Source

In the magnetic float polishing of ceramic ($Si3N4$) balls, the diameter of the contact area under a load of 1 N per ball can be calculated using the hardness of the shaft/ball material combination. Table I gives the contact diameters for different shaft materials.

For the calculation of the temperature field on the surface of the ball around the contact area in magnetic float polishing process, representative data given in Table II are used:

Total heat generated at the contact area in the process of polishing is given by:

$$q_{total} = P \cdot \mu \cdot v \cdot 0.2388$$

For P = 1 N/ball; μ = 0.25, q_{total} (cal/sec) for various values of v are given in Table III.

Of the total heat generated at the contact area in MFP, some of the heat flows into the ceramic ball, while the remaining flows into the abrasive. The heat partition is assumed to depend on the ratio of the thermal conductivities of the materials of the two contacting bodies.

The percentage of the fraction of the heat that flows into the ball, x, is given by :

$$x = \lambda_1 / (\lambda_1 + \lambda_2)$$

$$x = 0.026/(0.026 + 0.076) \cdot 100 \% = 25.5\%$$

Thus, $\qquad q_{dc} = 0.255 \cdot q_{total}$

Figure 6 is distribution of the temperature rise calculated on the surface (by substituting z = 0) of the contact area in MFP for v = 3 m/sec. Figure 7 is the calculated values of the temperature rise on the surface along the X-axis (y = 0, z = 0) for different sliding velocities, v = 1, 2, 3, 4, 5, and 6 m/sec, radius of the moving disc heat source r_0=12.6 μm, and location of the center of the heat source is X=0, y=0. It can be seen that the flash temperatures (maximum) generated can be very high, depending on the sliding speed. For a sliding speed of 1 m/sec, it is about 226 $^{\circ}$C and increases with increase in the sliding speed to 1038 $^{\circ}$C at 6 m/sec. Figure 8 shows the

isotherms of different temperatures on the surface for v = 3 m/sec, ro=12.6 μm which can be used to calculate the flash times at relevant flash temperatures. Each of it involves the area where the temperature rise is higher than that of the isothermal. The length of the area enclosed by relevant isotherms in the X-direction can be estimated from this figure.

The flash time is given by the following relationship:

$$\text{flash time} = \frac{L}{v} \cdot 10^6 \ \mu\text{sec}$$

where   L - length of the region where the temperature higher than a
               certain critical temperature in cm.
         v - velocity of motion of the moving heat source in cm/sec.

Based on this, the flash times at relevant flash temperatures can be obtained as shown in Table IV. The room temperature is assumed as 20 °C.

For the example shown in Table IV, for a flash temperature higher than 100 °C, the flash time is 12.6 μsec but for a flash temperature of higher than 500 °C, the flash time reduces to 2.1 μsec. Even this short time can be adequate for the chemo-mechanical action to take place.

4. DISCUSSION

A thermal model for a moving disc shaped heat source was developed in this investigation starting from the Jaeger's instantaneous point heat source. This model enables the calculation of the flash temperatures, flash times, and temperature distribution at the contact area. This model was then applied to calculate the flash temperature and flash times in MFP of silicon nitride balls.

It may be pointed out that many of the earlier models used approximate equations to calculate the maximum flash temperature while in this paper we have presented exact solutions starting from the Jaeger's instantaneous point heat source. Those approximate equations mentioned above can give acceptable values of maximum flash temperature only when the sliding speed is high and the heat source is a uniformly

distributed band or rectangular heat source. Such a model, however, may not represent cases of polishing, grinding, and most frictional sliding contacts. The consideration of using disc-shaped moving heat source with a normal distribution of the heat liberation intensity is closer to the practical cases. In the analysis presented here, one can calculate the temperatures over a wide range of sliding speeds. Also, using the equations developed here, one can also calculate not only the maximum and mean temperatures but also the complete map of temperature distribution in and around the heat source. This we believe is our contribution in this paper.

In the determination of chemical reaction products that may form in chemo-mechanical polishing, both flash temperatures and flash times have to be considered. The mathematical analysis presented here enables the calculation of flash times which is not possible with the use of approximate solutions mentioned above. Also, the mathematical analysis presented here imposes no restrictions on the size of the sample while that of using FEM analysis is by necessity limited by the mesh size.

Using chromium oxide abrasive in MFP of silicon nitride balls, at the pressures and sliding speeds used, the flash temperatures generated are reasonably high and the corresponding flash times sufficiently long to generate specific reaction products, such as oxidation of silicon, and the formation of chromium nitride and chromium silicate compounds [7,8]. Based on the Gibb's Free Energy (ΔG^0) calculations, it was shown that oxidation of silicon nitride in air can take place around 167 ^0C. It can be seen from Figure 7, that even at relatively low sliding speed (2 m/sec), the flash temperature in polishing far exceeds the temperature required for the oxidation of silicon nitride with sufficiently long duration of time for the reaction products to form. Of course, at the higher speed, namely, 6 m/sec, the temperature rise exceeds 1000 ^0C. At these conditions chemo-mechanical reactions can be formed between the silicon nitride balls and the chromium oxide abrasive in MFP resulting in the formation of chromium nitride and chromium silicate. Thus chemical reactions can be activated during polishing by proper choice of the abrasive for a given workmaterial, the environment and polishing conditions.

Examination of the wear debris (in the SEM with an X-ray microanalyzer and a low angle X-ray diffraction apparatus) obtained in MFP of silicon nitride balls using chromium oxide abrasive showed conclusively that Cr_2O_3 does participate in the chemo-mechanical polishing of Si_3N_4 forming chromium nitride and chromium silicate

[7,8]. This work establishes the role of Cr_2O_3 not as a mere catalyst but one actively taking part in the chemical reactions during chemo-mechanical polishing [8]. Based on it, models were developed for the chemo-mechanical polishing of Si_3N_4 in water (i.e. water based magnetic fluid) and dry with Cr_2O_3 abrasive. These models are based on the formation of such reaction products as chromium silicate and chromium nitride in addition to the formation of silica layer on the surface of Si_3N_4 as well as the gaseous reaction products, such as ammonia (in water) and nitrogen (in air).

It may be pointed out that approximate equations for flash temperatures were used earlier, basically to reduce the mathematical computational time. However, with the advent of fast computers, use of exact equations, starting from the fundamental equation of Jaeger's instantaneous point heat source does not necessarily pose any serious limitation. Besides, the results are more accurate.

Although a circular disc heat source was considered in this investigation, it is possible to consider other geometries, such as elliptical, square, tear shaped heat sources using a similar approach as presented here starting with the Carlsaw and Jaeger's instantaneous point heat source solution. This way other manufacturing operations, such as high-energy beam machining, surface coatings, surface heat treatment, and welding as well as tribological problems where moving disc heat source plays an important role can be addressed.

5. CONCLUSIONS

1. A disc shaped moving heat source problem is solved mathematically. Equation 8 is the mathematically accurate solution for disc shaped moving heat source. It can be applied to calculate the flash temperatures generated at the contact point between the balls and the driving shaft surface in magnetic float polishing (MFP).

2. Using the equation for the moving disc heat source for a semi infinite body (Equation 8), a complete map of the temperature distribution around the moving disc heat source can be obtained as shown in Figures 6 - 8.

3. In the process of mathematical derivation, the limits of integration were taken as 0 and ∞. This is based on a rigorous analysis of the relevant function $f(\omega)$ as shown in Figure 5. No arbitrary assumptions are made. As shown in Figure 5, the function $f(\omega)$ converges when $\omega \rightarrow 10$. The practical upper limit of $v^2t/4a$ is generally much larger

than 10. Once the integration is from 0 to ∞, the variable ω becomes merely a dimensionless real number. Thus, the time variable disappears and the temperature rise will no longer depend on the time and the so-called quasi-steady state condition results.

4. In solving the numerical integration, however, the upper limit is taken as 10 (not ∞) and the lower limit as 0.01. As can be seen from Figure 5, no noticeable error results from this assumption, and at the same time it reduces the computational time significantly.

5. The equation for the moving disc heat source for a semi infinite body (Equation 8) is the general solution for a moving disc heat source. In this investigation it is applied for magnetic float polishing (MFP) of silicon nitride balls. However, a similar approach can be applied to address different manufacturing applications including high energy beam machining, surface coating, surface heat treatment, and welding.

6. The flash temperatures (maximum) generated can be very high, depending on the sliding speed. For a sliding speed of 1 m/sec, it is about 226 $^{\circ}$C and increases with increase in the sliding speed to 1038 $^{\circ}$C at 6 m/sec. However, the flash time decreases with increase in the flash temperature. For the example shown in Table IV, for a flash temperature higher than 100 $^{\circ}$C, the flash time is 12.6 μsec but for a flash temperature of higher than 500 $^{\circ}$C, it reduces to 2.1 μsec. Although the flash times are on the order of a few microseconds, it is possible to initiate reaction products between the workpiece and the abrasive as evidenced by the X-ray diffraction studies of the wear debris formed in magnetic float polishing [7, 8].

7. While flash temperatures can be used as a basis for thermodynamic analysis (free energy of formation) for the feasibility of initiating a particular chemical reaction product that can be formed between the workmaterial, abrasive, and the environment, flash times are needed to investigate the kinetics. However, an analysis of this type assumes equilibrium conditions while in practice, the conditions are far different from equilibrium.

ACKNOWLEDGMENTS

REFERENCES

1.   Kato, K, " Tribology of Ceramics, " Wear 136 (1990)117-133

2.   Umehara, N. and K. Kato, " Principles of Magnetic Fluid Grinding of Ceramic Balls," Int. J. of Applied Electromagnetics in Materials 1, (1990) 37-43

3.   Yasunaga, N., Tarumi, N., Obara, A., and O. Imanaka, "Mechanism and Application of the Mechanochemical Polishing Method Using Soft Powder," Science of Ceramic Machining and Surface Finishing II, Ed. B. J. Hockey and R. W. Rice, NBS Special Publication No. 562 (1979) 171

4.   Umehara, N., "Magnetic Fluid Grinding - A New Technique for Finishing Advanced Ceramics," Annals of CIRP 43/1, (1994) 185-188

5.   Akazawa, M., Kato, K., and K. Umeya, "Wear Properties of Silicon Nitride in Rolling Contact Fatigue," Wear 110 (1986) 285-293

6.   Raghunandan, M., Umehara, N., and R. Komanduri, "On the Possibility of Chemo-Mechanical Polishing of Silicon Nitride," Proc. of the Symposium on Tribology in Manufacturing, ASME/STLE Tribology Conference, Lahaina, Maui, Hawaii (1994) 81-89. Also, accepted for publication in Trans. ASME - J of Tribology (1995)

7.   Bhagavatula, S. R., "On the Chemo-Mechanical Polishing of Silicon Nitride with Chromium Oxide Abrasive," M.S. Thesis, Oklahoma State University, Stillwater, OK (1995)

8.   Bhagavatula, S. R. and R. Komanduri, "On the Chemo-Mechanical Polishing of Silicon Nitride with Chromium Oxide Abrasive," accepted for publication in thePhilosophical Magazine (1995)

9.   Akazawa, M. and K. Kato, "Wear Properties of Silicon Nitride in Rolling-Sliding Contact," Wear 124 (1988) 123-132

10.   Rosenthal, D., "The Theory of Moving Sources of Heat and Its Application to Metal Treatments," Trans ASME (Nov. 1946) 849-866

11.   Jaeger, J. C., "Moving Sources of Heat and the Temperature of Sliding Contacts," Proc. of the Royal Society of NSW 76 (1943) 203-224

12.   Carlsaw , H.S. and J. C. Jaeger," Conduction of Heat in Solids," Oxford University Press, 2nd Edition (1959)

13.   Archard, J. F., "The Temperature of Rubbing Surfaces," Wear 2 (1958/59) 438-455

14.   Francis, H. A., "Interfacial Temperature Distribution within a Sliding Hertzian Contact," ASLE Trans 14 (May 1970) 41-54

15.   Greenwood, J. A., "An Interpolation Formula for Flash Temperatures," Wear 150 (1991) 153-158

Table I   Contact Diameters for Different Shaft Materials

Material of Driving Shaft	Hardness, Kg/mm^2	Contact Diameter, μm
Silicon Nitride	1800	8.4
Steel (soft)	200	25.2
Silicon Carbide	2500	7.1
Aluminum Oxide	2100	7.8
Zirconia	1400	9.5

Table II   Representative Data for the Calculation of the Temperature Field

Material of the driving shaft   :   Stainless steel
Load on the ball (silicon nitride), P   :   1 N/ball
Sliding speed, v   :   1 ~ 6 m/sec

Thermal properties of silicon nitride:

   Thermal conductivity, λ_1 :   0.026 cal/cm·sec·°C
   Thermal diffusivity, a   :   0.039 cm^2/sec
   Specific heat, c   :   0.207 cal/g·°C
   Density, ρ :   3.19 g/cm^3

Thermal conductivity of chromium oxide, λ_2 :   0.076 cal/cm·sec·°C

Table III   Values of q_{total} for Different Sliding Velocities
(P = 1 N and μ = 0.25)

Sliding velocity,'v m/sec	q_{total} cal/sec
2	0.1194
3	0.1791
4	0.2388
5	0.2985
6	0.3582

Table IV   Flash Times for Different Flash Temperatures
(P=1N/ball,   v=3 m/sec)

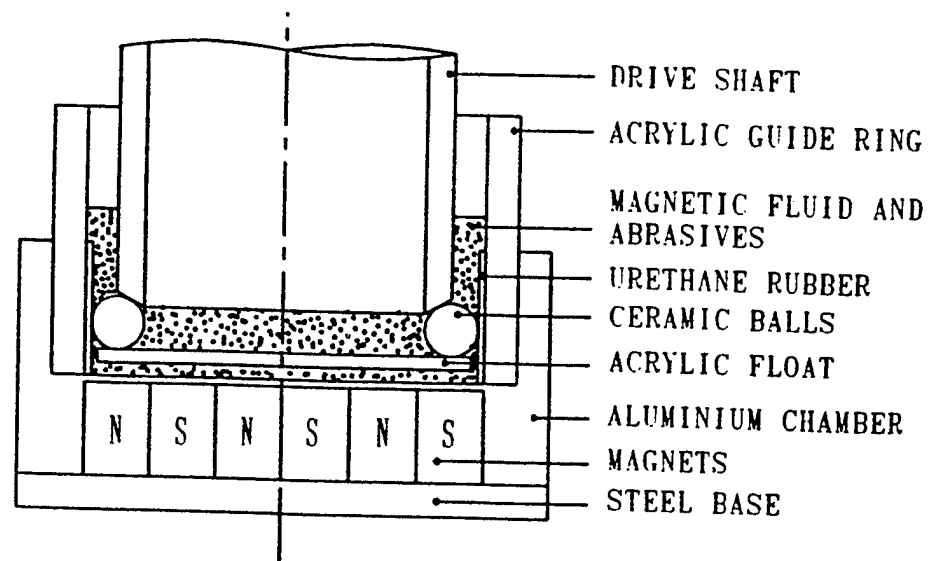| Flash temperature higher than, °C	100	200	300	400	500	600
Flash time, µsec	12.6	6.2	4.1	2.9	2.1	1.2

Figure 1 Schematic of the magnetic float polishing apparatus showing permanent magnets located at the base of the apparatus [4].
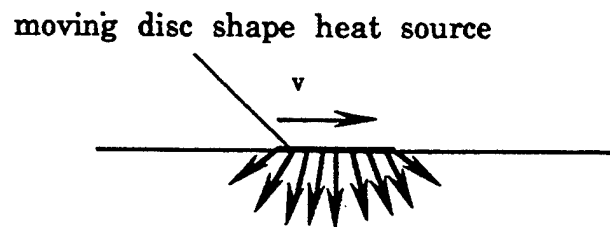

Figure 2 Schematic model used for simulating the heat transfer process during magnetic float polishing of ceramic balls
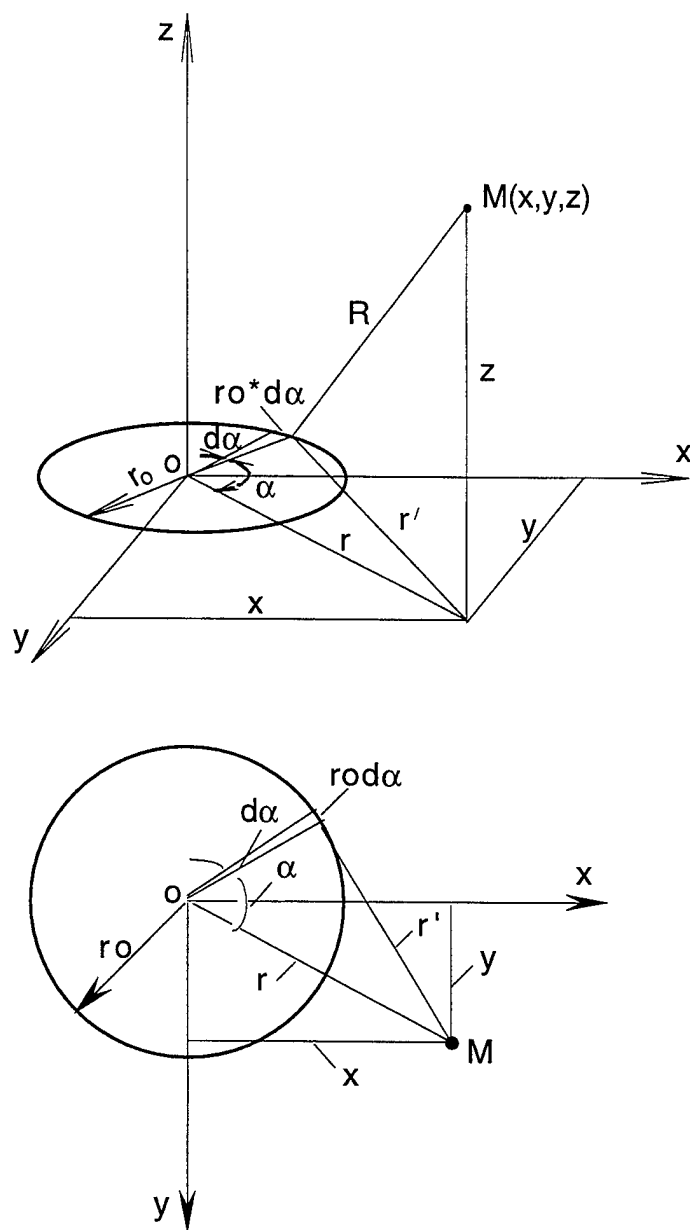
Figure 3   Illustration of the instantaneous ring heat source problem
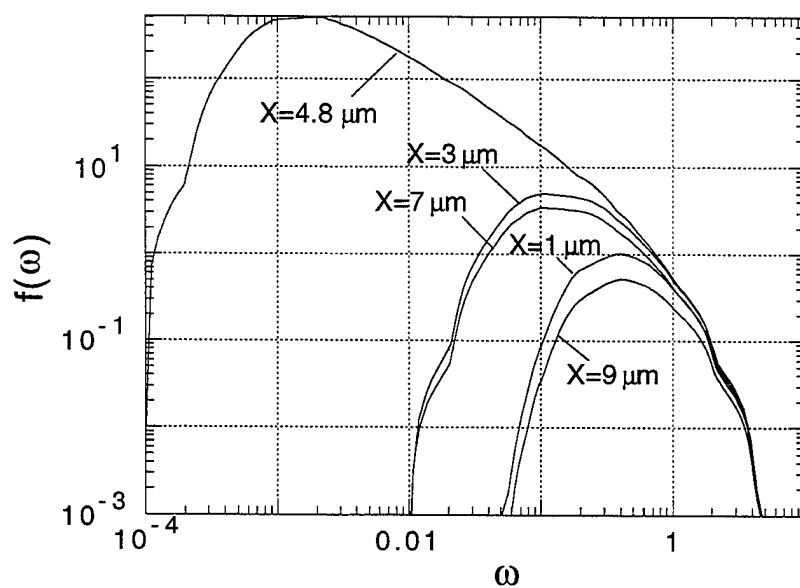
Figure 4   Representation of spatial and time relationships for a moving ring heat source

186

Figure 5 Variation of f(ω) with ω for different values of X,
X = 1, 3, 4.8, 7 and 9 μm
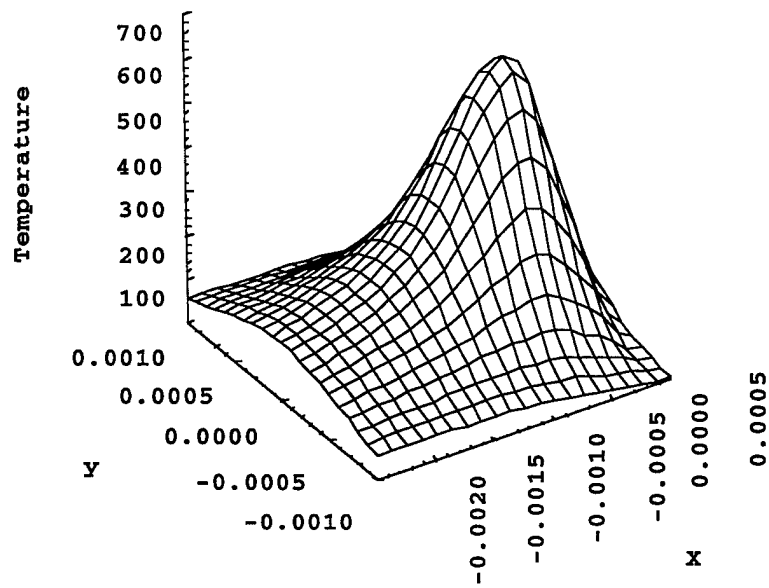
Figure 6   Temperature rises on the surface (x-y plane) for
different X and y (z=0), v=3 m/sec
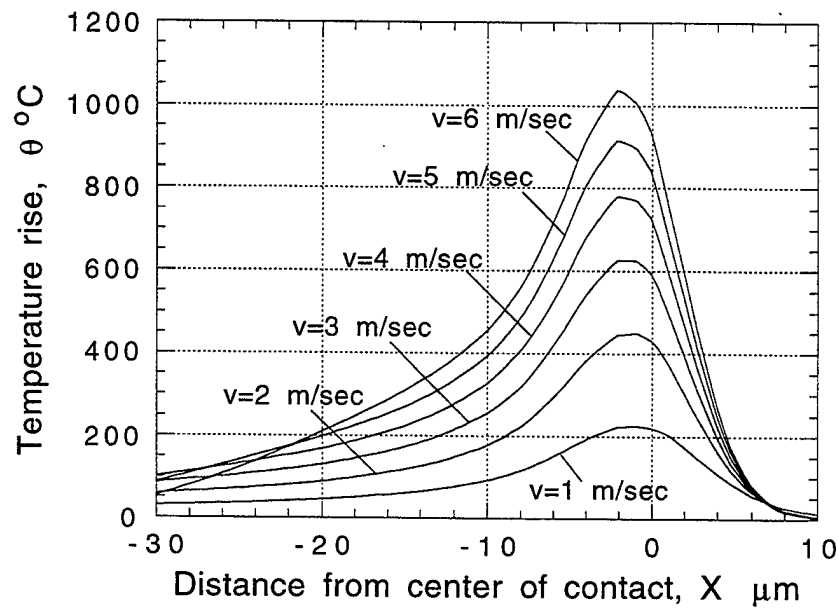
Figure 7   Calculated temperature rise on the surfac along the X-axis
(y = 0, z = 0) for various velocities, v = 1, 2, 3, 4, 5 and 6m/sec.
Radius of the moving heat source is 12.6 μm. P=1 N/ball. Location
of the center of the moving heat source: X=0, y=0.

APPENDIX L

A THERMAL MODEL OF MAGNETIC ABRASIVE FINISHING (MAF) OF CERAMICS

Zhen Bing Hou, S. R. Bhagavatula, and R. Komanduri

A THERMAL MODEL OF THE MAGNETIC ABRASIVE FINISHING (MAF) OF CERAMIC ROLLERS

Hou Zhen-Bing, S. R. Bhagavatula, and R. Komanduri
Mechanical and Aerospace Engineering
Oklahoma State University
Stillwater, OK 74078, USA

ABSTRACT

Using the moving disc heat source model developed by Hou and Komanduri [1], flash times and flash temperatures generated at the contact points between the workmaterial (silicon nitride roller) and the abrasive (chromium oxide) in magnetic abrasive finishing (MAF) process were calculated. The heat source between a magnetic abrasive particle and the contact point on the workmaterial (where the material removal takes place) was approximated to a disc. The flash temperatures generated were found to be a function of the polishing pressure as well as the rotational speed of the workmaterial. They were also found to be sufficient to activate chemo-mechanical action between the silicon nitride workmaterial and the chromium oxide abrasive. Examination of the wear debris indicated the formation of the reaction products, namely, chromium silicate and chromium nitride as shown elsewhere [3,4]. Surface finish on the order of 5 nm (Ra) were obtained in polishing of the silicon nitride rollers by this technique.

1. INTRODUCTION

The temperatures generated at the contact area between the workmaterial and the abrasive during polishing is an important parameter that can determine the possibility of chemical reaction in the contact regions. Similarly, the flash times determine the rate of chemical reaction and consequently the chemo-mechanical polishing of the workmaterial. It is, however, somewhat impractical to measure the temperatures at the points of contact experimentally. Therefore, one has to resort to analytical techniques, such as the heat transfer model developed recently by Bing and Komanduri [1]. That model uses a moving disc heat source and Jaeger's classical solutions to determine the flash temperatures generated at the point of contact

between the abrasive and the work material. In the following, a brief description of the magnetic abrasive finishing (MAF) process is given. This is followed by a brief description of the theoretical model of the moving disc heat source problem. An example calculation is presented in the Appendices and results of that work are presented under Discussion.

2. MAGNETIC ABRASIVE FINISHING

The magnetic abrasive finishing (MAF) process is a novel technique for fine polishing of cylindrical specimens such as rollers used in ceramic hybrid bearings [2]. The material removal rate is generally high (1 μm/min) and finish quality is also excellent (Ra 5 nm). Figures 1 (a) and (b) are schematic and photograph of the MAF process, respectively. The apparatus consists of an electromagnet for the generation of the magnetic field. A copper coil, wound in the form of solenoid, is used for the generation of the magnetic field in the core. The magnetic core material is generally a low carbon steel (0.16% C). Magnetic heads are designed such that the magnetic field is concentrated surrounding the air gap between the magnetic heads with minimum leakage for the roller, which is made of non-magnetic ceramic material. A pneumatic air vibrator is used to provide the vibratory motion to the magnetic head so that circumferential grooves that may form otherwise can be eliminated. The equipment is mounted on a 1.5 hp, Hardinge precision lathe with a continuous speed range of up to 3000 rpm. Table I gives the specifications of the magnetic abrasive finishing equipment.

The magnetic abrasive is an agglomerate of ferromagnetic particles and fine hard abrasive. The magnetic abrasive, when charged into the gap between the magnetic poles, forms two magnetic abrasive brushes around the periphery of the roller (Figure 2). When a nonmagnetic cylindrical workpiece, such as a ceramic roller, is placed in the magnetic field with rotary and vibratory motions (with or without a lubricant), surface and edge finishing operations are performed by these magnetic abrasive brushes. The process is highly efficient and the removal rate and finish depend on the workpiece circumferential speed, magnetic flux density, working clearance, workpiece material, size of the magnetic abrasive agglomerate, including the type of abrasive used, grain size, and volume fractions of the abrasive and magnetic material in the agglomerate. The diameters of the ferromagnetic particles of the agglomerates are in the range of 100 to 400 μm and the diameters of the fine hard abrasives are in the range of 5 to 10 μm.

192

Table I: Specifications of the Magnetic Abrasive Finishing Equipment

Machine capacities:

Machine Tool	: 1.5 hp, Hardinge high precision lathe
Lathe speed	: 500- 2,500 rpm
Workpiece size	: 5-25 mm diameter x 120 mm long cylindrical roller
Polishing capacity	: 45 mm long
Magnetic field intensity	: 0.5-1.2 T
Magnetic pressure	: 0-40 kPa
Magnetic core	: 0.16% carbon steel
Magnetic abrasives	: Cr_2O_3, CeO, Fe_2O_3, MgO, B_4C, SiC, SiO_2 abrasive (5-10 μm) in a matrix of iron particles (100-400 μm)

3. EXPERIMENTAL PROCEDURE

In the magnetic abrasive finishing process, magnetic field is generated using an electromagnet. Current in the range of 0.5-2 A is passed through the copper coil wound in the form of a solenoid. The magnetic field generated within the magnetic core passes through the magnetic head. Magnetic abrasives are introduced in the gap between the magnetic heads, i.e. between the N and S poles. Due to the presence of the field, the abrasives align in the direction of the field. The cylindrical roller to be polished is held in the chuck of the lathe. The roller is given a rotary motion and is positioned in the magnetic field. A small clearance between the magnetic head and chuck of the lathe is provided to avoid accidental collision. The vibratory motion is provided to the magnetic head by means of a pneumatic vibrator to eliminate circumferential grooves. Typical frequency of vibration of the head are in the range of 15-20 Hz. The abrasives are stirred at intervals of about 1 minute to achieve uniform wearing of the abrasives.

4. HEAT TRANSFER MODELING OF MAGNETIC ABRASIVE FINISHING

In the magnetic abrasive finishing of ceramic rollers, the pressure applied by ferromagnetic particles on the cylindrical surface of the roller causes a Hertzian contact, the radius of which can be determined analytically. During the rotation of the roller, the ferro-magnetic particles carrying hard fine abrasives interact with the surface of the roller, thus removing material (as shown schematically in Figure 3). The real area

of contact is assumed to be a disc with a diameter of about 10~20 μm depending upon the hardness of the workmaterial and the abrasive. During polishing, the rod rotates with a velocity v, and generates heat at the rate of q cal/sec at the real area of contact, which is given by,

$$q = P \bullet \mu \bullet v \bullet 0.2388 \quad cal/sec$$

where

P is the load, N.

μ is the coefficient of friction

v is the sliding velocity, m/sec

The moving disc heat source problem can be solved based on the solution of a moving ring heat source. Thus, a brief introduction of the moving ring heat source problem is given in the following [1].

Consider a moving ring heat source, q_{rg} (cal/sec), continuously liberating heat and moving along the X-axis with a velocity v (cm/sec) (Figure 4). The problem is to determine the temperature rise at any point M(x,y,z) at any time t (in seconds) after the heat source begins to work.

The solution to this problem for a semi-infinite conduction medium is given by the following equation [1] :

$$\theta M = \frac{q_{rg} \ v}{8\lambda a \pi^{3/2}} \bullet \exp(-XV) \int_0^{\frac{v^2 t}{4a}} \frac{d\omega}{\omega^{3/2}} \bullet \exp\left(-\omega - \frac{u^2}{4\omega}\right)$$

$$\bullet \ I_0 \left[\frac{r_0 V^2}{2\omega} \sqrt{\left(X + \frac{2\omega}{V}\right)^2 + y^2} \right] \tag{1}$$

where,
    q_{rg} the heat generated by a ring heat source, cal/sec.

    v   sliding velocity, cm/sec.

    λ   thermal conductivity of silicon nitride, cal/cm.sec. °C.

    a   thermal diffusivity of silicon nitride, cm²/sec.

    X,y   co-ordinates of the point of interest,

V v/2a

ω a dimensionless number which has its maximum
  value equals to the upper limit of the integration,

r_0 the radius of the ring, cm.

I_0 (p) a modified Bessel function of first kind order zero,

$$p = \frac{r_0 V^2}{2\omega} \sqrt{\left(X + \frac{2\omega}{V}\right)^2 + y^2} \; ;$$

$$u = \frac{R_h v}{2a}$$

$$R_h^2 = r_0^2 + X^2 + y^2 + z^2$$

when p < 1.6 I_0 (p) = 0.935•exp(0.352p)

when 1.6 <= p <= 3 I_0 (p) = 0.5293•exp(0.7348p)

when p > 3 I_0 (p) = exp(p)/(2πp)$^{0.5}$

   The disc heat source can be considered as a combination of a series of concentric ring heat sources with different radii from zero to r_0 (here r_0 is the radius of the disc heat source). Usually the intensity of heat liberation is not uniformly distributed from the center to the periphery. A reasonable assumption would be to consider it to be distributed normally.

   Based upon the above considerations, the solution to the moving disc heat source for a semi-infinite body, as in the present case is given by the following equation:

$$\theta_M = \frac{9qdc \cdot v}{4\lambda a\pi^{3/2}r_o^2} \cdot \exp(-XV) \int_0^{r_o} r_i \cdot \exp\left(-\left(\frac{3r_i}{r_o}\right)^2\right) \cdot dr_i \cdot$$

$$\int_0^{\frac{v^2t}{4a}} \frac{d\omega}{\omega^{3/2}} \cdot \exp\left(-\omega - \frac{u^2}{4\omega}\right) \cdot I_0(p) \qquad (2)$$

where

$$p = \frac{r_i V^2}{2\omega} \sqrt{\left(X + \frac{2\omega}{V}\right)^2 + y^2}$$

$$V = \frac{v}{2a}$$

$$u = R_h \cdot V$$

$$R_h^2 = r_i^2 + X^2 + y^2 + z^2$$

The various steps used in the calculation of the flash temperatures using the moving disk heat source model along with a sample calculation are given in Appendix A and Appendix B, respectively.

5. RESULTS AND DISCUSSION

Figures 5 and 6 show the variation of the temperature rise with polishing pressure and sliding speed of the moving disc heat source on the roller surface, respectively. It can be seen that as the polishing pressure increases, the maximum flash temperature produced also increases. For example, it is about 758 °C at a polishing pressure of 68.95 kPa and drops to about 502 °C at 34.48 kPa. Also, as the sliding speed of the heat source increases, the maximum flash temperature also increases. For example, at 2.62 m/sec, the maximum temperature rise is about 502 °C but increases to over 828 °C at 5.24 m/sec. Based on Gibbs Free Energy calculations, it can be shown that these temperatures are sufficiently high to initiate chemo-mechanical action between the

silicon nitride roller and the chromium oxide abrasive. However, the extent of the formation of the chemical compounds depend on the flash times. The calculation of the flash times is given in the following and in many cases is of sufficient duration to cause chemo-mechanical action.

Determination of the Flash Times

Flash times of the expected flash temperatures can be calculated by measuring the distance on the temperature distribution plot where the temperature is above a given value and dividing it by the velocity of the abrasives. The total flash time (T_1) is defined as the time from the beginning of the temperature rise to the time when it drops to the room temperature. If this time is more than the time taken (say T_2), for the next abrasive to reach this present location then there would be a cumulative effect on the rise of flash temperatures on the rod. Otherwise, there would be no cumulative effect.

Taking the temperature rise plot of Figure 5 as an example, the flash time can be found using the following equation:

$$\text{Flash time, } T_1 = \frac{L}{v} \cdot 10^6 \text{ sec}$$

where   L is the length of the region where the temperature is higher than a certain expected critical temperature in cm.
v is the velocity of the moving heat source in cm/sec.

Table 2 gives the flash times at various flash temperatures for different combinations of polishing pressure and sliding speed. It can be seen that depending on the pressure, the temperature, and the sliding velocity, the flash times can range from 1-21.2 μsec.

(a)   Referring to Figure 7, the total flash time T_1 is given by,

$$T_1 = 132/2.62 = 50.4 \text{ μsec.}$$

(b)   The time taken by the next abrasive to travel through the center to center between the abrasives, T_2 is given by (in this case, the minimum possible center to center distance is 250 μm)

$$T_2 = 250 / 2.62 = 95.4 \, \mu sec.$$

Since $T_1 < T_2$, there would be no cumulative effect of the abrasive on the flash temperature rise of the rod.

Table II Calculated Flash Times for Various Flash Temperatures

Expected flash temperature, ^oC			100	200	300	400	500	600	700
	P kPa	v m/sec							
Flash time,	34.48	2.62	13.0	6.2	4.0	2.6	1.1	--	--
μsec	34.48	3.93	10.0	5.7	3.7	2.7	1.9	1.3	--
	34.48	5.24	6.9	4.9	3.4	2.5	1.9	1.5	1.1
	51.71	2.62	17.9	8.9	5.9	4.2	3.0	1.8	--
	51.71	3.93	11.5	7.9	5.3	3.9	3.0	2.4	1.8
	51.71	5.24	7.6	6.0	4.8	3.6	2.9	2.3	1.9
	68.95	2.62	21.2	10.0	7.6	5.6	4.3	3.2	2.0
	68.95	3.93	12.5	9.4	6.9	5.1	4.0	3.3	2.6
	68.95	5.24	8.2	6.7	5.6	4.6	3.8	3.1	2.6

It can be shown that using chromium oxide abrasive in MAF of silicon nitride rollers, at the pressures and sliding speeds used, the flash temperatures generated are high and the corresponding flash times are sufficiently long to form specific reaction products, such as, oxidation of silicon, and formation of chromium nitride and chromium silicate [3]. It can also be shown that based on Gibb's Free Energy (ΔG^o) calculations, the oxidation of silicon nitride in air can take place around 167 ^oC. It can be seen from Table II, that even at relatively low pressure (34.48 kPa) and low sliding speed (2.62 m/sec), the flash temperature in polishing far exceeds the temperature required for the oxidation of silicon nitride with sufficiently long duration of time for the reaction products to form. They are close to the conditions where chemo-mechanical reactions involving the formation of chromium nitride and chromium silicate can be formed. Thus chemical reactions can be activated during polishing by proper choice of the abrasive and polishing conditions for a given workmaterial.

Examination of the wear debris (in the SEM with an X-ray microanalyzer and a low angle X-ray diffraction apparatus) obtained in MAF of silicon nitride rollers using chromium oxide abrasive showed conclusively that Cr_2O_3 does participate in the chemo-mechanical polishing of Si_3N_4 forming chromium nitride and chromium silicate [3,4]. This work establishes the role of Cr_2O_3 not as a mere catalyst but one actively taking part in the chemical reactions during chemo-mechanical polishing [4]. Based on it, we have developed models for the chemo-mechanical polishing of Si_3N_4 in air and in water with Cr_2O_3 abrasive. These models are based on the formation of such reaction products as chromium silicate and chromium nitride in addition to the formation of silica layer on the surface of Si_3N_4 as well as the gaseous reaction products, such as ammonia (in water) and nitrogen (in air).

6. CONCLUSIONS

1. A moving disc heat source model was applied to magnetic abrasive finishing (MAF) process to determine the flash temperatures and flash times. The workmaterial considered is silicon nitride roller and the abrasive is chromium oxide

2. The moving disc heat source problem was solved (for the case of MAF) by assuming normal distribution for the intensity of heat liberation over the disc.

3. The flash temperature was found to be a function of the polishing pressure as well as the sliding speed of the abrasives on the work surface.

4. As the polishing pressure increases, the maximum flash temperature produced also increases. For example, it is about 502°C at 34.48 kPa and increases to 758°C with increase in polishing pressure to 68.95 kPa. Also, as the sliding speed of the abrasives on the work surface increases, the maximum flash temperature also increases. For example, at 2.62 m/sec, the maximum temperature rise is 502°C. With increases in sliding speed, say 5.24 m/sec, the temperature rise increased to about 828 °C. The flash temperatures and corresponding flash times were found to be adequate for the chemo-mechanical action between the abrasive (chromium oxide) and the workmaterial (silicon nitride) under the conditions of polishing. Experimental evidence of the wear debris presented elsewhere [3,4] showed the formation of chromium nitride and chromium silicate by the polishing process.

5. Based on the total flash time calculation, it was found that there would be no cumulative effect of the abrasive on the flash temperature rise of the rod. Thus the average temperature rise of the bulk material of the work piece is very low.

ACKNOWLEDGMENTS

REFERENCES

1.   Hou Zhen-Bing and R. Komanduri, " A Thermal Model of Magnetic Float Polishing of Ceramics," accepted for publication in Trans ASME, J of Tribology (1996)

2.   Fox, M., Agrawal, K., Shinmura. T, and R. Komanduri, "Magnetic Abrasive Finishing of Rollers," Annals of CIRP, 43/1 (1994) 181-184

3.   Bhagavatula, S. R., "On the Chemo-Mechanical Polishing of Silicon Nitride with Chromium Oxide Abrasive," M.S. Thesis, Oklahoma State University, Stillwater, OK (1995)

4.   Bhagavatula, S. R. and R. Komanduri, "On the Chemo-Mechanical Polishing of Silicon Nitride with Chromium Oxide Abrasive," accepted for publication in Philosophical Magazine (1995)

APPENDIX - A

Calculation of the Flash Temperature Using the Moving Disk Heat Source Model

1. The surface velocity is determined from the resultant of the rotational velocity of the rod and the translational velocity of the abrasives sliding on the rod.

2. The number of ferro-magnetic particles taking part in the polishing were determined using the ratio of the areas of magnetic brush and the mean cross-sectional area of the ferro-magnetic particles multiplied by a coefficient of probability. The assumption used here is that the distribution of heights of the asperities on the surface of the magnetic brush is the same as that of a monolayer of particles with normal distribution of their sizes backed with a flat surface (see Figure A 1 for details).

3. The total force acting is the product of the polishing pressure and the area of magnetic brush. The force on each ferromagnetic particle is the ratio of the total force and the number of particles taking part in polishing.

4. The radius of contact was determined from the Hertzian stress equation:

$$r_0 = (1.5 \cdot w \cdot R'/E')^{1/3}$$

where w is the load per ferromagnetic particle, in N
R' is the equivalent radius, in m.
E' is the equivalent Young's modulus.
r_0 is the radius of contact

where

$$\frac{1}{R'} = \frac{1}{R_1} + \frac{1}{R_2}$$

R_1 is the radius of the ferromagnetic particle,
R_2 is the radius of the cylindrical surface of the work

Where

$$\frac{1}{E'} = \frac{1- v_1^2}{E_1} + \frac{1- v_2^2}{E_2}$$

E' is the equivalent Young's modulus,
E_1 is the Young's modulus of the work piece,
E_2 is the Young's modulus of the ferromagnetic particle,
v_1 is the Poisson's ratio of workmaterial,
v_2 is the Poisson's ratio of the ferromagnetic particle.

5. The heat generated is determined from the product of the load, the sliding velocity, and the coefficient of friction.

6. The fraction of the heat contributing to the temperature rise is assumed to be a linear function of thermal conductivities of the silicon nitride workmaterial, chromium oxide abrasive, and the ferromagnetic powder used in the polishing.

7. The heat dissipated into the workmaterial causes temperature rise (flash temperatures) at the contact point.

8. The flash time (i.e. duration of the expected temperature) is calculated in the following manner: (Consider for example, the flash temperatures as 100, 200, 300, 400, 500, 600, and 700 °C, respectively)

i) Calculate from the temperature distribution plots along the X-axis, the total distance in the vicinity of the working ferromagnetic particle where temperature exceeds 100, 200, 300, 400, 500, 600 or 700 °C, respectively.

ii) Divide this distance by the sliding velocity obtained in step i to yield the flash time.

9. To determine whether the particle adjacent to the particle under consideration has any effect on the cumulative rise in the flash temperature, the time taken by the adjacent particle to reach the present one's position is calculated. This is simply the ratio of the center to center distance between the neighboring particles and the sliding velocity. If this time is longer than the total flash time from the beginning of temperature rise to the moment when the flash temperature rise drops down to zero, then, there is no cumulative effect.

APPENDIX-B

Specimen Calculations Using the Moving Disk Heat Source Model

Table B1 gives the polishing conditions used and Table B2 gives the relevent material properties of the workmaterial and the abrasive.

Table B1: Polishing Conditions Used

Polishing pressure p:	34.48 kPa
Diameter of the silicon nitride rod D:	25 mm
Rotational speed of the rod N:	2000 rpm
Oscillational frequency of the magnetic head, f:	25 Hz
Amplitude of oscillation of the magnetic head A:	0.25 cm
Width of the magnetic head L:	1.0 cm
Size of the ferromagnetic particles :	100-400 μm
(means diameter = 250 μm)	
Volume fraction of Iron powder v:	60%

Table B2: Material Properties of the Workmaterial and the Abrasive

Thermal conductivity of silicon nitride, λ_1:	0.026 cal/cm.sec.^oC
Thermal conductivity of chromium oxide, λ_2:	0.076 cal/cm.sec.^oC
Thermal conductivity of iron powder:	0.174 cal/cm.sec.^oC
Thermal diffusivity of silicon nitride, a:	0.039 cm^2/sec.
Heat capacity of silicon nitride, C:	0.202 cal/gm. ^oK
Density of silicon nitride, ρ:	3.3 gm/cm^3
Elastic modulus of silicon nitride, E_1:	304 GPa
Elastic modulus of ferromagnetic particles, iron, E_2:	160 GPa
Poisson's ratio of silicon nitride, ν_1:	0.25
Poisson's ratio of iron particles, ν_2:	0.28

Surface velocity of the magnetic particles, $V_1 = \pi D N / 60$
$$= 3.14 \bullet 25 \bullet 10^{-3} \bullet 2000/60$$
$$= 2.618 \text{ m/sec.}$$

Oscillational speed of the magnetic head, $V_2 = 2 \bullet A \bullet f /100$

$$= 2 \bullet 0.25 \bullet 25/100 = 0.125 \text{ m/sec}$$

Relative velocity between the abrasive and work piece,

$$V = [V_1{}^2 + V_2{}^2]^{\frac{1}{2}}$$

$$V = 2.621 \text{ m/sec.}$$

Number of magnetic abrasives in
the monolayer
$$= \pi \bullet 0.5 \bullet D \bullet L / (\text{abr. size})^2$$
$$= 3.14 \bullet 0.5 \bullet 25 \bullet 10/ (250 \bullet 250 \bullet 10^{-6})$$
$$= 6283$$

Referring to Figure B1, it can be seen that initially only a few particles which are of the highest height of the asperities are under contact. With the application of polishing pressure by means of the magnetic field, the contact points of those particles will undergo a certain deformation. It consequently causes the work surface to approach closer to the magnetic brush as shown in Figure B1.

With a load about 1- 2.5 N/particle, the deformation of the contact points can be estimated to be in the range of 0.6 to 1.8 μm. The total range of distribution of the heights of different particles is around 300 μm (assuming normal distribution). Due to deformation of the initial contact points, the number of particles with actual contact (number of active particles) increases. The deformation is very small (0.6-1.8 μm) compared to the total range of distribution (300 μm). The probability of the heights of asperities falling into this small range (0.6--1.8 μm) is very low. The probability calculations show that it is almost constant (about 0.14%) when the deformation of the initial contacts is in the range of 0.6-1.8 μm.

Effective young's modulus, E' is given by,

$$E' = \frac{1}{\dfrac{1 - v_1{}^2}{E_1} + \dfrac{1 - v_2{}^2}{E_2}}$$

$$E' = \frac{1}{\dfrac{1-0.28^2}{160 \times 10^9} + \dfrac{1-0.25^2}{304 \times 10^9}}$$

$$E' = 1.131 \cdot 10^{11}$$

Effective radius of contact, R' is given by,

$$R' = \frac{1}{\dfrac{1}{R_1} + \dfrac{1}{R_2}}$$

where R_1 is the radius of the ferromagnetic particle, and R_2 is the radius of the roller at the point of contact.

$$R' = \frac{1}{\dfrac{1}{0.5 \times 250 \times 10^{-3}} + \dfrac{1}{12.5}}$$

R' = 0.124 mm.

Total load on the rod, W = polishing pressure • 0.5 • π • (rod. dia.) •
$$\text{(length of heat source)}$$
$$= 3.45 \cdot 0.5 \cdot \pi \cdot 2.5 \cdot 1.0$$
$$= 13.54 \text{ N.}$$

Load per magnetic particle, w = Total load / number of particles under contact

$$= 13.54 / (6283 \cdot 0.0014)$$
$$= 1.54 \text{ N/particle}$$

Radius of contact, r_0 is given by,
$$r_0 = (1.5 \cdot w \cdot R'/E')^{1/3}$$
$$= [(1.5 \cdot 1.54 \cdot 0.124 \cdot 10^{-3})/1.131 \cdot 10^{11}]^{1/3}$$
$$= 13.64 \ \mu m.$$

Total amount of heat produced during polishing at the disc plane heat source, Q is given by (assuming $\mu = 0.25$),

$$Q = (w \bullet \mu \bullet v \bullet .2388)$$

$$= (1.54 \bullet 0.25 \bullet 2.62 \bullet .24)$$
$$= 0.241 \text{ cal/ sec.}$$

The fraction of heat that goes into the workmaterial, x is given by,

$$x = \frac{\lambda_{Si_3N_4}}{\lambda_{Si_3N_4} + \{[\frac{100 - \% \text{ of Iron content}}{100}] . \lambda_{Cr_2O_3} + [0.01 . \% \text{ of Iron content}. \lambda_{Fe}]\}}$$

$$x = 0.026/(0.026 + (0.076 \bullet .4) + (0.174 \bullet .6))$$
$$= 0.1617$$

Amount of heat that goes into the silicon nitride workmaterial, Q_{wp} is given by,

$$Q_{wp} = Q \bullet x$$
$$= 0.2410 \bullet 0.1617$$
$$= 0.039 \text{ cal/sec.}$$

206
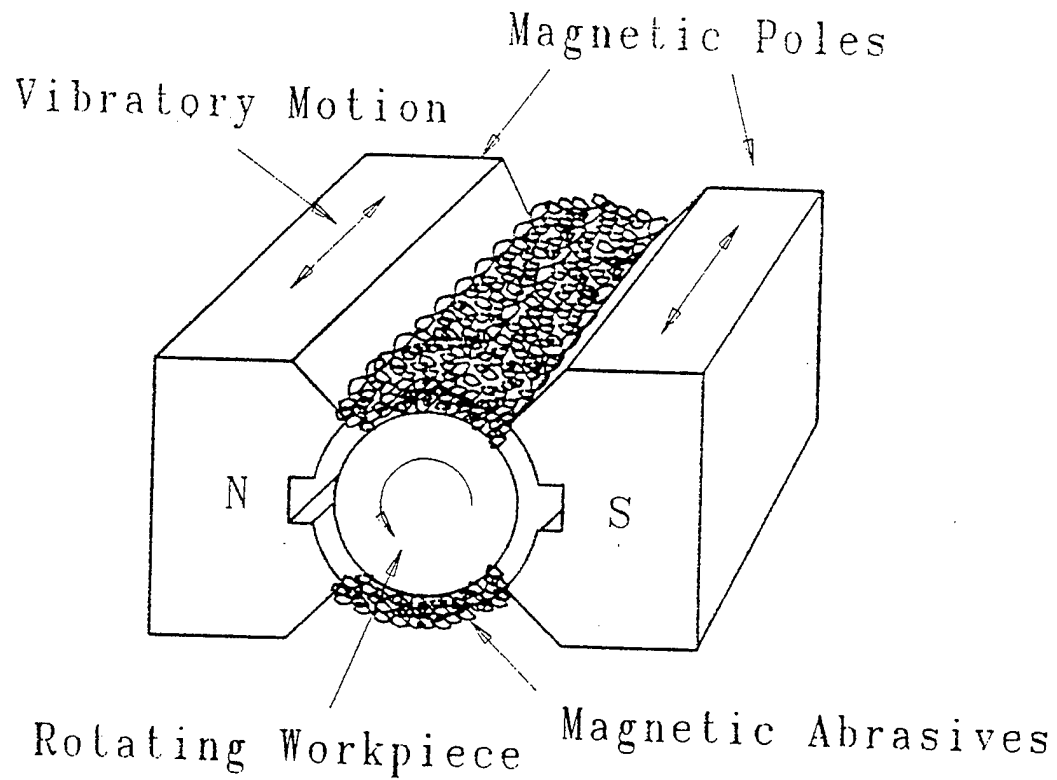
Figure 1 (a)   Schematic of the magnetic abrasive finishing (MAF)
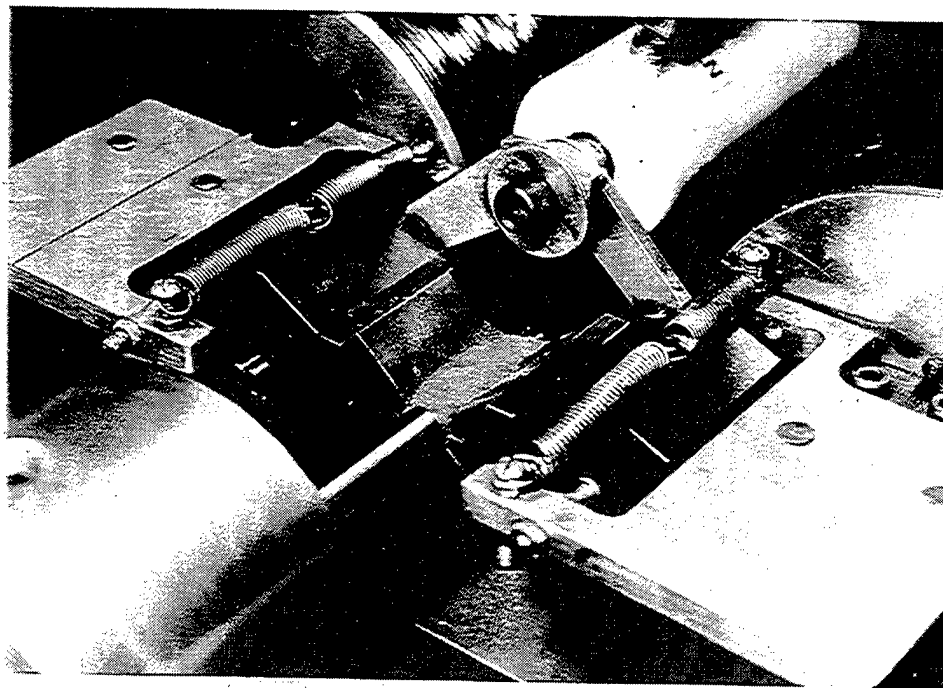process for polishing ceramic rollers [2]

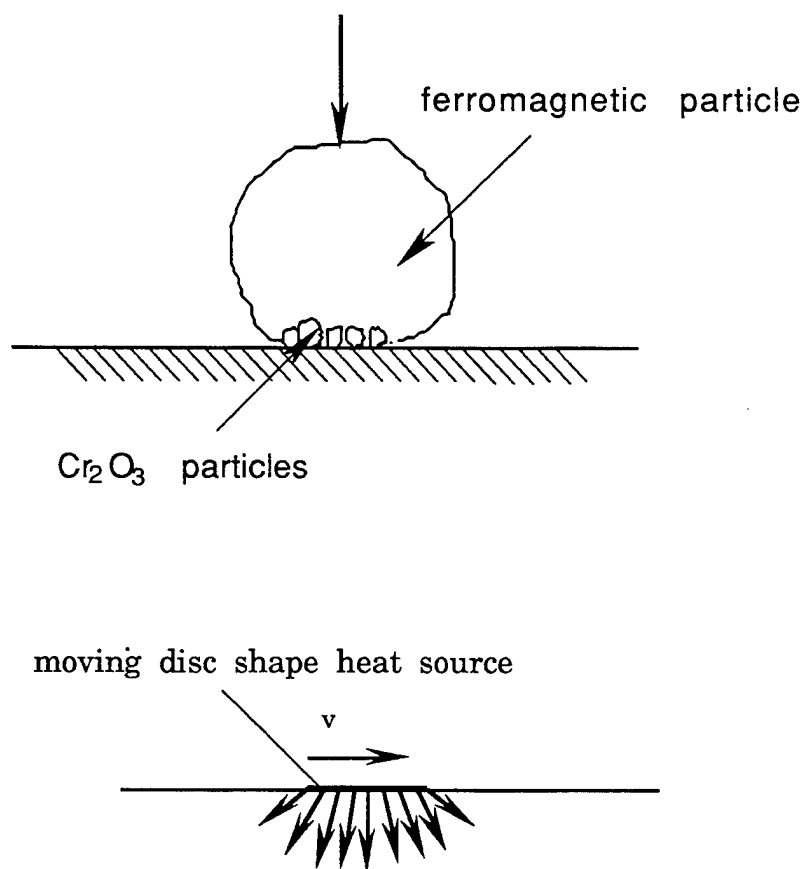Figure 1 (b)   Photograph of the magnetic abrasive finishing (MAF)
apparatus [2]

ferromagnetic particle

Cr_2O_3 particles

moving disc shape heat source

v

Figure 3   Schematic of the moving disc heat source problem [1]
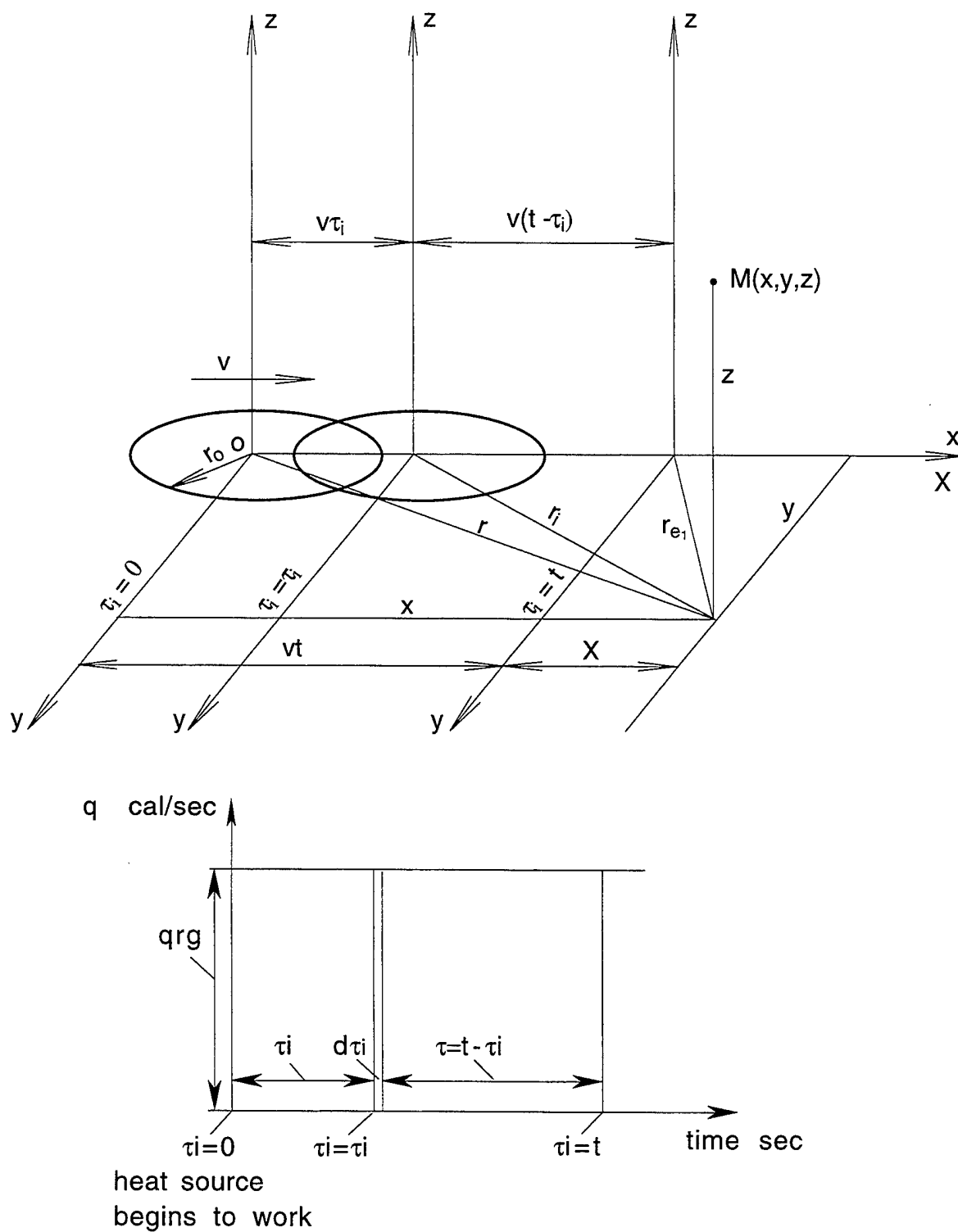
Figure 4   Moving ring heat source problem in an infinitely large conducting
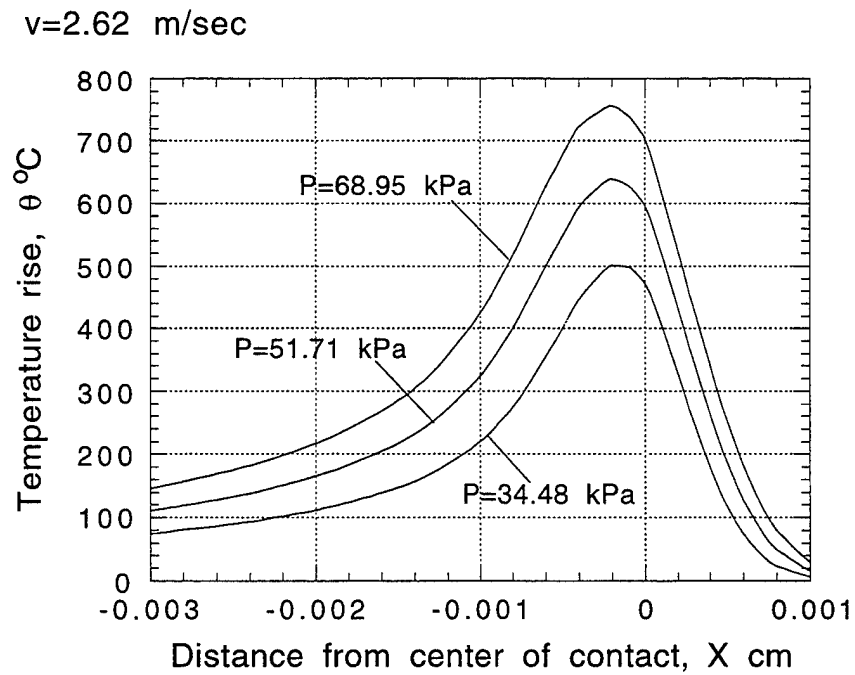   medium (after Hou Zhen Bing and R.Komanduri [1])

v=2.62 m/sec

Figure 5   Variation of flash temperature rise with polishing presure

P=34.48 kPa

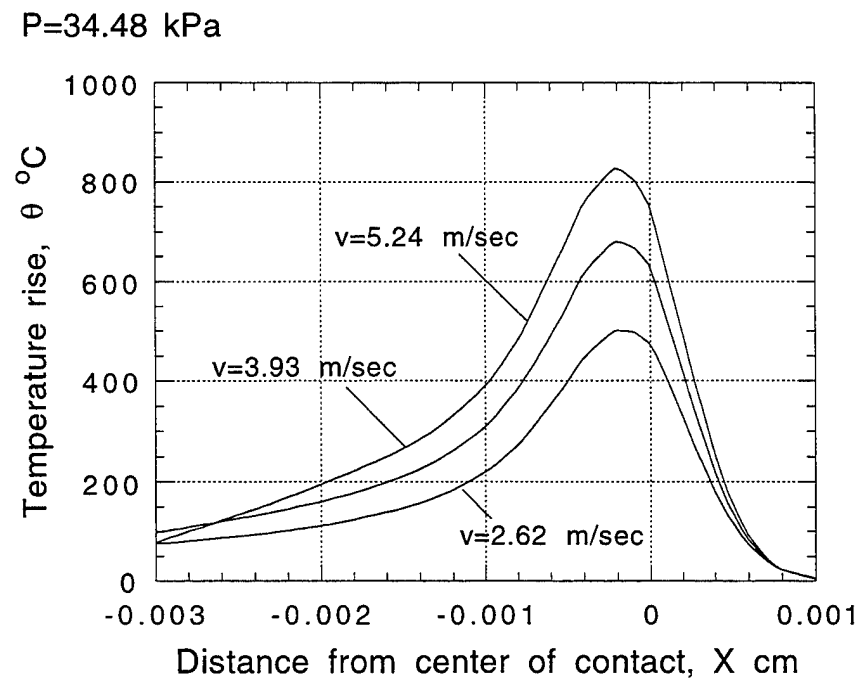Figure 6   Variation of flash temperature rise with sliding speed of
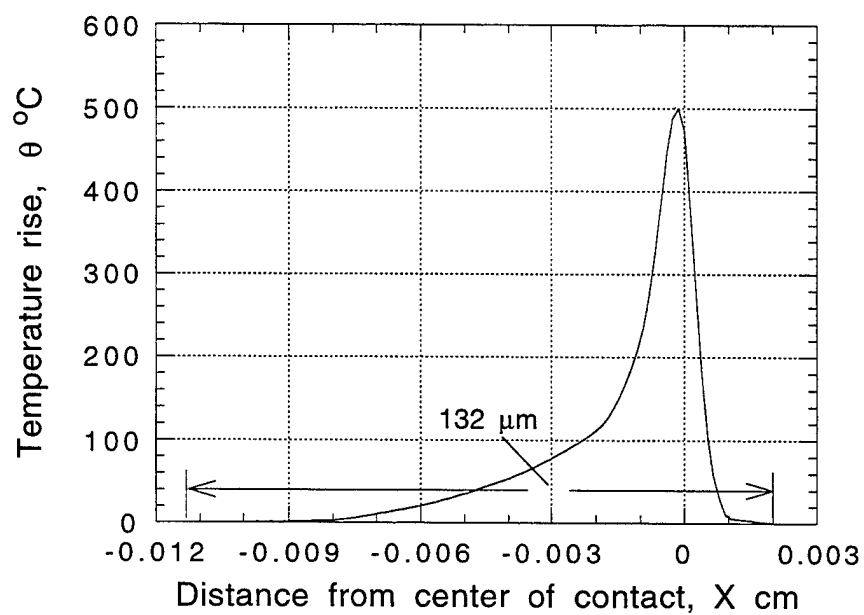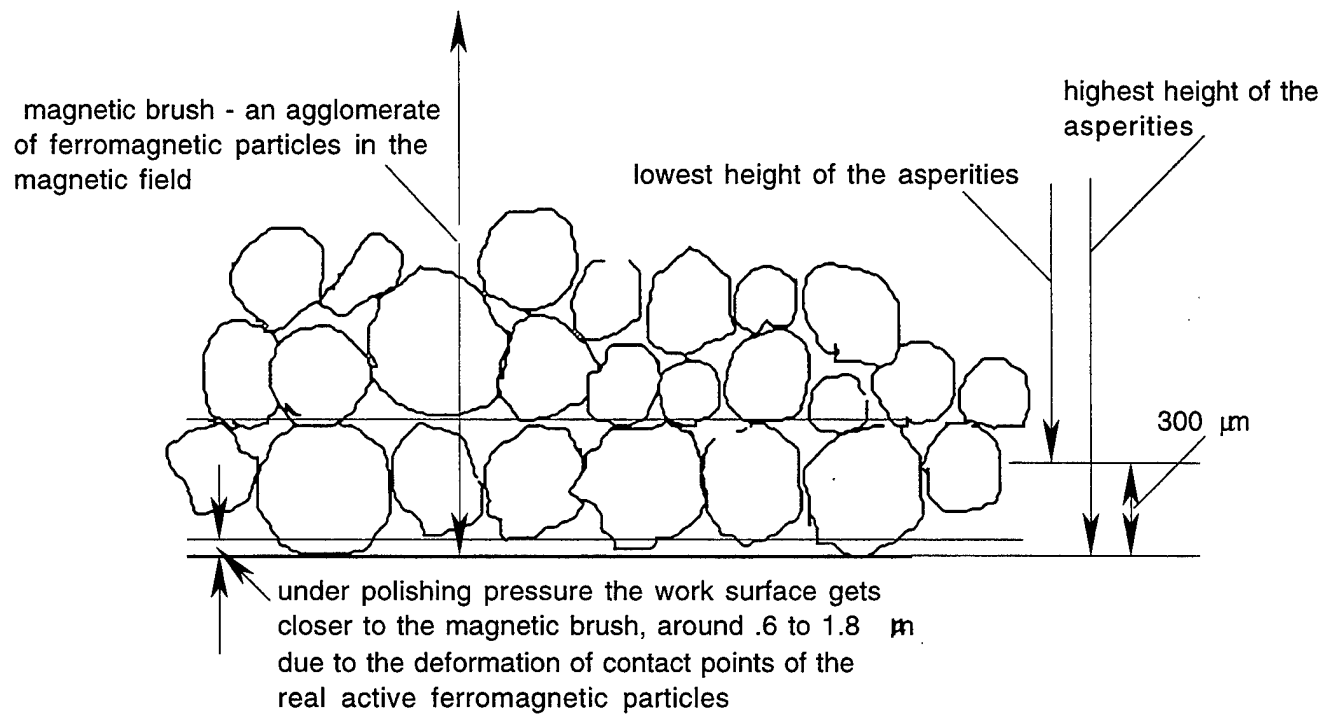   abrasives on the work surface

210

P=34.48 kPa   v=2.62 m/sec

Figure 7   Total flash temperature rise

magnetic brush - an agglomerate of ferromagnetic particles in the magnetic field

lowest height of the asperities

highest height of the asperities

300 µm

under polishing pressure the work surface gets closer to the magnetic brush, around .6 to 1.8 µm due to the deformation of contact points of the real active ferromagnetic particles

The deformation of the real contacting points causes the increase of probability of real contact from nearly zero to about .14 %.

Figure B1   Coefficient of probability of real contact